Exploring CO_2 as C_1 building block in synthetic processes: Steps towards a circular economy

Dissertation

in partial fulfillment of the requirements for the degree of

Doctor rerum naturalium (Dr. rer. nat.)

at the University of Rostock

Faculty for Mathematics and Natural Sciences

submitted by

Thea Siri Mayer, M.Sc.

born August 18th, 1997

in Lübeck, Germany.

Leibniz Institute for Catalysis

at the University of Rostock

2024

https://doi.org/10.18453/rosdok_id00005032

Leben ist die entschleunigte Totaloxidation des energiereichen Kohlenstoffs.

A. Börner, 2017

Selbstständigkeitserklärung

Ich versichere hiermit an Eides statt, dass ich die vorliegende Arbeit selbstständig angefertigt und ohne fremde Hilfe verfasst habe, keine außer die von mir angegebenen Hilfsmittel und Quellen dazu verwendet habe und die den benutzten Werken inhaltlich und wörtlich entnommenen Stellen als solche kenntlich gemacht habe.

Rostock, den 14.05.2024

……..

Thea Siri Mayer

Die vorliegende Dissertation wurde vom 01.04.2021 bis 14.05.2024 am Leibniz-Institut für Katalyse e.V. an der Universität Rostock unter Anleitung von Dr. Jola Pospech und Prof. Dr. Matthias Beller erstellt.

1. Gutachterin: Dr. Jola Pospech (Leibniz-Institut für Katalyse e.V.)
2. Gutachterin: Prof. Dr. Ivana Fleischer (Universität Tübingen)

Tag der mündlichen Prüfung: 15.10.2024

Acknowledgements

Zunächst möchte ich meiner Doktormutter Dr. Jola Pospech dafür danken, dass sie mich meine ganze Karriere hinweg unterstützt hat. Du hast mir zu einem Auslandsaufenthalt und einem Industriepraktikum verholfen und trotzdem immer klar gemacht, dass du mich danach wiederhaben möchtest. So habe ich immer gewusst, dass ich wertgeschätzt werde. Wir haben zusammen das Tief Ralli überstanden und auch die Betreuung auf Distanz während der Schwangerschaft und Elternzeit hat gut funktioniert. Danke für dein Vertrauen, als du mich in deiner Elternzeit zur stellvertretenden Laborleiterin gemacht hast und ich Bestellzettel etc. selbst unterschreiben durfte. Du hast mich für Lindau vorgeschlagen und mir so ermöglicht, Nobelpreisträger zu treffen; ich durfte nach Kopenhagen, Namur, und Vancouver reisen. Auch bei der Jobsuche hast du mich bestmöglich unterstützt, mir Empfehlungsschreiben geschrieben und Kontakte geknüpft und vermittelt. Selbst wenn ich nur aufmunternde Worte oder eine Umarmung brauchte, warst du da. Nun geht eine Ära zu Ende, wie du es ausgedrückt hast – 2018 bis 2024 ist eine lange Zeit. Du warst die beste Chefin, die ich mir hätte wünschen können. Danke für alles.

Anschließend möchte ich Prof. Dr. Matthias Beller danken. Als die geplante Haushaltsstelle für meine Promotion nicht mehr zur Verfügung stand, bist du ohne zu zögern eingesprungen und hast mir eine Stelle unter Betreuung von Jola und dir angeboten. Und tatsächlich war das eine viel bessere Stelle als die ursprünglich Geplante, denn ich habe so die Chance bekommen, weiterhin mit meiner liebgewonnenen Arbeitsgruppe in Aarhus in Kontakt zu stehen, jährlich dorthin zu reisen und sogar einen erneuten Auslandsaufenthalt zu erleben. Die Co-Betreuung hat in meinen Augen wunderbar funktioniert (viel besser, als mir alle prophezeit haben), du hast dich in regelmäßigen Meetings eingebracht und viele neue Impulse für meine Forschung geliefert. Als du eine Weile keine Updates bekommen hast, hast du nachgehakt, was bei deinem Arbeitspensum wirklich nicht selbstverständlich ist. Du warst immer verständnisvoll und unterstützend, hast uns aber auch ehrlich mitgeteilt, wenn wir in eine Sackgasse geraten waren, was mindestens genauso wertvoll war. Danke!

Durch ein großzügiges Funding des CADIAC-Projekts und der DFG konnte ich Chemikalien, einen Autoklav und alles, wovon man im Labor sonst noch träumen könnte, finanzieren. Danke dafür. Ich hatte während meiner Promotion am Likat zudem das Privileg, drei Monate in Aarhus verbringen zu dürfen und viele Konferenzen besuchen zu können – in diesem Punkt möchte ich auch dem DAAD für ein großzügiges Reisestipendium für meine Reise nach Vancouver danken.

Liebe Pospeople, euch danke ich für die Begleitung meiner Promotion und das fantastische Gruppengefühl. Tobi möchte ich danken, weil wir vor allem zu Beginn meiner Arbeit ein klasse Team waren. Dank der Gewöhnung an deinen starken Kaffee, der am Anfang noch zu Lachflashs und riesigen Energieschüben geführt hat, kann mich jetzt nichts mehr schocken. Mit so einer Laborfamilie habe ich

sehr gerne auch mal bis spätabends gearbeitet. Andranik hat vor allem mein erstes Jahr liebevoll begleitet mit Bossa Nova-Musik, selbstgemachtem Hummus zu jeder Gelegenheit und motivierenden Sprüchen im Labor. Danke an Luisa, die immer ein fester Teil des AKs war, egal ob sie sich gerade in Rostock, Wuppertal oder Bath aufgehalten hat. Dir, Johannes, danke ich dafür, dass du die Betreuung von Huy übernommen und mir eine Riesenlast von den Schultern genommen hast. Du wusstest zudem immer einen Rat bei allen Laborproblemen, ohne diesen jemals jemandem aufzudrängen. Danke an Jannik, dass du meinen Kiosk gebührend wertschätzt und den regelmäßigen fachlichen Austausch wieder eingeführt hast, nachdem ich so lange allein im Labor gewesen bin. Ihr alle seid Kollegen, mit denen man gerne die Arbeitstage UND Feierabende verbringt. Danke an dieser Stelle auch an Jacqui, die von Anfang an ein Mitglied ehrenhalber war, süße Nachrichten an den Abzügen hinterlassen hat und immer am meisten von uns allen auf die Einhaltung der Sicherheitsvorschriften in unserem Labor geachtet hat. Danke, dass du meine Freundin bist.

Vom AK Skrydstrup möchte ich vor allem natürlich Prof. Dr. Troels Skrydstrup danken, der mich nach den 4 Monaten im Master noch ein zweites Mal herzlich aufgenommen hat und auf den CADIAC-Konferenzen allen erklärt hat, wie sehr er sich auf meinen Besuch freut. Danke an Karoline, die alles aus der Ferne organisiert hat und mir ein Vorbild für die Arbeit als Projektkoordinatorin gewesen ist. Ich danke auch Clemens, mit dem ich zusammen an Nylon verzweifelt bin – die Chemie hat zwar nein gesagt, aber wir waren trotzdem ein gutes Team! Julia danke ich dafür, dass wir dieses und letztes Mal so eine schöne Zeit abseits des Labors hatten. Zum Schluss danke ich allen anderen Mitgliedern der Skrydstrup-Gruppe, auf die ich mich jeden November freuen durfte.

Aus dem AK Beller danke ich zuallererst Caro. Seit unserer gemeinsamen Zeit als Doktorandensprecherin sind wir zu tollen Kolleginnen und Freundinnen geworden, darüber habe ich mich sehr gefreut. Danke für deine Unterstützung und Mitarbeit am Phenanthrolin-Projekt, welches du trotz deiner vielen Aufgaben nie aus den Augen verloren hast. Ohne dich hätte meine Dissertation kein so rundes Ende. Danke an Gordon, dass du immer ein offenes Ohr für mich hattest und mich aufgebaut hast. Ihr und noch einige andere habt mir trotz aller Widrigkeiten immer das Gefühl gegeben, auch zum Bereich Beller zu gehören und mit Fragen immer zu euch kommen zu dürfen.

Ab dem zweiten Jahr meiner Promotion gehörte ich zudem zum AK Beweries, dem ich für die tolle Arbeitsatmosphäre danken möchte. Vor allem Prof. Dr. Torsten Beweries danke ich für die gute Betreuung, obwohl ich offiziell ja gar nicht unter seiner Fittiche stand. Dein Interesse und dein Blickwinkel auf meine Forschung haben mich motiviert weiterzumachen, wenn ich innerlich schon aufgegeben hatte. In Jahresabschlussgesprächen haben wir gemeinsam das Jahr Revue passieren lassen und du hast mich an all die tollen Dinge erinnert, die neben der oftmals frustrierenden Forschung noch passiert sind, wie mein Engagement als Doktorandensprecherin oder die Reise nach Lindau.

Alex – traditionell bekommt der Partner ja einen Abschnitt weiter hinten in der Danksagung, bei Familie und den Freunden, aber du warst (und bist) ja nicht nur mein Lieblingsfreund, sondern auch mein Lieblingskollege. Neben der seelischen Unterstützung zuhause (dein regelmäßiges „ich bin stolz auf dich“ hat mich durch die Monate des Schreibens an dieser Diss begleitet) hast du mich auch auf Arbeit mit Rat, Tat, trockenen Lösemitteln, Skills im Umgang mit luftempfindlichen Substanzen, und Berechnungen meines sich-selbst-zersetzenden Liganden unterstützt. Du hast immer auf meine Work-Life-Balance aufgepasst. Danke für alles.

Auch vielen übrigen LIKAT-Angestellten habe ich zu danken. Claas, danke für die Hilfe mit den Autoklaven und für unsere Mensa-Donnerstage, eine Tradition, die wir nie vernachlässigt haben. Hutti danke ich für die Erreichbarkeit rund um die Uhr – egal welches Anliegen ich hatte, es war stets am nächsten Morgen gefixt. Danke an Andreas Koch und Susann Buchholz für die Unterstützung bei der Verteidigung der Rechte der Doktorand*innen beim Selbstmessen von NMRs. Ich danke Dr. Wolfgang Baumann für die (zeit)aufwendigen quantitativen ^{13}C NMR und die ^{1}H-^{15}N HMBC-Spektren sowie für die Diskussion der Ergebnisse. Ohne beides wäre eine gründliche Analyse meines Liganden nicht möglich gewesen. Anke und Hajo möchte ich für die fixe Messung von Kristallstrukturen danken, auch wenn meine Substanzen selten schwere Elemente enthalten haben. Ich danke zudem Anja für die Hilfe beim Beantragen von finanzieller Unterstützung für meinen Aarhus-Aufenthalt und Anne und Nicole, die immer nur liebe Worte übrighatten.

Ohne Freunde außerhalb des LIKAT wäre meine Promotion sicherlich schwieriger gewesen. Danke also an Michelle für unsere regelmäßigen Telefonate, die meine Doktorarbeit begleitet haben. Mit dir konnte ich mich aufregen, freuen, und diskutieren. Lucas und Basti, ihr habt die Einhornherde am Leben gehalten. Danke, dass wir uns nach dem Studium nicht aus den Augen verloren haben, obwohl wir in so unterschiedlichen Bereichen gelandet sind. Danke an Max und die restlichen Physiker, dass ihr mich bei euch aufgenommen habt, als ich eine Zeit lang kollegenlos und einsam war. Außerdem möchte ich meinen Französischmädels danken für die tolle Atmosphäre in unseren Französischkursen während meiner Promotion, aber noch viel mehr dafür, dass wir danach in Kontakt geblieben sind.

Zuletzt habe ich meiner Familie zu danken. Neben allen anderen geht mein Dank vor allem an meine Eltern, meinen Opa und meinen Bruder. Notwendigerweise ist unser Zusammenhalt während meiner Promotion noch stärker geworden und für den Teil bin ich sehr dankbar. Danke für die Unterstützung und Liebe während des Studiums. Danke für eure Besuche in Aarhus, durch die ich mich weniger allein gefühlt habe. Danke an Opa für unsere WG-Zeit während meines Praktikums bei Bayer, wir waren so ein gutes Team. Danke, dass ich euch alle jederzeit anrufen kann.

Abstract

This thesis explores various approaches for utilizing CO_2 as a C_1 building block in synthetic processes, with the overarching aim of integrating carbon dioxide into a circular economy framework. Initially, the release of CO_2 was investigated through the photomediated pyrimidopteridine-catalyzed hydro- and deuterodecarboxylation of pharmaceutically relevant carboxylic acids. The representative scope includes 26 primary, secondary, and tertiary carboxylic acids. By using analytical methods such as Stern-Volmer fluorescence quenching, EPR spectroscopy and cyclic voltammetry, it was possible to propose a reasonable reaction mechanism. Furthermore, the thesis outlines an approach for CO_2 capture involving the chemical modification of waste material, specifically nylon-6, to yield an economically relevant and readily available material. This initiative aligns with the "waste to value" concept. Optimization of this process was achieved using *N*-hexylhexanamide as a model system. Given the necessity to close the anthropogenic carbon cycle, CO_2 conversion is imperative. The methodology employed in this thesis involves rational nitrogen-based ligand design, with the aim of facilitating CO_2 conversion at low concentrations, while avoiding the use of phosphorus-based ligands.

Zusammenfassung

Diese Dissertation beinhaltet die Erforschung verschiedener Ansätze zur Nutzung von CO_2 als C_1-Baustein in synthetischen Prozessen. Das übergeordnete Ziel war die Integration von Kohlenstoffdioxid in eine Kreislaufwirtschaft. Zunächst wurde die Freisetzung von CO_2 durch die photomediierte Pyrimidopteridin-katalysierte Hydro- und Deuterodecarboxylierung von pharmazeutisch relevanten Carbonsäuren untersucht. Der repräsentative Scope umfasst 26 primäre, sekundäre und tertiäre Carbonsäuren. Durch den Einsatz analytischer Methoden wie Stern-Volmer Fluoreszenzquenching, EPR-Spektroskopie und Cyclovoltammetrie war es möglich, einen Reaktionsmechanismus zu formulieren. Darüber hinaus wird in dieser Arbeit ein Ansatz zur CO_2-Abscheidung vorgestellt, bei dem Abfallstoffe, insbesondere Nylon-6, chemisch modifiziert werden, um ein wirtschaftlich relevantes und leicht verfügbares Material zu erhalten. Dieses Ziel steht im Einklang mit dem "waste to value"-Konzept. Die Optimierung dieses Prozesses wurde mithilfe *N*-Hexylhexanamids als Modellsystem erreicht. Angesichts der Notwendigkeit, den anthropogenen Kohlenstoffkreislauf zu schließen, ist die Umwandlung von CO_2 zwingend erforderlich. Die in dieser Arbeit angewandte Methodik beinhaltet ein rationales Design von Liganden auf Stickstoffbasis mit dem Ziel, die Umwandlung von CO_2 in niedrigen Konzentrationen zu realisieren und gleichzeitig die Verwendung von phosphorbasierten Liganden zu vermeiden.

Table of Contents

ACKNOWLEDGEMENTS ..... **II**

ABSTRACT ..... **V**

TABLE OF CONTENTS ..... **VI**

LIST OF ABBREVIATIONS ..... **VII**

1 CIRCULAR ECONOMY **1**

2 OBJECTIVES **4**

3 CO_2 RELEASE BY PHOTOMEDIATED HYDRO- AND DEUTERO-DECARBOXYLATION **5**

3.1 INTRODUCTION 5

3.2 RESULTS AND DISCUSSION 9

3.2.1 Optimization using a Design of Experiment Approach *9*

3.2.2 Scope of the Reaction *13*

3.2.3 Mechanistic Investigations *24*

4 CO_2 CAPTURE BY (POLY)AMINES SYNTHESIZED FROM WASTE NYLON **30**

4.1 INTRODUCTION 30

4.2 RESULTS AND DISCUSSION 39

4.2.1 Synthesis of Triphos Derivatives *39*

4.2.2 Optimization using N-Hexylhexanamide as Model Substrate *43*

4.2.3 Reduction of Nylon *51*

5 CO_2 CONVERSION BY TRANSITION METAL CATALYSIS **57**

5.1 INTRODUCTION 57

5.2 RESULTS AND DISCUSSION 70

5.2.1 Alkoxycarbonylation as a Model for the Dimerization of CO_2 via Metallacarboxylic Acids *70*

5.2.2 Rational Ligand Design for Carbon Capture and Utilization *77*

5.2.2.1 Synthesis and Evaluation of Pyrox-C_4N 79

5.2.2.2 Synthesis and Evaluation of Phen-NCCN 85

6 SUMMARY AND OUTLOOK **98**

7 EXPERIMENTAL SECTION **101**

7.1 GENERAL REMARKS 101

7.2 GENERAL PROCEDURES 105

7.3 EXPERIMENTAL DATA 108

8 REFERENCES **207**

9 CURRICULUM VITAE **217**

List of Abbreviations

3D	3-dimensional
Å	Ångström
acac	acetylacetonate
Ad	adamantyl
atm.	atmosphere
ATR	attenuated total reflection
BA	phenylboronic acid
BCF	tris(pentafluorophenyl)borane
BDE	bond dissociation energy
bipy	2,2‘-bipyridine
Bn	benzyl
Boc	*tert*-butyloxycarbonyl
br	broad
Bu	*n*-butyl
Bu-O_3-Bu	butyl diglyme
°C	degree Celcius
calcd.	calculated
Cbz	benzyloxycarbonyl
CCS	Carbon Capture and Storage
CCU	Carbon Capture and Utilization
cm	centimeter
COD	cyclooctadiene
CRI	Carbon Recycling International
CV	cyclic voltammetry
Cys	L-cysteine
δ	chemical shift
d	doublet
DAB	1,4-diaminobutane
DAC	Direct Air Capture
DACCS	Direct Air Carbon Capture and Storage
DCM	dichloromethane
DDQ	2,3-dichloro-5,6-dicyano-1,4-benzoquinone
depe	1,2-bis(diethylphosphino)ethane
DES	deep-eutectic solvent
DFT	density function theory
DIBAL-H	di-*iso*-butylaluminum hydride
DIC	*N,N’*-di-*iso*-propylcarbodiimide
DIPAE	di-*iso*-propylaminoethanol
DIPEA	di-*iso*-propylethylamine
DMAP	dimethylaminopyridine
DMC	dimethylcarbonate
DMF	*N*,*N*-dimethylacetamide
DMM	dimethoxymethane
DMO	dimethyloxalate
DMSO	dimethylsulfoxide
DoE	Design of Experiment
dppf	1,1‘-bis(diphenylphosphino)-ferrocene
d.r.	diastereomeric ratio
dtbbpy	di-*tert*-butylbipyridine
E^*_{red}	excited-state reduction potential
$E^{ox}_{1/2}$	ground-state oxidation potential
$E^{red}_{1/2}$	ground-state reduction potential
ECH	epichlorohydrin
eCO_2RR	electrochemical CO_2 reduction reaction
EDA	ethylene diamine
ee	enantiomeric excess
e.g.	for example
EI	electron ionization

EMEA	2-(ethylamino)ethanol	HPLC	high-performance liquid chromatography
EPR	electron paramagnetic resonance	HRMS	high resolution mass spectroscopy
equiv.	equivalent	*I*	spin
ESI	electrospray ionization	IL	ionic liquid
Et	ethyl	i.o.	instead of
Et_2O	diethyl ether	IPDA	isophorone diamine
EtOAc	ethyl acetate	*i*Pr	*iso*-propyl
EtOH	ethanol	*i*PrOH	*iso*-propanol
EU	European Union	IR	infrared spectroscopy
eV	electron volt	*J*	coupling constant
EWG	electron-withdrawing group	*k*	specific rate constant
FA	formic acid	kg	kilogram
Fc	ferrocene	kJ	kilojoule
FE	Faradaic efficiency	K_{SV}	Stern-Volmer quenching constant
FID	flame ionization detector	l	liter
FLP	frustrated Lewis pair	LC	liquid chromatography
g	*g*-factor	LDPE	low-density polyethylene
g	gramm	LED	light-emitting diode
G	Gibbs free energy	Lys	L-lysine
GC	gas chromatography	*m*	*meta*
GHC	guanidinium hydrochloride	m	multiplet
h	hour	m^2	square meter
H	enthalpy	m^3	cubic meter
HABA	2-(4-hydroxyphenylazo)benzoic acid	M	molar (= mol/l)
		$[M]^+$	molecular ion peak
HAT	hydrogen atom-transfer	MACHO	ligand type, $HN(CH_2CH_2PR_2)_2$
HBpin	pinacolborane	MALDI	matrix-assisted laser desorption/ ionization
HDPE	high-density polyethylene		
hept	heptet	mbar	millibar
HFIP	hexafluoro-*iso*-propanol	MCA	metallacarboxylic acid
HMBC	heteronuclear multiple bond correlation	MCE	metallacarboxylic ester
		*m*CPBA	*meta*-chloroperbenzoic acid
$HNTf_2$	bistriflimidic acid		

Me	methyl	OAT	oxygen-atom transfer
MEA	monoethanolamine	OD	oxygen-derived
MeCN	acetonitrile	o/n	over night
MEK	methylethylketone	OTf	triflate
MeOH	methanol	*p*	*para*
mg	milligramm	p	pentets
MHz	megahertz	PA6	polyamide-6
min	minutes	PC	propylene carbonate
µl	microliter	PEI	polyethyleneimine
ml	milliliter	PEHA	pentaethylenehexamine
µmol	micromol	Ph	phenyl
mmol	millimol	phen	1,10-phenanthroline
MOF	metal-organic framework	pK_a	negative logarithm of the acid dissociation constant
mol%	mol percent		
m.p.	melting point	PP	polypropylene
MS	mass spectrometry	ppm	parts per million
MSA	methylsulfonic acid	PPT	pyrimidopteridine
Mt	megatons	PPTNO	pyrimidopteridine *N*-oxide
m/z	mass-to-charge ratio	PPTS	pyridinium *p*-toluenesulfonate
NASA	North-American Space Agency	Pr	propyl
*n*Bu	*n*-butyl	Pro	L-proline
nBu_2O	dibutyl ether	*n*PrOH	*n*-propanol
n.d.	not detected	PS	polystyrene, Styrofoam
NHC	*N*-heterocyclic carbene	PT	proton transfer
nm	nanometer	PTFE	polytetrafluoroethylene
NMP	*N*-methyl-2-pyrrolidinone	*p*TSA	*para*-toluenesulfonic acid
NMR	nuclear magnetic resonance spectroscopy	PVC	polyvinyl chloride
		PVP	polyvinyl pyrrolidone
NOESY	nuclear Overhauser effect spectroscopy	pyrox	pyridyloxazoline
		q	quartet
NSAID	non-steroidal anti-inflammatory drug	quant.	quantitative
		R	rest
OAc	acetate	ref	reference

R_f	retention factor	TMA	tetramethylammonium
rt	room temperature	TMG	1,1,3,3-tetramethylguanidine
s	singlet	TMM	2-methylallyl, trimethylmethane
S	spin quantum number	TMS	trimethylsilyl
sat.	saturated	TOF	time-of-flight
*s*Bu	*sec*-butyl	TOF	turn-over frequency
SCE	standard calomel electrode	TON	turn-over number
SDS	sodium dodecyl sulfate	t_R	retention time
SET	single-electron transfer	tribromide	1,1,1-tris(bromomethyl)ethane
SV	Stern-Volmer	triphos	1,1,1-tris(diphenylphosphino-methyl)ethane
t	time		
t	triplet	UV	ultraviolet
T	temperature	V	volt
TBA	tetrabutylammonium	Val	L-valine
TBD	1,5,7-triazabicyclo[4.4.0]dec-5-ene	vs	versus
		v/v%	volume percent
*t*Bu	*tert*-butyl	W	watt
TEA	triethylamine	WGSR	water-gas shift reaction
TEMPO	(2,2,6,6-tetramethylpiperidin-1-yl)oxyl	WHO	World Health Organization
		wt%	weight percent
TGA	thermogravimetric analysis	XTB	semiempirical tight-binding model
THF	tetrahydrofuran		
TLC	thin layer chromatography		

1 Circular Economy

Since the dawn of the industrial revolution, the standard of living has increased tremendously whereas less consideration was given to the environment.[1] The extensive use of resources has already led to current or future depletion of fossil fuels, including crude oil, coal, and natural gas, and of lithium, which is needed for batteries. Also certain other metals used in the technology sector and as catalysts in the chemical industry, or phosphorus applied as fertilizer in agriculture are available in limited amounts, among many others.[2-6] At the same time, fossil fuels and (in)organic waste have been incinerated for energy supply, releasing tons of CO_2, a prominent greenhouse gas, into the atmosphere.[3, 7] According to the North American Space Agency (NASA), "human activities have raised the atmosphere's carbon dioxide content by 50% in less than 200 years"[8], resulting in a new geological era that is informally called the *Anthropocene*.[9] The CO_2 concentration is regularly measured from Antarctic ice cores and directly from the atmosphere in Mauna Loa (Hawaii), Barrow (Alaska), Cape Matatula (American Samoa), at the South Pole, in Cape Grim (Australia), on the Shetland Islands (Scotland), and on Lampedusa Island (Italy).[10] According to these measurements, the atmospheric CO_2 concentration has recently surpassed 420 ppm, which is substantially higher than the average of 280 ppm that was obtained from Antarctic ice core samples representing the past 2000 years before the industrial revolution (Figure 1).[11-12] The impact of this increased amount of CO_2 became clear soon as it resulted in environmental troubles such as associated ocean acidification and global warming.[13]

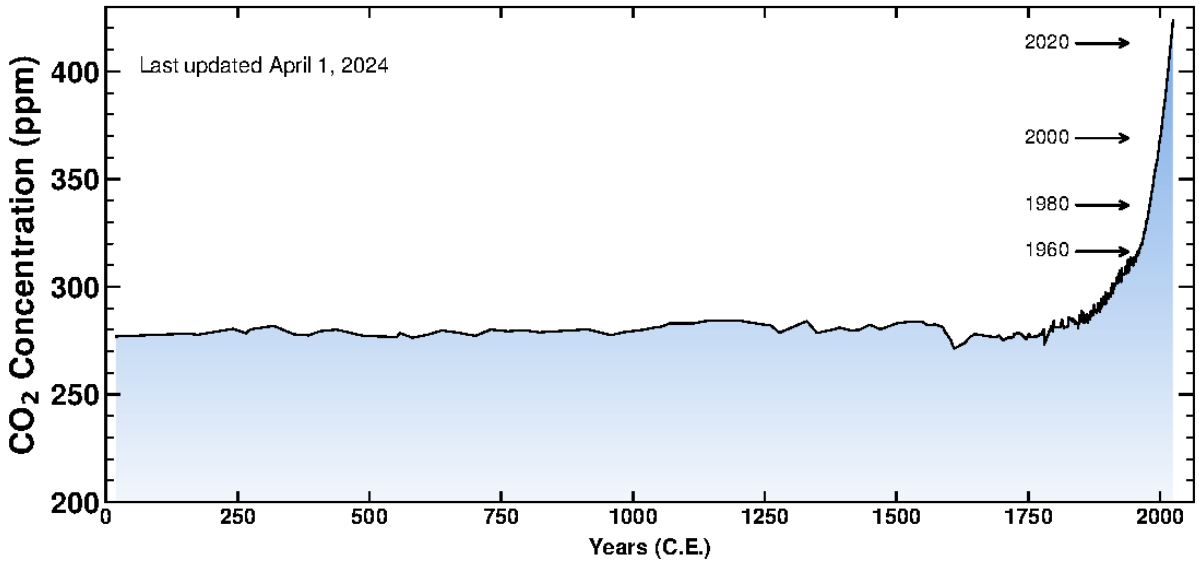

Figure 1. The Keeling Curve of the global atmospheric carbon dioxide concentration of the last 2000 years published by the Scripps Institution of Oceanography.[12]

The planet further suffers from an enormous pollution of the environment by waste, with the major contributor being plastic waste. According to Bergmann *et al.*, plastic pollution has even reached areas without permanent human activities like the Arctic deep seafloor.[14] Plastic waste stems mainly from

single-use packaging. Therefore, some countries have recently started a plastic packaging tax and others have already completely banned the use of single-use plastics.[15] However, the EU still produced 188.7 kg packaging waste per inhabitant in 2021.[16] The generation of waste, that is incinerated, landfilled, or dumped in the environment, is always accompanied by a loss of the raw materials contained in the waste, which inevitably leads to an increased demand for new raw materials from nature for the manufacture of new products.[17]

The concept of a circular economy was created to encounter these environmental problems and to reconstruct the ecological balance.[15] It includes the efficient use of resources so that less raw materials are needed, less waste is produced, and fewer emissions are released in the atmosphere.[18] This can be achieved by a smart product design, sustainable manufacturing, or the possibility to repair broken parts. Most of all, a circular economy is built on a thoughtful waste management that brings the raw materials of end-of-life products back to the production process (Figure 2).[6, 18] The goals of this concept can be summarized in the 3R policy (reduce, reuse, recycle).[15]

Figure 2. The circular economy model depicted by the European Parliament Research Service.[18]

As the first country, Germany established legally binding guidelines for plastics recycling that match the circular economy goal already in 1991. It is now the country with the highest recycling rate and the largest market for post-consumer plastics.[19] To be able to recycle plastics accordingly, it is important to separate the different plastic types from each other and from residuals like food waste.[20] Recycled plastics might have different properties than newly manufactured ones though, including differences in crystallinity, stiffness, ductility, or melt viscosity, that must be taken into account for potential applications.[21-22] These changes are caused by structural modifications in the polymer chains during the mechanical or chemical recycling processes.[22] The recycling of glass as part of a circular economy is mostly executed in Europe.[23] In many countries, there is a refundable deposit on glass bottles. The bottles are returned to the filler, cleaned, and refilled.[24] On the other hand, waste glass is collected

and sorted by color, then melted and reused for new glass bottles or the production of glass wool or foam glass.[23] In principle, glass can be recycled an unlimited number of times without loss of quality.[25] Additionally, a novel recycling approach, the so-called glass up-casting, delivers thick-walled products and can tolerate a higher rate of contamination.[26] Likewise, end-of-life electronics and batteries can be recycled to obtain many different metals.[2, 27] The applied methodologies for precious metals comprise selective dissolution, organometallic coordination, or reductive precipitation, *inter alia*.[27] Aluminum can be recycled from scrap by melting the metal, which would save 95% of the energy that is required for isolating aluminum from its ores.[28] Furthermore, lithium can be regained from lithium-ion batteries as lithium carbonate by electrochemical extraction, hydrometallurgy, or pyrolysis.[2] However, since less than 1% of the most important metals are currently recycled, partly caused by the huge market demand, there is a lot of room to improve the recycling of metals.[2, 29-30]

The concept of the circular economy is also applicable to counter the rising CO_2 concentrations in the atmosphere.[31] According to the scheme from the European Parliament Research Service, different steps are to be considered (Figure 2). Nowadays, approx. 95% of all manufactured carbon-based products, including materials, commodity chemicals, or pharmaceuticals, are made of petrochemicals stemming from fossil fuels.[32] At the end of their life, these products are usually landfilled or incinerated together with biomass and municipal solid waste, among others.[33] Both processes release CO_2, which is considered to be the final product of the chemical and biological combustion.[34] To close the carbon cycle, it is imperative to utilize CO_2 as carbon source to synthesize new materials, fuels, or pharmaceuticals.[35] By this means, the so far used petrochemicals from fossil fuels can be replaced, whilst reducing the emission of CO_2 into the atmosphere.[34] At the same time, the environment is polluted by carbon-based materials like plastics in the sea or pharmaceuticals in wastewater.[14, 36] Thus, there is also a need to degrade these compounds and re-feed them into the carbon cycle. This can be accomplished by (partly) transforming the pollutants into CO_2 which can be reduced and reused as a sustainable C_1 building block.

In this thesis, carbon dioxide was studied regarding its application as a C_1 component in synthetic processes. Different approaches to establish an anthropogenic chemical carbon cycle were examined.

2 Objectives

This thesis comprised approaches to explore CO_2 as C_1 building block in synthetic processes. The work included efforts about CO_2 release from pharmaceutically relevant and natural carboxylic acids, carbon capture utilizing (poly)amines and CO_2 conversion by transition metal catalysis (Figure 3). The overarching goal was the utilization of carbon dioxide in terms of a circular economy.

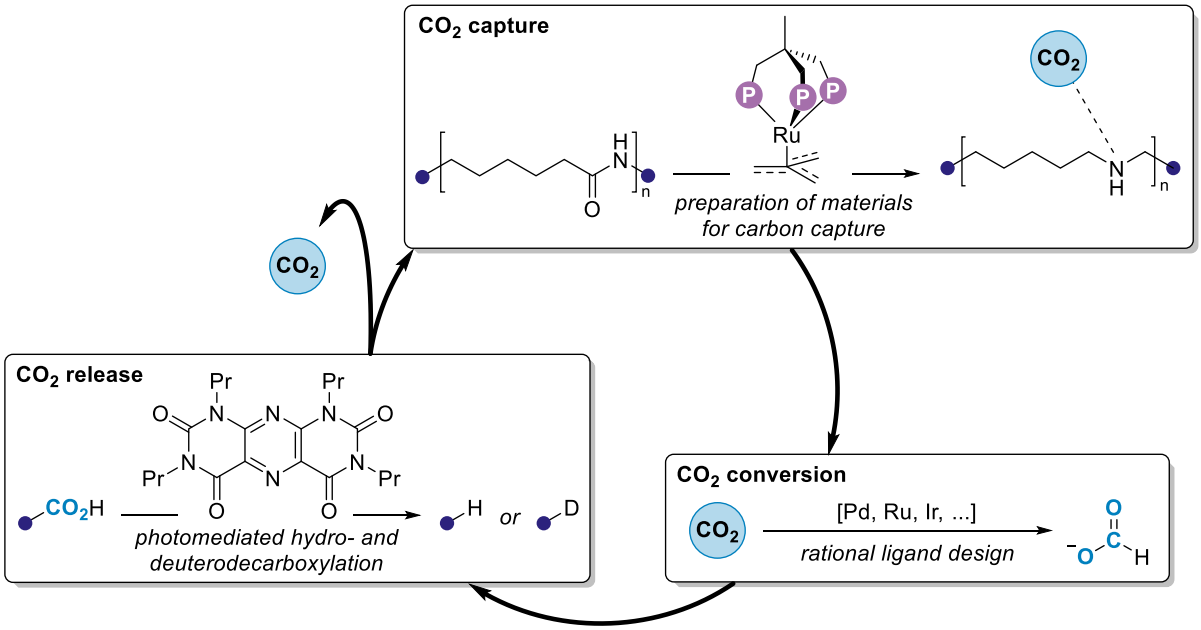

Figure 3. Steps towards a circular economy for the use of CO_2 that are presented in this dissertation.

For CO_2 release, the photomediated pyrimidopteridine-catalyzed hydro- and deutero-decarboxylation of primary, secondary, and tertiary carboxylic acids was envisioned, aiming for the thorough investigation including the utilization of different diagnostic tools to present a rational reaction mechanism. The approaches to CO_2 capture were conceptualized to apply commodity materials like nylon-6 for carbon dioxide removal from air. Aligning with the 'waste to value' concept, this approach ought to fulfil the goal of waste polymer to carbon capture through chemical modification. CO_2 conversion is the ultimate challenge to close the anthropogenic carbon cycle. For reusing carbon dioxide as a highly available carbon source, new concepts are required. By using rational ligand design and avoiding the implementation of phosphorus, which is available in limited quantities, the conversion of CO_2 in low concentrations was targeted.

3 CO_2 Release by Photomediated Hydro- and Deutero-decarboxylation

Pharmaceutically relevant carboxylic acids were efficiently hydro- and deuterodecarboxylated applying a pyrimidopteridine photoredox catalyst. This work has been published as part of the present dissertation.[37]

3.1 Introduction

The release of CO_2 from organic molecules has been known for a long time, since the first fossil fuel had been incinerated for energy supply (Scheme 1).[38] Such combustion needs much energy and the addition of external oxygen. Nevertheless, combustion in general is not selective, as SO_x and NO_x will be formed as acidic by-products if heteroatoms are present in the pyrolyzed compounds or if N_2 from air is oxidized.[39] Oxy-combustion is an elegant tool to avoid especially NO_x formation from N_2. Prior to the incineration, the air is separated into its main components, N_2 and O_2. The fuel is then combusted in pure oxygen, producing up to 100% CO_2.[40] Furthermore, CO_2 can be released by the electrochemical oxidation of glucose and glucose derivatives, such as sorbitol, glucaric acid, or oxalic acid, in fuel cells.[41] This reaction takes place in a cascade manner on its way to the full oxidation of all carbon atoms to CO_2. Again, oxygen is needed as the oxidant.

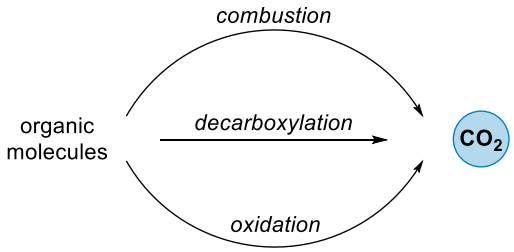

Scheme 1. Partly or full degradation of organic molecules to CO_2.

By combustion and oxidation, the complete molecular scaffold is destroyed. In contrast, organic molecules like carboxylic acids can be degraded in a controlled way by decarboxylation. The products of this reaction are CO_2 and a hydrodecarboxylated product that can be further utilized. Traditional approaches to selectively release carbon dioxide from carboxylic acids require high temperatures, strong oxidizing agents, or the application of transition metal catalysts (Scheme 2a-c).[42-44] The mild decarboxylation of carboxylic acids can alternatively be achieved by photoredox catalysis (Scheme 2d).[45]

a) Kharaka *et al.*, **1983**: thermal

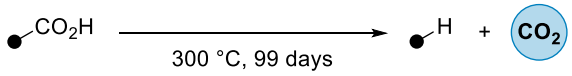

b) Baran *et al.*, **2017**: transition metal-catalyzed

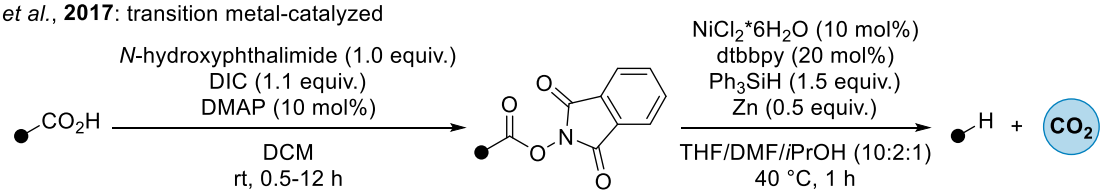

c) McLean *et al.*, **2022**: strong oxidants

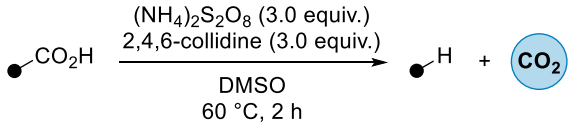

d) Sun *et al.*, **2022**: photomediated

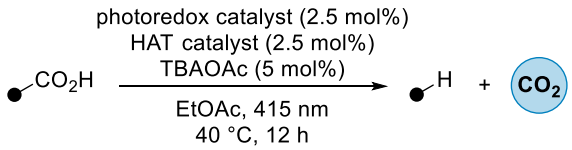

Scheme 2. Examples for the (a) thermal, (b) transition metal-catalyzed, (c) oxidizing, and (d) photomediated decarboxylation.[42-45]

In 1983, Kharaka *et al*. reported the thermal decarboxylation of acetic acid to CO_2 and methane.[42] Reasonable conversions of at least 50% were observed after 99 days at 300 °C. This example showed that traditional thermal protocols require much energy. If applied for more complex molecules, such harsh conditions can lead to undesired cracking or coke formation. Transition metal-catalyzed procedures, applying reductive conditions, have been published by the Baran group, among many others.[43, 46] First, the acid was activated by reaction with *N*-hydroxyphthalimide and *N,N'*-di-*iso*-propylcarbodiimide (DIC). The redox-active ester was then decarboxylated using nickel catalysis, zinc as the reducing agent, and triphenyl silane as the hydrogen atom donor.[43] This activation of the carboxylic acid *via* a redox-active ester was necessary to avoid the competing reduction to aldehydes or alcohols, which is also known to proceed using the combination of a Ni-catalyst, zinc, and silanes.[47] Alternatively, the decarboxylation of carboxylic acids can be realized under oxidative conditions. The metal- and light-free approach of McLean *et al*. applied ammonium persulfate, a strong oxidant, in excess.[44] Although the protocol was operationally simple, the researchers observed a limited functional group tolerance and competitive homocoupling. Recently, Sun and co-workers reported a mild photomediated decarboxylation of aliphatic carboxylic acids.[45] Again, the direct oxidation of carboxylic acids required strongly oxidizing conditions including a photoredox catalyst with a high excited state reduction potential. Hence, the researchers applied an acridinium photoredox catalyst. They further added di-*p*-tolyl disulfide as an additional hydrogen atom-transfer (HAT) co-catalyst. A similar combination of potent acridinium photoredox catalysts with H-atom donors has also been reported by Nicewicz and co-workers and by the Sumerlin group, *inter alia*.[48-49]

Pyrimidopteridines (PPT) have already been known since 1951.[50] From then, it took more than 30 years until the first application of substituted pyrimidopteridines under photochemical conditions has been reported.[51] During their investigations, the group of Maki used the corresponding *N*-oxides (PPTNO) as stoichiometric reagents to transfer the oxygen atom onto a substrate (oxygen atom-transfer, OAT) or mediate dehydrogenative cyclizations.[52-55] Also, first stoichiometric oxidative decarboxylation reactions have been known, leading to CO_2 and an aldehyde as the products.[56-57]

In 2019, Pospech and co-workers characterized differently substituted PPTNOs.[58] Photophysical and electrochemical studies revealed that these photoactive heterocycles and their deoxygenated counterparts, the PPTs, were potent excited state oxidants (E^*_{red} = +2.10 V vs SCE in MeCN for PrPPT),[59] and on a par with the well-known acridinium photoredox catalysts (E^*_{red} ≤ +2.08 V vs SCE in MeCN).[60] Among other applications,[61-62] these PPTs were used as photoredox catalysts for the photomediated decarboxylative Giese-type reaction (Scheme 3).[63]

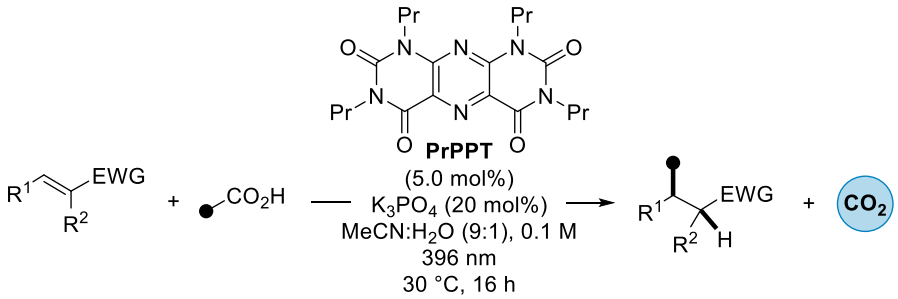

Scheme 3. Photomediated PrPPT-catalyzed C–C bond formation.[63]

Our group discovered that aliphatic carboxylic acids could efficiently be decarboxylated and subsequently coupled with electron-deficient alkenes to synthesize complex compounds in 17-92% yield. According to the proposed mechanism, the deprotonated carboxylate was oxidized in an initial single-electron transfer (SET) with the PrPPT* in the excited state, delivering the $PrPPT^{\bullet-}$ radical anion. After successful decarboxylation, the alkyl radical added to the electron-deficient olefine, which was then reduced by the $PPT^{\bullet-}$ radical anion to the corresponding carbanion and PrPPT in a second SET. Final protonation delivered the C–C-coupled product.

However, this second SET does only work for electron-deficient molecules. The reduction potentials of unstabilized aliphatic alkyl radicals is low ($E^{ox}_{1/2}$ ≤ –1.6 V vs SCE in MeCN) and prevents the catalytic turnover of most photoredox catalysts.[64] Therefore, HAT co-catalysts are usually added in the literature, as drawn from the work of Sun, Nicewicz, or Sumerlin.[45, 48-49] These help to close the catalytic cycle independently of any reduction potential. In earlier investigations of the PPT photoredox catalyst, our group found out about the dual role as photoredox and HAT catalyst by detecting a $PPTH^{\bullet}$ radical species *via* EPR spectroscopy.[61] According to the proposed reaction mechanism, the radical species was formed by protonation of the $PrPPT^{\bullet-}$ radical anion and underwent HAT with the substrate

intermediate to yield the product and the photoredox catalyst. This might enable the application for the hydrodecarboxylation of aliphatic carboxylic acids without addition of external HAT co-catalysts.

Indeed, in the course of investigating the photomediated decarboxylative Giese-type reaction, Pospech *et al.* observed a non-coupled hydrodecarboxylated by-product, meaning that carboxylic acids were transformed into the corresponding C_{n-1} alkanes by extruding CO_2.[63] This is especially interesting for degradation of pharmaceutically relevant carboxylic acids and decreasing their solubility in wastewater. One prominent example, among many others[36], is ibuprofen (**1**). Being the world's third most consumed drug and a popular representative of the non-steroidal anti-inflammatory drug (NSAID) family, it is often prescribed in high doses of up to 1200 mg per day.[65] While most of the drug is metabolized in the body, around 15% is excreted unchanged and remains highly active when it enters water and food cycles.[66] So far, biodegradation, together with sorption processes, is the main pathway to remove ibuprofen (**1**) from wastewater[66], proceeding mainly *via* enzymatic hydroxylation, acylation, glucuronidation, and demethylation.[67-69] Since bioremediation can be inhibited if pollutants exceed microbially toxic concentrations, the photomediated hydrodecarboxylation of pharmaceuticals can be a promising alternative.

3.2 Results and Discussion

Based on the findings of our group, the photomediated decarboxylation of aliphatic carboxylic acids like ibuprofen (**1**) was examined during the work on this thesis. The investigation revealed that tetra-*N*-propylpyrimidopteridine (PrPPT) could be applied for the photomediated hydro- and deuterodecarboxylation of primary, secondary, and tertiary carboxylic acids.[37]

3.2.1 Optimization using a Design of Experiment Approach

Ibuprofen (**1**) was used as model substrate for all optimization reactions. A thorough screening of different solvents, bases, and photoredox catalysts was conducted by Sina Brandt, M.Sc., during an internship in our laboratory. Next to MeCN, also the aprotic solvents 1,4-dioxane, acetone, DMSO, DMF, and toluene and MeOH as a candidate for protic solvents were tested (Table 1). Except for toluene, all tested solvents were chosen due to their miscibility with water, which was found to be crucial in the original procedure by Pospech and co-workers.[63]

Table 1. Solvent screening for the photomediated decarboxylation.

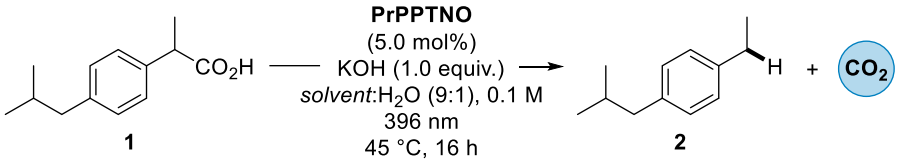

entry	solvent	yield[a]
1	MeCN	32%
2	1,4-dioxane	16%
3	acetone	13%
4	DMSO	10%
5	DMF	8%
6	toluene	13%
7	MeOH	12%

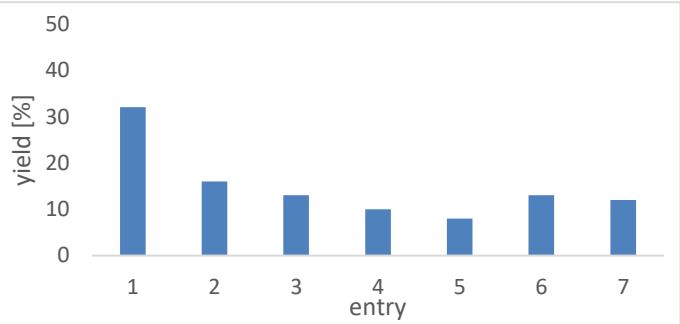

[a] Yields were determined by calibrated GC using biphenyl as internal standard.

The decarboxylated product 1-ethyl-4-isobutylbenzene (**2**) was detected in 32% yield using aqueous MeCN. Neither of the alternative solvents outcompeted the performance of MeCN, delivering the desired product **2** in diminished yields of 8-16%. Next, different bases were screened as an alternative to KOH (Table 2). The screening comprised various inorganic bases like hydroxides, carbonates, bicarbonates, phosphates, and monohydrogen phosphates. As a candidate for the organic bases, urotropin was chosen.

Table 2. Base screening for the photomediated decarboxylation.

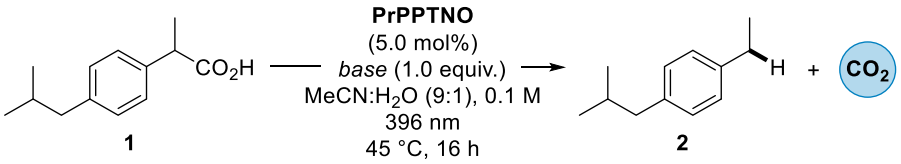

entry	base	yield[a]
1	KOH	32%
2	NaOH	20%
3	Na_2CO_3	36%
4	K_2CO_3	37%
5	Cs_2CO_3	29%
6	$NaHCO_3$	29%
7	K_3PO_4	39%
8	K_2HPO_4	20%
9	urotropin	13%

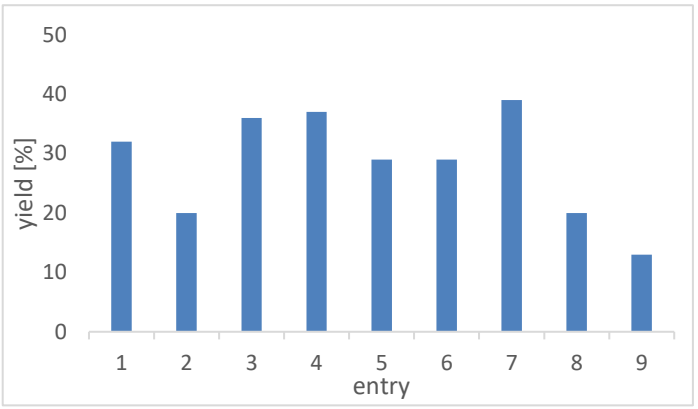

[a] Yields were determined by calibrated GC using biphenyl as internal standard.

From the results of the base screening, it was obvious that the reaction worked best applying either carbonate or phosphate bases, affording the desired product **2** in 36-39% yield, respectively. Thus, the screenings were continued using K_3PO_4 as the base. Afterwards, differently substituted PPTNO and PPT photoredox catalysts were screened (Table 3).

Table 3. Catalyst screening for the photomediated decarboxylation.

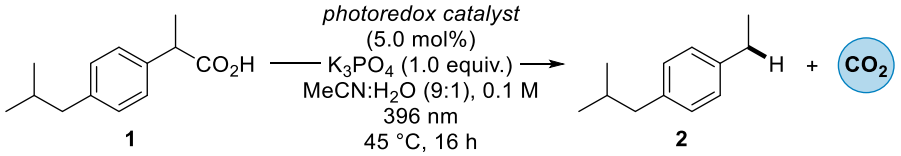

entry	photoredox catalyst	yield[a]
1	PrPPTNO	39%
2	PrPPT	42%
3	MePPTNO	24%
4	BuPPTNO	34%
5	BuPPT	38%
6	PhPPTNO	10%

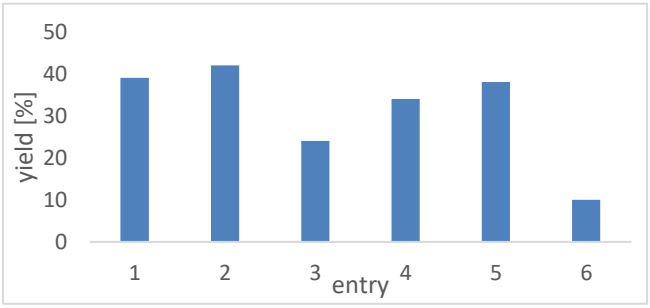

[a] Yields were determined by calibrated GC using biphenyl as internal standard.

The catalyst screening revealed that PrPPTNO could be easily replaced by its deoxygenated analogue, PrPPT, yielding the product in an even higher yield of 42% (entry 2). When applying MePPTNO or PhPPTNO, 1-ethyl-4-isobutylbenzene (**2**) was formed in a lower yield of 24% and 10%, respectively (entries 3 and 6). BuPPTNO appeared to be a suitable alternative for the propyl-substituted photoredox catalyst, affording the product in 34% (entry 4). Again, the deoxygenated analogue, BuPPT, gave an increased yield of 38% (entry 5).

All in all, these initial screenings gave the product 1-ethyl-4-isobutylbenzene (**2**) in up to 42% yield. Attempts to reproduce this yield revealed the crucial importance of the reaction set-up. While an open set-up, consisting of two LED panels (396 nm, 30 W each) on opposite sites and a magnetic stirrer in between, led to yields around 16%, higher yields were obtained using a closed set-up that was placed inside of a metallic box, being shielded from any cooling air flow. The energy of the LED panels led to increased reaction temperatures of up to 50 °C, which caused the difference in yield. To maintain a constant temperature for all reactions, an oil bath was added and heated to 50 °C (Figure 4), leading to reproducible results in both set-ups.

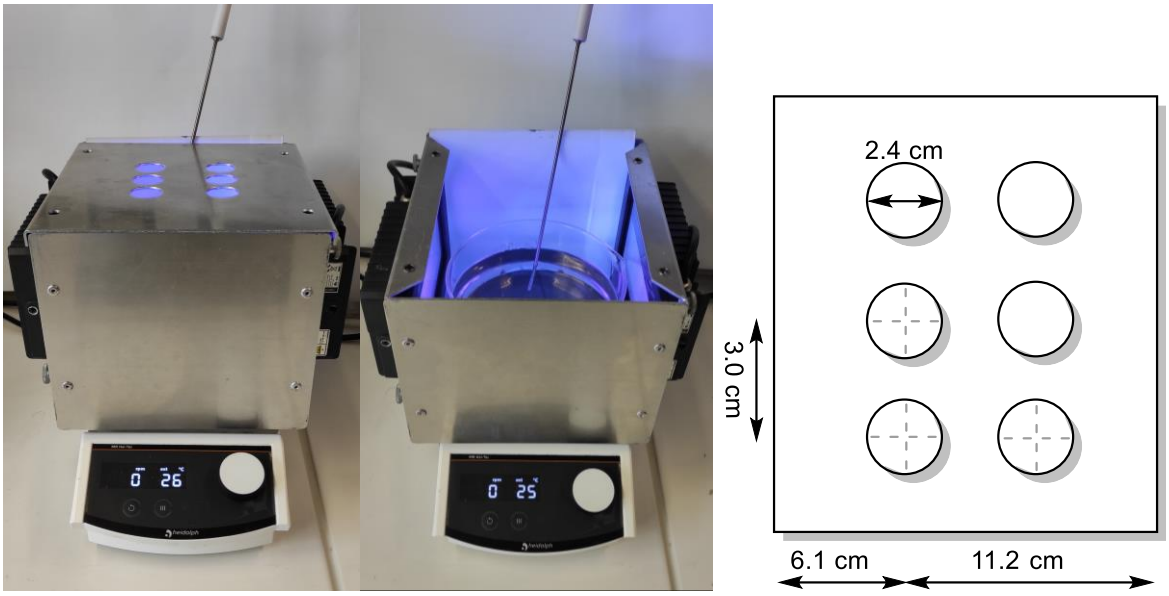

Figure 4. Optimized reaction set-up.

With the pre-optimized conditions in hand, the Design of Experiment (DoE) concept was used to finetune the reaction conditions.[70] By experimental design, the reaction outcome (response) can be calculated over a pre-defined reaction space, providing a global knowledge of the whole experimental domain. The interactions among the chosen variables are considered by using mathematical models. For the photomediated hydrodecarboxylation, a face-centered factorial design with three variables was chosen, being (i) amount of base, (ii) water content, and (iii) reaction time. The resulting 13 experiments were conducted in random order in collaboration with Dr. Tobias Täufer, who calculated the response surfaces by using a quadratic model (R^2 = 0.9511, Figure 5). Six additional experiments were performed to improve the quality of the model. The applied equation (Equation 1) included a constant b_0, three linear terms (b_1, b_2, b_3), three two-term interactions (b_{12}, b_{13}, b_{23}), and three quadratic terms (b_{11}, b_{22}, b_{33}).

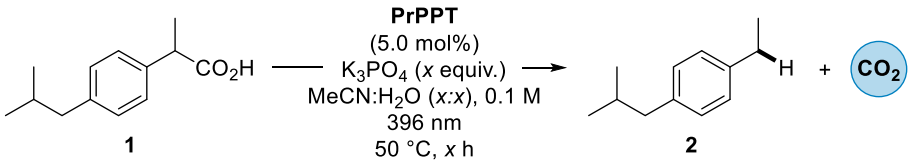

Equation 1. Quadratic model used to plot the response surface.

$$y = b_0 + b_1x_1 + b_2x_2 + b_3x_3 + b_{12}x_1x_2 + b_{13}x_1x_3 + b_{23}x_2x_3 + b_{11}x_1^2 + b_{22}x_2^2 + b_{33}x_3^2$$

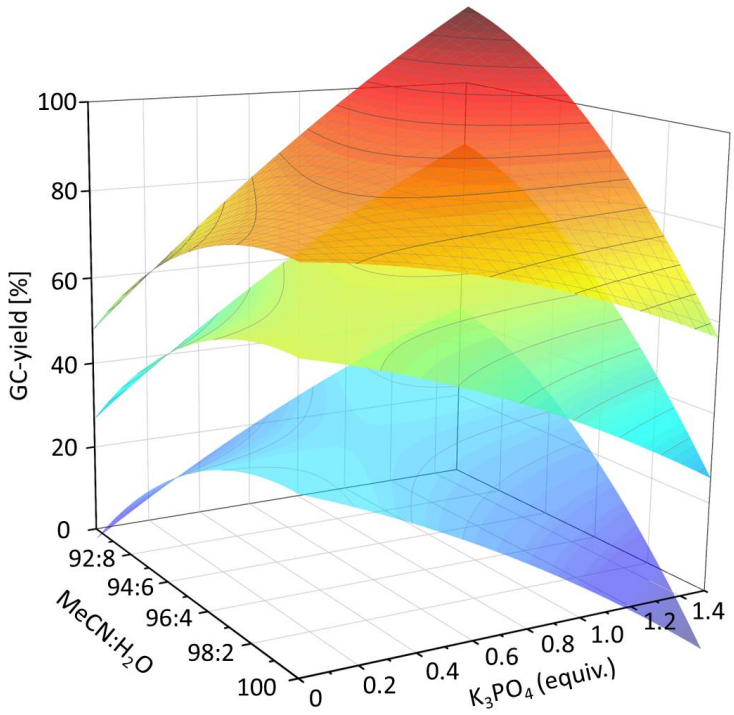

Figure 5. 3D surface plots. From bottom to top: 8, 16, and 24 h reaction time. Yields were determined by calibrated GC.

The 3D surface plots show that the yields are generally increased by prolonging the reaction time. Furthermore, the curved form of the plots underlined the relation between the amount of water and the amount of base that is caused by the insolubility of K_3PO_4 in pure MeCN.[71] Accordingly, more base could be dissolved in the reaction medium and take part in the reaction if more water had been added. This relation was also reflected by yields as depicted in the 3D surface plots. When the amount of base was increased without water present, the yield decreased. Also, when no base was present and the amount of water was increased, the yield became lower. In contrast, when both amounts were increased, also the yield was increased, since the base could be completely dissolved.

The outcome of the DoE led to fully optimized reactions conditions consisting of 1.33 equiv. of base, a 94:6 ratio of MeCN/H_2O and 24 h reaction time. All in all, the isolated yield of the decarboxylation of the model substrate ibuprofen (**1**) was increased from 42% to 90%. Finally, the optimization of the photomediated decarboxylation was concluded by control reactions (Table 4).

Table 4. Control reactions.

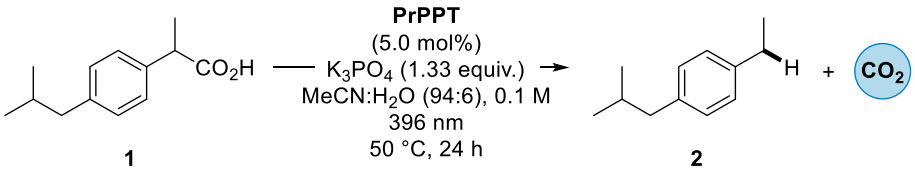

1 **2**

entry	deviation from optimized reaction conditions	yield[a]
1	none	90%
2	no photocatalyst	n.d.
3	in the dark	n.d.
4	no base	35%

No conversion was observed in the control reactions without photocatalyst or light (entries 2 and 3). Therefore, a thermic reaction was excluded. Running the reaction in absence of base gave the product in 35% yield (entry 4). This can be explained by the high oxidation potentials of carboxylic acids if compared to the corresponding carboxylates, as discussed later (Chapter 3.2.3).

3.2.2 Scope of the Reaction

With the optimized reaction conditions in hand, the scope of the photomediated hydrodecarboxylation of carboxylic acids was explored. Beyond ibuprofen (**1**), various other secondary benzylic carboxylic acids and one amino acid were converted into the corresponding alkanes with moderate to excellent yields (Table 5).

Table 5. Scope of secondary carboxylic acids for the pyrimidopteridine-catalyzed photomediated hydrodecarboxylation.

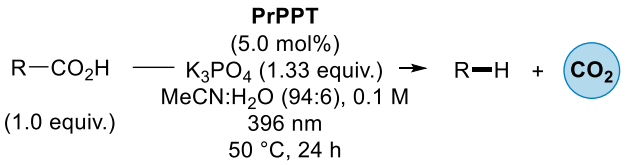

entry	secondary carboxylic acid	product	yield[a]
1	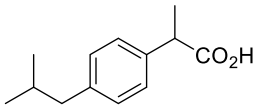 ibuprofen (**1**)	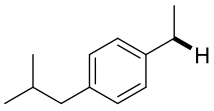 **2**	90%
2	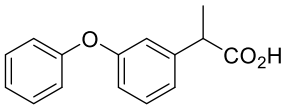 fenoprofen (**3**)	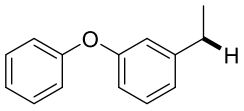 **4**	93%
3	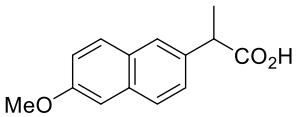 naproxen (**5**)	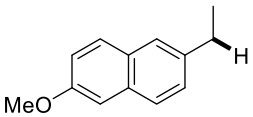 **6**	quant.
4	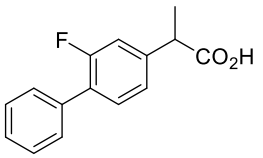 flurbiprofen (**7**)	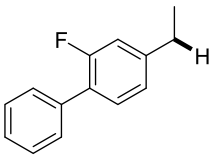 **8**	95%
5	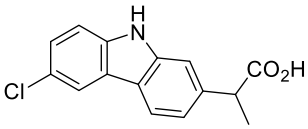 carprofen (**9**)	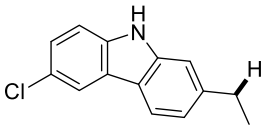 **10**	58%
6	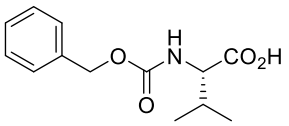 Cbz-Val-OH (**11**)	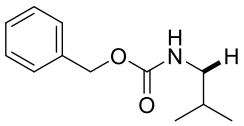 **12**	59%
7	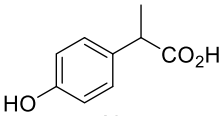 **13**	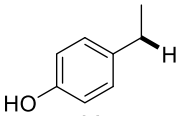 **14**	79%
8	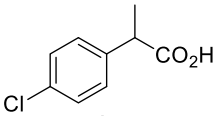 **15**	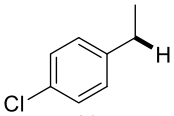 **16**	77%

[a] Reactions were performed on a 0.5 mmol scale. Isolated yields are shown, calculated as the average of two experiments.

The present structural motif is widely distributed among NSAIDs. Decarboxylating fenoprofen (**3**) and naproxen (**5**) with electron-rich ether groups gave the corresponding products **4** and **6** in 93% and quantitative yield, respectively (entries 2 and 3). The halide substituents in flurbiprofen (**7**) and 2-(4-chlorophenyl)propanoic acid (**15**) were well tolerated in this reaction and gave the products **8** and **16**

in 95% and 77% yield, respectively (entries 4 and 8). The hydrodecarboxylation of carprofen (**9**), which carries a 6-chlorocarbazole moiety, afforded the product **10** in a moderate yield of 58%, possibly due to the nitrogen atom of the carbazole unit (entry 5). Despite reduced nucleophilicity of the carbazole motif[72], partial action as a radical scavenger is conceivable as a side reaction.[73] The lower yield of 59% from the decarboxylation of Cbz-protected L-valine (**11**) can be interpreted similarly (entry 6). In contrast, 2-(4-hydroxyphenyl)propanoic acid (**13**) was efficiently decarboxylated, although phenols are prominent radical scavengers (entry 7).[74] The product 4-ethylphenol (**14**) was obtained in a very good yield of 79%.

The decarboxylation of naproxen (**5**) was also accomplished in quantitative yield on a gram scale (Scheme 4). In the same experiment, also the photoredox catalyst was re-isolated after the reaction in an excellent yield of 90%. However, the reaction time had to be extended to 72 h, as a larger number of photons are required to convert a larger amount of starting material.[75]

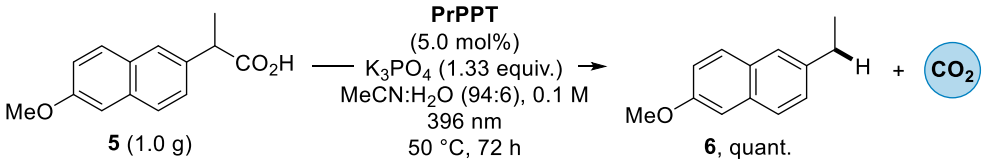

Scheme 4. Scale-up of the photomediated decarboxylation of naproxen (**5**).

In contrast to the secondary carboxylic acids, primary carboxylic acids were only poorly converted into the corresponding alkanes (Table 6).

Table 6. Scope of primary carboxylic acids for the pyrimidopteridine-catalyzed photomediated hydrodecarboxylation.

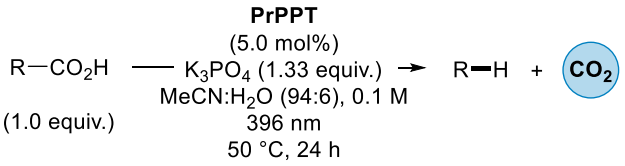

entry	primary carboxylic acid	product	yield[a]
1	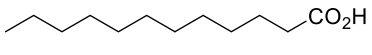 **17**	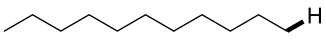 **18**	20%[b]
2	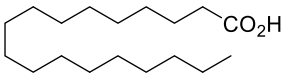 stearic acid (**19**)	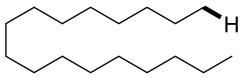 **20**	20%
3	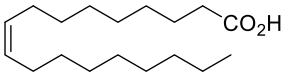 oleic acid (**21**)	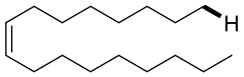 **22**	15%
4	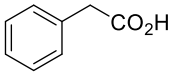 **23**	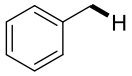 **24**	17%[b]
5	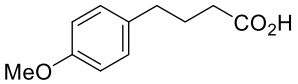 **25**	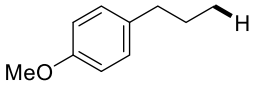 **26**	17%
6	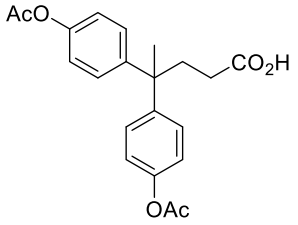 **27**	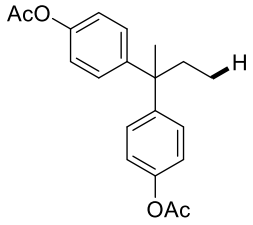 **28**	15%
7	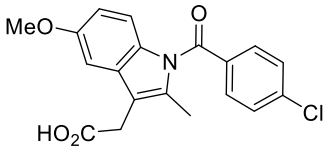 indometacin (**29**)	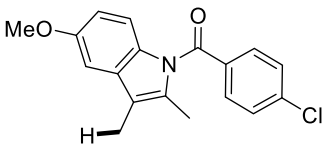 **30**	34%

[a] Reactions were performed on a 0.5 mmol scale. Isolated yields are shown, calculated as the average of two experiments. [b] GC yield using biphenyl as internal standard.

Different long-chained alkanes and alkenes (**18**, **20**, **22**) and alkyl benzene derivatives (**24**, **26**, **28**) were synthesized with low yields between 15% and 20% (entries 1-6). A possible explanation is the instability of primary alkyl radical intermediates.[76] An alternative explanation, focusing on hindered proton transfers, was ruled out by adding 20 mol% benzoic acid, or decreasing the amount of base to 0.33 equiv., respectively. None of these adjustments impacted the yields. Nevertheless, this method can be seen as an alternative way of converting fatty acids into long-chain hydrocarbons as a substitute for fossil fuels.[77-78] Intriguingly, NSAID derivative indomethacin (**29**), bearing an indole moiety, gave the hydrodecarboxylated product **30** in a higher yield of 34% (entry 7). This can be rationalized by resonance effects of the radical intermediate **31** (Scheme 5).

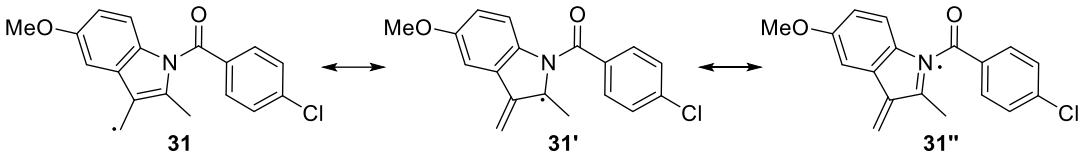

Scheme 5. Stabilization of a primary alkyl radical by resonance effects.

Tertiary carboxylic acids are sterically very demanding. The hydrodecarboxylation of different examples has been accomplished in varying yields between 23% and 67% (Table 7).

Table 7. Scope of tertiary carboxylic acids for the pyrimidopteridine-catalyzed photomediated hydrodecarboxylation.

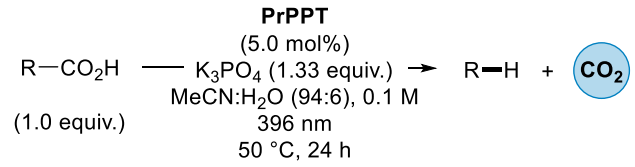

entry	tertiary carboxylic acid	product	yield[a]
1	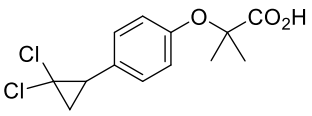 ciprofibrate (**32**)	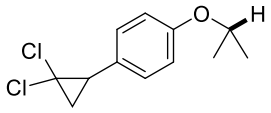 **33**	39%
2	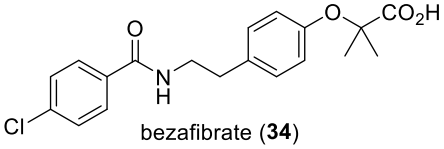 bezafibrate (**34**)	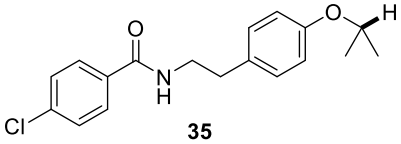 **35**	33%
3	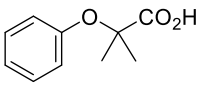 **36**	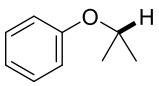 **37**	35%[b]
4	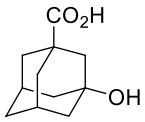 **38**	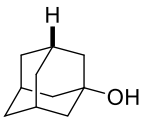 **39**	67%
5	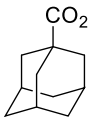 **40**	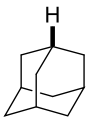 **41**	23%[c]
6	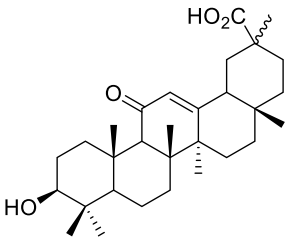 enoxolone (**42**)	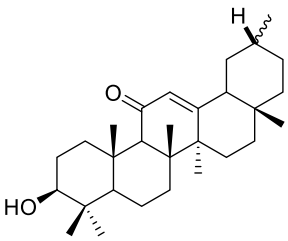 **43**	66%[d]

[a] Reactions were performed on a 0.5 mmol scale. Isolated yields are shown, calculated as the average of two experiments. [b] NMR yield using 1,3,5-trimethoxybenzene as internal standard. [c] GC yield using biphenyl as internal standard. [d] 10 v/v% EtOAc was added to enhance the solubility of the substrate.

Fibrates, such as ciprofibrate (**32**) and bezafibrate (**34**), are known as lipid-lowering agents.[79-80] Together with the related 2-methyl-2-phenoxypropanoic acid (**36**) they were decarboxylated to products **33**, **35**, and **37** in 33% to 39% yield (entries 1-3). Surprisingly, adamantane carboxylic acid (**40**) gave product **41** in only 23% yield, whereas 3-hydroxyadamantane carboxylic acid (**38**) was successfully converted to **39** in 67% yield (entries 4 and 5). A support of the HAT by product **39** was ruled out by adding hydroxyadamantane (**39**) to the decarboxylation reaction of adamantane carboxylic acid (**40**). For both substrates, a (hydroxy)adamantyl methyl ketone was identified as side product by GC-MS in approximately 10% and 20% yield, respectively. Mechanistically, this can be explained by attack of an alkyl radical on the solvent, MeCN, and subsequent hydrolysis. The highly functionalized bioactive compound enoxolone (**42**), usually found in licorice[81], is poorly soluble in the reaction medium. The addition of EtOAc increased the solubility and the corresponding decarboxylated product **43** was isolated in 66% yield (entry 6). The product was isolated as a mixture of diastereomers. Crystals suitable for X-ray crystallography were obtained by recrystallization from hot DMSO (Figure 6).

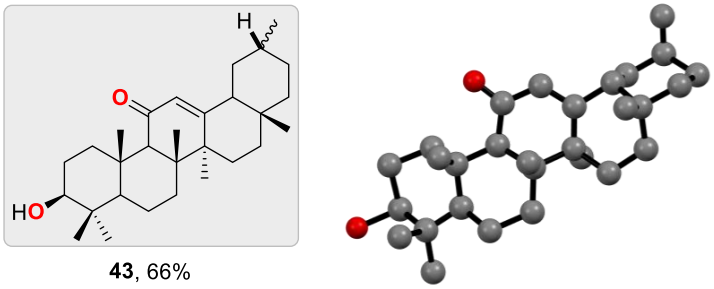

43, 66%

Figure 6. X-ray structure of steroid **43**. Color code: grey (C), red (O). Hydrogen atoms were omitted for clarity. Due to the poor quality of the crystals, the structure could only be solved but not refined.

Due to the poor quality of the crystals, the structure could only be solved but not refined. However, the data set was sufficient to confirm the structural identity of compound **43**.

The hydrodecarboxylation method using PrPPT as a robust photoredox catalyst was further developed into a protocol for deuterodecarboxylation. Isotope labeling of organic compounds is an important tool in synthetic and medicinal chemistry. It facilitates the identification and understanding of (bio)chemical transformations.[82] In this way, the pharmacodynamic properties and preclinical toxicity of drugs can be investigated directly in living organisms.[83] The radioactive hydrogen isotope tritium in particular is considered a valuable marker in drug research.[82] If a minimum amount of 50% of a product is labeled with tritium, the compound can already be applied in tritium-labeling studies.[84-85] Since the use of tritium sources is comparatively expensive, deuteration is often used as a model reaction. However, the selective introduction of one deuterium atom at a specific site in an organic molecule is challenging. Decarboxylative deuteration in an aqueous reaction medium is an elegant methodology for selectively replacing a carboxyl group with a deuterium atom from D_2O, an

inexpensive source of deuterium.[86] Furthermore, the applied carboxylic acids are readily available and abundant starting materials.

By simply replacing water with deuterated water in our system, a high deuterium incorporation of up to 95% was achieved. A representative scope is depicted in below (Table 8).

Table 8. Scope of the pyrimidopteridine-catalyzed photomediated deuterodecarboxylation.

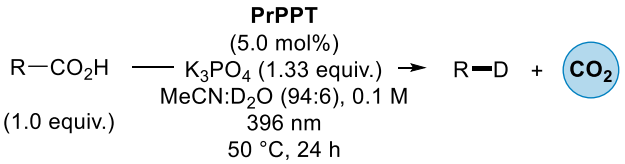

entry	carboxylic acid	product	yield[a] (*d*-content)
1	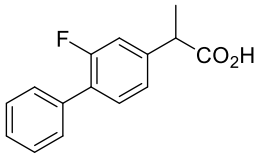 flurbiprofen (**7**)	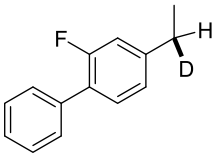 ***d*-8**	a) 98% (88%) b) 93% (53%)[b]
2	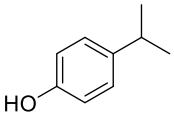 **13**	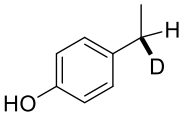 ***d*-14**	79% (80%)
3	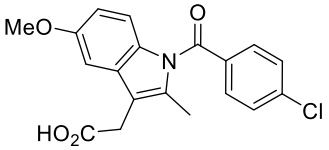 indometacin (**29**)	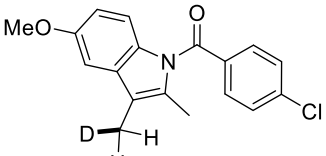 ***d*-30**	34% (91%)
4	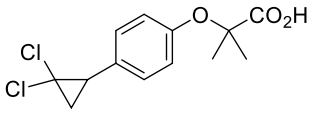 ciprofibrate (**32**)	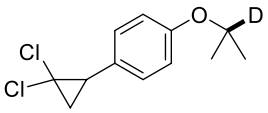 ***d*-33**	a) 35% (83%) b) 19% (58%)[b]
5	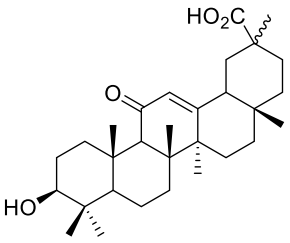 enoxolone (**42**)	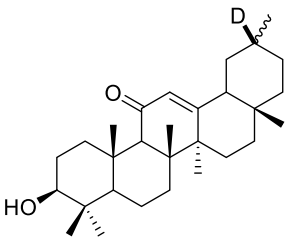 ***d*-43**	64%[c] (95%)[d]

[a] Reactions were performed on a 0.5 mmol scale. Isolated yields are shown, calculated as the average of two experiments. [b] D_2O (5.0 equiv.) was used. [c] 10 v/v% EtOAc was added to enhance the solubility of the substrate. [d] The deuterium content was calculated using GCMS.

The pyrimidopteridine-catalyzed photomediated deuterodecarboxylation was successfully applied on primary, secondary, and tertiary carboxylic acids. A high deuterium incorporation of 80-95% was found for all tested substrates (entries 1-5). No predeuteration of protic groups like carboxylic acid or phenol moieties was required even though protic groups are prone to undergo H/D-exchange with

D_2O. Under standard reaction conditions, the applied amount of D_2O was 33.3 equiv. It was shown that the deuterium content still exceeds the 50% threshold even in the presence of only 5.0 equiv. D_2O (entries 1b and 4b). These results indicate that the method shown is potentially applicable for important tritium-labeling studies.[84-85]

In contrast, literature studies showed that a photomediated deuterodecarboxylation reaction could also proceed *via* deuterium transfer from deuterated acetonitrile, CD_3CN, instead of deuterated water.[87] To confirm or deny this possibility for the present reaction, the decarboxylation of ciprofibrate (**32**) was conducted in a 94:6 mixture of CD_3CN/H_2O (Scheme 6).

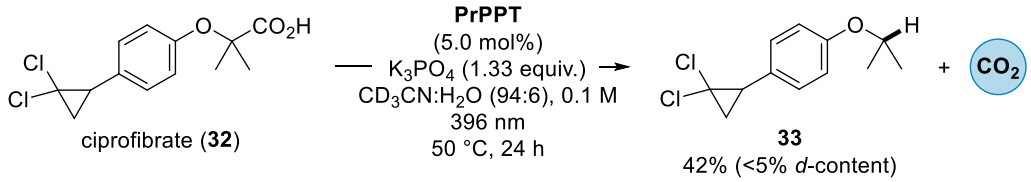

Scheme 6. Deuterium labeling using MeCN-d_3.

The reaction pathway *via* a cyanomethyl radical was ruled out though, as no deuterium content was detected in the formed product. Instead, the hydrodecarboxylated product **33** was isolated in 42% yield. However, while those 26 examples showed how versatile the discussed method is, there were also some molecules that did not react selectively to the corresponding decarboxylated product. Specifically, some functional groups were not tolerated at all (Table 9).

Table 9. Unsuccessful substrates sorted by the postulated reason for the failure.

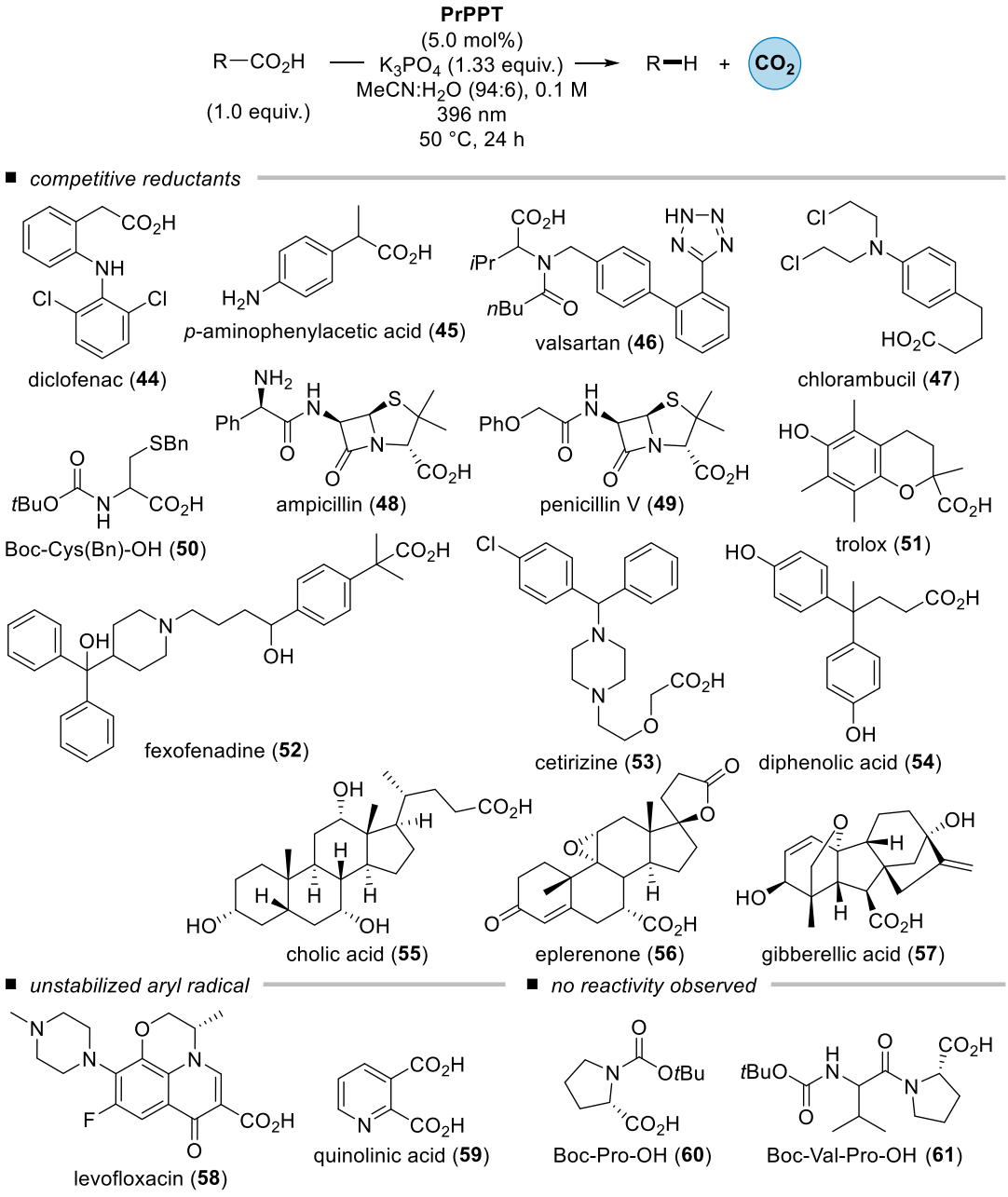

The functional groups, which were not tolerated, included especially unprotected amine groups that undergo competitive quenching of the excited state of the photoredox catalyst. Hence, NSAID candidate diclofenac (**44**), benzylic carboxylic acid *p*-aminophenylacetic acid (**45**), valsartan (**46**), which is used to treat high blood pressure, and anti-cancer agent chlorambucil (**47**) were not converted in the photomediated hydrodecarboxylation. The penicillin derivatives ampicillin (**48**) and penicillin V (**49**), bearing oxidizable thioethers, were unreactive as well. Double-protected L-cysteine (**50**), on the other hand, unselectively underwent multiple side reactions. Trolox (**51**) is a durohydroquinone derivative that is used as an antioxidant due to its property as a radical scavenger being easily oxidized to give a duroquinone derivative.[88] Therefore, it was not hydrodecarboxylated under these reaction conditions. Also, the antihistamines fexofenadine (**52**) and cetirizine (**53**), and diphenolic acid (**54**)

showed only little reactivity due to competitive reductants within the molecular structure. Same applied to cholesterol metabolite cholic acid (**55**), aldosterone antagonist eplerenone (**56**), and phytohormone gibberellic acid (**57**). Since the antibiotic levofloxacin (**58**) and quinolinic acid (**59**) contain sp^2-hybridized carboxylic acid groups that lead to a less stabilized aryl radical upon slow decarboxylation, no reaction was observed here either.[76, 87] Surprisingly, the amino acid Boc-L-proline (**60**) and the dipeptide Boc-Val-Pro-OH (**61**) were not converted in the photomediated decarboxylation as well.

A sensitivity assessment was conducted to gain more information about the robustness of the reaction. This is especially important for potential industrial applications.[89] Since a reaction can be differently robust for varying substrates, the assessment was conducted for both naproxen (**5**) and ibuprofen (**1**, Tables 10 and 11).

Table 10. Sensitivity assessment of naproxen (**5**).[a]

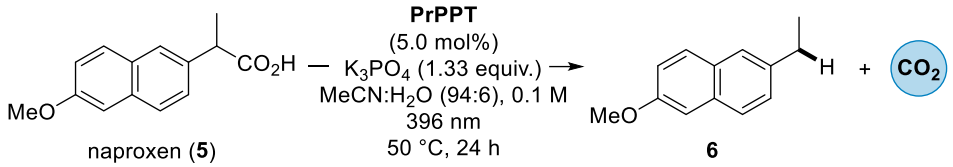

entry	deviation from optimized reaction conditions	yield[b]
1	none	quant.
2	sat. with Ar after adding degassed solvents	quant.
3	sat. with Ar after adding MeCN HPLC grade	quant.
4	sat. with Ar after adding deionized water	quant.
5	reaction under air, degassed solvents	27%
6	CO_2 atmosphere, degassed solvents	97%
7	Naproxen axicur® 250 mg	quant.
8	room temperature	81%

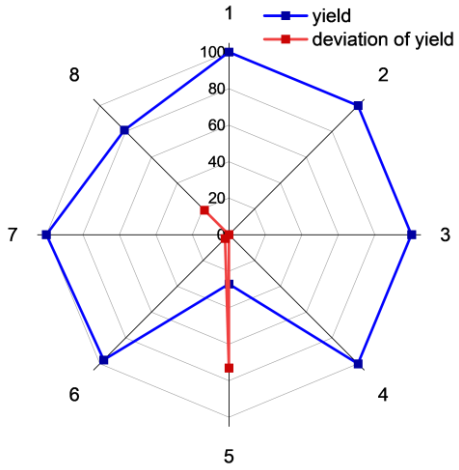

[a] Reactions were performed on a 0.5 mmol scale. Saturated with argon by bubbling the inert gas through the reaction mixture using a stainless-steel needle for 10 min. [b] Isolated yields are shown.

Under optimized conditions, naproxen (**5**) could be decarboxylated quantitatively. In a first experiment, the reaction vessel was filled with the solid reagents under air but was not evacuated three times and filled with argon before the degassed solvents were added. Instead, the resulting solution was saturated with argon for ten minutes. By using this procedure, product **6** was still isolated in quantitative yield (Table 10, entry 2). The yield also remained quantitative when using non-degassed solvents stored in air and then saturating this solution with argon before starting the irradiation (entries 3 and 4). Since the presence of atmospheric oxygen usually serves to quench the photoreaction, it was not surprising that the yield decreased drastically when the reaction itself was

carried out in air (entry 5). In contrast, under CO_2 atmosphere, which is a by-product of the decarboxylation reaction, the yield was only slightly affected (entry 6). Commercially available naproxen in tablet form also contains lactose monohydrate, cornstarch, iron(III) oxide, cellulose, crospovidone and magnesium stearate. Nevertheless, the active substance **5** could be decarboxylated quantitatively here (entry 7). Performing the reaction at room temperature led to a slightly decreased isolated yield of 81% (entry 8). Thus, in contrast to ibuprofen (**1**), setting the temperature to 50 °C appeared to be important but not crucial for the decarboxylation of naproxen (**5**). In summary, the photomediated decarboxylation of naproxen (**5**) emerged to be a very robust reaction.

However, the substrate ibuprofen (**1**) behaved differently (Table 11).

Table 11. Sensitivity assessment of ibuprofen (**1**).[a]

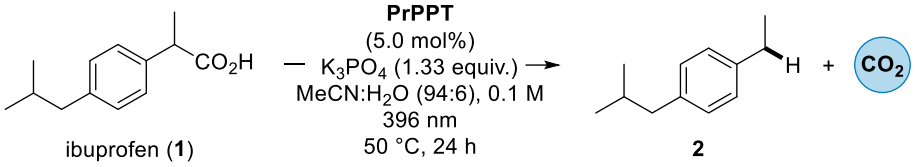

entry	deviation from optimized reaction conditions	yield[b]
1	none	90%
2	sat. with Ar after adding degassed solvents	48%
3	sat. with Ar after adding MeCN HPLC grade	66%
4	sat. with Ar after adding deionized water	58%
5	reaction under air, degassed solvents	10%
6	CO_2 atmosphere, degassed solvents	22%
7	IbuHEXAL® 200 mg	48%

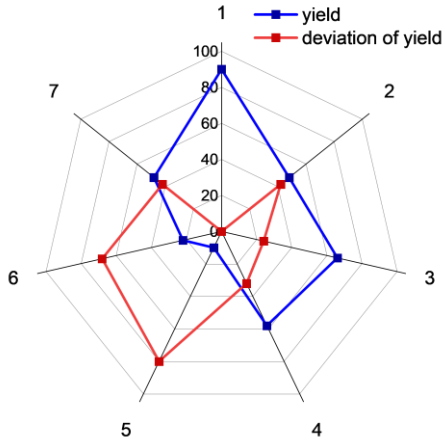

[a] Reactions were performed on a 0.5 mmol scale. Saturated with argon by bubbling the inert gas through the reaction mixture using a stainless-steel needle for 10 min. [b] GC yields using biphenyl as internal standard are shown.

Although generally similar trends were observed, the reaction studied was more sensitive to varying reaction conditions. Again, the first experiment included that the Schlenk tube was filled with the solid reagents under air but was not evacuated three times and purged with argon before the degassed solvents were added. The reaction mixture was then saturated with argon for ten minutes, which led to a slight reduction in yield (entry 2). Similarly, the reaction worked well when non-degassed solvents were used as long as the solution was saturated with argon prior to irradiation (entries 3 and 4). Similarly to naproxen, running the reaction under air caused a reduction in yield to 10% on the decarboxylation of ibuprofen (**1**, entry 5). The addition of a CO_2 atmosphere had a much greater impact, as the yield dropped to 22% (entry 6). Commercially available ibuprofen in tablet form, containing cellulose, sodium croscarmellose, hypromellose, polyethylene glycol, magnesium stearate,

silicium dioxide, talcum and titanium dioxide as additive, was decarboxylated with only a slightly decreased yield of 48% (entry 7).

In summary, the PrPPT-catalyzed photomediated hydro- and deuterodecarboxylation presented herein comprises a scope of 26 examples including primary, secondary, and tertiary carboxylic acids. A high deuterium incorporation of up to 95% was achieved under optimized conditions. More than 50% deuterium incorporation was reached in the presence of 5.0 equiv. D_2O, rendering the method viable for tritium labeling. Moreover, the reaction was successfully applied on a gram scale and with commercially available NSAIDs in tablet form.

3.2.3 Mechanistic Investigations

Different experiments were conducted aiming to elucidate the reaction mechanism. First, an on/off experiment was performed (Figure 7). After 4 h irradiation time, a sample was taken and analyzed by GC, and the light was turned off for 2 additional hours, followed by taking another sample. This procedure was repeated several times.

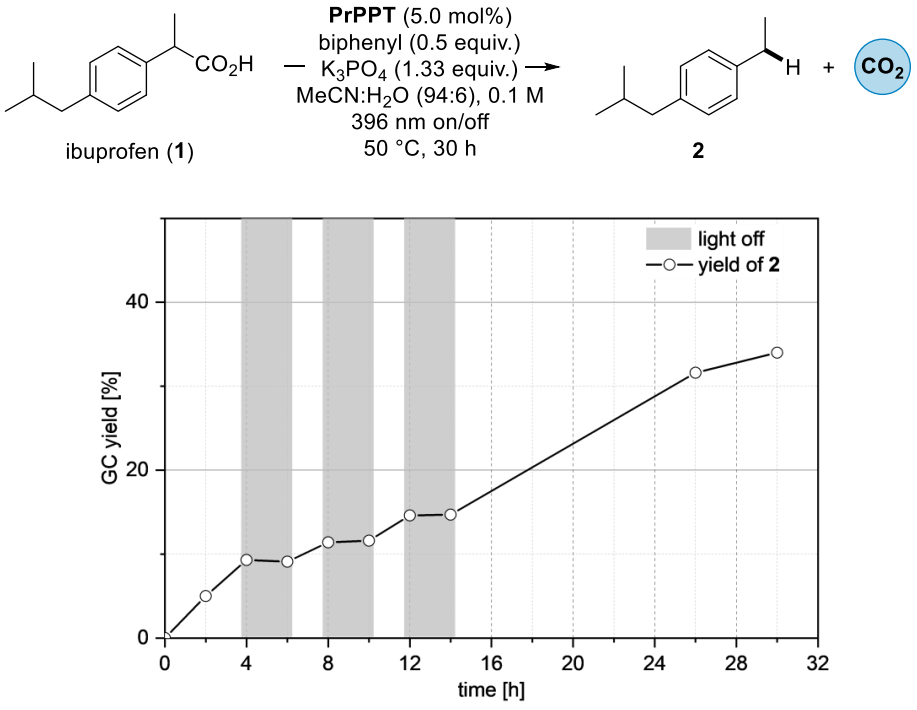

Figure 7. Light on/off experiment.

It was observed that no product was formed during the off phases. Thus, the reaction mixture must be constantly irradiated to proceed the transformation. Hence, a radical propagation mechanism can be excluded. The decreased overall yield, on the other hand, was caused by the raising water content in the reaction mixture, since the sample was taken exclusively from the MeCN phase. Although both solvents are generally miscible, the addition of the base and the resulting difference in density led to a two-phase system.

The applied PrPPT photoredox catalyst is a strong excited-state oxidant (E^*_{red} = +2.10 V vs SCE in MeCN).[59] To analyze which species is most likely oxidized by PrPPT, cyclic voltammograms (CV) were recorded in collaboration with Sina Brandt, M.Sc., and Dr. Tobias Täufer (see Experimental Section). Those analyses revealed high ground-state oxidation potentials for the carboxylic acids, e.g., ibuprofen (**1**, $E^{ox}_{1/2}$ = +2.15 V vs SCE in MeCN, ΔG = +14.5 kJ/mol) and hydroxyadamantane carboxylic acid (**38**, $E^{ox}_{1/2}$ = +2.48 V vs SCE in MeCN, ΔG = +36.7 kJ/mol), that are not accessible by most excited-state photoredox catalysts. The corresponding carboxylates, on the other side, were observed to have lower oxidation potentials, e.g., tetrabutylammonium (TBA) ibuprofen carboxylate (**62**, $E^{ox}_{1/2}$ = +1.04 V vs SCE in MeCN, ΔG = –102.3 kJ/mol) and TBA hydroxyadamantane carboxylate (**63**, $E^{ox}_{1/2}$ = +1.31 V vs SCE in MeCN, ΔG = –76.2 kJ/mol), as determined by CV. This indicated that a single-electron transfer (SET) from the carboxylic acid to the PPT is unlikely whereas it can happen from the carboxylate after deprotonation by the applied base.

Next, Stern-Volmer quenching experiments were conducted (Figure 8). A solution of PrPPT in MeCN was irradiated and the intensity of the fluorescence was measured by a fluorometer. Then, either a solution of ibuprofen (**1**) or TBA ibuprofen carboxylate (**62**) in MeCN was added dropwise. The decreasing intensity of the fluorescence was used to calculate a quenching constant K_{SV}.

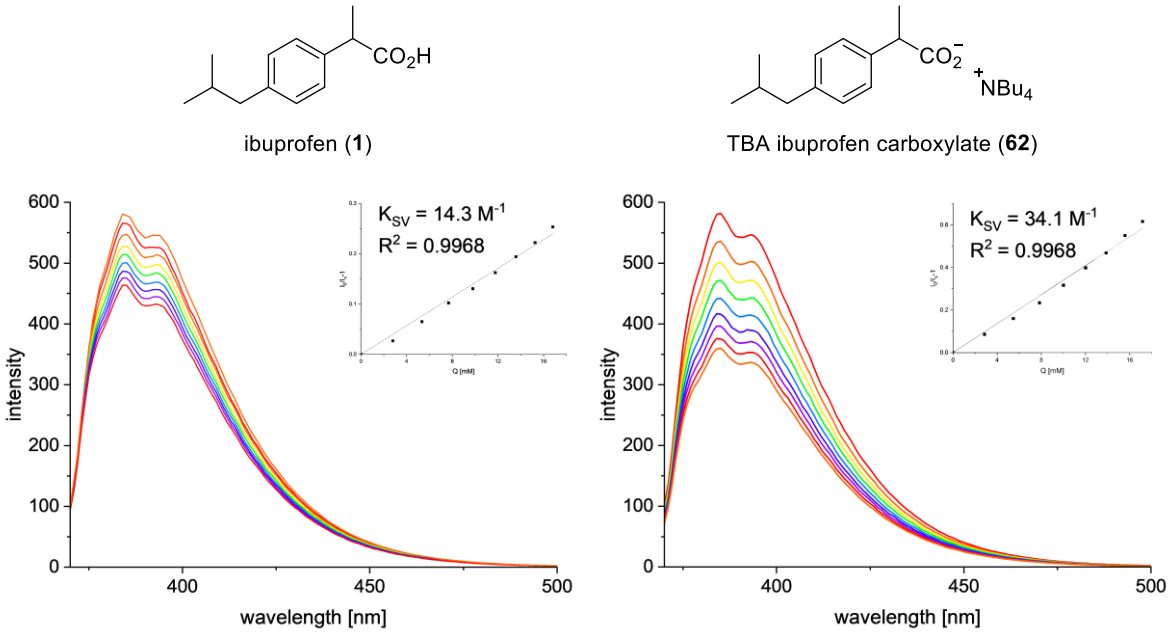

Figure 8. Quenching of the luminescence of PrPPT with varying concentrations of ibuprofen (**1**, left) and TBA ibuprofen carboxylate (**62**, right).

When comparing the quenching constants K_{SV} of the exemplary carboxylic acid and its carboxylate, it became clear that the carboxylic acid ibuprofen (**1**) was a moderate quencher for the excited state of PrPPT (K_{SV} = 14.3 M^{-1}), while TBA ibuprofen carboxylate (**62**) efficiently quenched the excited state of PrPPT (K_{SV} = 34.1 M^{-1}). This was in agreement with the observation from the CV measurements.

To confirm that the quenching of the excited state of the photoredox catalyst by the carboxylate proceeded *via* an SET, electron paramagnetic resonance (EPR) spectroscopy was applied in collaboration with Dr. Jabor Rabeah. Aromatic carboxylic acids do not undergo decarboxylation under the applied reaction conditions. Thus, benzoic acid (**64**) was utilized in a first EPR experiment, striving to accumulate an on-cycle species. A mixture of benzoic acid (**64**), PrPPT, varying amounts of base, and dry MeCN was irradiated while recording the EPR spectra (Figure 9).

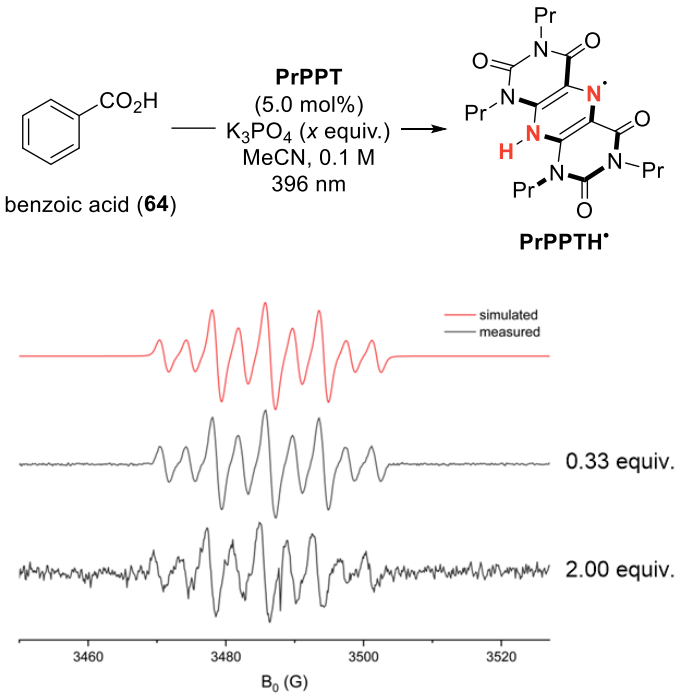

Figure 9. EPR spectrum of benzoic acid (**64**, 0.5 mmol), K_3PO_4 (0.33 equiv. or 2.00 equiv., respectively) and PrPPT (5.0 mol%, black line) in MeCN (5 ml); simulation (red) with two nonequivalent N and one H nuclei (g = 2.005; A_{N1} = 7.84 G, A_{N2} = 3.72 G; A_{H1} = 7.45 G) corresponding to PrPPTH•.

A strong nine-line signal was observed at g = 2.005 (Figure 9). The simulated signal matched with the radical intermediate PrPPTH• bearing a radical (S = ½) interacting with one ^{1}H nucleus (I = ½; A_H = 7.45 G) and two nonequivalent ^{14}N nuclei (I = 1; A_{N1} = 7.84 G, A_{N2} = 3.72 G). The measured signal was much stronger when less base was used. Hence, a proton transfer (PT) from benzoic acid (pK_a(benzoic acid) = 4.2)[90] to the PPT•⁻ radical anion was proposed, yielding a PrPPTH• radical. Different from the optimized reaction conditions, an aprotic environment was used for the EPR spectroscopy. Therefore, water was excluded as the proton source. The PrPPTH• species, however, accumulated in the reaction mixture because there was no aryl radical as an acceptor for the necessary HAT to close the catalytic cycle. An excess amount of base acted as competitive proton abstractor and resulted in a diminished signal.

After the EPR spectroscopy of benzoic acid, the experiment was repeated with ibuprofen (**1**), which readily extrudes carbon dioxide under the applied conditions. Again, the carboxylic acid **1**, PrPPT,

varying amounts of base, and dry MeCN were irradiated and the EPR spectra were recorded (Figure 10).

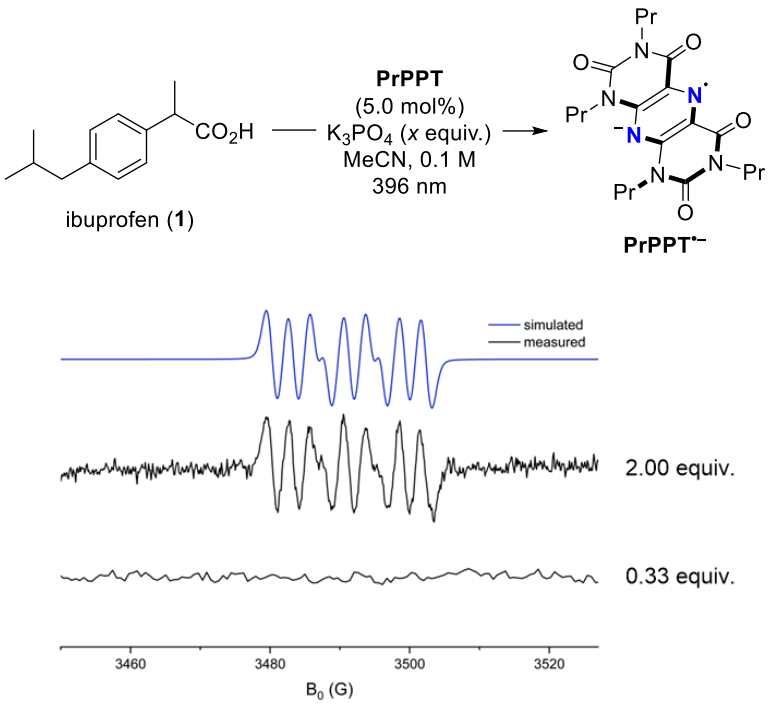

Figure 10. EPR spectrum of ibuprofen (**1**, 0.5 mmol), K_3PO_4 (0.33 equiv. or 2.00 equiv., respectively) and PrPPT (5.0 mol%, black line) in MeCN (5 ml); simulation (blue) with two nonequivalent ^{14}N nuclei (g = 2.005; A_{N1} = 7.87 G, A_{N2} = 3.14 G) corresponding to PrPPT$^{\bullet-}$.

When ibuprofen (**1**) was treated with substoichiometric amounts of base in the presence of PrPPT in pure MeCN, the reaction proceeded smoothly. Thus, no on-cycle species could be accumulated. In contrast, when the base was used in excess, the reaction was partly inhibited by deprotonation of ibuprofen (pK_a(ibuprofen) = 5.3)[91], and a nine-line signal was observed in the EPR spectrum at g = 2.005. The signal correlated well with the simulated interaction of a radical (S = ½) with two nonequivalent ^{14}N nuclei (A_{N1} = 7.87 G, A_{N2} = 3.14 G), as present in a PrPPT$^{\bullet-}$ radical anion. This supported the assumption of an initial SET as part of the operating mechanism.

Following the mechanistic proposal, an initial SET from the carboxylate to the PrPPT photoredox catalyst would not only lead to the formation of the PrPPT$^{\bullet-}$ radical anion but also of a carboxyl radical that would undergo rapid decarboxylation even at room temperature ($k \approx 10^9$ s^{-1} at 20 °C) driven by entropy increase.[92-93] The product of this decarboxylation step, the alkyl radical, can be trapped by stabilized radical species like (2,2,6,6-tetramethylpiperidin-1-yl)oxyl (TEMPO). To investigate this assumption, TEMPO (1.25 equiv.) was added to the decarboxylation reaction with adamantane carboxylic acid (**40**) under otherwise unaltered conditions (Scheme 7).

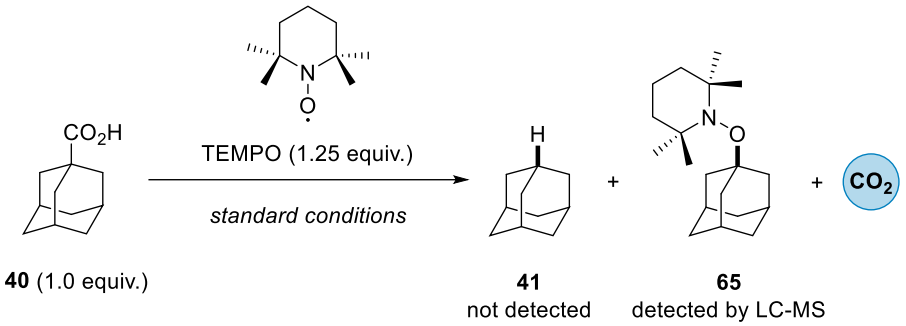

Scheme 7. TEMPO radical trapping experiment.

Indeed, an adamantyl TEMPO adduct **65** from the reaction of the adamantyl radical with TEMPO was identified by LC-MS. At the same time, the formation of adamantane (**41**) was effectively inhibited, as no product was detected.

However, there were two competing mechanistic proposals to close the catalytic cycle: either by H-atom transfer (HAT) from the PrPPTH• radical intermediate to the alkyl radical to form the product, or by direct reduction of the alkyl radical to the corresponding radical anion followed by protonation to give the product. The latter possibility was ruled out by thermodynamic reasons, as the SET from the PPT radical anion ($E_{1/2}^{red}$[PrPPT/PrPPT•⁻] = –1.21 V vs SCE in MeCN)[59] to the alkyl radical ($E_{1/2}^{red}$ ≤ –1.6 V vs SCE in MeCN)[64] was thermodynamically unfavorable (Δ*G* = +9.0 kcal/mol).

The dual role of PrPPT as photoredox and HAT catalyst was already known from previous publications of the Pospech group.[61-62] This was supported by the present mechanistic experiments. Nevertheless, a control experiment was performed to investigate whether adding an additional HAT co-catalyst further promotes the photomediated hydrodecarboxylation. In literature, thiols and disulfides are often used for this purpose.[94-95] Thus, a catalytic amount of diphenyl disulfide (10 mol%) was added to the hydrodecarboxylation of adamantane carboxylic acid (**40**, Table 12).

Table 12. Control experiment with an additional HAT co-catalyst.

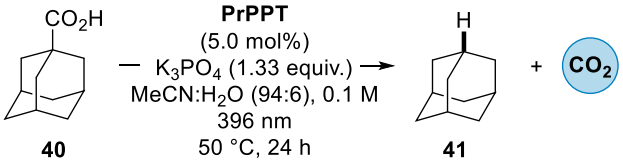

entry	deviation from optimized reaction conditions	yield[a]
1	none	23%
2	10 mol% diphenyl disulfide	18%

[a] Yields were determined by calibrated GC using biphenyl as internal standard.

The addition of diphenyl disulfide as an HAT co-catalyst did not enhance the yield of the reaction. It could hence be concluded that PrPPT functioned as an efficient HAT catalyst while the HAT was not

the yield-limiting step. In combination, the conducted mechanistic experiments allowed to propose a plausible reaction sequence (Scheme 8).

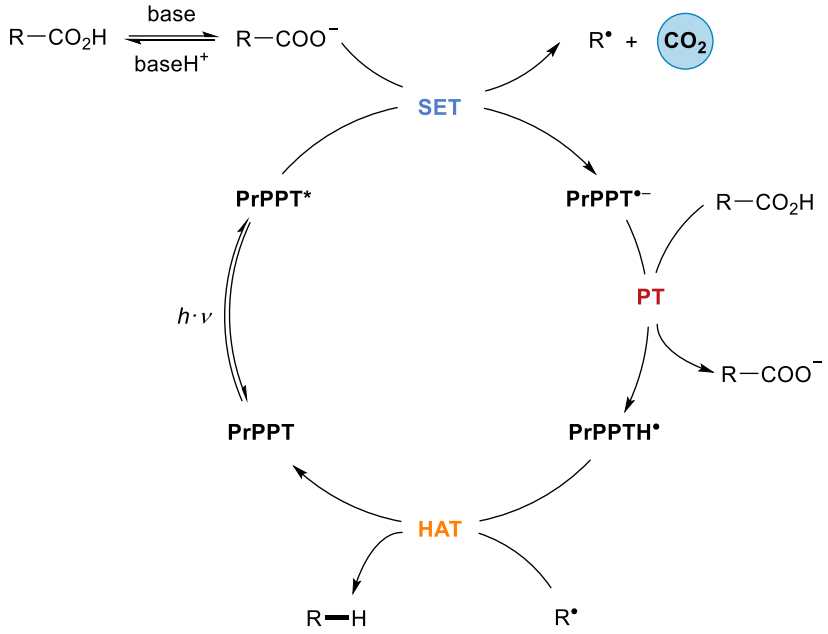

Scheme 8. Proposed reaction mechanism of the photomediated hydrodecarboxylation.

First, the photoredox catalyst PrPPT was irradiated by UV light (396 nm). Due to its property as a potent excited state oxidant (E^*_{red} = +2.10 V vs SCE in MeCN), the excitation of PrPPT was followed by the oxidation of the carboxylate, that had been formed from the applied carboxylic acid by deprotonation, *via* single-electron transfer. The direct SET from the carboxylic acid substrate had been ruled out with the help of CV measurements and Stern-Volmer experiments. The SET led to the formation of the radical intermediate PrPPT$^{\bullet-}$ and a carboxyl radical, which directly underwent decarboxylation to give an alkyl radical. Both species had been detected using EPR spectroscopy and a radical trapping experiment, respectively. Next, the PrPPT$^{\bullet-}$ radical anion was protonated by the applied carboxylic acid to form a PPTH$^{\bullet}$ radical, which had also been detected by EPR spectroscopy. Subsequent HAT from PrPPTH$^{\bullet}$ to the alkyl radical delivered the desired product. At the same time, the photoredox catalyst was recovered.

4 CO_2 Capture by (Poly)Amines Synthesized from Waste Nylon

Polyamide-6 (nylon-6, PA6) was modified by reduction with molecular hydrogen and tested for its capability to capture carbon dioxide. This research project was carried out in collaboration with Clemens Kaussler, M.Sc., during a research stay in the Skrydstrup group at Aarhus University from April to June 2023.

4.1 Introduction

Capturing CO_2 from the air is an effective way to face the increased atmospheric concentration of the greenhouse gas that is driving climate change. Carbon capture can either be realized at stationary points and by direct air capture (DAC).[96] Stationary points are characterized by much higher CO_2 concentrations up to 15%, rendering it easier to efficiently remove the gas.[97] These point sources are mostly located near power plants, since more than 75% of the annual global CO_2 emissions is associated with power generation.[98] These emissions also include the power generation of industrial facilities and the transportation sector, emitting CO_2 due to combustion of fossil resources. DAC, on the other hand, can be performed at any place and can, thus, compensate for emissions that are difficult to eliminate. This includes, among others, marine transport and air traffic.[99] Due to the lower concentration of roughly 400 ppm CO_2, though, the efficiency is decreased whereas the energy demand is increased. According to a technology developed by Carbon Engineering, DAC is accomplished best with high-powered fans pulling air into the system where it is chemically captured, purified, and compressed.[100]

Two main concepts have been developed throughout the last centuries, which are carbon capture and storage (CCS) and carbon capture and utilization (CCU).

CCS combines CO_2 capture with compressing the captured carbon dioxide, which is then brought to underground storage sites on land or in the ocean.[98] CCS is often combined with DAC (DACCS), which has the advantage that it can be used wherever storage is possible and does not have to take place near point sources. In principle, CCS offers the possibility to remove enough CO_2 from the atmosphere to meet the requirements of the 2014 Paris Agreement, as the technical geological storage capacity is considered large enough.[101] CCS is already being used on an industrial scale by more than 70 different companies around the world, including Aker Carbon Capture (400 kilotons per year), Shell (1.2 million tons per year), or Carbfix (1 billion tons per lifetime), among others.[102-105] They store the captured CO_2 in basaltic rock formations, saline reservoirs, or depleted oil and gas fields. Additionally, more than 30 facilities are currently in construction and are expected to be operational within the next years.[105]

Nevertheless, there are some issues related to CCS. First, CCS is not in line with a circular economy, because the carbon is not reused but stored underground. Additionally, the storage underground is threatened by geological incidents such as earthquakes or slides that can lead to abrupt liberation.[31] Storing CO_2 as minerals might be a solution to dangerous pressured CO_2, although mineral carbonation is known to proceed very slowly, requiring a geological time scale.[34] The actual implementation of CCS on big scale is further limited by "technological, economic, institutional, ecological-environmental and socio-cultural barriers".[101]

Therefore, researchers and industry nowadays focus on CCU as a concept to develop a chemical carbon cycle. From 2019 to 2021, the EU has financed the first industrial project, the George Olah Renewable Methanol Plant in Iceland, with more than 1.8 million €.[106] This plant, that is run by Carbon Recycling International (CRI), is able to annually produce 4000 tons of green methanol from green H_2 and CO_2. The hydrogen is produced by water splitting using renewable energy, while 5500 tons of CO_2 are captured per year for this process. The plant is located close to a geothermal power plant as the stationary point. Since then, CRI has planned and built many more facilities with adjacent manufacturers, producing more than 100 kilotons green MeOH each.[107] This corresponds to more than 150 kilotons CO_2 per year that are recycled this way. Another benefit of the proximity of industrial parks and facilities is cheap hydrogen from onsite processes that allow to spare water electrolysis. Columbus, a Belgian company that has been approved for funding by the EU Innovation Fund in 2023, puts its focus on the synthesis of methane from carbon dioxide and green hydrogen, aiming to capture and utilize up to 187 kilotons CO_2 per year.[108] The so-produced methane could be applied as a full replacement for natural gas without the requirements to modify any infrastructure. A commercial conversion of CO_2 into C_2 products has been developed by LanzaTech in 2022. They targeted the formation of high-value products like ethanol, acetone, or isopropanol by designing an enzyme suitable for fermentation of CO_2.[109]

However, both methods, CCS and CCU, have in common that CO_2 needs to be captured first. Various methods exist for carbon capture.[110] In the following paragraphs, capture by metal-organic frameworks (MOFs), amines, ionic liquids (ILs), and polymers are explained, although these represent just a few of the many active research areas in carbon capture. The capture by bases like NaOH, leading to inorganic salts like Na_2CO_3 and $NaHCO_3$ is not further discussed. This chemisorption suffers from a low absorption performance and high temperatures above 927 °C that are required for the regeneration of the carbon capture material.[38]

MOFs are highly porous materials that are typically synthesized from transition metal ions and organic ligands, also referred to as linkers, which build a periodic 3D network. They are characterized by a high surface area, while the chemical and physical properties including the pore size can be easily

tuned by altering the metal or the linker.[111] These materials are often explored as solid carbon capture agents, as depicted by the Xing group (Scheme 9).[112]

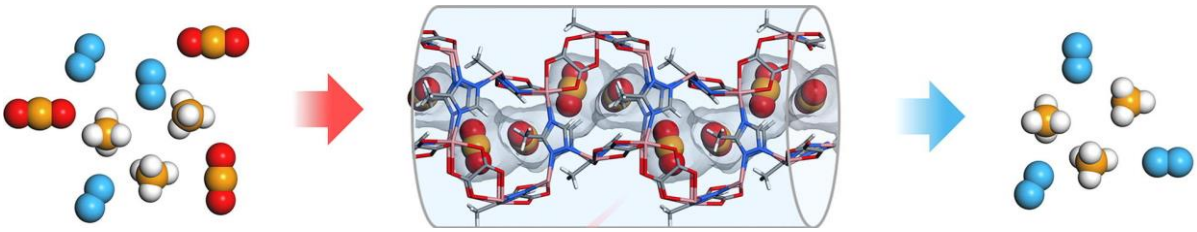

Scheme 9. Selective capture of CO_2 by a metal-organic framework of Xing and co-workers, replicated with the permission of Elsevier.[112]

In 2017, the group of Das reported on a microporous MOF, which they had synthesized from zinc nitrate and a V-shaped sulfonyldibenzoate linker together with a *N*-rich spacer, 2,5-bis(3-pyridyl)-3,4-diaza-2,4-hexadiene.[113] While their material had a moderate maximum CO_2 loading capacity of 2.04 mmol/g at 1 bar CO_2, the researchers were able to separate carbon dioxide from gas mixtures with methane and N_2 with good selectivities of 152:1 and 436:1, respectively. Thus, the system was assumed to be applicable to flue gas separation. However, real flue gas contains water, and most MOFs are not moisture stable, as they co-adsorb water. Hence, Boyd *et al.* used computational methods to screen a library of more than 300000 MOFs for identifying specific properties of water-tolerant systems.[114] Based on the obtained information, they synthesized two different water-stable MOFs starting from aluminum(III) salts and a porphyrin- or pyrene-based linker, respectively. Afterwards, both MOFs were tested regarding their stability towards water by immersing them in water for 7 days. Promisingly, no change in crystallinity was observed. The CO_2 uptake capacity from 15 v/v% CO_2 was in good agreement with the predicted values with 0.95 mmol/g and 0.30 mmol/g, respectively. The impact of water on the binding of CO_2 was further studied by varying the humidity of the N_2/CO_2 (85:15) gas mixture. Only minor differences of the capacities were observed. To develop a material that is able to capture trace amounts of CO_2, as present in the atmosphere, Hu and co-workers engineered a MOF with a specific pore size and geometry.[115] By reacting cobalt nitrate with a dihydroxyterephthalate linker, the researchers created a regular, hydrophobic MOF with a hexahedral morphology. The free coordination sites of the metal were saturated by pyrazine vapor, leading to a structure featuring a fast diffusion and a strong CO_2 binding force. The MOF showed a good performance at 1 bar and even at atmospheric concentration, achieving a CO_2 uptake of 7.87 mmol/g and 1.36 mmol/g, respectively.

Despite these promising examples, carbon capture by using MOFs can suffer from a weak binding affinity, caused by the labile nature of physical sorption in comparison to chemisorption. Powder agglomeration further leads to a decreased surface area. Additionally, many MOFs are characterized by a stagnant diffusion kinetics.[111]

The most common carbon capture agents are amines which have been used to separate CO_2 from other gases for almost 100 years.[116] In general, the mechanism of the chemisorption with primary, secondary, and tertiary amines proceeds *via* carbamate or bicarbonate formation, depending on the amount of water present (Scheme 10).[96]

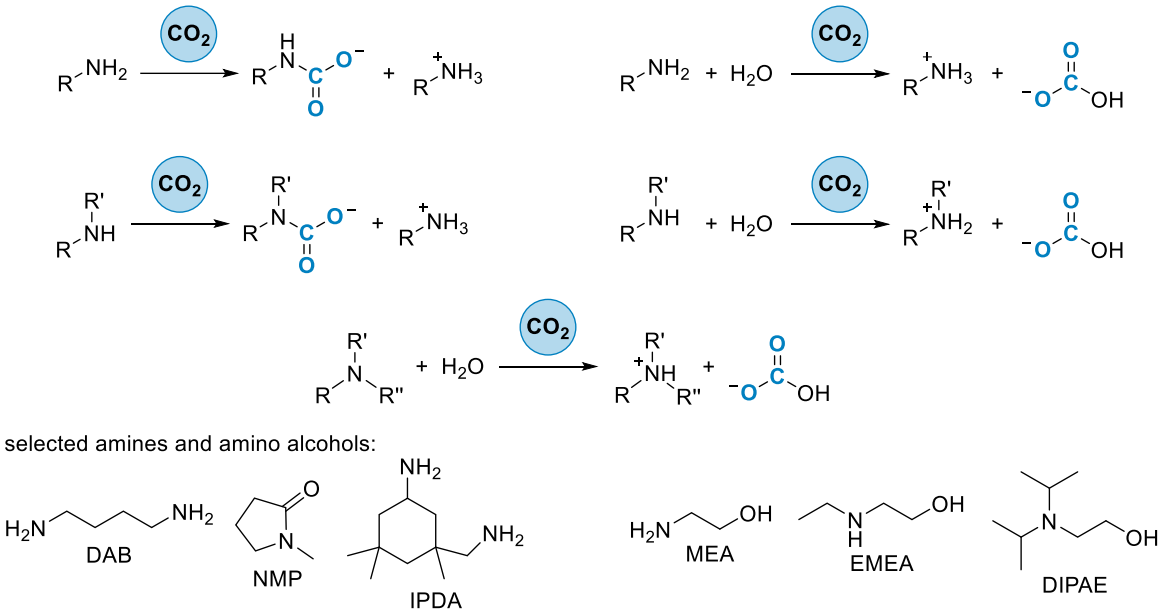

Scheme 10. Top: Chemisorption *via* amine moieties in the absence or presence of water either by carbamate formation (left) or by bicarbonate formation (right).[96] Bottom: Selected amines (left) and amino alcohols (right).

Among those amines are also amino alcohols, that can react with CO_2 by the formation of organic carbonates while the charge is stabilized by the amine moiety.[117] Amines are popular carbon capture agents because they quickly respond to carbon dioxide and are even most efficient in DAC. For example, aqueous solutions of unhindered amines and amino alcohols like monoethanolamine (MEA) show a CO_2 uptake efficient of up to 88% from atmospheric concentrations of CO_2.[38] In 2022, Kikkawa *et al.* found isophorone diamine (IPDA) to have an even higher CO_2 uptake efficiency of more than 99%.[118] They saturated a solution of IPDA in DMSO or in water with an CO_2/N_2 mixture (400 ppm CO_2) to mimic DAC and compared the obtained data with the capturing ability of an equimolar solution of MEA, which had been clearly outperformed. The efficient CO_2 removal by IPDA, that remained consistent at a high speed of 201 mmol/h for 100 h, was caused by an equilibrium shift to the solid carbamic acid product. Next to recent results on novel amines with high activities, there are also many already commercialized methods for the utilization of aqueous solutions of different amines or amine combinations. The company Advanced Carbon Capture has, for instance, reported on their technique to capture CO_2 in a patent from 2013.[119] They have found that an aqueous solution of a mixture of a tertiary amine with a primary or secondary amine formed a two-phase system upon saturation with CO_2. Since the CO_2-rich phase and the CO_2-lean phase were not miscible, they could easily be separated to re-run the process with the CO_2 lean phase. This was true, among others, for the combination of 2:1

di-*iso*-propylaminoethanol (DIPAE) and 1,4-diaminobutane (DAB), which absorbed more than 2 mol CO_2 per kg of solution with an initial rate of $50 \cdot 10^5$ mol l^{-1} s^{-1}. However, aqueous solutions require much energy for the CO_2 release due to the high specific heat of water.[117, 120] Thus, so-called water-lean solvents have been developed in the past years. These amine blends are meant to mimic the great selectivity of purely aqueous systems but improve the efficiency and reduce the energy consumption.[117] Even though the term water-lean solvent suggests the total absence of water, it may be present as part of mixtures with alcohols or amines. Recently, Qi and co-workers have investigated the properties of a solution of 2-(ethylamino)ethanol (EMEA) in *N*-methyl-2-pyrrolidinone (NMP) and water, which is known to have a 20% higher CO_2 absorption rate than the respective purely aqueous EMEA solution.[120] In addition, the regeneration energy was up to 69% lower than comparable water-based systems. One of the main drawbacks of using amines is the high volatility, which causes solvent reduction. In the discussed example, the amine emission was proven to be expectably high with 1891 mg/m^3 at 54 °C. This substrate loss renders the application of liquid amine systems for carbon capture quite expensive. Other downsides of amines are their corrosive and potentially toxic nature. They are further prone to oxidative decomposition.[38, 121]

To overcome the disadvantages of amines, additional types of carbon capture agents are being investigated. One of those are ionic liquids (IL), that have first been explored for CO_2 capture by Blanchard *et al.* in 2001.[122] ILs are salts with a melting point below 100 °C.[123] They exhibit unique properties like high thermal stability, a negligible vapor pressure, and designability, because both cation and anion can easily be modified.[121] Furthermore, it is state-of-the-art that the cation plays a minor role, whereas the interaction with the anion is most relevant for CO_2 uptake. Interestingly, the basicity of the anion is not the only factor relevant for carbon capture since the capture efficiency does not completely correspond to the basicity order.[121] Instead, longer alkyl chains create free space within the solvent that increase the solubility of CO_2.[124] Other factors that are beneficial for the carbon capture efficiency are hydrogen bonding, halogen bonding, and electrostatic interactions.[121] In 2015, de Leeuw and co-workers have examined the solubility of CO_2 in various conventional ILs containing five different anions while keeping a phosphonium cation.[125] Both dry and wet conditions, as present in fuel gas, were tested. Depending on anion, the CO_2 uptake capacity differed between 0.23 and 1.20 mol/mol but was mostly equimolar. Equally, the effect of water on the system differed. While the phenolate anion was protonated by water and showed a reduced CO_2 uptake of 0.16 mol/mol (from 1.00 mol/mol under dry conditions), another IL with benzotriazolide as the anion revealed an increased CO_2 uptake of 0.59 mol/mol (from 0.23 mol/mol under dry conditions). Unfortunately, the researchers do not give reasons for the observed trends. Popular reasons why commercializing ILs for carbon capture remains challenging are that these solvents are hardly recyclable and highly viscous, which may even increases up to 200 times during carbon capture.[121] However, the group of de Leeuw has

shown that under wet conditions, the viscosity rather decreased upon CO_2 absorption.[125] They were also able to recycle one of their ILs 6 times without significant reduction in its CO_2 capacity, thus, riposting all mentioned disadvantages of ILs. To improve the carbon capture efficiency, amino-functionalized ILs have been developed. With this additional CO_2-capturing site, a multimolar absorption could be achieved, not dependent on whether the cation or the anion is bearing the amino group.[126] In 2020, the group of Li reported on a novel amino-functionalized IL that they had combined with the organic solvents ethylene glycol and *n*PrOH to maintain a low viscosity despite the additional H-bonding by the amine.[127] With this mixture, they afforded a CO_2 uptake of up to 1.72 mol/mol. After regenerating the system 5 times, the capacity was still 91% of the original value. According to mechanistic experiments by ^{13}C NMR, a mixture of carbamates and carbonates was present in the IL. To avoid the increased viscosity by H-bonding while keeping the increased carbon capture capacity, other researchers have rather focused on the functionalization with *N*-heterocycles like pyridines or pyrrolide anions.[126] Applying liquid salts as solvents can also enhance the CO_2 uptake of MOFs, as recently shown by Zhang *et al.* and Noorani and Mehrdad.[128-129] In the work of Zhang and co-workers, an amino-functionalized IL was added during the synthesis of the MOF.[128] This resulted in the formation of an ultramicroporous network where the IL served as a competing ligand through coordination of the metal center by the amino group. By this treatment, the absorption capacity of the MOF was increased by 1.5 times. Instead of using an IL, Noorani and Mehrdad impregnated a MOF with a deep-eutectic solvent (DES), which is a mixture of an acid with a base that is liquid once it is combined.[129] As the DES, they use a mixture of choline chloride and urea. Successfully, the absorption capacity of their MOF for CO_2 increased by 1.7 times after the impregnation. The authors rationalize this effect by an additional interaction of the gas with the DES in the pores of the MOF.

Researchers further focus on polymers including – though not limited to – polyamines due to their stability, recyclability, and low volatility.[110] In 2019, the group of Jones prepared a porous polyethyleneimine (PEI)-based material for carbon capture.[130] While cross-linking the polymer strands using poly(ethylene glycol) diglycidyl, the aqueous reaction mixture was quickly frozen by the addition of liquid N_2 and kept on the freezer for two days. After thawing, washing, and drying the sample *in vacuo*, the new connectivity of the polymer was retained, affording a highly porous structure that had been built around the water crystals. At ambient temperature, a CO_2 uptake capacity of 2.8 mmol/g was achieved, reaching 80% within only 18 minutes. This could even be increased to 5.5 mmol/g under humid conditions and recycled more than 50 times. More recently, Chen *et al.* combined an alkaline solution of cellulose, a bio-based polymer, with epoxy-functionalized PEI and epichlorohydrin (ECH), responsible for cross-linking the polymers.[131] They afforded a rigid aerogel with a porous structure by freeze-drying the reaction mixture. Interestingly, the researchers attested the stability of the material by putting a water-filled Erlenmeyer flask with a total weight of 4 kg on top of 1 g aerogel. The

maximum absorption capacity was 6.5 mmol/g at room temperature and did not decrease upon recycling the system 5 times. It further outcompeted the carbon capture ability of freeze-dried cellulose aerogel and ECH-cross-linked PEI cellulose aerogel without epoxy-functionalization.

Polyamines do not necessarily have a big surface area. Thus, they are often immobilized on porous materials, such as silica, clay, graphene, alumina, and MOFs (Scheme 11).[96] As stated by Hack *et al.*, "amine-functionalized porous materials outperform all others in terms of CO_2 adsorption capacity and regeneration efficiency".[132] This increased carbon capture ability of amine-functionalized materials is caused by the combination of physisorption *via* the porous structure and chemisorption by the amine moieties.[96]

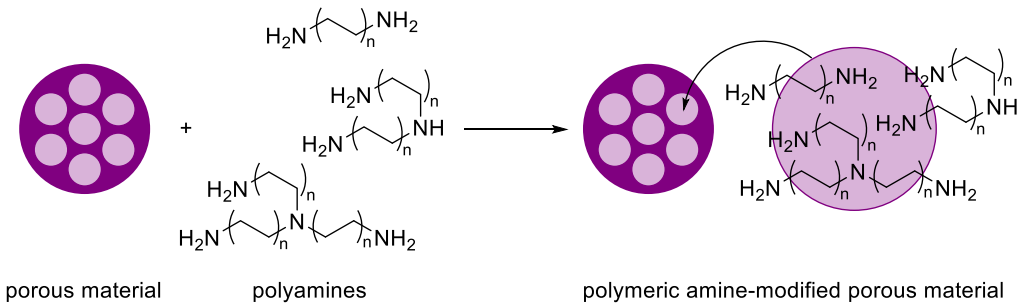

Scheme 11. Functionalization of porous materials with polyamines.[96]

According to Hamdy *et al.*, there is one highly promising candidate for industrial carbon capture among the many procedures available.[133] The presented immobilization of PEI on porous silica had been published by Jones and co-workers in 2019.[134] The researchers have impregnated macro- (750 nm) and mesoporous (5 nm) silica with PEI and investigated its activity towards CO_2. They applied simulated dry air and flue gas with CO_2 concentrations of 400 ppm and 10%, respectively. Unexpectedly, the adsorption capacity at a temperature of 30 °C was the same for both CO_2 concentrations and just dependent on the amount of PEI per SiO_2. Therefore, it was assumed that the adsorption of CO_2 was kinetically limited and thus reached a limit independent on the amount of CO_2. If that was true, the researchers explained, increasing the temperature should support the CO_2 uptake. Whereas the expected effect has been observed for simulated flue gas, reaching adsorbtion capacities around 15 mmol/g SiO_2 (4.1 mmol/g sorbent) at 80 °C, the opposite effect occurred when atmospheric concentrations were applied. The maximum CO_2 uptake first increased from 2.4 mmol/g sorbent at 30 °C to 2.6 mmol/g at 50 °C before it rapidly decreased to 0.1 mmol/g at 80 °C. The group of Jones ascribed this to unfavorable amine arrangements on the surface. A more recent example of an amine-functionalized porous material has been reported by Shan and co-workers.[111] The researchers combined chromium nitrate with aminoterephthalate to prepare a MOF with the amine units as part of the MOF-network. This type of MOFs is called MIL-101 and had been known for years to bear the largest pore volume and the highest surface area, until extensive research in this field has led to even

exceeded values.[135-136] The nanoparticles were immobilized on bamboo powder cellulose, a carbon capture agent itself, to avoid particle aggregation.[111] With this system, a CO_2 uptake of 13.4 mmol/g was achieved at ambient temperature and a pressure of 1 bar CO_2. The remarkable performance was assigned to a synergistic effect of amine, MOF, and cellulose by comparing the CO_2 uptake capacity to that of the single components and the physical mixture of all. The attachment of the MOFs to cellulose also enabled recycling the systems 15 times without noticeable decrease of productivity.

Polymeric and polymer-derived carbon capture agents taking waste plastics as the starting material have come up in the past years. These plastics are very cheap and available on large scale, which is required to encounter the rising amount of carbon dioxide in the atmosphere.[137] The groups of Lau and Changkun have modified waste Styrofoam (polystyrene, PS) by cross-linking the polymer strands *via* formaldehyde dimethyl acetal and carbon tetrachloride, respectively.[138-139] This treatment led to an increased porosity of the PS. The cross-linked Styrofoam of Changkun and co-workers showed a moderate CO_2 uptake capacity of 2.52 mmol/g at 0 °C and a selectivity of 38 when applying a post-combustion-like 15% CO_2/N_2 mixture.[138] On the other hand, the cross-linked PS of Lau and co-workers was slightly less efficient with a CO_2 uptake of 2.1 mmol/g at the same conditions but more selective towards CO_2. From a 25% CO_2/N_2 gas mixture, the material showed a superior selectivity of more than 400.[139] In 2022, the group of Tour treated high-density polyethylene (HDPE) plastic waste with KOAc in a 1:4 molar ratio and pyrolyzed the reaction mixture to afford an efficient CO_2 sorbent with a CO_2 uptake capacity of 3.8 mmol/g at 1 bar CO_2.[140] The porous carbon sorbent had a nanometer-scale pore size and a high surface area of up to 1055 m^2/g. Since the sorbent had been synthesized from waste materials, carbon capture is with less than 21 \$/ton CO_2 much cheaper than with amine-based systems that have been commercially applied for years and produced costs of 80-160 \$/ton CO_2. Comparable results were obtained from low-density polyethylene (LDPE), polypropylene (PP), and mixed postconsumer plastics. All in all, using waste plastics-derived materials for carbon capture supports the circular economy approach.

A common type of waste plastics, that has not yet been applied in carbon capture, is nylon. More than 8 million tons of nylons – predominantly nylon-6 and nylon-6,6 – are produced every year.[141] The polymeric material is synthesized by ring-opening polymerization of ε-caprolactam (**66**) or by condensation polymerization of hexamethylenediamine (**67**) and adipic acid (**68**), respectively (Scheme 12).[142] Common applications include textile fibers (for clothing, fishing nets, etc.), food packaging, toothbrush bristles, and even biomaterials (for dental implants, skin sutures, etc.).[142] However, the nonbiodegradable thermoplastic material causes increased pollution of the sea and soil.[143] Therefore, methodologies to recycle or modify the polymer for application in a second lifecycle, e.g., carbon capture, are desired.

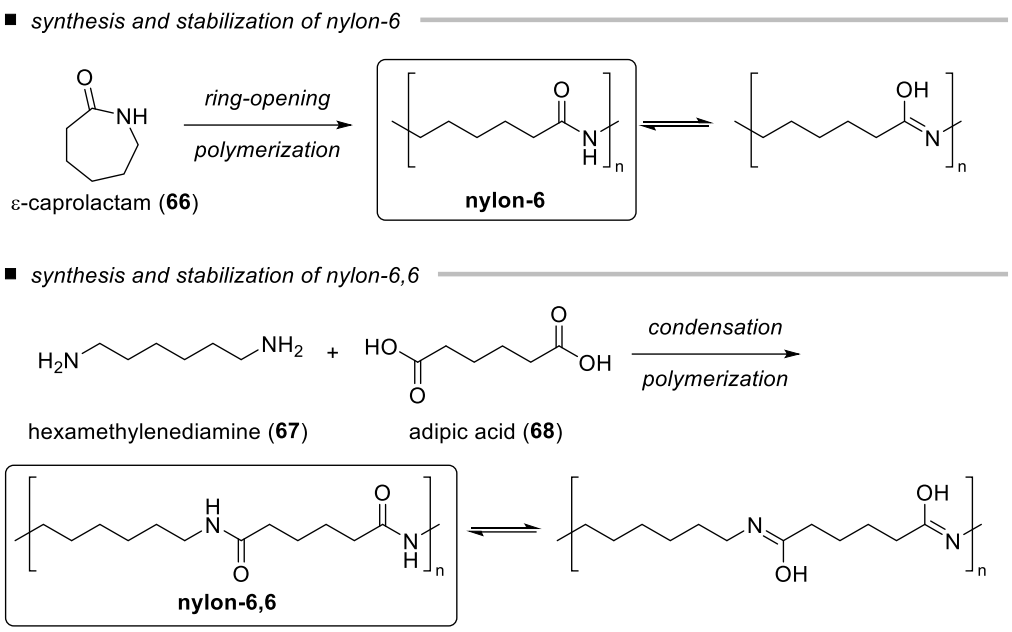

Scheme 12. Synthesis, structure, and tautomerism of nylon-6 and nylon-6,6.

Nylon is known to be thermically and chemically very stable, rendering it difficult to get the polymer to react.[142] In general, the carbonyl group in amides is less activated because of the resonance with the iminol form caused by delocalization of the lone pair at the nitrogen, raising the stability and inertness of nylon (Scheme 12).[144] Furthermore, inter- and intramolecular hydrogen bonding makes the robust material insoluble in most organic solvents.[143] In addition, the rigid structure of nylon renders the secondary amide bonds poorly accessible. Thus, common chemical recycling of nylon-6, leading to the monomer ε-caprolactam (**66**), needs high temperatures above the melting point (>220 °C), high pressures, or strongly basic or acidic conditions.[145-146] For the purpose of CO_2 capture, amine functionalities are needed rather than amide moieties as present in nylon because of the higher nucleophilicity of the amine.[147]

4.2 Results and Discussion

In the present work, the development of a transition metal-based protocol for the reduction of nylon-6 to the respective polyamine was envisioned. Preliminary results established that nylon-6 can be stoichiometrically reduced by using borane. Thermogravimetric analysis (TGA) of the polyamine product revealed reversible CO_2 sorption (Figure 11).

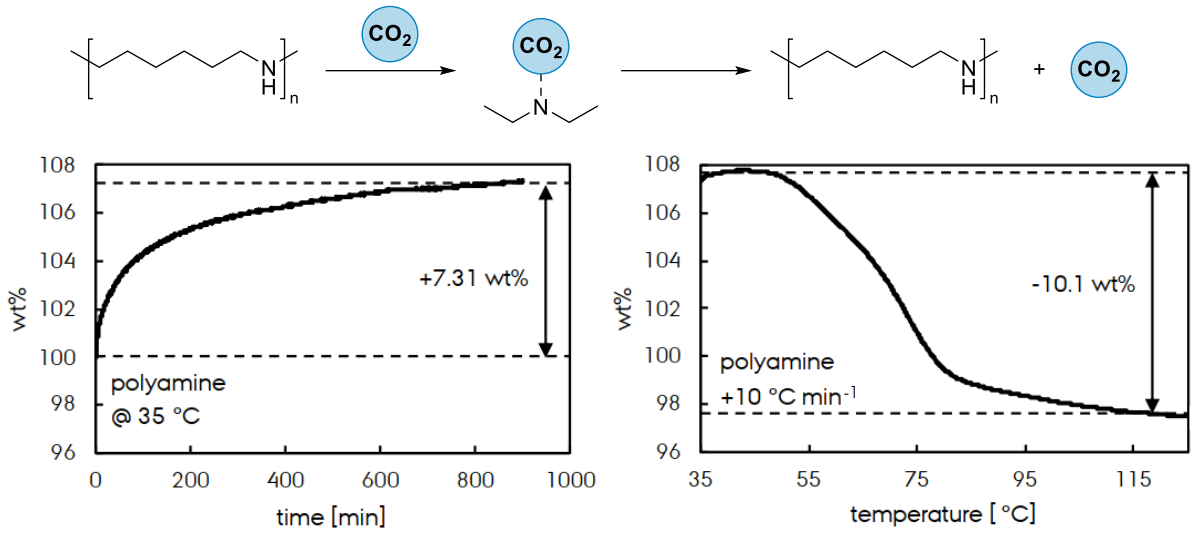

Figure 11. Preliminary TGA results recorded by Clemens Kaussler that show the reversible CO_2 sorption of PA6-derived polyamine. *Left*: Isothermic measurement at 35 °C with a CO_2 flow rate of 20 ml/min. *Right*: Desorption with a heating rate of +10 °C/min.

While 7.3 wt% CO_2 had been sorbed – equaling 16.5 mol% (roughly 17 CO_2 molecules per 100 monomer units) –, a weight loss of 10.1 wt% was observed upon heating of the polymer. This additional weight loss is explained by residual water that was adsorbed to the polyamine in the beginning. Having these promising results in hand, effort was put into developing a catalytic procedure for polyamine synthesis using hydrogen as green reductant,[148-149] that is applicable on large scale while avoiding the production of stoichiometric waste. Due to solubility issues observed for both the polyamide and the polyamine, the smaller molecule *N*-hexylhexanamide was investigated instead as a model system for polymeric aliphatic secondary amides.

Although the development of hydrogenation processes for (semi)aromatic amides has recently made new progress, not many routes are yet known to catalytically reduce aliphatic secondary amides with H_2.[144, 150] A method patented by Klankermayer and Leitner in 2019 was used as the starting point.[151] They utilized a ruthenium cyclooctadiene (COD) 2-methylallyl (TMM) precursor together with a substituted 1,1,1-tris(diphenylphosphinomethyl)ethane (triphos) ligand as the complex [Ru((OMe)$_2$-triphos)(TMM)] to successfully reduce *N*-hexylhexanamide (**69**) to dihexylamine (**70**) in 84% yield (Scheme 13). High temperature and hydrogen pressure were required (160 °C, 100 bar), as well as catalytic amounts of tris(pentafluorophenyl)borane (BCF) as the Lewis acid.

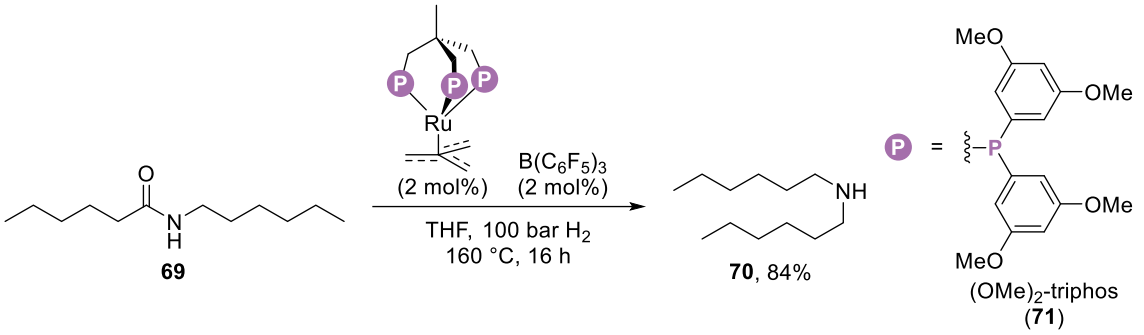

Scheme 13. Hydrogenolysis of *N*-hexylhexanamide by Klankermayer and Leitner.[151]

Different mechanisms of the amide hydrogenation have been proposed. They have in common that the amide functionality is reduced stepwise, leading to intermediary primary amines and alcohols, nitriles and imines, and tertiary amines as possible side products (Scheme 14).[144] The possibility of C–N cleavage instead of C–O cleavage is particularly undesirable in connection with polyamide reduction, as this can lead to a lower degree of polymerization and cross-linking events that further complicate the analysis of the polymer. In their publication, Klankermayer and Leitner showed that neither hexylamine nor hexanol were formed. However, trihexylamine was detected in 16% yield.[151]

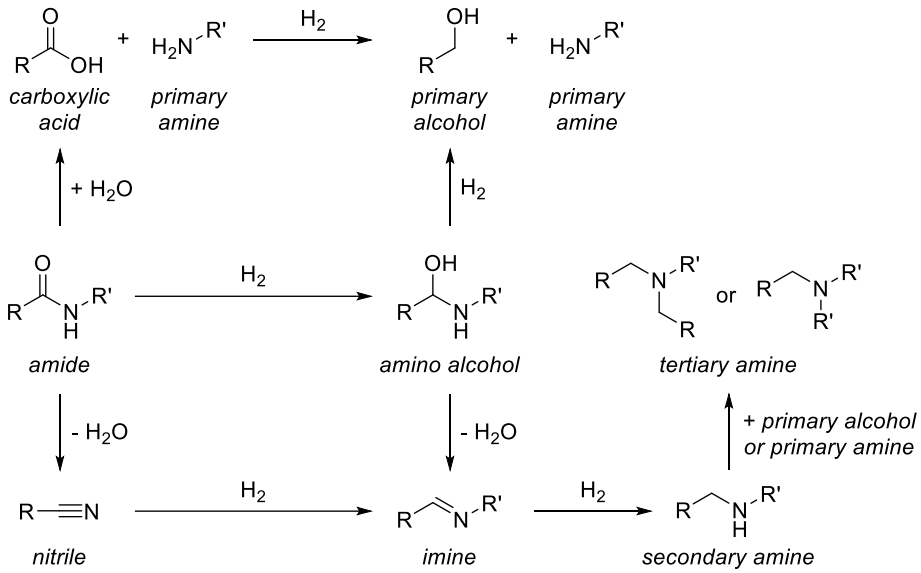

Scheme 14. Formation of possible side products as depicted by Beller and co-workers.[144]

The sterically hindered triphos ligand prevented the catalyst from deactivation by dimerization[152] or formation of a carbonyl complex.[153] Therefore, at the outset of the project, differently substituted triphos derivatives were synthesized and tested in the amide reduction as published by Klankermayer, Leitner and co-workers.

4.2.1 Synthesis of Triphos Derivatives

Aiming to produce a library of differently substituted triphos ligands with various electronic properties, six triphos derivatives **71**-**76** were targeted following a modified literature procedure (Scheme 15).[151] Initially, the respective aryl bromide was reacted with diethyl phosphite *via* a Grignard reaction to give the diarylphosphine oxides **71-*a*** to **76-*a***. Subsequent reduction of the phosphine oxide to the corresponding diarylphosphines **71-*b*** to **76-*b*** was conducted using pinacolborane (HBpin) instead of aluminum hydrides ($LiAlH_4$ or DIBAL-H) applied by Klankermayer and Leitner due to the simplified work-up. In the end, the phosphine was deprotonated and treated with 1,1,1-tris(bromomethyl)ethane (**77**, tribromide) to afford triphos **71**-**76**. The triphos products were then crystallized from toluene and pentane, respectively.

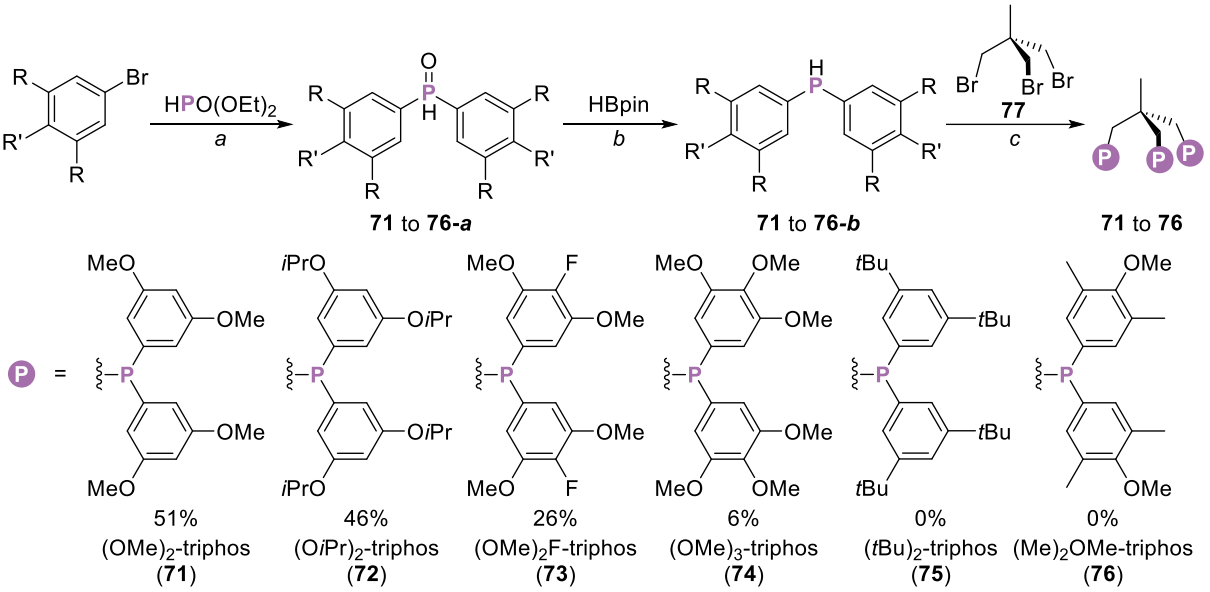

Scheme 15. Synthesis of differently substituted triphos structures. Reaction conditions: *a*) aryl bromide (3.0 equiv.), Mg (3.3 equiv.), THF (1.5 M), rt, o/n; *then* diethyl phosphite (1.0 equiv.), rt, 1 h; *b*) diarylphosphine oxide (1.0 equiv.), pinacolborane (2.5 equiv.), MeCN (0.2 M), 60 °C, o/n; *c*) diarylphosphine (3.2 equiv.), KOtBu (3.2 equiv.), tribromide (1.0 equiv.), DMSO (0.1 M), rt, o/n.

Following the described procedure, sterically hindered $(OMe)_2$-triphos (**71**) and $(OiPr)_2$-triphos (**72**) were synthesized in three steps in 51% and 46% overall yield, respectively. Analogously, the more electron-deficient $(OMe)_2F$-triphos (**73**) and the more electron-rich $(OMe)_3$-triphos (**74**) were obtained in lower overall yields of 26% and 6%, respectively.

The synthesis of $(tBu)_2$-triphos (**75**) yielded an inseperable mixture of compounds. For $(Me)_2OMe$-substituted phosphine (**76-*b***), no formation of triphos derivative **76** was observed when the tribromide (**77**) was added. A single product was isolated in 24% yield after crystallization from toluene and pentane (Figure 12).

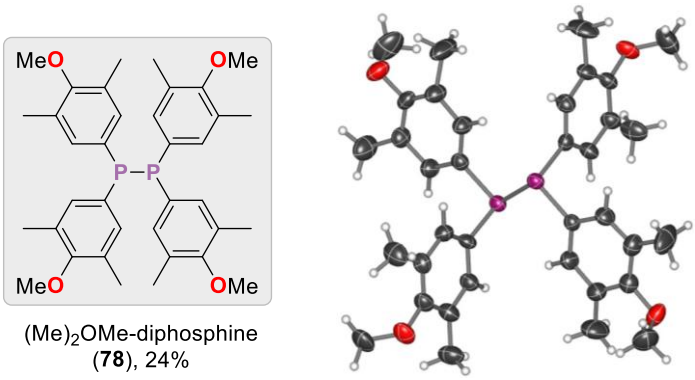

Figure 12. X-ray structure of $(Me)_2$OMe-diphosphine (**78**). Color code: black (C), red (O), purple (P). Selected interatomic distances [Å]: P1-P2 2.231.

First, the compound was analyzed by NMR spectroscopy. Even though the ^{31}P NMR shift was comparable to a typical triphos signal, no signals were found in the ^{1}H and ^{13}C NMR spectra that could be assigned to the backbone. Indeed, X-ray crystallography of the crystals revealed the formation of tetrakis(3,5-dimethyl-4-methoxyphenyl)diphosphine ($(Me)_2$(OMe)-diphosphine, **78**) instead of the respective $(Me)_2$OMe-triphos (**76**). The P–P distance was 2.231 Å. This was in line with the bond length of a P–P single bond, as reported by Pyykkö and Atsumi.[154] A similar structure was already known for alkylphosphines, since Burk and Harlow reported on this kind of P–P coupling during a reaction of the trichloride with dimethylphospholane in 1990.[155] It was assumed that the mechanism proceeded *via* a metal halogen exchange with the deprotonated phospholane (Scheme 16).[156]

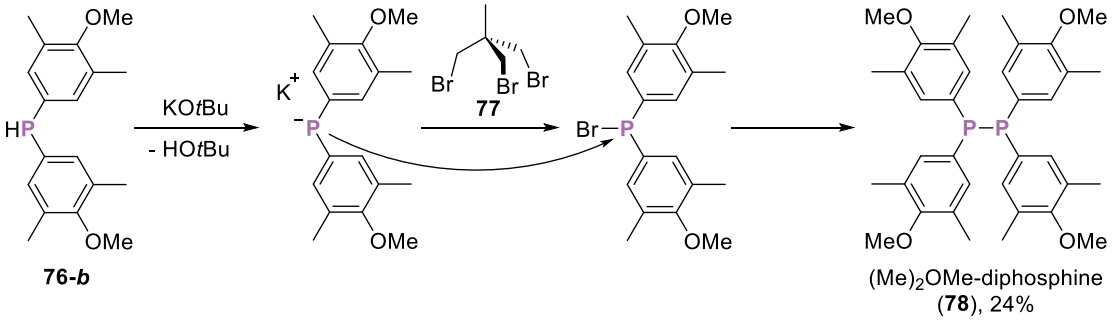

Scheme 16. Proposed formation of diphosphine **78**.

In summary, four differently substituted triphos derivatives (**71**-**74**) were synthesized, having various steric and electronic characteristics. Additionally, diphosphine **78** was synthesized and characterized by NMR spectroscopy and X-ray crystallography. These new ligands were then tested in the homogeneous hydrogenation of *N*-hexylhexanamide (**69**) as a model for PA6.

4.2.2 Optimization using N-Hexylhexanamide as Model Substrate

The reaction conditions were optimized by screening the reaction conditions including the applied metal precursor, acid, ligand, and solvent. Hexanol, hexylamine, hexanenitrile, and trihexylamine were detected as side products. Nevertheless, the yields of the side products were omitted for clarity (for complete screening tables including all side products, see Experimental Section). Initially, the original reaction reported by Klankermayer and Leitner was reproduced. For this, *N*-hexylhexanamide (**69**), $(OMe)_2$-triphos (**71**), the metal precursor $Ru(COD)(TMM)_2$, and the Lewis acid BCF were dissolved in dry THF. The reaction mixture was placed in an autoclave and pressurized with 100 bar of hydrogen before it was heated to 160 °C for 18 h (Scheme 17).

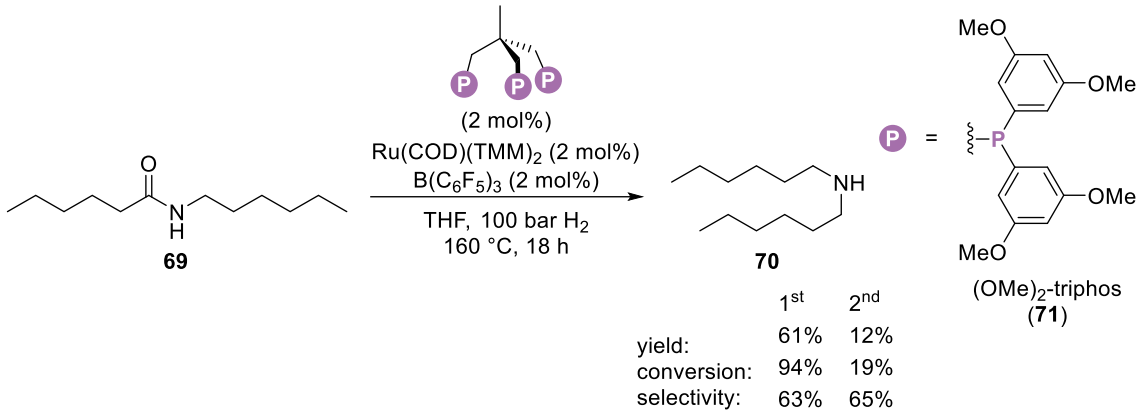

Scheme 17. Reproduction of the original reaction conditions for the hydrogenation of *N*-hexylhexanamide, as claimed by Klankermayer and Leitner.[151]

The original reaction had so far only been claimed by Klankermayer and Leitner in a patent.[151] However, it became evident that the outcome was difficult to reproduce. In two independent experiments, dihexylamine (**70**) was formed in 61% and 12% yield, respectively. Likewise, the conversion amounted to 94% and 19%, respectively. In contrast, the selectivity towards the desired product **70** remained the same, numbering 63% and 65%. Nevertheless, the optimization was continued, and the obtained data was checked against both reference experiments (labeled as ref) without deviations to maintain the comparability. The reported results are depicted below colored in red (Table 13). First, different ruthenium sources were screened. The screening included mostly Ru(II) complexes to maintain the comparability to the patented reaction conditions. As an exception, $Ru(acac)_3$ was also tested.

Table 13. Screening of ruthenium precursors for the hydrogenation of *N*-hexylhexanamide (**69**).

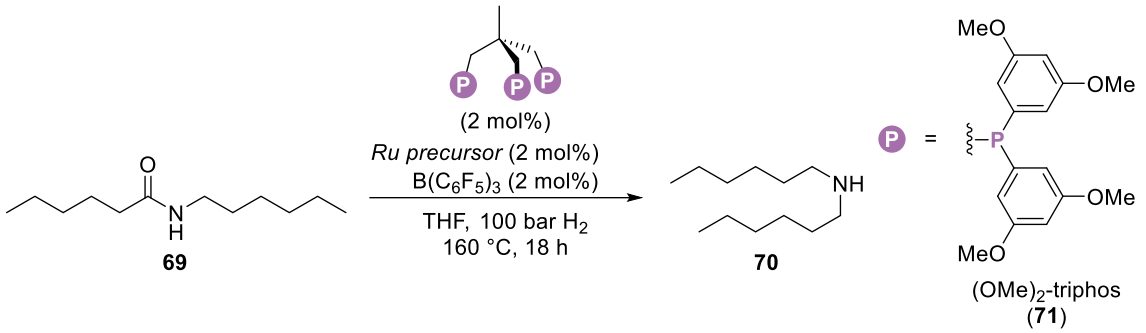

entry	metal precursor	yield[a] (conversion)
ref	$Ru(COD)(TMM)_2$	61% (94%)
ref	$Ru(COD)(TMM)_2$	12% (19%)
1	$Ru(TMM)((OMe)_2$-triphos) (**79**)	54% (79%)
2	$Ru(acac)_3$	15% (15%)
3	$Ru(H)_2(PPh_3)_4$	29% (29%)
4	$Ru(H)_2(PPh_3)_3(CO)$	-- (--)
5	$RuCl_2(PPh_3)_4$	-- (--)
6	$[RuCl_2(COD)]_n$	-- (--)
7	$[RuCl_2(p\text{-cymene})]_2$	-- (--)
8	Ru-MACHO	-- (--)
9	Ru-MACHO-BH	-- (--)

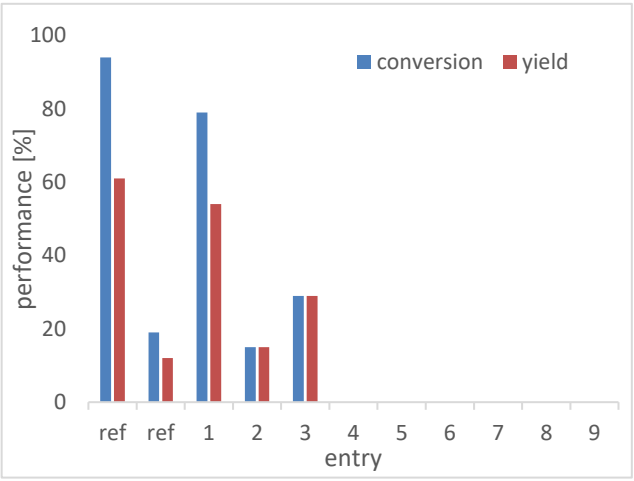

[a] Yield and conversion were determined by calibrated GC using mesitylene as internal standard.

When applying pre-synthesized [Ru(TMM)((OMe)$_2$-triphos)] (**79**), as the researchers did in the patent, a comparable yield of 54% was obtained as with the formation of the complex *in situ* (Table 13, entry 1). The ruthenium precursors [Ru(acac)$_3$] and [Ru(H)$_2$(PPh$_3$)$_4$] showed a decreased conversion but a very high selectivity towards the dialkylamine product (entries 2 and 3). Unfortunately, it was equally difficult to reproduce these data. Attempts to isolate the respective active triphos complexes failed because neither precursor reacted cleanly with the ligand when heated in toluene. Additionally, structurally similar Ru(H)$_2$(PPh$_3$)$_3$(CO), RuCl$_2$(PPh$_3$)$_4$, [RuCl$_2$(COD)]$_n$, and [RuCl$_2$(*p*-cymene)]$_2$ were applied in the hydrogenation of amide **69**. Neither of the metal precursors led to the formation of amine **70** (entries 4-7). Both Ru-MACHO complexes, that had been successfully applied in literature to hydrogenate lactams[157], did not convert *N*-hexylhexanamide (**69**) under the applied conditions (entries 8 and 9).

The screening of metal precursors was followed by the screening of appropriate solvents (Table 14). Initially, the influence of the water content of THF was investigated. Then, THF was exchanged for other ethers but also for polar aprotic solvent DMSO and the alcohols *m*-cresol and ethylene glycol.

Table 14. Solvent screening for the hydrogenation of *N*-hexylhexanamide (**69**).

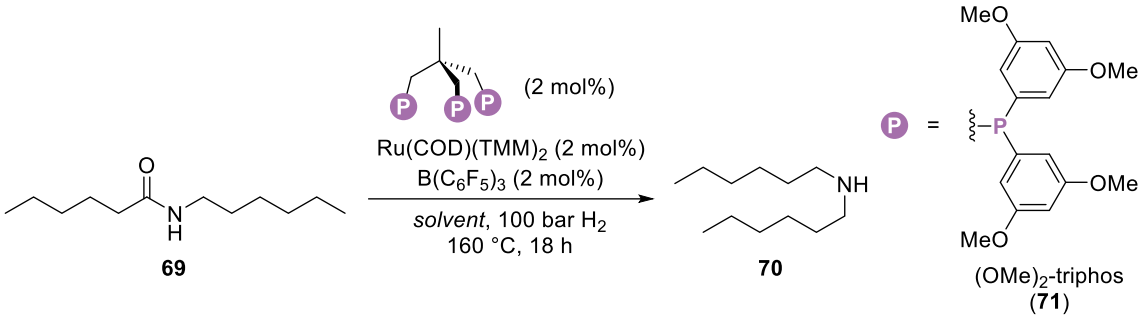

69 **70** (OMe)$_2$-triphos (**71**)

entry	solvent	yield[a] (conversion)
ref	THF	61% (94%)
ref	THF	12% (19%)
1	THF[b]	19% (22%)
2	THF[c]	42% (46%)
3	*n*-Bu$_2$O	-- (5%)
4	DMSO	-- (--)
5	*m*-cresol	-- (--)
6	Bu-O$_3$-Bu	40% (53%)
7	ethylene glycol	-- (8%)

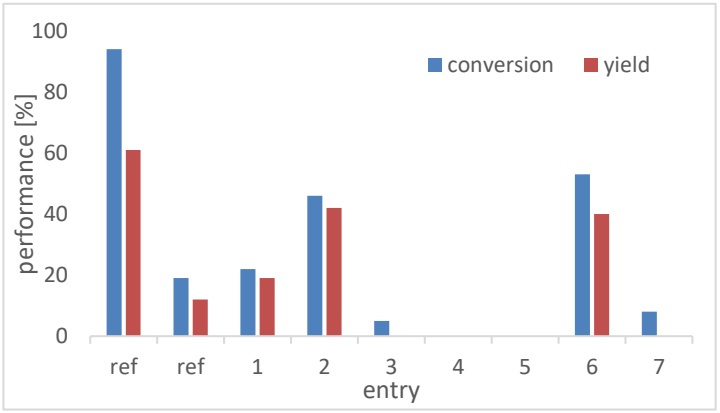

[a] Yield and conversion were determined by calibrated GC using mesitylene as internal standard. [b] Water (5.0 equiv.) was added. [c] Molecular sieves were added.

Increasing the water content of THF by adding extra water (5.0 equiv.) was observed to decrease the yield of amine **70** (entry 1). This was in line with the postulated reaction mechanism, where water was formed during the reaction but was also capable of cleaving the amide bond.[144] In contrast, adding molecular sieves to the reaction afforded the hydrogenated product in 42% yield (entry 2). While DMSO was utilized for the hydrogenative depolymerization of nylons, as demonstrated by Milstein and co-workers[143], it inhibited the investigated reaction completely (entry 4). This is in line with the deactivating effect of DMSO on Ru, as stated by Zhou *et al*. in 2021.[158] Neither of the tested alcohols *m*-cresol and ethylene glycol converted amide **69** (entries 5 and 7). Interestingly, THF could be exchanged for butyl diglyme (Bu-O$_3$-Bu) but not for dibutyl ether (entries 3 and 6). The advantage of using butyl diglyme was its high boiling point of 255 °C, which was above the reaction temperature and even above the melting point of PA6.[159] Furthermore, structurally similar diglyme, bearing two methyl groups instead of butyl groups, was known to be a better solvent for nylon-6 than THF.[143] Diglyme itself was not tested. However, due to the price of Bu-O$_3$-Bu, the optimization was continued with THF whereas butyl diglyme was later used for the hydrogenation of polyamide-6.

The previously synthesized, novel triphos ligands **71**-**74** and diphosphine **78** were screened next. Additionally, a few triphos ligands known in literature were tested (Table 15).

Table 15. Screening of ligands for the hydrogenation of *N*-hexylhexanamide (**69**).

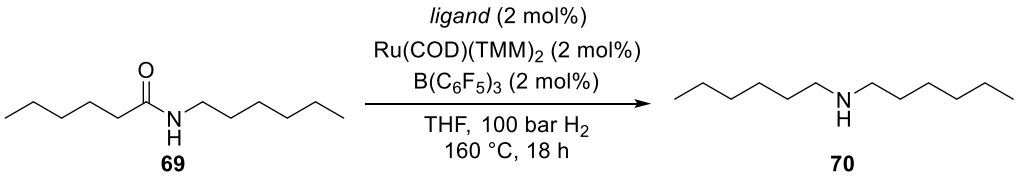

entry	ligand	yield[a] (conversion)
ref	$(OMe)_2$-triphos (**71**)	61% (94%)
ref	$(OMe)_2$-triphos (**71**)	12% (19%)
1	$(OiPr)_2$-triphos (**72**)	8% (11%)
2	$(OMe)_2$F-triphos (**73**)	10% (10%)
3	$(OMe)_3$-triphos (**74**)	-- (--)
4	$(Me)_2$OMe-diphos (**78**)	-- (--)
5	$(Me)_2$-triphos	39% (68%)
6	Me-triphos	-- (--)
7	CF_3-triphos	-- (--)
8	triphos	-- (--)
9	P(*n*-octyl)$_3$	-- (--)

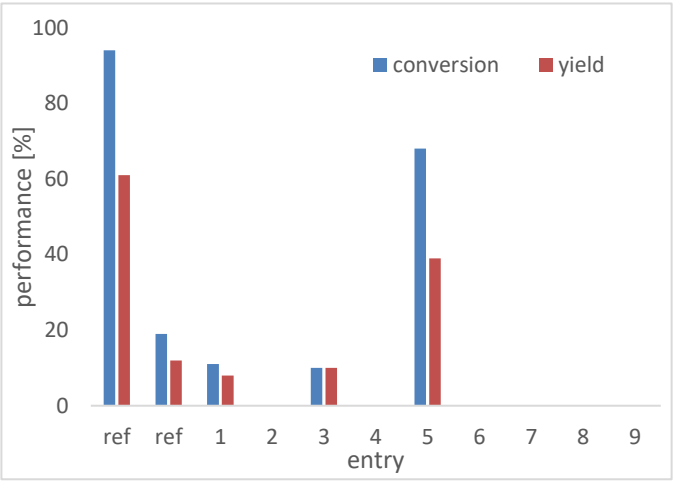

[a] Yield and conversion were determined by calibrated GC using mesitylene as internal standard.

Sterically demanding (O*i*Pr)$_2$-triphos (**72**) selectively gave the product **70** in 8% yield (entry 1). Additional substituents in *para*-position altered the $(OMe)_2$-triphos ligands' electronic properties. While electron-poor ligand **73** led to 10% yield of product **70** (entry 2), electron-rich ligand **74** inhibited the reaction completely (entry 3). The same applied to diphosphine **78** (entry 4). $(Me)_2$-triphos, having a lower steric bulk than $(OMe)_2$-triphos (**71**), yielded the product in 39% (entry 4). Furthermore, amide **69** was not converted in the presence of *para*-substituted Me-triphos, CF_3-triphos, and unsubstituted triphos, which do not have any steric bulk. Commercially available monodentate P(*n*-octyl)$_3$ gave no product either. In conclusion, steric bulk seemed to be essential to the reaction. Tridentate phosphine ligands were supporting the reaction better than bi- or monodentate phosphines.

Finally, different Lewis and Brønsted acids were screened. An acidic co-catalyst is generally needed for the activation of the amide and of the ruthenium catalyst by removing the TMM ligand and creating a free coordination site while stabilizing the cationic active complex (Table 16).[160]

Table 16. Acid screening for the hydrogenation of *N*-hexylhexanamide (**69**).

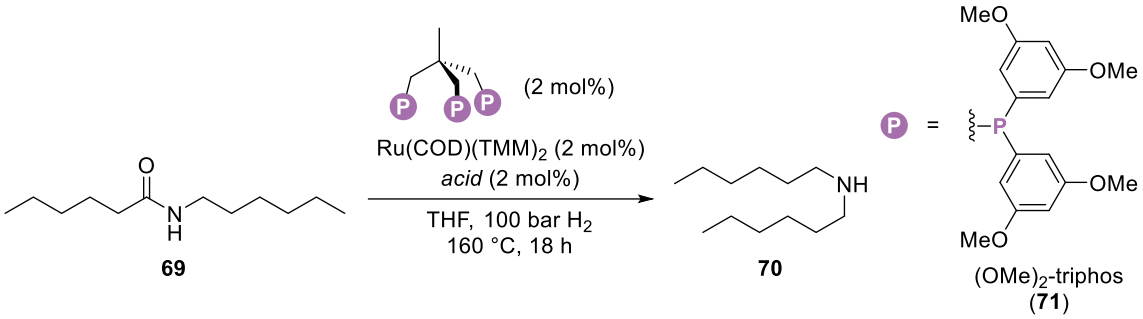

entry	acid	yield[a] (conversion)
ref	$B(C_6F_5)_3$	61% (94%)
ref	$B(C_6F_5)_3$	12% (19%)
1	*p*TSA*H_2O	50% (83%)
2	MSA	-- (--)
3	formic acid	-- (22%)
4	$HNTf_2$	54% (87%)
5	$Al(OTf)_3$	21% (28%)
6	$Yb(OTf)_3$	55% (64%)
7	$Hf(OTf)_4$	45% (62%)
8	AgOTf	12% (13%)
9	$ZnCl_2$	-- (--)
10	TMSOTf	-- (--)

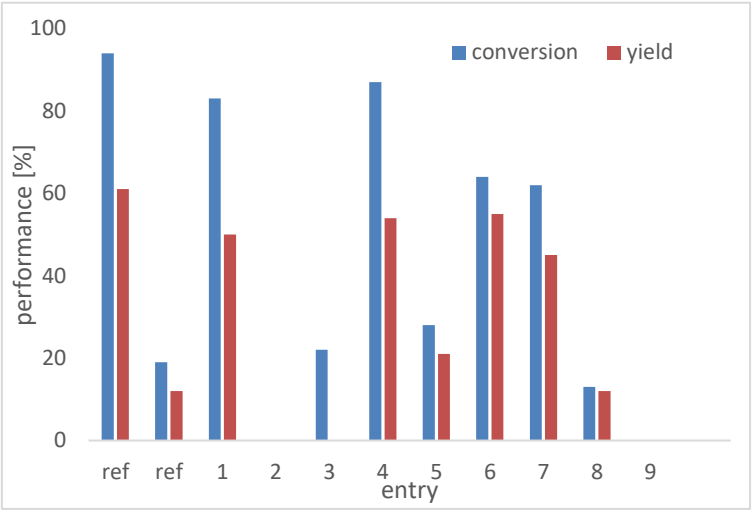

[a] Yield and conversion were determined by calibrated GC using mesitylene as internal standard.

In the present reaction, BCF could be replaced by the Brønsted acid *p*-toluenesulfonic acid monohydrate (*p*TSA*H_2O), hydrogenating the amide to the secondary amine in 50% yield but rather unselectively (entry 1). Surprisingly, the reaction did not preceed with the related derivative methanesulfonic acid (MSA) (entry 2). The same applied to formic acid (entry 3). The so-called superacid bistriflimidic acid ($HNTf_2$), on the other hand, gave the desired product **70** in 54% yield (entry 4). Likewise, Lewis acids such as triflate (OTf) salts yielded the amine **70** selectively, although the yields were lower compared to the standard conditions (entries 5-8). Applying the Lewis acids $ZnCl_2$ or TMSOTf did not lead to the formation of dihexylamine (**70**, entries 9 and 10).

To get more insights into the reaction mechanism, 0.5 equivalents *n*-octylamine were added to the reaction mixture under otherwise unaltered conditions (Scheme 18).

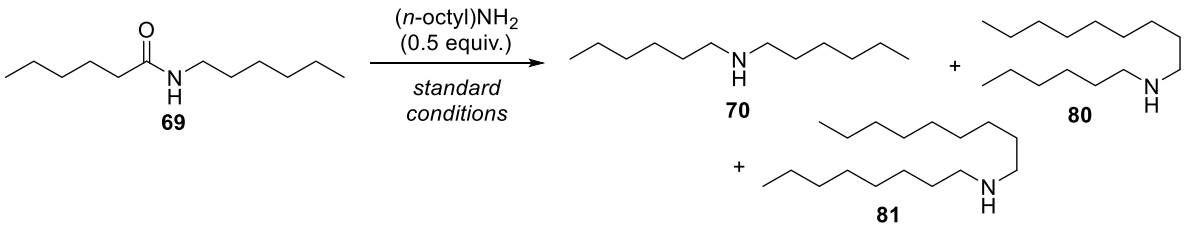

Scheme 18. Mechanstic investigation using *n*-octylamine.

Interestingly, the addition of *n*-octylamine led to equimolar amounts of dihexylamine (**70**), hexyloctylamine (**80**), and dioctylamine (**81**). This underlined the proposed reaction mechanism, which proceeded *via* C–N cleavage, and confirmed the assumption that the condensation of two primary amines is also possible under the standard reaction conditions.

The solubility of PA6 in THF and in butyl diglyme is low. Therefore, the screening of the reaction conditions was repeated in hexafluoro-*iso*-propanol (HFIP) as the solvent (Table 17). Being able to separate polymer chains from each other due to its strong H-bonding, HFIP is apt to dissolve polymers.[161] Even though HFIP is a costly solvent (min. 267 €/l)[162], recycling of the alcohol by distillation decreases the total costs of the reaction when performed on big scale.[163]

Table 17. Screening of metal precursors for the hydrogenation of *N*-hexylhexanamide (**69**) in HFIP.

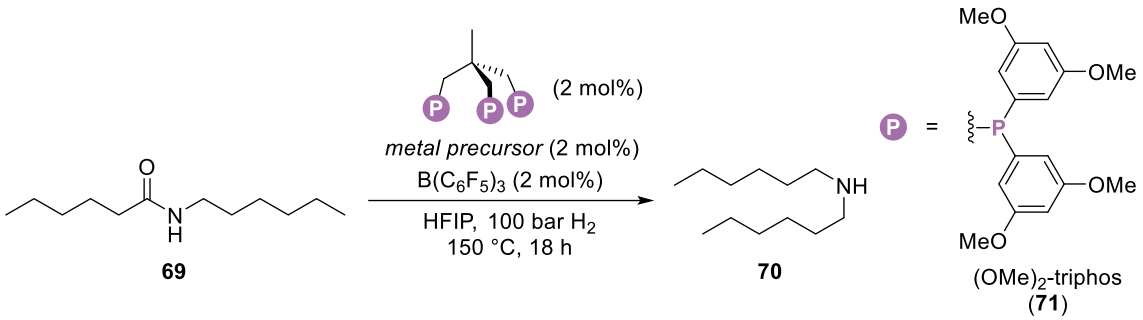

entry	metal precursor	comment	yield[a] (conversion)
1	$Ru(COD)(TMM)_2$	--	61% (86%)
2	$Ru(COD)(TMM)_2$	--	53% (100%)
3	$Ru(COD)(TMM)_2$	60 bar H_2	61% (100%)
4	$Ru(COD)(TMM)_2$	120 °C	21% (26%)
5	$Co(NTf_2)_2$	--	-- (12%)
6	$Co(NTf_2)_2$	no acid	-- (24%)
7	$Co(BF_4)_2(H_2O)_6$	--	-- (20%)
8	$Co(BF_4)_2(H_2O)_6$	no acid	-- (14%)
9	$Co(acac)_3$	--	-- (15%)

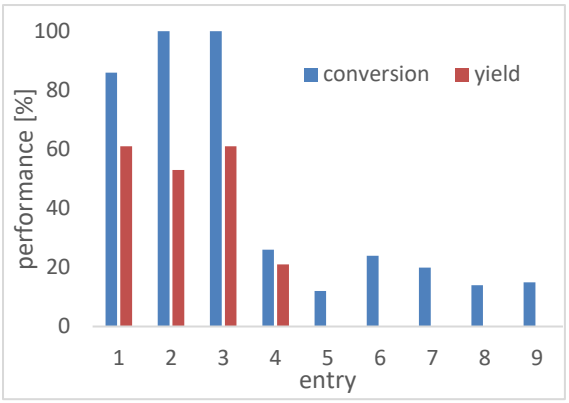

[a] Yield and conversion were determined by calibrated GC using mesitylene as internal standard.

Encouragingly, using HFIP as solvent led to reproducible yields, as the yields of two experiments only differed in 8% (entries 1 and 2). In HFIP, the only detectable side product was trihexylamine. A general investigation of the reaction conditions revealed that it was possible to decrease the pressure needed to 60 bar while the yield was maintained at 61% with full conversion of the starting material (entry 3). Notably, reducing the temperature to 120 °C led to a reduced yield of 21% (entry 4). Additionally, several metal precursors were screened. In literature, cobalt is used as a more sustainable alternative to ruthenium.[160] However, no product was formed, neither with nor without BCF as acidic additive (entries 5-9).

Next, the newly synthesized triphos ligands **71**-**74** were tested again in HFIP (Table 18).

Table 18. Ligand screening for the hydrogenation of *N*-hexylhexanamide (**69**) in HFIP.

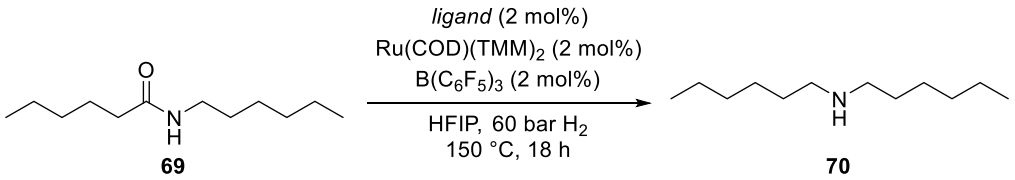

entry	ligand	yield[a] (conversion)
ref	$(OMe)_2$-triphos (**71**)	61% (100%)
1	$(OiPr)_2$-triphos (**72**)	18% (37%)
2	$(OMe)_2$F-triphos (**73**)	-- (39%)
3	$(OMe)_3$-triphos (**74**)	-- (20%)
4	$(Me)_2$-triphos	40% (100%)
5	OMe-triphos	21% (64%)
6	Me-triphos	-- (51%)
7	triphos	-- (32%)

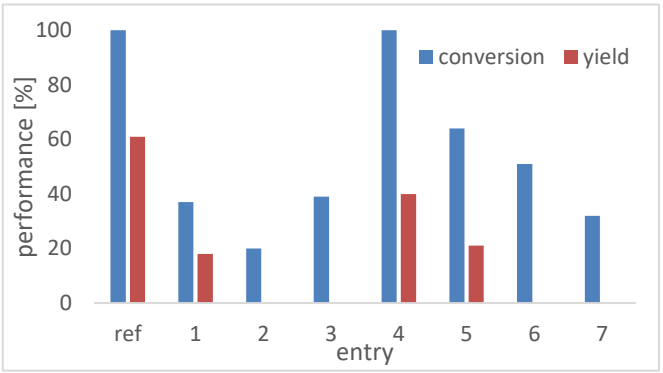

[a] Yield and conversion were determined by calibrated GC using mesitylene as internal standard.

The ligand screening gave very similar results to the screening performed in THF. $(OMe)_2$-triphos (**71**) could be exchanged for other sterically hindered triphos derivatives, even though the hydrogenation of amide **69** became less successful. Applying a triphos derivative with an increased steric bulk, like (O*i*Pr)$_2$-triphos (**72**), gave the amine **70** in 18% yield (entry 1). When a triphos derivative with a decreased steric bulk is applied, like $(Me)_2$-triphos, the amine **70** was detected in 40% yield while full conversion of the amide **69** (entry 4). Altering the electronic properties by introducing a substituent in *para*-position did not allow the formation of amine **70** (entries 2 and 3). Surprisingly, the application of sterically unhindered but electron-rich OMe-triphos gave amine **70** in 21% yield (entry 5). Using Me-triphos or unsubstituted triphos did not support the hydrogenation reaction (entries 6 and 7).

Based on the results obtained from the first screening of acids conducted in THF, various Brønsted acids were tested next in HFIP (Table 19). Since BCF is commonly used in Ru-catalyzed hydrogenation reactions, mainly other boron-based additives were chosen for the screening.

Table 19. Screening of acids for the hydrogenation of *N*-hexylhexanamide (**69**) in HFIP.

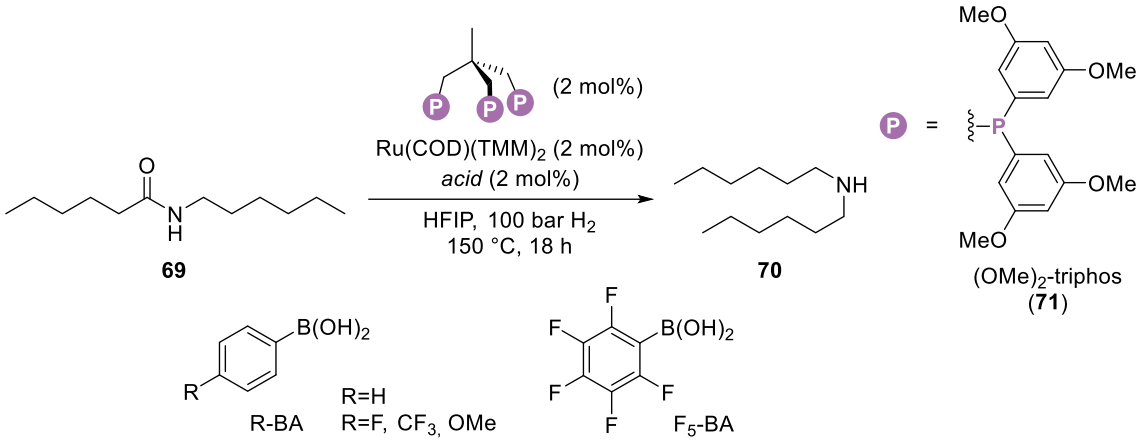

entry	acid	yield[a] (conversion)
ref	$B(C_6F_5)_3$	61% (100%)
1	*p*TSA*H_2O[b]	-- (40%)
2	$B(OH)_3$[c]	55% (75%)
3	BA	55% (75%)
4	BA[b]	60% (89%)
5	F-BA[b]	43% (71%)
6	CF_3-BA[b]	-- (18%)
7	F_5-BA[b]	61% (94%)
8	OMe-BA[b]	24% (38%)

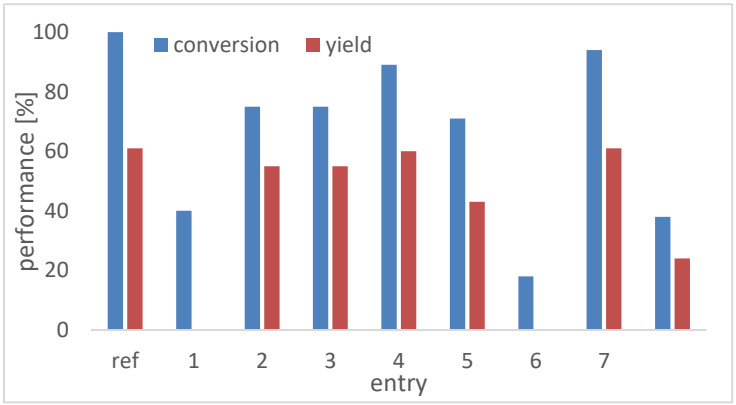

[a] Yield and conversion were determined by calibrated GC using mesitylene as internal standard. [b] 4 mol% of the acid were used. [c] $B(OH)_3$ (5 mol%) was used.

Differently to the first acid screening in THF, the use of *para*-toluenesulfonic acid did convert the starting material **69** but did not lead to any product formation (entry 1). The reaction gave comparable yields though when boric acid or phenylboronic acid (BA) were used, affording amine **70** in 55% and 60% yield, respectively (entries 2-4). The selectivity was even better than with BCF. Surprisingly, electron-deficient *para*-fluorophenylboronic acid (F-BA) and *para*-(trifluoromethyl)phenylboronic acid (CF_3-BA) yielded the product **70** in a decreased yield of 43% or not at all (entries 5 and 6), while perfluorophenylboronic acid afforded amine **70** in 61% yield (entry 7). The product **70** was detected in a decreased yield of 24%, when electron-rich *para*-methoxyphenylboronic acid (OMe-BA) was used (entry 9).

In summary, similar trends were observed when performing the hydrogenation of *N*-hexylhexanamide in THF and in HFIP. The patented combination of $Ru(COD)(TMM)_2$ and $(OMe)_2$-triphos worked best, whereas the Lewis acid BCF could be replaced by substituted phenylboronic acids or boric acid. In comparison with the THF-based system, the reaction in HFIP was more robust. The required hydrogen pressure was reduced from 100 bar to 60 bar. The reaction temperature of 150 °C proved necessary.

4.2.3 Reduction of Nylon

Because the strong hydrogen bonding in nylon-6 and in the reduced polyamine makes the polymers hardly soluble in common organic solvents and thus challenging to analyze, the success of the hydrogenation reaction is challenging to quantify. In protein synthesis, the Kaiser test is a common method to investigate the presence of free amino groups.[164] This colorimetric analysis relies on the transformation of ninhydrin (**82**) into Ruhemann's blue (**83**) by the condensation reaction with a primary amine. It is also applied in forensic chemistry to detect fingerprints.[165] Due to its high sensitivity also towards free secondary amino groups, forming a blue pigment similar to Ruhemann's blue (**83**), it was chosen herein as a potential analytical test for quantitative analysis (Scheme 19).[166]

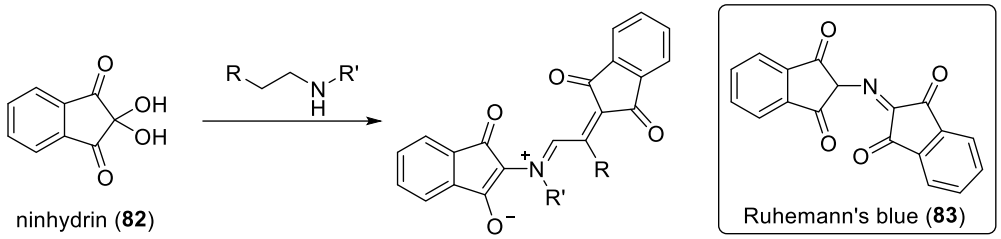

Scheme 19. Reaction of ninhydrin (**82**) with secondary amines next to 2-(1,3-dioxoindan-2-yl)iminoindane-1,3-dione, also known as Ruhemann's blue (**83**).[166]

Additionally, IR was chosen as a method to identify potential carbonyl groups present after the reaction. The characteristic C=O stretching frequency of the amide group was expected to vanish while the N–H band of the corresponding amine should increase. However, preliminary tests showed that the results of the Kaiser test did not correspond to the results of the IR analysis and led to an overestimation of the success of the reaction. This is explained by the fact that a bigger part of the sample is analyzed by IR spectroscopy *via* radiation slightly penetrating the material whereas only the surface of the solid nylon sample, where hydrogenation might have partly happened, is examined by the Kaiser test. Furthermore, the Kaiser test is influenced by side reactions and by hydrolytic, oxidative, and photolytic instability.[167] Therefore, all future samples were exclusively analyzed by IR. The spectra were then compared with the IR spectra of nylon-6 and the corresponding polyamine, as obtained from the stoichiometric reduction (Figure 13).

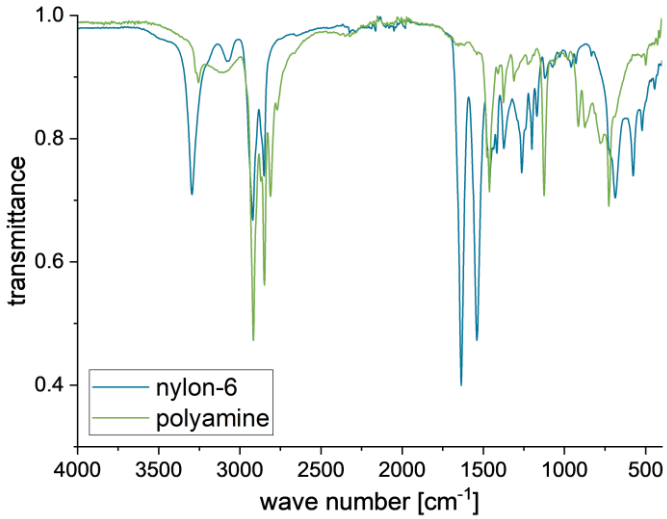

Figure 13. IR spectra of nylon-6 (blue) and the corresponding polyamine (green).

The optimized conditions were employed on different nylon-6 samples in THF or butyl diglyme, respectively. The polymer used was either cut into small pieces with scissors or reprecipitated from hot DMSO to create a bigger surface area. However, the external appearance of all PA6 samples remained unaltered after they had been filtered off, washed with EtOAc, water, and MeOH, and dried. Furthermore, no change of the IR bands was observed. Therefore, additional reagents were required to support the dissolving or at least swelling of the polymer. Chaotropic additives are known to break the hydrogen bonding, e.g., in aqueous systems.[168] Since polyamides also show strong H-bonding resulting in a decreased solubility, those additives may support dissolving these types of polymers. Thus, a selection of chaotropic agents was applied in another screening (Table 20).

Table 20. Screening of chaotropic additives for the hydrogenation of nylon-6.

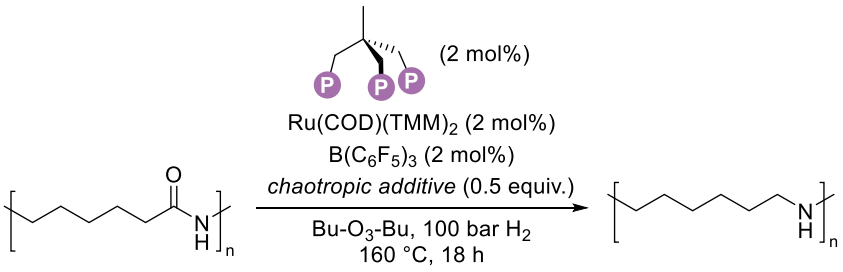

entry	chaotropic additive	yield[a]
1	LiCl	n.d.
2	$MgCl_2$	n.d.
3	SDS	n.d.
4	GHC	n.d.
5	urea	n.d.
6[b]	--	n.d.

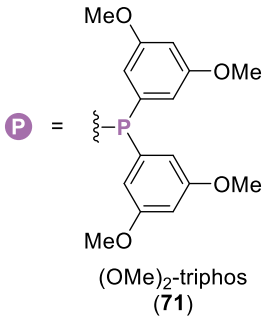

$(OMe)_2$-triphos (**71**)

[a] Yield was determined by IR spectroscopy. [b] HFIP was used as the solvent under a decreased pressure of 60 bar H_2.

The screening included salts like LiCl, $MgCl_2$, sodium dodecyl sulfate (SDS), and guanidinium hydrochloride (GHC) as well as urea. Unfortunately, no reduced product was observed in the IR spectra recorded after the reaction (entries 1-5). When the hydrogenation reaction was performed under optimized conditions in HFIP at 60 bar, no change of the respective bands in the IR spectrum was observed either, although the starting material was completely dissolved. It was recovered after the reaction by removing HFIP *in vacuo* and then adding EtOAc, which precipitated the compound and allowed to isolate the thin polymeric film with tweezers (entry 6).

However, as many literature procedures for chemical recycling of polyamides require harsher conditions with temperatures above their melting points, another reaction was run over 2 days applying a reaction temperature of 240 °C (Scheme 20). Due to the increased temperature, the high-boiling solvent Bu-O_3-Bu and a glassy stirring bar were chosen. For safety reasons, the initial hydrogen pressure was lowered to 85 bar.

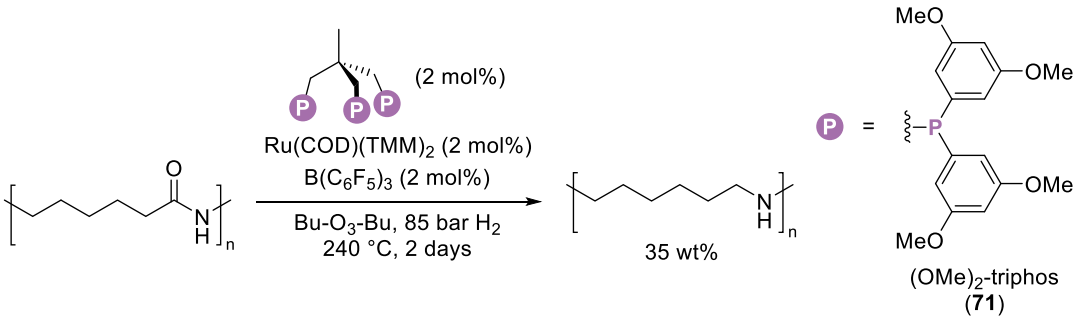

Scheme 20. Nylon hydrogenolysis at increased temperature.

A jelly-like solid was separated from the reaction mixture by filtration, dried, and analyzed by IR (Figure 14). The mass of the gel amounted to 35 wt% of the starting material.

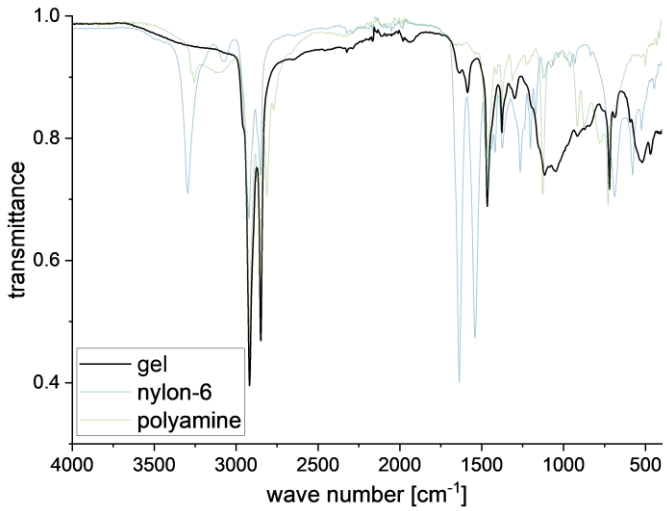

Figure 14. IR spectrum of the gel obtained from the hydrogenation reaction at 240°C (black) compared to the IR spectra of nylon-6 (blue) and the corresponding polyamine (green).

The IR spectrum of the gel contained only minor C=O vibrations, hinting towards a successful hydrogenation of the polymer. Interestingly, no increased N–H vibration was observed either. This suggested cross-linking of the polymer chains, resulting in tertiary amine motives. To support this assumption, the gel was further analyzed by mass spectrometry using matrix-assisted laser desorption/ionization (MALDI) and a time-of-flight (TOF) detector (Figure 15).

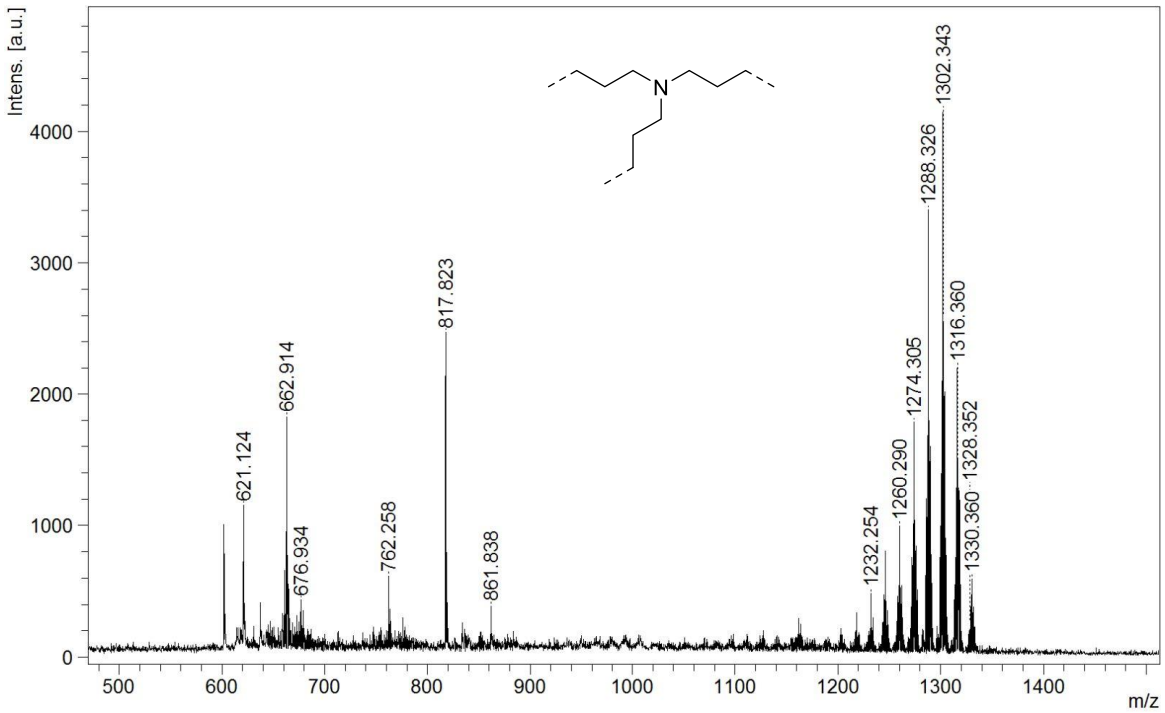

Figure 15. MALDI-TOF spectrum of the gel obtained from the hydrogenation reaction at 240 °C using a 2-(4-hydroxyphenylazo)benzoic acid (HABA) matrix. The MS was measured by Dr. Simon S. Pedersen.

The observed peaks between *m/z* 1204 and 1330 could be assigned to possible oligomeric structures, e.g., as depicted below (Figure 16).

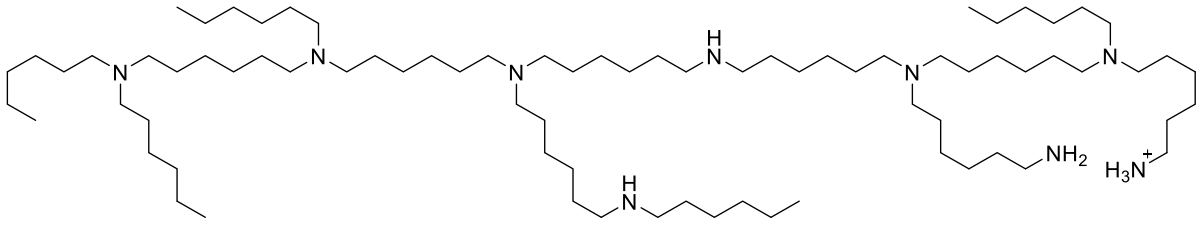

Figure 16. Possible oligomer with a molecular weight of 1232.26 g/mol.

However, multiple cross-linked structures were found to cause similar masses. Thus, no clear assumption on the constitution of the molecule can be drawn. Surprisingly, the gel was soluble in chloroform and therefore it was possible to record NMR spectra. However, the ^{1}H and ^{13}C NMR spectra did not solely support one of the suggested molecular structures. The absence of N–H signals in the ^{1}H NMR spectrum generally supported the theory of a cross-linked oligomer, while the lack of signals above 80 ppm in the ^{13}C NMR spectrum that could have been assigned to amide units confirms the absence of C=O vibrations in the IR spectrum.

The gel was further analyzed *via* TGA in collaboration with Dr. Simon S. Pedersen to investigate whether it was capable of capturing CO_2 (Figure 17). The resolution of the TGA curve is rather low due to the small sample size. The material captured around 1.8 wt% of CO_2, which equals 4.0 mol% and is around 4 CO_2 molecules per 100 monomer units. However, the gained mass was quickly lost when the gas was changed back to helium, indicating that carbon dioxide is loosely bound by physisorption rather than by chemisorption.

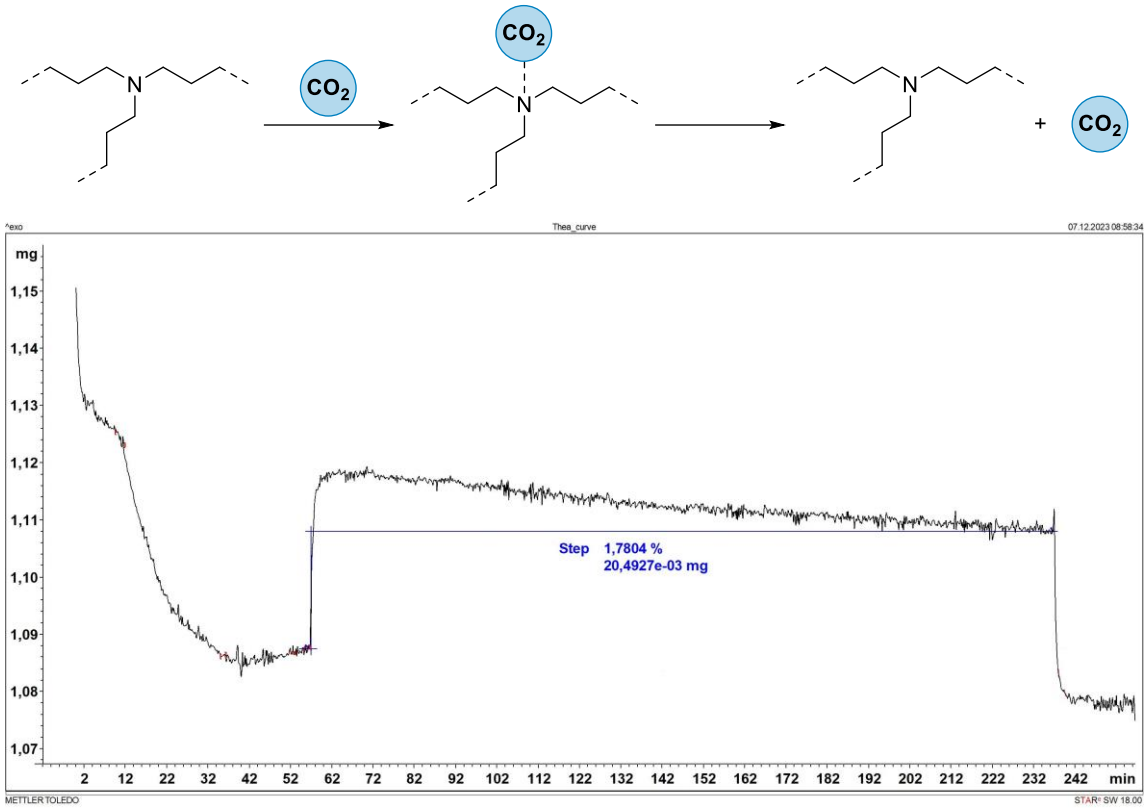

Figure 17. TGA graph of the gel while streaming 100% CO_2 over its surface for 3 h, recorded by Dr. Simon S. Pedersen.

Next to the jelly-like solid, also the liquid phase of the reaction was investigated. Due to the high-boiling solvent, rendering it difficult to be removed, no IR or NMR analysis was possible. In the MALDI-TOF-MS, however, signals between *m/z* 580 and 779 were detected (Figure 18). Distances between two signals with $\Delta m/z$ = 14 pointed towards the successful reduction of an amide to an amine unit. Furthermore, distances between the signals with $\Delta m/z$ = 100 were found, which hinted at the loss of one amine repeating unit. Thus, it was assumed that the soluble fraction of this experiment contained semi-reduced oligomers with a degree of polymerization between 5 and 7 monomers.

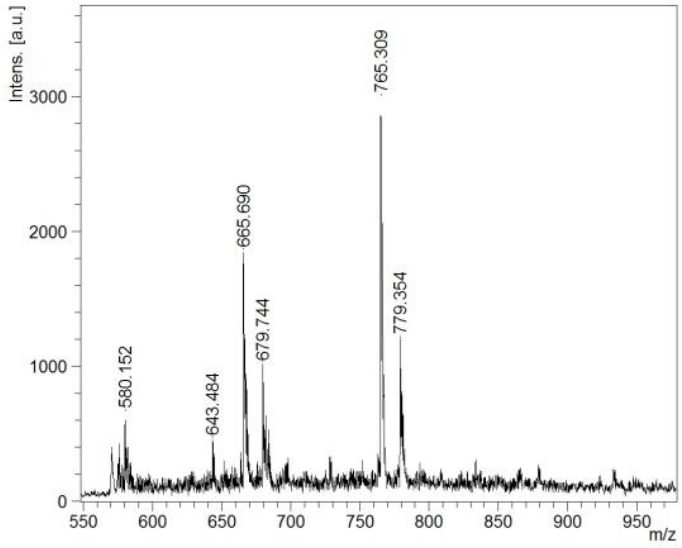

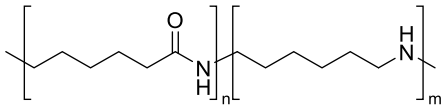

Figure 18. MALDI-TOF spectrum of the Bu-O_3-Bu solution after the hydrogenation reaction at 240 °C using a 2-(4-hydroxyphenylazo)benzoic acid (HABA) matrix. The MS was measured by Dr. Simon S. Pedersen.

In summary, the hydrogenation of secondary amides was investigated using *N*-hexylhexanamide (**69**) as a model system. The transfer of the optimized reaction conditions to nylon-6 samples was challenging and did not lead to satisfactory results in THF, Bu-O_3-Bu, or HFIP, although the latter solvent completely dissolved the polymer. The use of chaotropic agents did not improve the conversion of the polyamide. Solely the hydrogenation at elevated temperature above the melting point of nylon-6 yielded a reduced reaction product in 35 wt%. This oligoamine was examined by IR, NMR, and MS and assigned to different cross-linked structures with a low efficiency in CO_2 capture, as shown by TGA.

5 CO_2 Conversion by Transition Metal Catalysis

5.1 Introduction

Carbon dioxide is a rather inert molecule. Since the carbon atom is fully oxidized, most transformations require a reduction step. Albeit, the reduction potential of CO_2 is highly negative ($E_{1/2}^{red}$ = –2.21 V vs SCE in DMF).[169] At the same time, the C=O bond dissociation energy (BDE) is high (BDE = 750 kJ/mol) due to the three-center, four-electron-delocalized π-bonds.[13] Thus, the direct reduction is thermodynamically unfavored and has to be accomplished with the help of suitable catalysts or reagents.[169] Due to the structural rearrangement that is required for the geometric change of the linear molecule during a reaction, the transformation of CO_2 is also kinetically unfavored.[170] Additionally, the conversion of gaseous CO_2 is associated with a decrease in entropy that can render even an exothermic reaction unfeasible.[34] All in all, the transformation of thermodynamically stable CO_2 is not trivial and has been part of ongoing investigations for decades.

Despite all difficulties, researchers have developed a variety of protocols on how to utilize CO_2 as a chemical feedstock.[99, 171-172] When combined with amine-based carbon capture, the structural rearrangement has been overcome. This is due to formation of a carbamate species, which is no longer a linear molecule. Some of the procedures have already been implemented into CCU facilities, others are still conducted on a laboratory scale.

5.1.1 CO_2 Reduction to C_1 Compounds

The reduction to C_1 compounds is widely applied. Those compounds are common reagents in chemical transformations, serve as hydrogen storage materials, or are value-added compounds themselves (Scheme 21).

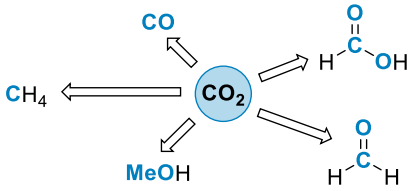

Scheme 21. C_1 chemicals synthesized from CO_2.

Carbon monoxide is the product of the one-electron reduction of CO_2. It can be produced by electrochemical CO_2 reduction reactions (eCO_2RR), by photochemical processes, or by thermal means.[173] A recent example for the photochemical CO_2 reduction to CO is the study of Rotundo *et al.* published in 2021.[174] They investigated the effect of different electronic and steric properties on the performance of a photoactive rhenium tricarbonyl complex. In comparison to the parent compound $Re(bipy)(CO)_3Cl$ (bipy = 2,2'-bipyridine), especially the *p*-aniline substituted complex showed an

improved UV-vis absorption. It was the same complex that showed the best photocatalytic performance in CO_2 reduction to CO, reaching a TON of 120 when substituted benzimidazole was used as the sacrificial reductant (Scheme 22).

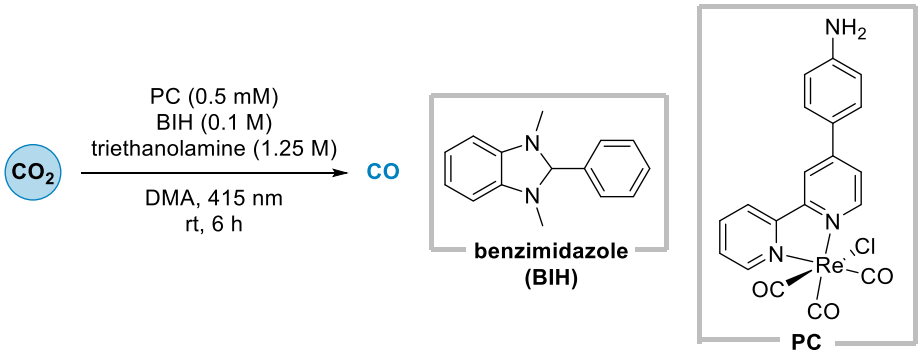

Scheme 22. Photomediated CO_2 reduction to CO.[174]

In contrast, CO is more efficiently formed in the eCO_2RR, reaching a Faradaic efficiency (FE) above 95%.[13] This was, for instance, achieved by Li *et al*. in 2023, who reported the selective electrolysis of CO_2 to CO catalyzed by an antimony copper alloy.[175] The introduction of Sb single atoms weakened the *CO binding strength on the surface of the electrode and lead to the selective and efficient desorption of CO. Generally, carbon monoxide is, *inter alia*, applied as a more reactive surrogate for inert CO_2.[176] Since CO can be produced in many ways, like the incomplete combustion of materials, it has a rather low market price.[177] The reduction of CO_2 to formic acid (FA) or formate is thermodynamically less favored than the reduction to CO due to the additional entropy decrease. The reaction can be achieved using a base and a catalyst, producing a compound with a hydrogen content of 4.4 wt% (Scheme 23).

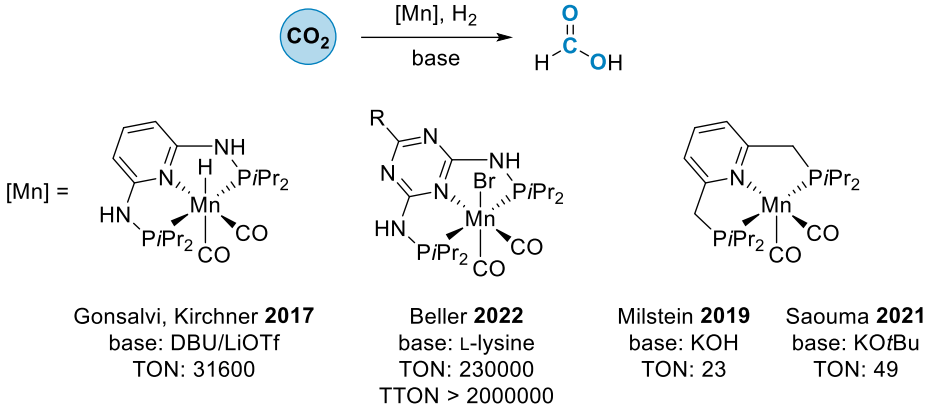

Scheme 23. Comparison of the Gonsalvi/Kirchner, Beller, and Milstein/Saouma manganese pincer complexes.[178-181]

Gonsalvi, Kirchner and co-workers have observed already in 2017 that formic acid can be produced with a high TON of 31600 by using a manganese pincer complex.[178] Very small catalyst loadings of 0.002 mol% were required. LiOTf was further used as the co-catalyst, as the presence of Li^+ cations enhanced the stability of crucial intermediates. The performance of the manganese catalyst was even

improved by Beller *et al.* in 2022 by exchanging the pyridine backbone by a triazine ring and additional promotion by the amino acid L-lysine.[179] They argued that the increased TON of 230000 was caused by deprotonation and dearomatization of the pincer ligand, thus leading to the active catalytic species. The total TON over ten runs exceeded 2 million albeit the formate yield decreased after each run. In contrast, the groups of Milstein and Saouma have shown that a PNN pincer ligand without amine bridges only produced formate with maximum TONs of 23 and 49, respectively.[180-181] In general, FA is the most value-added C_1 compound and applied as preservative agent, antibacterial agent, and hydrogen storage material.[177] Formaldehyde is industrially synthesized from methanol that is oxidized in air.[182] However, it can also be produced from CO_2 although it remains challenging to suppress the full reduction to methanol, which has a low energy barrier.[183] In 2023, Kim *et al.* reported a novel heterogeneous photocatalyst that was able to produce formaldehyde (259.1 µmol/g after 24 h) with 61% selectivity upon irradiation with visible light.[184] The researchers claimed that the synergic nature of their dual-atom-site catalyst having neighboring Sn(II) and Cu(II) ions caused the high selectivity towards formaldehyde from a CO_2-saturated $KHCO_3$ solution. While Sn/C_3N_4 was observed to favor the formation of formic acid, the introduction of 25% Cu(II) led to an enhanced reduction of FA to formaldehyde. The required protons and electrons were delivered by the TEA additive. Furthermore, methanol is a popular product from CO_2 reduction that is already commercially implemented into CCU facilities.[106] The reduction requires much energy (ΔH = 676 kJ/mol) if compared to photosynthesis (ΔH = 479 kJ/mol)[185] but generates a high-value product with a rather high market price due to its applications as gasoline additive and for formaldehyde and acetic acid production.[177] Interestingly, in 2022, Leitner and co-workers investigated the CO_2 hydrogenation to MeOH using a modified Ru-MACHO catalyst and dimethyl ethylenediamine.[186] By using *n*-decane as the solvent for the nonpolar catalyst, they found a multiphasic system where the polar products MeOH and water separated into a second phase. Through this self-separating catalytic system and the following removal of the product phase from the reaction systems, a high total TON of 19235 was achieved. The performance of this multiphasic system was among the highest known so far, rendering the method potentially interesting for industrial applications. However, recent research into the methanol production from CO_2 mainly focuses on the elaboration of mechanistic details that have remained unclear so far as many potential intermediates may be involved.[187] Finally, CO_2 can be reduced to methane that is, *inter alia*, used as a renewable fuel.[177] In 2023, McCarver and co-workers computationally examined the efficiency of MOF-74 doped with different metals in the eCO_2RR to methane.[188] They detected iron as a promising candidate for selective methane formation due to a strong binding affinity to possible reaction intermediates and a less favorable hydrogen reduction. Almost 100% selectivity to methane was also found by Xiong *et al.* in 2021.[189] The researchers investigated the photocatalytic hydrogenation of CO_2

with Ag_{25} clusters at 100 °C under irradiation with visible light (450 nm). Up to 29 µmol h^{-1} mg^{-1} methane was produced.

5.1.2 Reductive Homocoupling of CO_2 to C_{2+} Compounds

Research on the homocoupling of carbon dioxide is mainly conducted applying electrochemical methodologies. Among others, a wide variety of short-chain alkanes, alkenes and alcohols can be produced *via* eCO_2RR. These products can be summarized as synthetic fuels with C_2 or C_3 chains.[190-191] The reduction of CO_2 takes place *via* the intermediate *CO bound to the mostly heterogeneous catalysts, that subsequently reacts further to form various products. Next to homocoupled products, also undesired carbon monoxide can be formed, since the desorption of *CO is kinetically preferred.[190, 192] The heterogeneous catalyst OD-Cu (oxide-derived) is known as an excellent electrocatalyst in the synthesis of multi-carbon species.[193-194] However, catalysts of this type often yield product mixtures. In 2019, the group of Ager identified three different, product-specific active sites of OD-Cu using the carbon isotopes ^{12}C and ^{13}C.[195] By introducing $^{12}CO_2$ and ^{13}CO into the electrolyte solution in a 30:70 mixture – to ensure a comparable formation rate of $*^{12}CO$ and $*^{13}CO$ due to the different solubilities of the two gases – they were able to determine that the coupling products ethylene, ethanol/acetate, and *n*-propanol each had different isotope ratios. Consequently, the three product-specific active sites had to show different turn-over frequencies (TOF) during the reduction of $^{12}CO_2$ to $*^{12}CO$. To develop more selective copper-based electrocatalysts, Grätzel and co-workers have doped OD-Cu nanowires with silver.[196] Having these in hand, they were able to improve the overall FE for C_{2+} products from 58% to 76%. Interestingly, the group achieved an FE of 52% specifically for the product ethylene. Mechanistic investigations showed that silver acted as a co-catalyst for the formation of the main product ethylene. To tune the selectivity of their system towards *n*-propanol, the groups of Li and Zheng have added double sulfur vacancies to their CuS electrocatalyst.[197] The formation of *n*-propanol is challenging due to two stepwise C–C bond formations and the stabilization of the $*C_2$ intermediate. With their CuS catalyst, the researchers achieved 15% FE for the selective formation of *n*-propanol. This efficiency remained high even after 10 h of continuous electrolysis.

One of the most atom-economic conversions of carbon dioxide is its dimerization to oxalic acid. With an annual production of 350 kilotons, oxalic acid or its anion oxalate can serve as the starting materials for the production of a variety of high-value products like ethylene glycol or glyoxylic acid, *inter alia*.[198-199] Both homogeneous and heterogeneous electrocatalysts have been applied in the eCO_2RR to oxalate. In 2000, the group of Jäger focused on the selective electrochemical formation of oxalate utilizing a macrocyclic nickel catalyst.[200] Mechanistically, they suggested either a dimerization of the $CO_2^{\bullet-}$ radical anions or a coordinative interaction with the complex. The oxalate product was formed in high amounts and with 98% FE. The same reaction was realized by Tanaka and co-workers in 2015

applying a trinuclear, sulfur-bridged Co complex.[201] The controlled potential electrolysis in MeCN using tetramethylammonium (TMA) bromide as electrolyte yielded TMA oxalate in 80% FE. Deposition of the product on the working electrode inhibited the reaction. Recently, Costa *et al.* produced oxalic acid by eCO_2RR with hybrid silver-carbon material.[202] They prepared their catalyst from coconut biomass by carbonization. Oxalic acid, produced in 29% FE, was quantified by HPLC.

In addition to eCO_2RR, thermal processes also play an important role in the studies into the homocoupling of carbon dioxide. However, the thermoreductive coupling of carbon dioxide to oxalate is till date rather a stoichiometric reaction than a catalytic transformation.[192] It can be achieved by applying homogeneous transition metal or *f*-block metal complexes, while the latter show a stronger coordination to the product due to their increased oxophilicity. For instance, the group of Ziller was able to crystallize a samarium oxalato complex from CO_2 already in 1998.[203] Recently, Bernskoetter and co-workers liberated potassium oxalate in 98% yield from their iron(0) complex with the use of KC_8 as reducing agent.[204] A disproportionation of CO_2 was observed as the side reaction, yielding $Fe(depe)_2(CO)$ (depe = 1,2-bis(diethylphosphino)ethane) and $Fe(depe)_2(CO_3)$. The first – and so far the only – catalytic process was published by Cook *et al.* in 2018 (Scheme 24).[205]

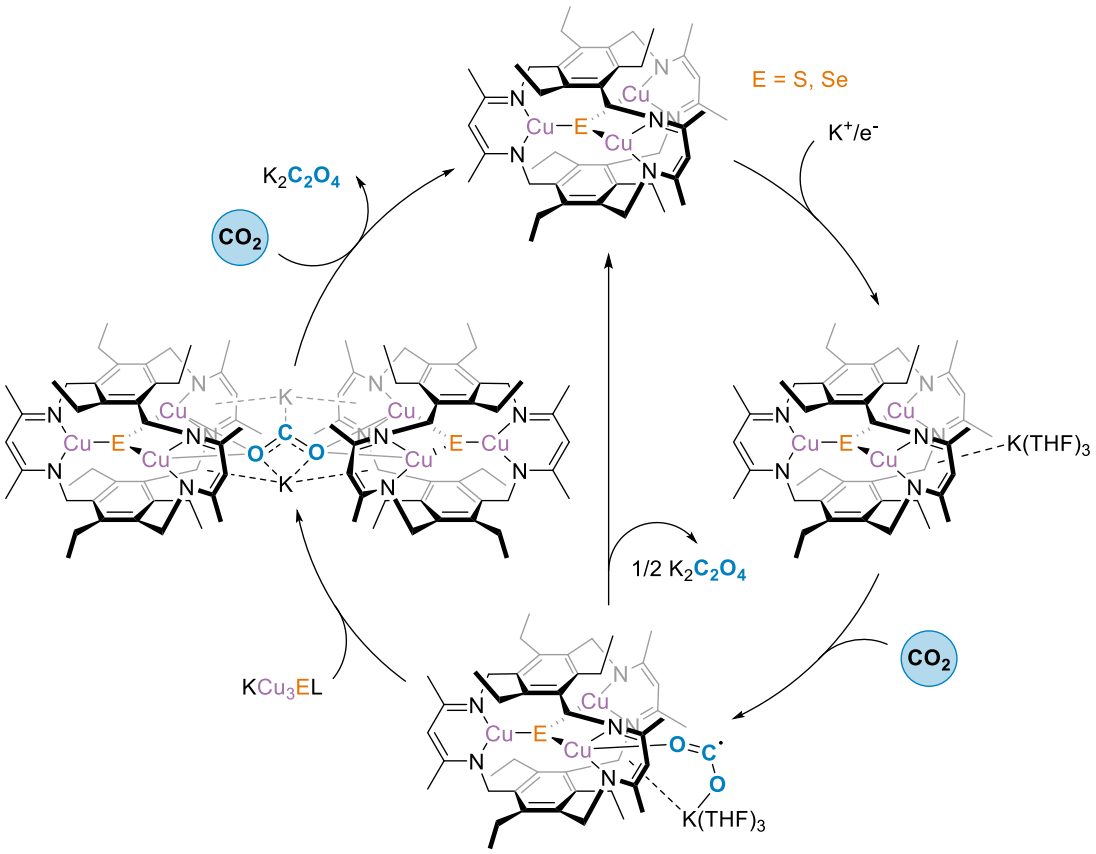

Scheme 24. Catalytic cycle of oxalate formation from CO_2 as proposed by Cook and co-workers.[205-206]

They applied a trinuclear Cu complex surrounding a sulfur or selenium atom and [K(18-crown-6)] as the reducing agent to achieve a TON of 24. The process was shown to strongly depend on the solvent

and the counterion, which were assumed to stabilize the transition state of this transformation. However, some procedures for the thermoreductive coupling of carbon dioxide suffer from misinterpretation of the obtained results.[207-208] In one example, for instance, the real carbon source for oxalate was oxidized ascorbate instead of reduced CO_2.[207] In another example, the reduced products formate or carbonate were thought to be oxalate if they were only analyzed by ^{13}C NMR spectroscopy or by oxidative titration with $KMnO_4$.[208] Misinterpretation can be avoided, though, by thoroughly analyzing the product or applying isotope labeling.

A first thermal variant of artificial photosynthesis in the classical sense, which led from one atmosphere of CO_2 to a C_3 carbohydrate, was presented in 2019 by the group of Bontemps.[209] Initially, bis(boryl)acetal **84** was prepared by the iron-catalyzed 4-electron reduction of carbon dioxide *via* the reaction with the borane 9-BBN. The researchers then achieved the C–C coupling by adding an *N*-heterocyclic carbene (NHC) to the reaction mixture (Scheme 25).

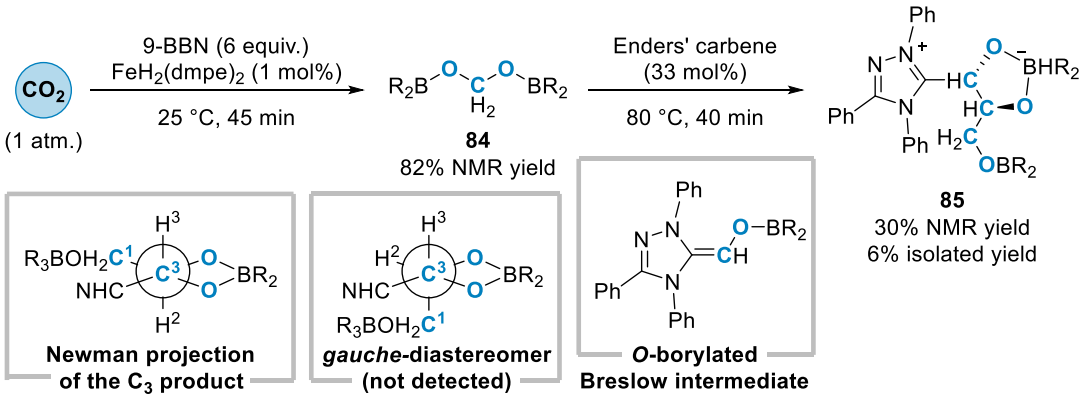

Scheme 25. Artificial photosynthesis reported by Bontemps and co-workers.[209]

A short reaction time of less than 2 h and mild reaction conditions were the benefits of this formose-type reaction. DFT calculations helped to propose a rational reaction mechanism, which involved a so-called Breslow intermediate, an *N*-heterocyclic, *O*-borylated alkene. According to these calculations, the undetected *gauche* product had a higher energy level than carbohydrate **85**. The calculated diastereoselectivity was later confirmed by X-ray crystallography. In 2021, Bontemps and co-workers reported the thermoreductive dimerization of CO_2 to C_2-C_4 aldoses.[210] Different to the C_3 product **85** obtained above, these carbohydrates were not connected to an NHC nor to a borane. Applying identical reaction conditions for the formation of bis(boryl)acetal **84**, the product was then treated with 10 equiv. D_2O to release formaldehyde in 94% within 30 minutes. In the same reaction vessel, formaldehyde was di- or oligomerized to C_2-C_4 aldoses like glycolaldehyde, erythrose or threose in up to 100% total yield using Enders' carbene. The selectivity of this reaction was mainly influenced by the solvent and the reaction time, as glycolaldehyde tended to dimerize after 30 minutes.

Bis(boryl)acetal **84** had also been applied by the same group to transfer a methylene unit onto *C*-, *N*-, and *O*-acceptors.[211] Products like hemiacetals, imines, and methylene-bridged bisphenols were obtained in up to 92% yield.

5.1.3 (Non-)Reductive Heterocoupling by C–C, C–N, and C–O Bond Formation

The first heterocoupling of CO_2 has already been reported in 1860 by Kolbe and later mechanistically explained by Schmitt.[212-213] The researchers reacted sodium phenolate with CO_2 to afford an intermediate that formed salicylic carboxylate upon rearrangement at increased temperatures. Pure salicylic acid was obtained after an acidic work-up (Scheme 26).

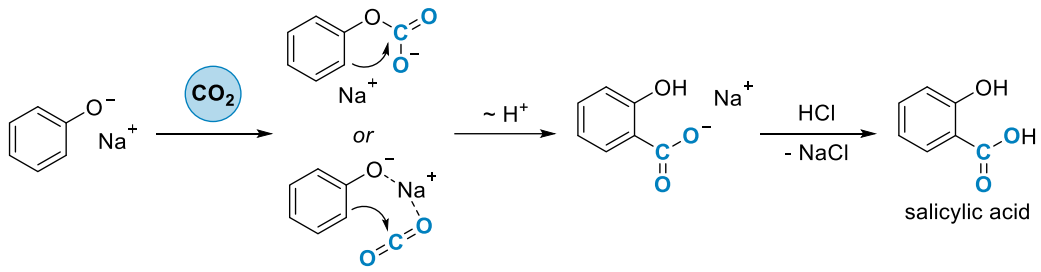

Scheme 26. Kolbe-Schmitt reaction including the originally postulated mechanism (top) and the mechanistic alternative (bottom).[212-214]

This reaction was selective towards the *ortho*-substituted product and became known as Kolbe-Schmitt reaction. However, there were some discussions within the scientific community on whether this reaction proceeded *via* sodium phenyl carbonate or rather *via* a phenolate carbon dioxide complex surrounding a sodium cation.[214] The latter theory would explain the increased formation of the *para*-substituted product if potassium phenolate was used as the starting material, since the ion radius of potassium is bigger than that of sodium. Furthermore, IR studies revealed bands that were located at higher wave numbers than that of a stable model substrate, sodium methyl carbonate, hinting towards the sodium complex as the intermediate. Regardless of the correct mechanistic proposal, the Kolbe-Schmitt reaction is still widely applied in industry.[34] It is mainly used for the synthesis of acetylsalicylic acid, a non-steroidal anti-inflammatory drug on the WHO list of essential medicines, primarily known as Aspirin.[215]

Since then, many research groups have investigated the reaction of CO_2 with a wide variety of reaction partners. In 2021, the group of Martin developed a nickel-catalyzed synthesis of natural and artificial β-amino acids from the reaction of one atmosphere of CO_2 with aziridines.[216] Initial mechanistic investigations indicated ring opening of the aziridines with the participation of nickel *via* formation of an aza-nickelacylobutane. Subsequent insertion of CO_2 into the metal-carbon bond afforded the C–C coupled products. An excess of manganese was used as the reducing agent. In another study, the same group used a MnCr alloy instead of manganese as the reductant to enable the Ni-catalyzed C–H carboxylation of *ortho*-alkynyl-substituted arenes with 1 bar of CO_2.[217] Cyclized

benzoic acids were obtained by a so far unknown 1,4-Ni migration. Interestingly, if the alloy was replaced by Mn/$CrCl_2$, the carboxylation of the internal alkyne was favored. Likewise, the group of Yu required superstoichiometric amounts of zinc as the reducing agent in their enantioselective carboxylic cyclization of terminal olefins to indolinones under one atmosphere of CO_2 (Scheme 27).[218]

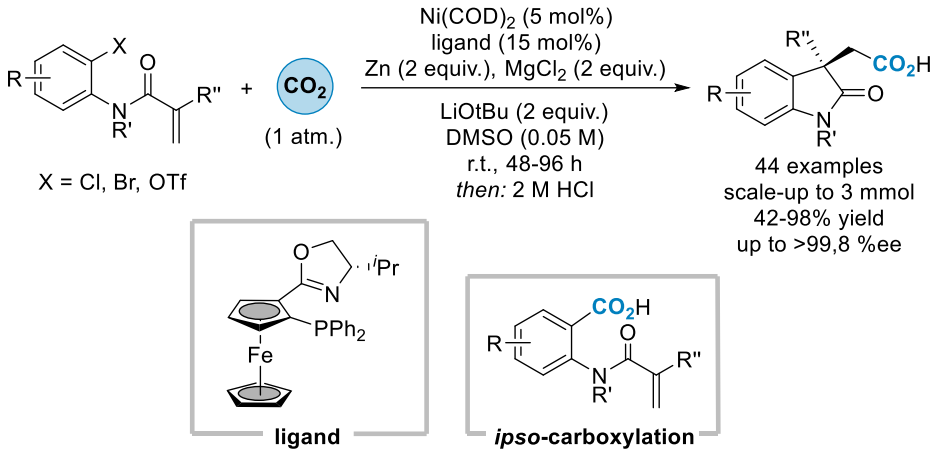

Scheme 27. Carboxylic cyclization of terminal olefins reported by Yu and co-workers.[218]

Mainly 5-exo-products were afforded with enantiomeric excesses of maximum 99.8 %ee in 42% to 98% yield. Preliminary mechanistic experiments revealed two possible pathways within the catalytic cycle. Both have in common that the chiral Ni(0) catalyst was oxidized to Ni(II) by addition of the aryl (pseudo)halide followed by one-electron reduction to Ni(I) by excess Zn metal. The possible routes differed in the order of reduction event and cyclization. The *ipso*-carboxylation side product, obtained from the 'reduction-cyclization' route, was detected in 3%. The authors claimed that their method was generally suitable to prepare many products interesting for the total synthesis of natural products. In an alternative approach, the group of Leitner has recently reported a redox-neutral carboxylation of arenes without the need for any reducing agent.[219] While avoiding the traditional oxidative addition/reductive elimination mechanism, the researchers followed a base-assisted concerted metalation-deprotonation pathway to carboxylate nonactivated aryl C–H bonds. Both the catalytic cycle and the molecular structure of the applied phosphine sulfonamido ligand had been computed prior to the experimental work. Interestingly, the substrate was used as the solvent and only the amount of base limited the yield since it was necessary to stabilize the product as carboxylate salt. Maximum TONs of 77 were achieved.

The full reduction of carbon dioxide to a methylene unit was achieved by Xia and co-workers in 2017 (Scheme 28).[220]

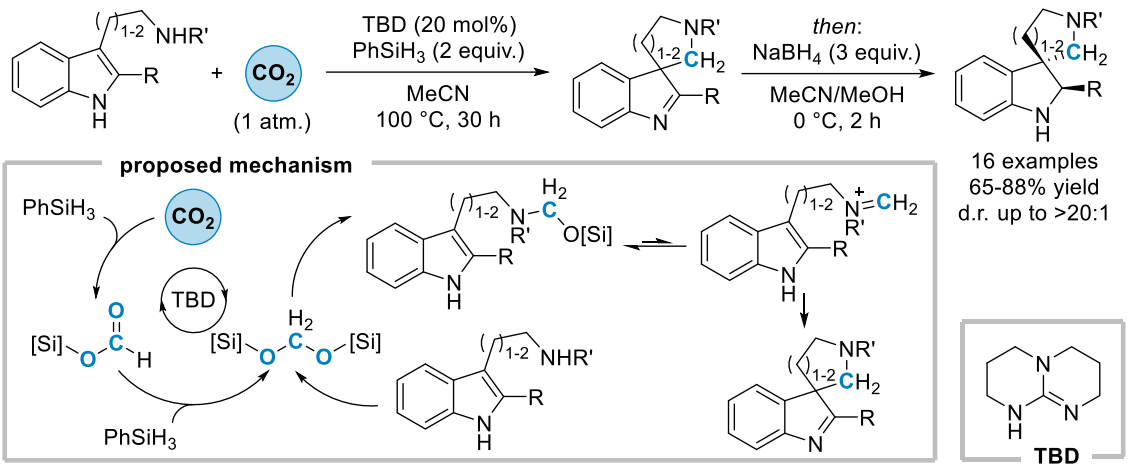

Scheme 28. Synthesis of chiral spiroindolines as reported by Xia and co-workers.[220]

They used phenylsilane as the reducing agent and catalytic amounts of the organic base 1,5,7-triazabicyclo[4.4.0]dec-5-ene (TBD). The reaction of tryptamine derivatives and an atmosphere of CO_2 *via* an intermediary bis(silyl)acetal led to the simultaneous formation of a C–C and a C–N bond. The spiro[4.4]indolpyrrolidine and spiro[4.5]indolpiperidine products gave the corresponding chiral spiroindoline compounds after reduction with sodium borohydride. Diastereomeric ratios between 2.3:1 and >20:1 were achieved.

In addition to C–C bond formations with CO_2 as the C_1 building block, reductive and non-reductive C–N bond formation reactions with CO_2 as reactant are also subject of extensive research.[149] For example, urea is the product of the non-reductive C–N coupling reaction of CO_2 and ammonia. The latter is traditionally produced from nitrogen and subsequently reacts with CO_2 at temperatures of up to 200 °C and pressures of up to 250 bar. Patented in 1922, this technology has, like the synthesis of salicylic acid, a long history.[221] It is nowadays still applied on a large scale of 130 Mt/year by the fertilizer industry.[99] In contrast to the harsh conditions employed so far, the group of Wang has developed a process to electrocatalytically synthesize urea directly from CO_2 and nitrogen in water as the solvent.[222] They utilized an electrocatalyst containing TiO_2 nanosheets with PdCu alloy nanoparticles on the surface to couple the intermediates *CO and *N=N*. At room temperature, their procedure achieved an FE of approximately 9% and a rate of 3.36 mmol g^{-1} h^{-1} urea, while carbon monoxide and ammonia were obtained as side products. Besides urea, research groups have also focused on the non-reductive synthesis of heterocycles from CO_2. In 2017, Beller and co-workers utilized CO_2 for the preparation of *N*3-substituted quinazoline-2,4(1*H*,3*H*)-diones (Scheme 29).[223]

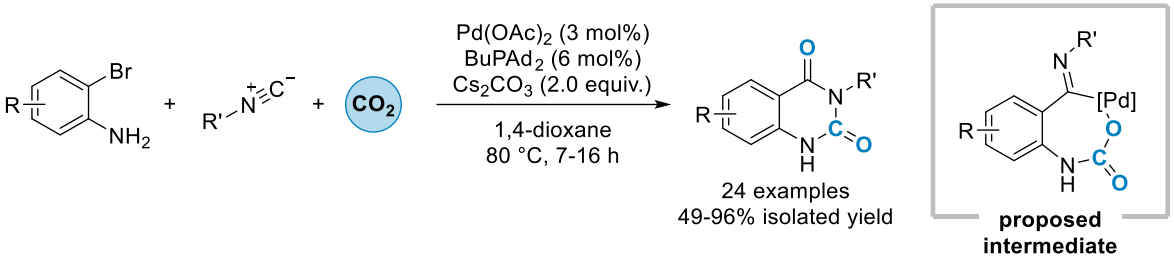

Scheme 29. Synthesis of *N*3-substituted quinazoline-2,4-diones as reported by Beller and co-workers.[223]

The Pd-catalyzed three-component-reaction of 2-bromoanilines, CO_2 and isocyanides afforded the respective products regio- and chemoselectively. Selective ^{13}C-labeling is possible by introducing the isotope either via CO_2 or the isocyanide building block. More recently, Vecchio *et al.* used a Staudinger/aza-Wittig approach for the late-stage isotope labeling of pharmaceuticals.[224] By converting aliphatic or aromatic azido amines with CO_2 in presence of dimethylphenylphosphine, ^{11}C-, ^{13}C-, and ^{14}C-labeled cyclic ureas were obtained within 5 minutes in 23-99% yield. The efficiency of this method was shown for six drug candidates including an unprotected peptide.

In contrast, the reductive C–N bond formation yielding formamides was investigated by the group of Hulla in 2023.[225] The researchers were able to improve the functional group tolerance, which is usually low, by avoiding the use of transition metal catalysts. Instead, they utilized different tin-based Lewis acids that form frustrated Lewis pairs (FLPs) with the amine substrates. The FLPs managed to activate H_2 by Sn–H bond formation and selectively hydrogenate CO_2 during amine formylation. Other reducible groups such as carboxylic acids, esters, amides, or alkenes were not affected. The fully reductive C–N coupling with CO_2 being reduced to methyl groups was published by Lei and co-workers in 2017.[226] Both primary and secondary alkyl- and arylamines were converted to the corresponding mono- and dimethylated tertiary amine products in up to 95% yield by using phenylsilane as the reducing agent. An isotope labeling experiment with $^{13}CO_2$ confirmed that the methyl groups in this catalyst-free *N*-methylation originated from carbon dioxide instead of the solvent DMF. An intermediary formamide species was excluded by control experiments. More recently, Ma *et al.* have reported a Co-catalyzed procedure to afford dimethylamines from nitroarenes, CO_2, and a combination of two hydrosilanes as the reducing agents.[227] Both substrates were reduced during the reaction with nitrosoarenes and silyl formate as the key intermediates. During the coupling step, a cooperative effect of the two hydrosilanes was observed. Functional groups like ethers and halides were tolerated, while competitive experiments showed the preferred reduction of electron-rich substrates. Next to hydrosilanes, also boranes have been used for the reductive C–N bond formation with CO_2. In 2022, Li and co-workers investigated the simultaneous formation of a C–S and a C–N bond during the synthesis of benzothiazoles from bis(2-aminophenyl) disulfide and carbon dioxide (Scheme 30).[228]

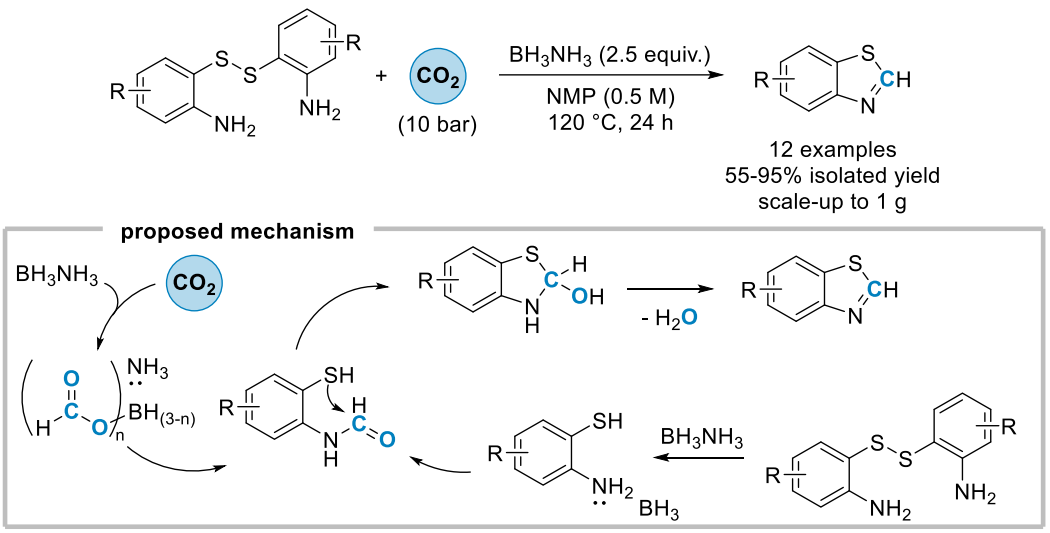

Scheme 30. Synthesis of 2-unsubstituted benzothiazoles from CO_2 as reported by Li and co-workers.[228]

Ammonia borane was applied as the reducing agent in this catalyst-free procedure. From the work of Zhao *et al.*, it was already known that ammonia borane can activate both CO_2 and the N–H bond of amines.[229] However, herein it was found that ammonia borane is further able to break disulfide bonds.[228] Finally, there are also electrocatalytic procedure within the field of reductive C–N bond formations, which are not further discussed herein.[230-232]

The field of C–O bond formation reactions comprises, *inter alia*, the formation of organic and inorganic carbonates. The latter is already used on an industrial scale to produce CO_2-cured concrete as material for buildings, for instance by the companies CarbonCure and Solidia Technologies.[233-234] Concerning price and performance, this CO_2-cured concrete is already competitive to conventionally produced concrete.[235] The direct environmental impact is built from two sides: less raw materials are required and the CO_2 is permanently stored in the building.[234] Among the formation of organic carbonates, the non-reductive reaction of epoxides with CO_2 producing cyclic organic carbonates is the most common one.[236] For example, the addition of CO_2 on simple methyl-substituted epoxide leads to the formation of propylene carbonate (PC), a popular polar-aprotic and green solvent in organic chemistry, which is also used as electrolyte in batteries.[237] In 2021, Martínez *et al*. explored the oxidation of unsaturated natural fatty acids to epoxides using *meta*-chloroperbenzoic acid (*m*CPBA).[238] This was followed by the La-catalyzed reaction with 10 bar CO_2 to afford bio-derived cyclic carbonates in yields between 41% and 98%. Tetrabutylammonium halides were applied as the co-catalyst whereas the absence of a solvent was well tolerated. Even highly substituted terpene epoxides were efficiently converted into the corresponding cyclic carbonates. The synthesis of cyclic carbonates derived from epoxidized waste fatty acid esters was successfully accomplished applying an increased pressure of 20 bar CO_2. While the formation of cyclic carbonates has been known for a long time, new approaches are needed to increase the structural variety within the cyclic carbonate product range. Thus, researchers have developed procedures to form new C–O bonds.[239] Recent advances in this field

were made by the group of Kleij.[240-241] In 2020, they published a regio- and diastereoselective coupling of CO_2 with an unsaturated cyclic epoxy alcohol.[240] By addition of an aluminum complex, altered selectivities were obtained for the bicyclic carbonate products. Novel 6-membered cyclic carbonates instead of the usual 5-membered heterocycles were prepared by the same group in 2022 (Scheme 31).[241]

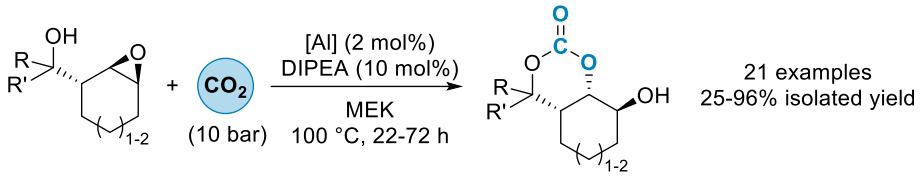

Scheme 31. Synthesis of cyclic carbonates from epoxy alcohols published by the group of Kleij.[241]

Without the need of using reactive oxiranes, rigid bicyclic 6-membered cyclic carbonates were obtained from the Al-catalyzed reaction of β-epoxy alcohols and 10 bar CO_2 even on a gram scale. As observed in both examples, the cyclic carbonate product was formed *via* incorporation of the free hydroxy group, followed by ring opening of the epoxide. The oxygen atom of the epoxide motif then formed a new hydroxy substituent. Recently, the group of Kleij has reported on the C–O bond formation starting from alkyne-1,*n*-diols and CO_2 (Scheme 32).[242]

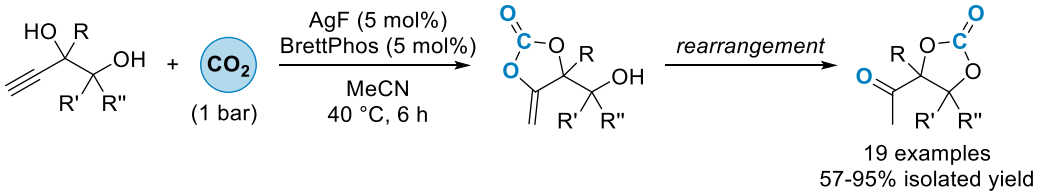

Scheme 32. Cascade reaction to synthesize highly substituted cyclic carbonates.[242]

By reaction of carbon dioxide with the hydroxy group and subsequent attack of the carbonate on the triple bond, an α-alkylidene carbonate was formed. An intermolecular rearrangement by involvement of the second hydroxy substituent finally led to the formation of a keto-functionalized cyclic carbonate.

In addition to the widely explored non-reductive C–O bond formation reactions, there are also reductive C–O bond formations yielding products like esters, alcohols, or acetals.[243] In 2019, Klankermayer and co-workers published the efficient hydrogenation of CO_2 in methanol.[244] The esterification of the intermediary formic acid with methanol gave methyl formate with high TONs exceeding 9500. In this study, they utilized a Ru-catalyst with a cyclohexyl-substituted triphos ligand having a tertiary amine as the backbone and a TMM ligand. $Al(OTf)_3$ was applied as Lewis acid. In comparison to earlier studies of the same group, the TON was increased 13-fold by increasing the total pressure to 120 bar (30 bar CO_2, 90 bar H_2), and optimizing the triphos ligand.[243] The esterification of formates with alcohols was further extended by Dyson and co-workers in 2023.[245] Using only 1 bar

CO_2, the group showed that they could reduce the gas with readily available $NaBH_4$ to sodium triformatoborohydride. The subsequent reaction with various structurally complex alcohols delivered the formyl esters in 70% to 99% yield. Mechanistic investigations revealed an autocatalytic behavior of the intermediary formic acid. However, the hydrogenation of CO_2 in methanol did not only yield methyl formate but was further optimized by Siebert *et al.* to selectively afford the acetal dimethoxymethane (DMM).[246] Again, a [Ru(triphos)(TMM)] catalyst with an amine backbone was applied. In a second step, DMM could be hydrolyzed to formaldehyde. Structurally more complex acetals were prepared by Beydoun and Klankermayer in 2019.[247] By combining CO_2, H_2, and biomass-derived diols, the researchers afforded a small scope of 9 (a)cyclic acetals. A Ru/triphos combination was again used as the catalyst, whereas $Al(OTf)_3$ was added as the Lewis acid.

In summary, multiple opportunities have been reported so far to convert CO_2 into useful chemicals and fuels. Most approaches, to date, require the pure gas in pressures higher than or equal to one atmosphere. However, it was emphasized that a lot of research has already been conducted in the field of CO_2 coupling reactions and is still ongoing, raising hope that the concept of CCU will in future be competitive to CCS facilities. The products of the utilization of CO_2 can replace gas and oil for the generation of power and serve as starting materials to produce more complex chemicals. When combined with the CO_2 release from degradation, oxidation, or combustion of pharmaceuticals and other end-of-life chemicals, a circular economy regarding the anthropogenic chemical carbon cycle is still reachable.[99]

5.2 Results and Discussion

In course of the work on the presented dissertation, the CO_2 conversion by transition metal catalysis was pursued using two different approaches. First investigations aimed at the transition metal-catalyzed dimerization of CO_2 *via* metallacarboxylic acids to form oxalic acid or oxalates by reductive elimination (Chapter 5.2.1). Another approach was the rational design of a ligand apt to bind CO_2, that can then forward the molecule to a metal center followed by the transfer to a substrate (Chapter 5.2.2).

Both systems were aspired to be robust and air-stable to enable converting CO_2 from the atmosphere. Therefore, it was exclusively focused on bidentate *N*-based ligands rather than air-sensitive phosphines. Additionally, phosphines are to be avoided due to a prevailing shortage of phosphorus.[4] The metal of choice was palladium in form of $Pd(OAc)_2$, which is also known to be air-stable but easily decomposes to Pd^0 nanoparticles when heated in alcohols.[248]

5.2.1 *Alkoxycarbonylation as a Model for the Dimerization of CO_2* via *Metallacarboxylic Acids*

One possible strategy towards the oxalate formation from CO_2 involved the intermediacy of metallacarboxylic acids (MCA). In principle, a complex bearing two *C*-bound carboxylic acid ligands can form oxalic acid by reductive elimination. However, this illusive structure is unstable and readily releases CO_2 due to its intrinsic instability, as seen in the water-gas shift reaction (WGSR, Scheme 33).[249]

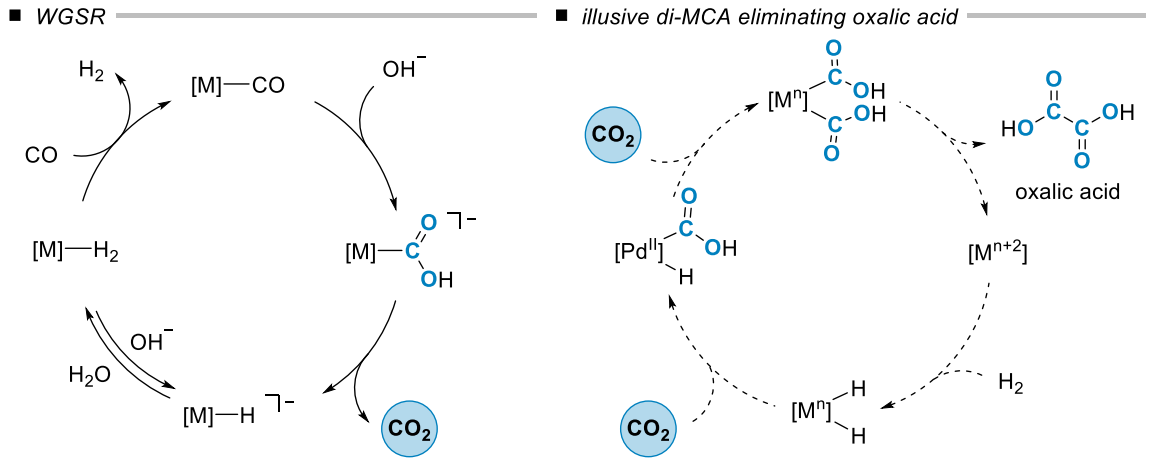

Scheme 33. Left: scheme of the WGSR.[249] Right: illusive catalytic cycle of the oxalic acid formation *via* dimetallacarboxylic acids.

Alternatively, it was focused on structurally related metallacarboxylic esters (MCE) to study the ligand effect on the oxalate formation. To date, (bis)alkoxycarbonyl complexes **86** have mostly been applied in the oxidative carbonylation of methanol to give dimethyl oxalate (DMO, **87**). Whereas the

homologous heterogeneous reaction on Pd/C – known as Ube process – has already been established on industrial scale in the 1980s,[250] the research on corresponding homogeneous palladium catalysts is still ongoing today. The air-stable MCE complexes reductively eliminate DMO (**87**) at increased temperatures (Scheme 34).[251-252] A similar behavior was observed for the less studied nickel[253], rhodium[254], and platinum[255] complexes. Although the DMO (**87**) formation initially was a stoichiometric reaction, the addition of a stoichiometric oxidant like O_2, benzoquinone, alkyl nitrites, Cu^{2+} salts, or a combination thereof enabled Pd-catalyzed processes with TONs up to 1110.[256-260]

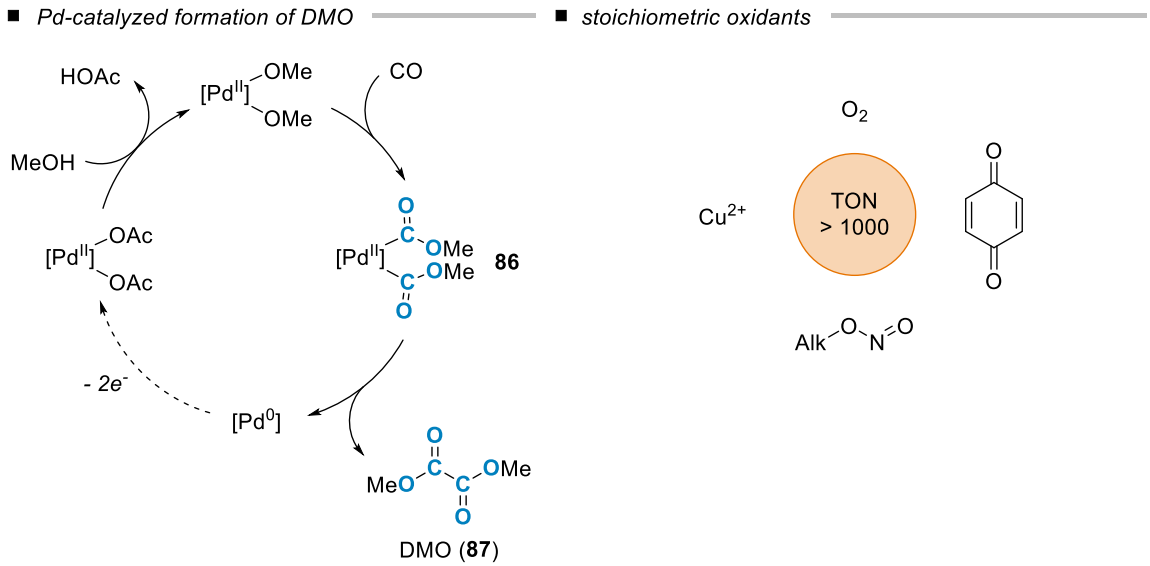

Scheme 34. Left: mechanism of the DMO (**87**) formation as proposed by Rivetti and co-workers.[251] Dashed arrow represents the required oxidation step to close the catalytic cycle. Right: stoichiometric oxidants that have been applied for Pd-catalyzed processes.[256-260]

In order to enable a dimerization to oxalates starting from CO_2 instead of CO, which is a much more difficult reaction, effort was put into the design of sterically sophisticated, bidentate, and air-stable *N*-based ligands. The concept of combining robust bipyridine (bipy) and phenanthroline (phen) ligands with bis(alkoxycarbonyl) ligands has already been explored in the 1990s.[261-263] However, the steric bulk in proximity to the Pd center has not exceeded a methyl group and the reactivity of these complexes with respect to DMO (**87**) formation remained unexplored. By having sterically more demanding substituents in *ortho*-position to the coordinating nitrogen atom, the support of the reductive elimination step by pushing the two MCE or MCA ligands closer together was anticipated.[264-265]

Thus, a library of substituted phen and bipy ligands **90**-**97** was envisioned (Table 21). Starting from unsubstituted phenanthroline (**88**) or bipyridine (**89**), steric bulk was generated by arylation or alkylation using commercially available solutions of organolithium compounds. The corresponding products **90**-**96** were obtained in varying isolated yields of 15% to quantitative yield.

Table 21. Scope of the nucleophilic *ortho*-substitution of phenanthroline and bipyridine.

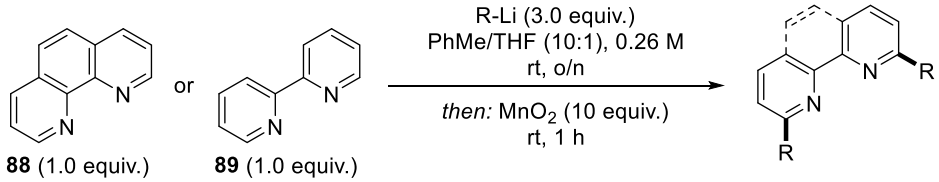

88 (1.0 equiv.) **89** (1.0 equiv.)

entry	reagent	product	yield[a]	entry	product	yield[a]
1	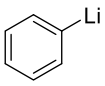	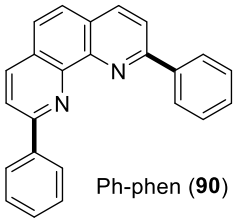 Ph-phen (**90**)	quant.	5	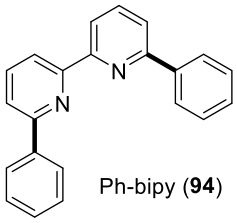 Ph-bipy (**94**)	19%
2	*n*BuLi	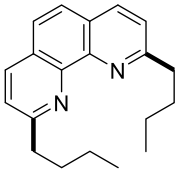 *n*Bu-phen (**91**)	69%	6	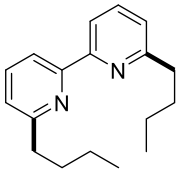 *n*Bu-bipy (**95**)	39%
3	*s*BuLi	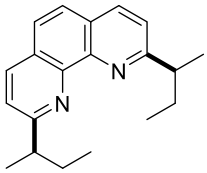 *s*Bu-phen (**92**)	24%[b]	7	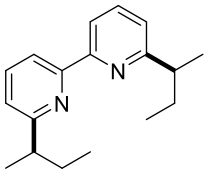 *s*Bu-bipy (**96**)	15%
4	*t*BuLi	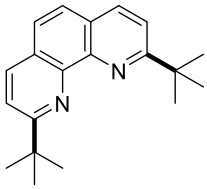 *t*Bu-phen (**93**)	33% 28%[c]	8	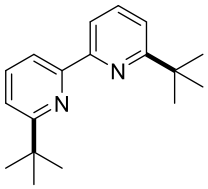 *t*Bu-bipy (**97**)	0%

[a] Reactions were performed on a 2.0 mmol scale. Isolated yields are shown. [b] The yield is calculated as the average of two experiments. [c] Scale-up (1 g).

The substituted phenanthrolines **90**-**93** were obtained in higher yields of 24% to quantitative yield (entries 1-4) than the substituted bipyridines **94**-**96**, which were isolated in 15-39% yield (entries 5-7). It can be concluded that the less sterically hindered products, bearing phenyl or *n*-butyl substituents, were isolated in increased yields (entries 1, 2, 5, and 6) when compared to the more sterically hindered products, **92**-**93** and **96**-**97**, bearing *sec*-butyl or *tert*-butyl substituents (entries 3, 4, 7, and 8). The reaction of phenanthroline (**88**) with *t*BuLi was successfully scaled up to 1 g, yielding the product *t*Bu-phen (**93**) in a slightly decreased yield of 28% (entry 4). Unfortunately, the reaction of bipyridine (**89**) with *t*BuLi (entry 8) did not result in product formation.

These ligands were next applied in the oxidative carbonylation of methanol as a mimic for the catalytic dimerization of CO_2. This reaction is usually catalyzed by palladium phosphine complexes

formed *in situ* from $Pd(OAc)_2$ as precursor.[252, 260] To the best of my knowledge, no homogeneous catalytic process using *N*-based ligands has been reported till date. Thus, the feasibility of the *in situ* complex formation was validated with *N*-based ligands by adding the unsubstituted ligands to $Pd(OAc)_2$ (Scheme 35).

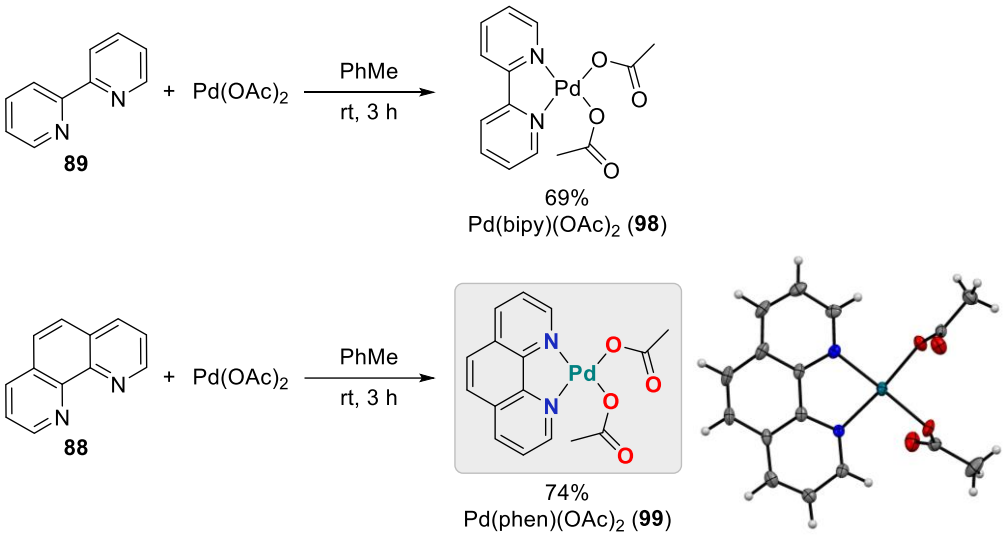

Scheme 35. Synthesis of $Pd(bipy)(OAc)_2$ (**98**) and $Pd(phen)(OAc)_2$ (**99**) and X-ray structure of $Pd(phen)(OAc)_2$ (**99**). Color code: grey (C), blue (N), red (O), teal (Pd). Since the complex is known in literature, no complete X-ray data was recorded.[266]

The complexes $Pd(bipy)(OAc)_2$ (**98**) and $Pd(phen)(OAc)_2$ (**99**) were obtained in 69% and 74% yield, respectively. X-ray crystallography of complex **99** confirmed a square-planar coordination of the palladium metal center, which correlates with literature reports.[263] In contrast, the *ortho*-substituted $Pd(Me\text{-}phen)(OAc)_2$ is known to have a bend structure.[266]

Next, the oxidative carbonylation of MeOH was investigated. A high CO pressure is required to avoid the undesired formation of dimethylcarbonate (DMC) as side-product, caused by incomplete CO insertion prior to the reductive elimination step.[252] Hence, an increased pressure of 40 bar CO was used in all reactions discussed below. Initially, the stoichiometric formation of DMO (**87**) was examined applying the substituted ligands **90**-**93** (Table 22).

Table 22. Screening of ligands for the stoichiometric DMO (**87**) formation.

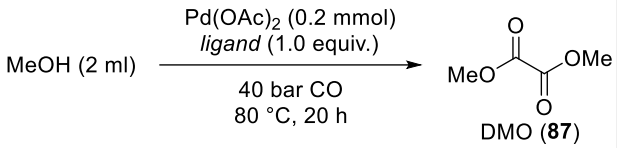

entry	ligand	yield[a]	2nd yield[a]
1	bipy (**89**)	20%	
2	phen (**88**)	28%	
3	*t*Bu-phen (**93**)	110%	61%
4	*n*Bu-phen (**91**)	85%	45%
5	*s*Bu-phen (**92**)	67%	61%
6	Ph-phen (**90**)	66%	28%[b]

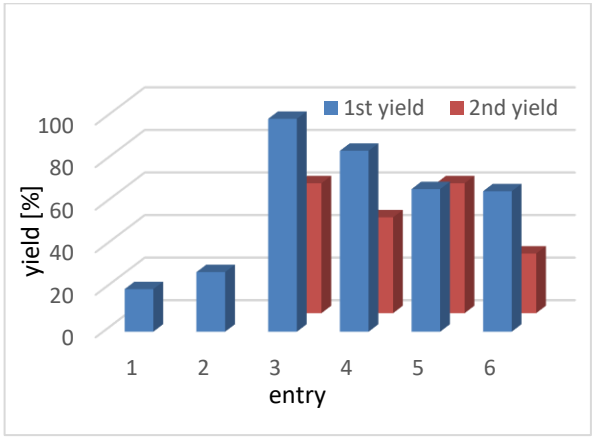

[a] GC yields calculated based on $Pd(OAc)_2$ as limiting reagent using tetradecane as internal standard. [b] PVP was added as nanoparticle dispersant.

As expected, the palladium complexes reductively eliminated dimethyl oxalate (**87**) with simultaneous formation of the free diamine ligand and precipitation of palladium black. The *N*-based ligands appeared to be too labilely bound to stabilize the reduced species Pd^0. If polyvinyl pyrrolidone (PVP) was added as nanoparticle dispersant to support the complex re-formation,[267] the yield of the reaction decreased as compared to the reaction without PVP (entry 6). However, reproducibility issues were observed. Thus, a first and a second yield were given for most entries. As a general trend, it can be concluded that all prepared ligands **90**-**93** (entries 3-6), bearing bulky substituents in *ortho*-position, showed an enhanced activity towards DMO than the unsubstituted ligands bipy (**89**) and phen (**88**, entries 1 and 2). The competing formation of DMC was avoided.

Afterwards, different oxidants were tested in an excess of 20 equiv. to promote a turn-over by re-oxidation of Pd^0 to Pd(II). Different Cu(II)-sources were assayed including $Cu(OAc)_2$, $Cu(OMe)_2$, and $CuCl_2$, even though halides are known to force the DMC formation.[268] Other oxidants, that were tested in these catalytic experiments, were MnO_2, I_2, different quinones, and oxygen (Table 23).

Table 23. Screening of oxidants for the catalytic DMO (**87**) formation.

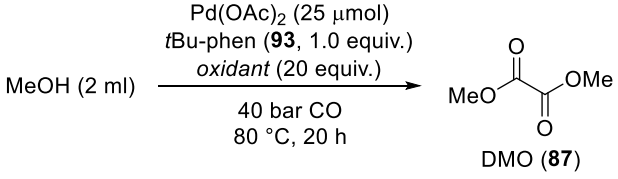

entry	oxidant	yield[a]
1	$CuCl_2$	n.d.
2	$Cu(OAc)_2$	n.d.
3	$Cu(OMe)_2$	n.d.
4	MnO_2	n.d.
5	I_2	n.d.
6	benzoquinone	n.d.
7	duroquinone	n.d.
8	DDQ	n.d.
9	O_2 (1 bar)	n.d.

[a] GC yield using tetradecane as internal standard.

However, no product **87** was observed according to GC analysis. This may either be due to the fact that there was no turn-over or that the DMO (**87**) concentration was below the detection limit, as only 25 µmol of Pd was used for the catalytic experiments instead of 0.2 mmol.

In the search for improved oxidative conditions, inspiration was drawn from the Wacker process that was found with the interesting concept of combining two oxidants, Cu(II) and oxygen.[269-270] While the Cu(II) source oxidized the Pd catalyst, the copper source itself was re-oxidized by oxygen. By this, the required amounts of precious metals were decreased. To implement Wacker process-like conditions for the catalytic formation of DMO (**87**), different Cu precursors and reaction conditions were screened (Table 24).

Table 24. Screening of reaction conditions for the catalytic DMO (**87**) formation.

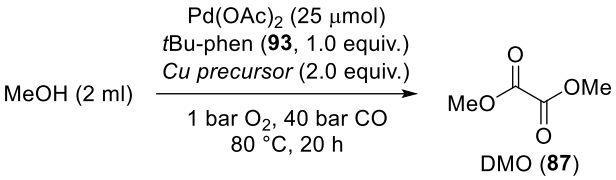

entry	Cu precursor	TON[a]
1	$Cu(OMe)_2$	6.4
2[b]	$Cu(OMe)_2$	1.4
3[c]	$Cu(OMe)_2$	<1
4[d]	$Cu(OMe)_2$	--
5	$Cu(OMe)_2$ (1.0 equiv.)	1.6
6	$Cu(OMe)_2$ (4.0 equiv.)	5.3
7	$Cu(OAc)_2$	--
8	Cu(0)	<1

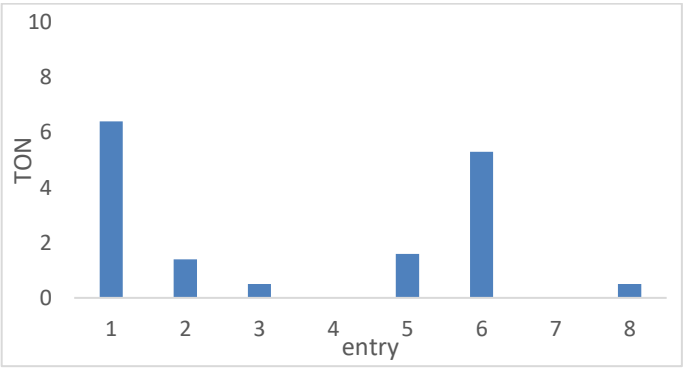

[a] GC yield using tetradecane as internal standard, calculated as the average of two independent experiments. [b] 12.5 µmol $Pd(OAc)_2$ was used. [c] 50 µmol $Pd(OAc)_2$ were used. [d] Control reaction without Pd.

This concept already worked in the first attempt (entry 1). DMO (**87**) was formed in an average yield of 640% based on the amount of Pd, corresponding to a TON of 6.4, when using *t*Bu-phen (**92**) as the ligand and $Cu(OMe)_2$ as co-catalyst. However, palladium black formation was still observed in the reaction mixture. A reduction of the catalyst loading from 25 µmol to 12.5 µmol led to a decreased TON of 1.3 (entry 2), while an increased catalyst loading, surprisingly, resulted in a TON smaller than 1 (entry 3). The importance of palladium in the oxidative carbonylation of MeOH was proven in a control experiment performed in the absence of Pd (entry 4). Altering the amount of the copper salt did not improve the TON (entries 5 and 6). Replacing $Cu(OMe)_2$ by copper metal or $Cu(OAc)_2$ gave no conversion (entries 7 and 8).

Next, the effect of the differently substituted ligands **90**-**96** on the catalytic formation of DMO (**87**) was investigated (Table 25). Their performance was compared to unsubstituted phenanthroline (**88**) and bipyridine (**89**), and to various commercially available substituted phen and bipy ligands.

Table 25. Ligand screening for the catalytic DMO (**87**) formation.

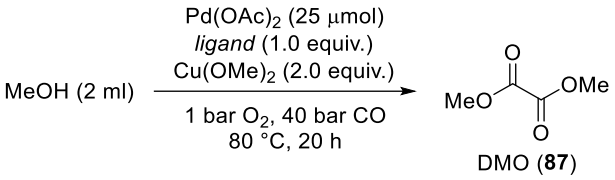

entry	ligand	TON[a]
1	*t*Bu-phen (**93**)	6.4
2	phen (**88**)	1.7
3	bipy (**89**)	4.5
4	Ph-phen (**90**)	19
5	*n*Bu-phen (**91**)	20
6	*s*Bu-phen (**92**)	5.4
7	Ph-bipy (**94**)	15
8	*n*Bu-bipy (**95**)	18
9	*s*Bu-bipy (**96**)	14
10	5,6-$(Me)_2$-phen	1.2
11	4,4'-$(Me)_2$-bipy	4.2
12	5,5'-$(Me)_2$-bipy	2.3
13	4,4'-$(OMe)_2$-bipy	<1
14	5,5'-$(CF_3)_2$-bipy	3.8
15[b]	--	16

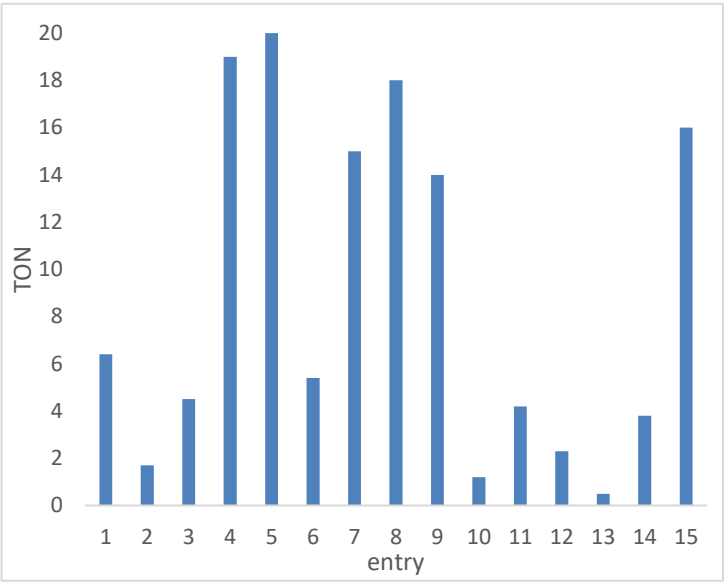

[a] GC yield using tetradecane as internal standard, calculated as the average of two independent experiments. [b] Control reaction without ligand.

As observed in the stoichiometric experiments (Table 22), the sterically demanding ligands prepared from alkylation and arylation of unsubstituted phen and bipy supported the DMO (**87**) formation better than their parent compounds **88** and **89** (entries 2 and 3). While the addition of 2,9-di-*tert*-butyl-1,10-phenanthroline (**93**) led to the formation of product **87** with a TON of 6.4 (entry 1), higher amounts of product were observed using Ph-phen (**90**) and *n*Bu-phen (**91**), giving dimethyl oxalate in high TONs of 19 and 20, respectively (entries 4 and 5). Applying 2,9-di-*sec*-butyl-1,10-phenanthroline (**92**) as the ligand yielded DMO (**87**) with a decreased TON of 5.4 (entry 6), comparable with the yield obtained using sterically hindered *t*Bu-phen (**93**). From these results, it was concluded that too much steric bulk (*t*Bu, *s*Bu) was not beneficial for this reaction either. The substituted bipy ligands followed the trend observed with the substituted phenanthrolines (entries 7-9). However, all ligands **90**-**96** prepared herein outcompeted the commercially available phen and bipy ligands having no steric bulk but altered electronic properties (entries 10-14).

Surprisingly, a high TON of 16 was achieved in a control reaction without adding any ligand (entry 15). It was therefore assumed that Pd nanoparticles catalyze this reaction rather than a homogeneous

Pd catalyst, as reported by Xu and co-workers.[271] This was supported by the well-known decomposition of palladium acetate in alcohols at increased temperatures.[248] Additional experiments with a range of Pd nanoparticles synthesized by Alexander Wotzka, M.Sc., did not confirm this assumption, as no detectable amounts of DMO (**87**) were formed.

Nevertheless, both 6,6'-diphenyl-2,2'-bipyridine (**94**) and 2,9-diphenyl-1,10-phenanthroline (**90**) together with *t*Bu-phen (**93**) were tested for the reductive coupling of CO_2 using H_2 as the reducing agent for the potential synthesis of oxalic acid, methanol, or formate (Table 26).

Table 26. Transfer of reaction conditions from the oxidative carbonylation to the reductive coupling of CO_2.

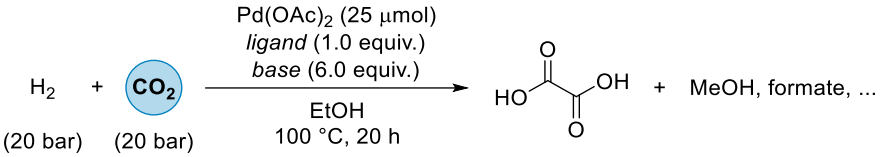

entry	ligand	base	product
1	Ph-bipy (**94**)	--	n.d.
2	Ph-phen (**90**)	--	n.d.
3	*t*Bu-phen (**93**)	--	n.d.
4	Ph-phen (**90**)	NaOEt	n.d.
5	Ph-phen (**90**)	K_3PO_4	n.d.
6	Ph-phen (**90**)	PPTS	n.d.

Next to varying the applied ligand (entries 1-3), also the addition of a base like sodium ethoxide, potassium phosphate, and pyridinium *p*-toluenesulfonate (PPTS) was tested (entries 4-6). None of the possible products could be identified by GC though.

In summary, the oxidative carbonylation of methanol to yield DMO (**87**) was realized using Wacker process-like reaction conditions and robust *N*-based bidentate ligands. The highest TON was 20 using Ph-phen (**90**) as the ligand. It remained unclear whether this was a homogeneously or heterogeneously catalyzed process due to the undesired formation of Pd nanoparticles in the reaction mixtures. First attempts to transfer the reaction conditions to the reductive coupling of CO_2 *via* MCAs have proved unsuccessful. Therefore, an alternative approach for the conversion of CO_2 was envisioned.

5.2.2 Rational Ligand Design for Carbon Capture and Utilization

In 2021, Beller and co-workers published their pioneering work about CCU using aliphatic amines.[272] They utilized the natural amino acid L-lysine to capture CO_2 and to reduce it afterwards to formate using a ruthenium catalyst (Scheme 36). When saturating an aqueous solution of lysine with air for 4 days, the researchers observed a CO_2 content of 0.48 per lysine molecule. When 20 bar of CO_2 were used instead, 0.61 molecules of CO_2 were captured per lysine in 3 h, either as carbamate or as bicarbonate. The addition of a Ru-MACHO catalyst, 80 bar H_2, and THF enabled the subsequent

reduction of the amine-bound CO_2 to formate in up to 55% yield. Other (oligo)amines like 1,5-diaminopentane, 1,1,3,3-tetramethylguanidine (TMG), or pentaethylenehexamine (PEHA) captured even more than 0.8 CO_2/amine, but they performed worse in the following reduction step.

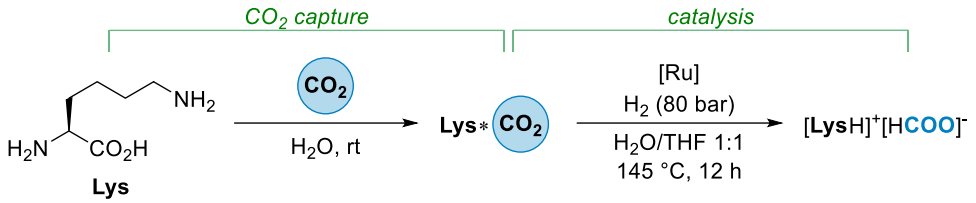

Scheme 36. Amino acid-assisted CO_2 conversion to formate.[272]

Based on these results, a novel ligand concept was envisioned. A similar approach was chosen by Aresta and co-workers, who investigated the reactivity of a 2-(pyridin-2-yl)ethan-1-amino iron complex with CO_2 and MeLi.[273] While they observed CO_2 insertion into the bond between Fe and the terminal amine starting at a pressure of 10 bar, no migration to the methyl nucleophile was noticed within 3 days. When changing the order of addition, the formation of a diacetate complex was observed. In analogy, the bifunctional molecules that have been rationally designed during the work on this dissertation were planned to have a rigid bidentate backbone with two *N*-donor atoms and a flexible side chain bearing a primary amine at the terminal position (Scheme 37).

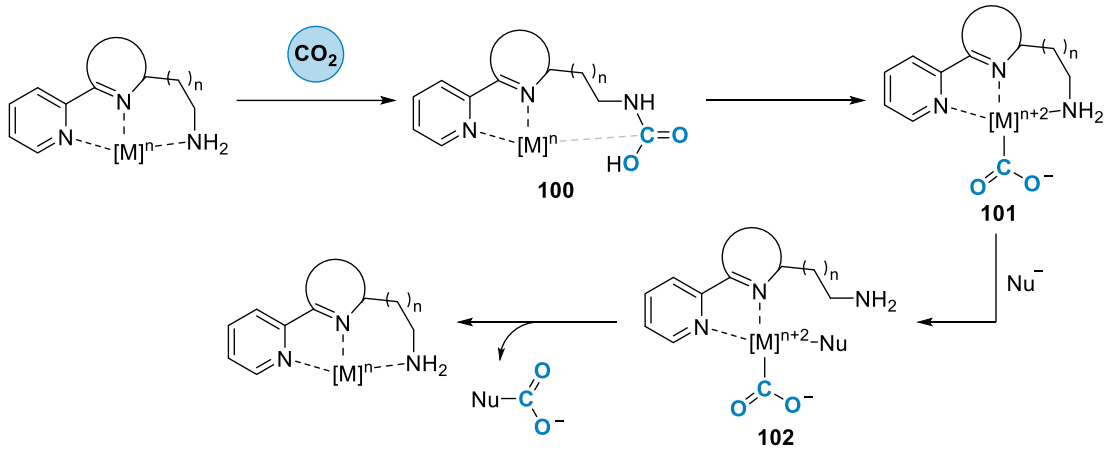

Scheme 37. Rationally designed *N*-donor ligand and its potential application as CO_2 transfer agent.

An appropriate flexibility of the side chain is needed to ligate the metal before and after the carbamate formation through CO_2 capture. It can be varied by modifying the number of carbon atoms (n = 0, 1, 2, 3, …) or by introducing heteroatoms (N, O, S, …). The rational reaction scheme for the potential transfer of carbon dioxide to an acceptor is shown above (Scheme 37). The reaction sequence might consist of CO_2 capture by formation of carbamate **100**, nucleophilic attack of the electron-rich metal center to form MCA **101**, coordination of a nucleophile and subsequent reductive elimination of the carboxylate. Suitable nucleophiles are organolithium compounds, alkenes, or alkynes, *inter alia*.

Many heterocoupling reactions with *C*-, *N*-, *O*-, and *S*-nucleophiles have been focused on in the past years, as discussed in the introduction (Chapter 5.1.3). They have in common that CO_2 pressures above or equal to 1 bar were required. However, the applied CO_2 pressure might be reduced by using a rationally designed bifunctional ligand that can assist in bringing CO_2 and the nucleophile closer together. Furthermore, the ligand might, due to its nature as a low-dentate ligand, provide additional free coordination sites that can bind to organic substrates and support organometallic reactions.[274]

5.2.2.1 Synthesis and Evaluation of Pyrox-C_4N

Starting from L-lysine, an amino acid from the chiral pool, the synthesis of a novel pyrox (pyridine-oxazoline) ligand **107** was envisioned. Although the arm of the designed ligand is rather long, potentially forming metallacycles with unfavorable ring sizes of 8 and 9 (for the carbamate), lysine was chosen as the starting material due to its commercial availability and low price. The chiral information of enantiopure L-lysine was not required for these first investigations but constituted an interesting approach to potential stereoselective applications. The retrosynthetic approach comprised a ring formation from **105** to **106** (B) and a reduction step to form **104** (D) besides two deprotection steps of the α-amine (C) and of the terminal amine in the side chain (A, Scheme 38). The reactions were successfully conducted on a gram scale.

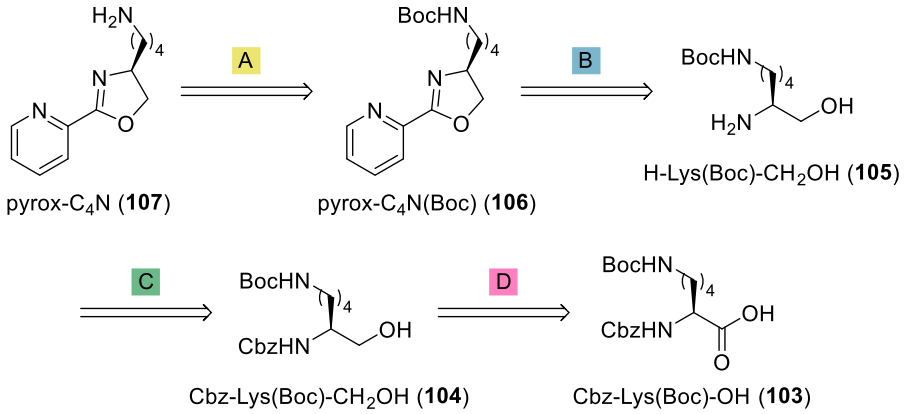

Scheme 38. Retrosynthetic strategy to synthesize Pyrox-C_4N starting from *N*-protected L-lysine **103**.

The starting material **103** contained two orthogonal protecting groups that enabled selective modifications during the synthetic process. The *N*-terminus of the amino acid was Cbz-protected and the primary amine in the side chain was Boc-protected. In the first step, Cbz-Lys(Boc)-OH (**103**) was reduced to the corresponding amino alcohol **104** (Scheme 39). For a successful reduction, amino acid **104** was transformed into a mixed anhydride using *iso*-butyl chloroformate and Hünig base (di-*iso*-propylethylamine, DIPEA). Then, it could be easily reduced adding $NaBH_4$ as a one-pot procedure.

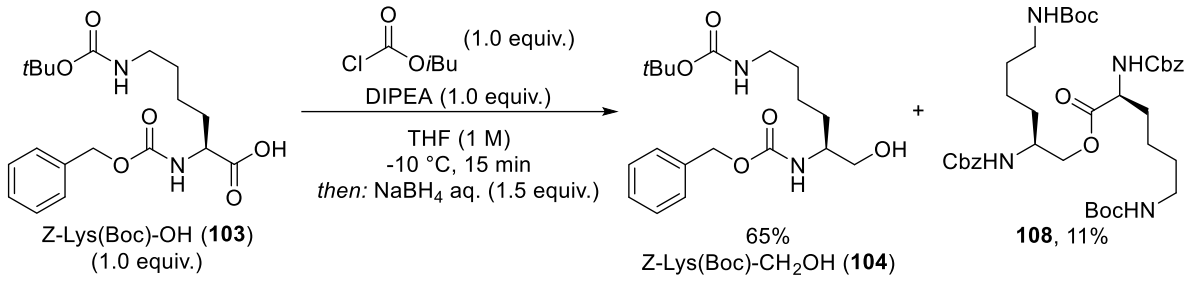

Scheme 39. Reduction of amino acid **103** to amino alcohol **104**.

The mild reaction conditions included a short reaction time together with a low temperature of –10 °C. Up to 3.2 g of the product were isolated in an average yield of 65%. Surprisingly, dimeric ester **108** was isolated as the side product in 11% yield, obtained from a reaction of the starting material with the product. Due to the lability of the Cbz-protecting group, no aluminum hydrides could be used. No conversion was observed after 24 h at ambient conditions or under reflux adding either borane or sodium borohydride solely.

Next, Cbz-protected lysinol derivative **104** was selectively deprotected catalyzed by 5 mol% Pd on activated carbon. The protecting group was removed by hydrogenation using a simple balloon with 1 atm. of hydrogen (Scheme 40).

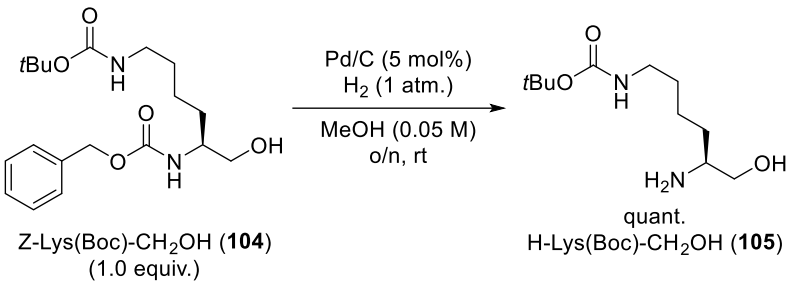

Scheme 40. Selective Cbz-deprotection of amino alcohol **105**.

The product H-Lys(Boc)-CH_2OH (**105**) was isolated by filtration in quantitative yield. The reaction could be scaled up to 2 g without loss in yield. Next, pyrox-C_4N(Boc) (**106**) was synthesized following a procedure of Li *et al*.[275] Amino alcohol **105** was cyclized with ethyl 2-pyridinecarboximidate (**109**), that was prepared by adding ethanol to 2-cyanopyridine. This procedure yielded mixtures of pyrox-C_4N(Boc) (**106**) and ester **110** in varying ratios (Scheme 41).

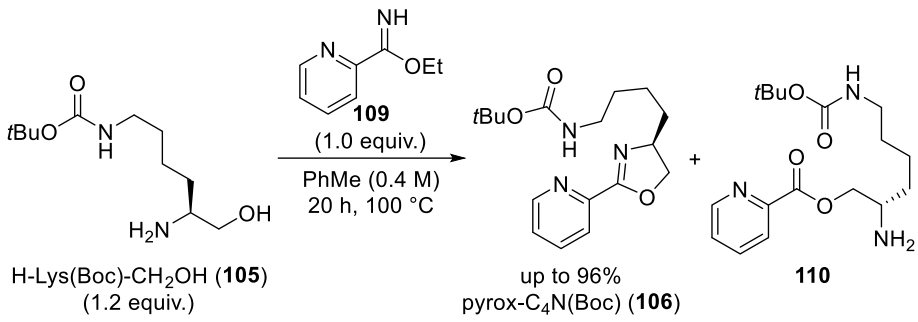

entry	ratio **106/110**[a]
1	26:74[b]
2	90:10
3	96:4
4	94:6 (90:10)[c]
5	86:14 (75:25)[c]

Scheme 41. Preparation of pyrox-C_4N(Boc) (**106**). [a] Ratio of products determined by ^{1}H NMR spectroscopy. [b] 24 h at 110 °C. [c] Ratio of products after 3 months on air.

Higher temperature and a longer reaction time favored the formation of by-product **110** (entry 1). If the reaction was run at 100 °C, the starting materials were fully converted after 20 h and the pyrox **106** was formed in an isolated yield of up to 96% (entry 3). The pyridyloxazoline structure of product **106** was confirmed by HRMS and NMR spectroscopy (Figure 19). Surprisingly, upon storage under air, pyrox-C_4N(Boc) (**106**) slowly changed into compound **110**.

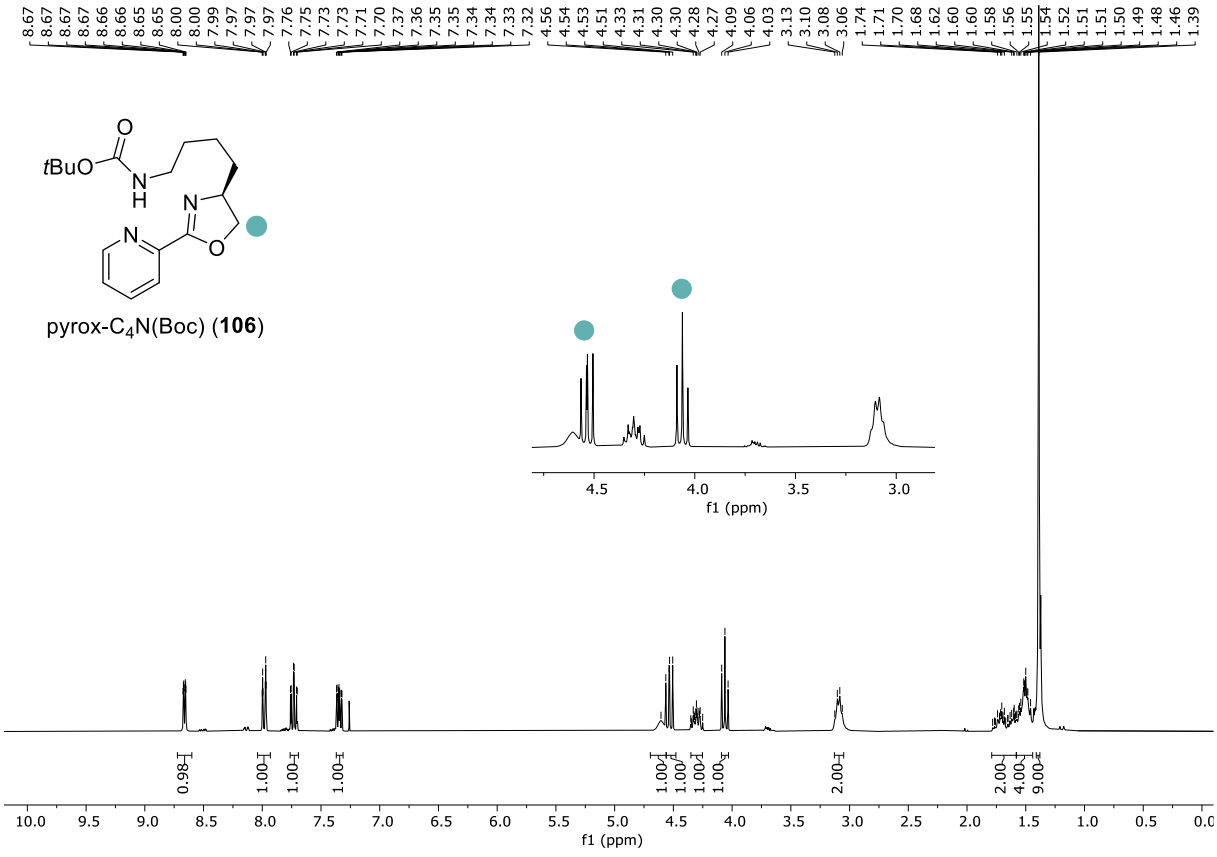

Figure 19. ^{1}H NMR spectrum of pyrox-C_4N(Boc) (**106**).

The signals of the side chain (between 1.00 and 3.50 ppm) remained the same as compared to the spectrum of the starting material, confirming that the Boc-protecting group remained intact during the reaction. A wide splitting of the signals of the methylene group in the oxazoline ring (green dot) into two down-field shifted sets of signals (4.06 ppm (dd, 1H, CH_2) and 4.53 ppm (dd, 1H, CH_2), colored in

turquoise) was observed. A connection of the wide splitting with the rigid and planar structure of the oxazoline ring was suggested, as the diastereotopic protons of the methylene group can move less and are, therefore, less equal. The down-field shift was caused by incorporation of the hydroxy group into the electron-withdrawing imidoester functionality.

As published by Schmidt and Qian for the cyclization of hydrazinopyridines with ethyl imidates, the mechanism of the cyclization reaction was proposed to include the nucleophilic attack of the amine **105** on the imidate **109**, followed by elimination of ethanol (Scheme 42). The nucleophilic attack of the hydroxy group, that resulted in a ring formation, was followed by elimination of ammonia.[276]

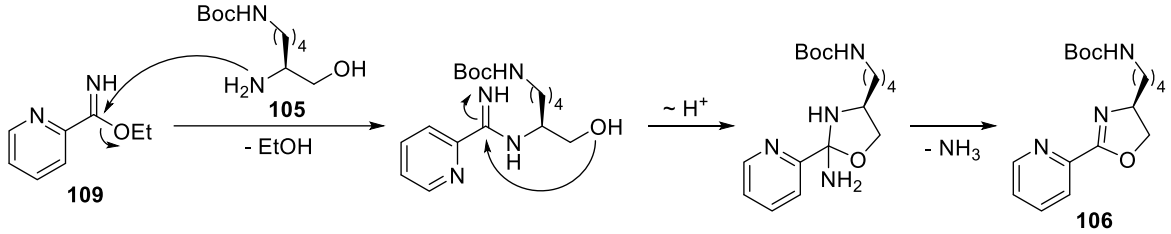

Scheme 42. Proposed mechanism for the oxazoline formation based on results by Schmidt and Qian.[276]

In the next step, the Boc-protecting group had to be removed to prepare a compound that can capture CO_2 *via* carbamate formation. The deprotection of pyrox-C_4N(Boc) (**106**) was accomplished using HCl in diethyl ether (Scheme 43). Afterwards, the amine hydrochloride salt **107*HCl** was treated with base to release the free amine **107**.

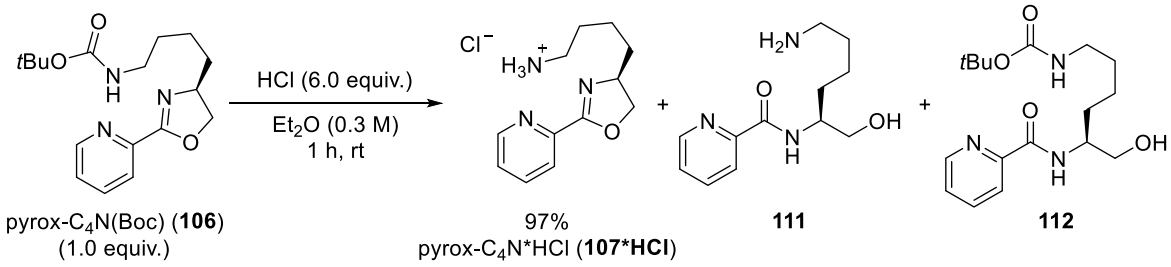

Scheme 43. Boc-deprotection reaction and competing ring opening.

In a first test reaction on small scale (0.1 mmol), pyrox-C_4N(Boc) (**106**) was reacted with 6 equivalents HCl followed by addition of aqueous NaOH solution. The crude NMR showed the pure amide product **111**, where the Boc-group had been successfully removed. If pyrox-C_4N(Boc) (**106**) was reacted with a decreased amount of 3 equivalents HCl followed by a basic work-up, no deprotection took place. Instead, the formation of Boc-protected amide **112** was observed in 48% yield. Thus, it was concluded that a high excess of HCl was required to remove the Boc-group whereas the basic work-up caused the opening of the oxazoline ring, that had been activated by the addition of an acid, and led to the formation of side products **111** and **112** *via* hydrolysis.[277] Indeed, when 6 equivalents HCl were added to pyrox-C_4N(Boc) (**106**) in dry solvents and without a basic work-up, the deprotected pyridyloxazoline **107** was isolated as a hydrochloride salt in 97% yield.

The amine hydrochloride salt was hygroscopic and slowly decomposed when stored under air (Figure 20). When the salt was dissolved in water, crystals of picolinic acid hydrochloride salt appeared. These were caused by decomposition of pyrox-C_4N*HCl (**107*HCl**) through acidic hydrolysis. To avoid such a decomposition, all compounds were from that point on handled under Schlenk conditions.

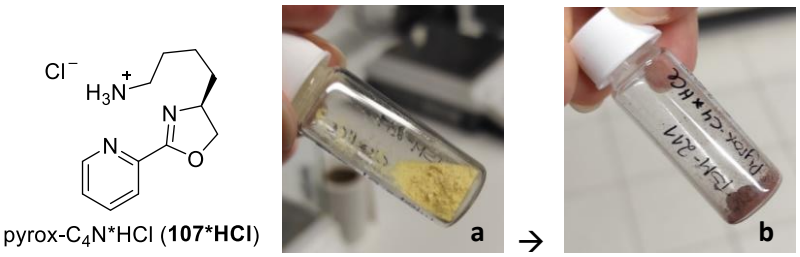

Figure 20. Pyrox-C_4N as hydrochloride salt **107*HCl**. The compound in a) was freshly prepared, while in b), it was stored under air for two weeks.

Aiming to gain final structural proof by X-ray crystallography, pyrox **106**, ester **110**, and amide **112** were reacted with a variety of different metal precursors (Figure 21). Especially the combination of amide **112** with $NiBr_2$ and of $FeBr_2$ with pyrox-C_4N(Boc) (**106**) led to promising results, precipitating colorful amorphous solids. Despite multiple attempts to grow single crystals from these precipitates, no crystal structure has been obtained yet. Other reaction mixtures seemed promising according to their NMR spectra (pyrox **106** with $PdCl_2(MeCN)_2$ or $Pd_2(dba)_3$) but yielded oily residuals. The issues in crystallizing the derivatives **106**, **110**, and **112** were most likely caused by the flexible side chain rendering it unfavorable for the molecules to stay in one conformation.[278]

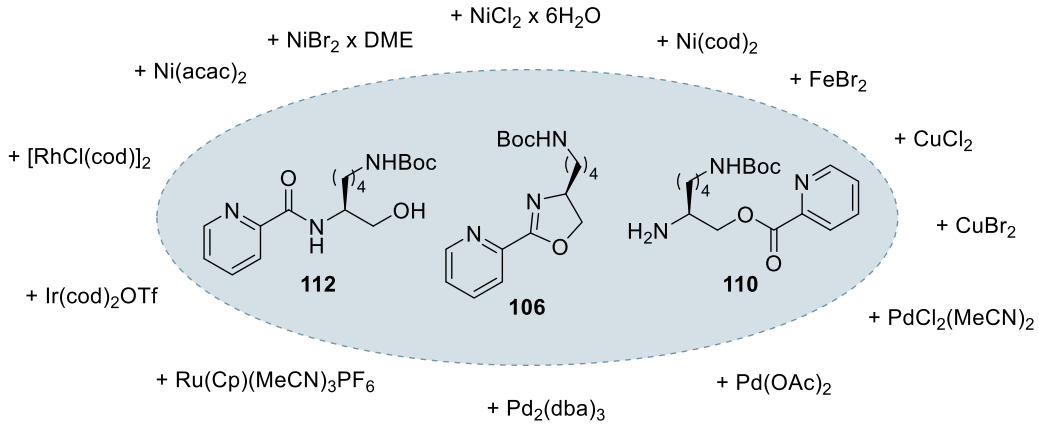

Figure 21. Different metal precursors were tested in combination with pyrox **106**, ester **110**, and amide **112**.

However, in order to find applications for pyrox-C_4N (**107**), the solubility in organic solvents had to be increased. To accomplish that, the chloride anion was exchanged with weakly coordinating BF_4^- using silver tetrafluoroborate (Scheme 44).

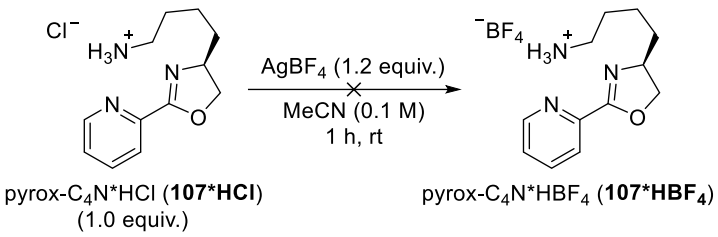

pyrox-C_4N*HCl (**107*HCl**) (1.0 equiv.)

pyrox-C_4N*HBF_4 (**107*HBF_4**)

Scheme 44. Anion exchange with silver tetrafluoroborate.

Whereas no reaction was observed in dry DCM, full conversion of the starting material was achieved using dry acetonitrile. AgCl was removed by filtration, and the crude product was dried *in vacuo* and analyzed. When examining the NMR spectra, however, it became obvious that the desired product decomposed under these reaction conditions. In a final attempt to investigate this reaction, the anion exchange was repeated using unaltered reaction conditions. However, the outcome of the first experiment was not reproducible. The ambiguous results of the anion exchange can be easily illustrated by comparing the aromatic region of the respective ^{13}C NMR spectra (Figure 22).

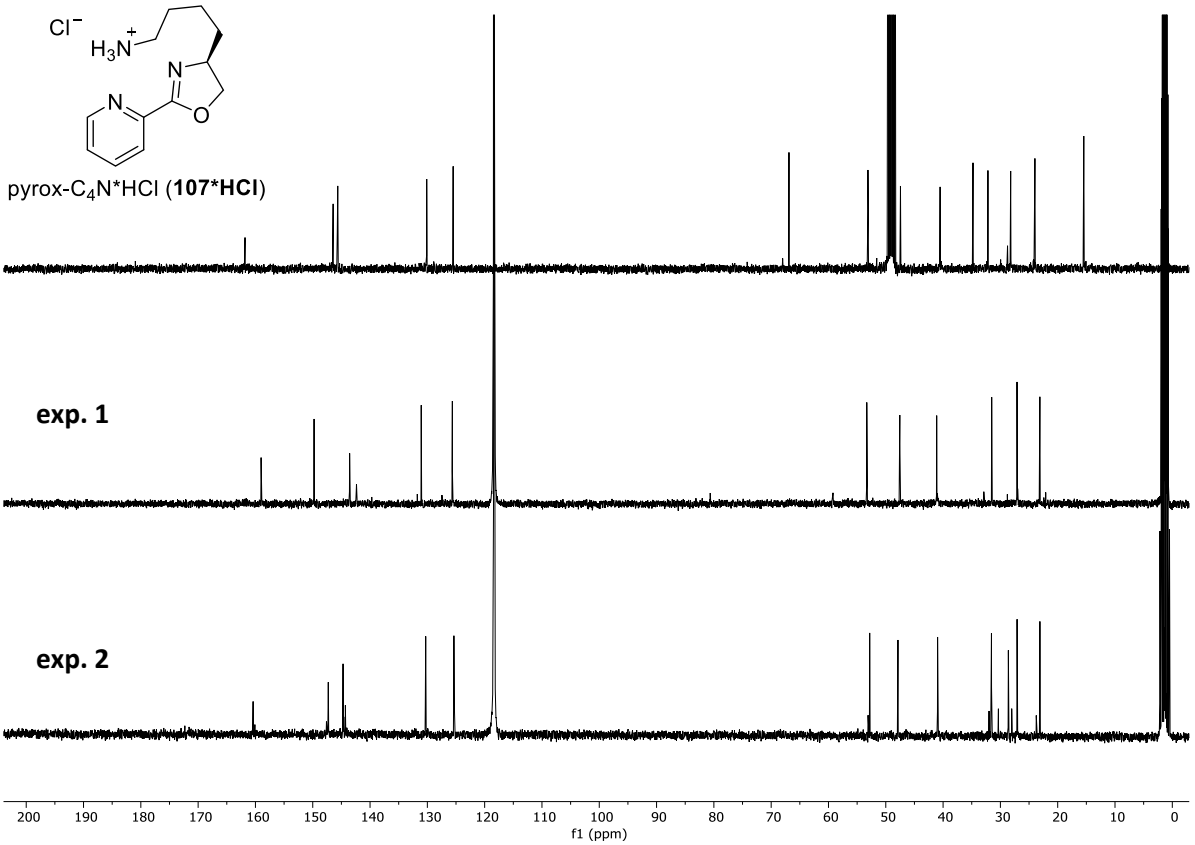

Figure 22. Comparison of ^{13}C NMR spectra of pyrox-C_4N*HCl (**107*HCl**), the product of experiment 1 and the product of experiment 2.

Questioning the stability of the deprotected pyridyloxazoline structure **107**, different conformers were calculated in collaboration with Dr. Alexander Linke using a semiempirical tight-binding model (XTB). The most stable conformer from the gas phase is depicted below (Figure 23, left). The flexible arm bearing a nucleophilic primary amine at the terminal position appeared to be able to

nucleophilically attack the carbonyl carbon atom of the oxazoline unit. This may result in the formation of an 8-membered diazocinol ring (Figure 23, right), followed by decomposition to multiple products. Based on these results, it became clear that replacing the C_4 side chain by a shorter hydrocarbon chain would not help to avoid this scenario, since the formation of 7-, 6-, and 5-membered rings is even more favorable.

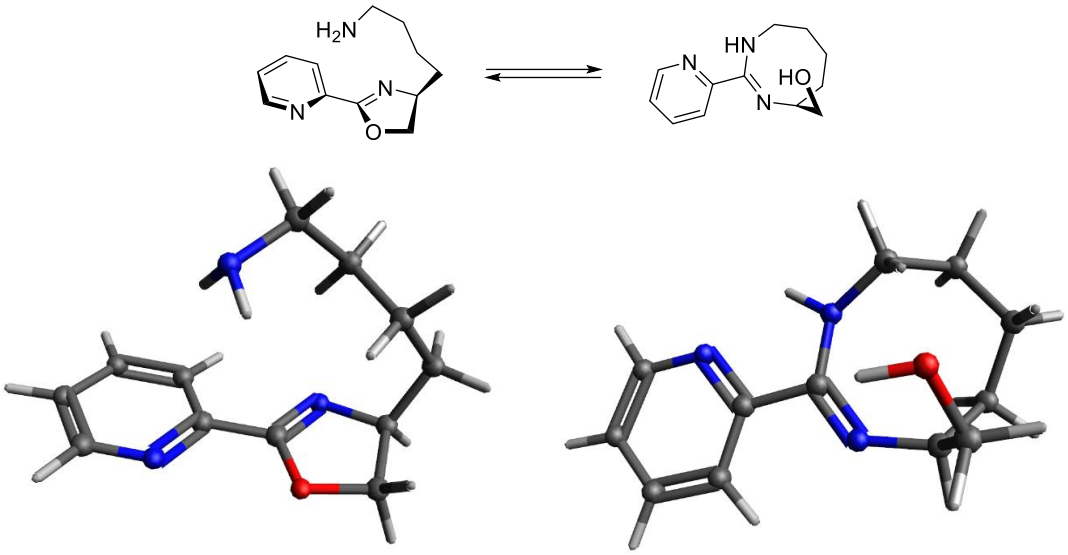

Figure 23. Stable conformer of pyrox-C_4N (**107**) and formation of an 8-membered diazocinol ring according to calculations using a semiempirical tight-binding model.

In summary, the synthesis of the novel pyrox-C_4N (**107**) was accomplished starting from L-lysine, a readily available amino acid from the chiral pool. The hydrocarbon chain bearing a free primary amine at the terminal position was meant to capture CO_2. By forwarding it to a metal center, which is ligated by the pyridine and the oxazoline units, an enhanced carbon dioxide capture at low pressure was targeted. However, the instability of the oxazoline ring was demonstrated experimentally and further rationalized by calculations. Additional attempts to gain structural proof *via* X-ray crystallography of a corresponding transition metal complex were unsuccessful. Since the aim was to synthesize a robust ligand for a variety of applications, a new structure had to be designed.

5.2.2.2 Synthesis and Evaluation of Phen-NCCN

Besides pyridyloxazoline structures, bipyridine and phenanthroline scaffolds are common bidentate *N*-based ligands in transition metal catalysis.[279] The revised target structure combined a bidentate phenanthroline ligand with an ethylene diamine side chain bearing a primary amine functionality (Scheme 45). The ligand was called phen-NCCN (**113**). The retrosynthetic approach comprised a C–N cross-coupling step (A) and, if necessary, the preparation of an appropriate phenanthroline halide from unsubstituted phenanthroline (**88**, B).

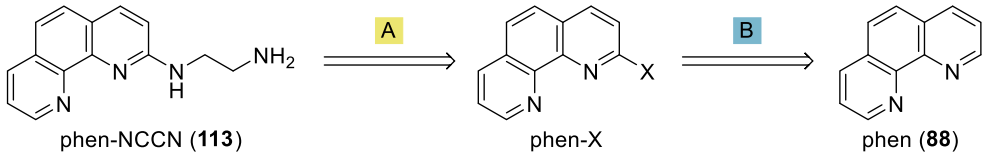

Scheme 45. Retrosynthetic strategy to synthesize phen-NCCN (**113**) starting from unsubstituted phenanthroline (**88**).

Inspiration for the ligand design as synthetic approach was drawn from the work of Ballestero, Abarca and co-workers, who published a strategy to synthesize new polynitrogenated ligands based on 3-(2-pyridyl)-[1,2,3]triazolo[1,5-*a*]pyridine.[280] Starting from the aryl iodide (**114**), they applied a Cu-catalyzed Ullmann-Goldberg cross-coupling-type reaction using only 4.0 equivalents ethylene diamine (EDA).

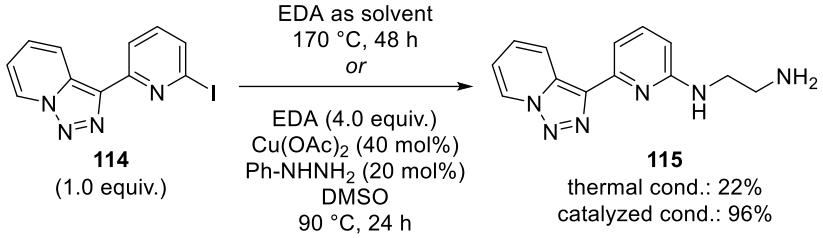

Scheme 46. Synthesis of polynitrogenated compound **115** according to Ballestero, Abarca and co-workers.[280]

They were able to isolate the coupling product **115** in 96% yield. When the commonly used thermal conditions were applied, only 22% of the desired product **115** were afforded. For this aromatic nucleophilic substitution reaction, the amine was taken as the solvent and the reaction mixture was refluxed for 2 days. However, Cu-catalyzed cross-coupling reactions were tested first for synthesizing phen-NCCN (**113**). Since phen-I (**116**) was not commercially available, it was aimed at synthesizing the compound starting from unsubstituted 1,10-phenanthroline (**88**). However, the direct oxidation using I_2 did not work. Thus, a longer route based on the procedure of Böttger *et al*. was chosen (Scheme 47).

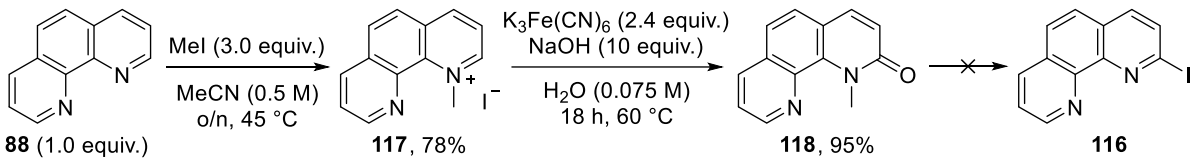

Scheme 47. Preparation of phen-I according to Böttger *et al*.[281]

The synthetic procedure proceeded *via* 1-methyl-1,10-phenanthrolin-1-ium iodide (**117**) and 1-methyl-1,10-phenanthrolin-2(1*H*)-one (**118**). Those two intermediates were successfully prepared and isolated in high yields of 78% and 95%, respectively.[281] Again, the subsequent reaction with I_2 did not afford the desired aryl iodide **116**. Therefore, the test reactions to synthesize phen-NCCN (**113**) from an aryl halide were carried out with commercially available 2-bromo-1,10-phenanthroline (**119**, Table 27).

Table 27. Test reactions for synthesizing phen-NCCN (**113**).

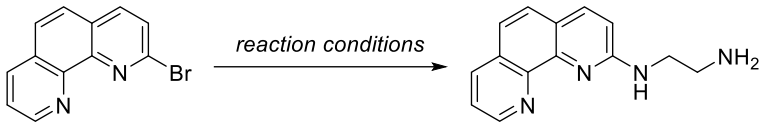

119 (1.0 equiv.) phen-NCCN (**113**)

entry	reaction conditions	observed product(s)
1	EDA (2.0 equiv.) $Cu(OAc)_2$ (10 mol%) KOH (2.0 equiv.) DMF (0.4 M) 100 °C, 2 d *or* EDA (2.0 equiv.) CuI (1.0 equiv.) NaOAc (2.5 equiv.) DMF (0.4 M) 100 °C, o/n	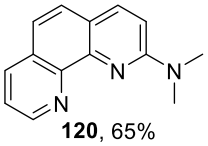 **120**, 65%
2	EDA (5.0 equiv.) Cu (5 mol%) H_2O (0.4 M) 100 °C, o/n	no conversion
3	EDA (1.5 equiv.) $Pd(dppf)Cl_2$ (5 mol%) KO*t*Bu (3.0 equiv.) THF (0.4 M) 100 °C, o/n	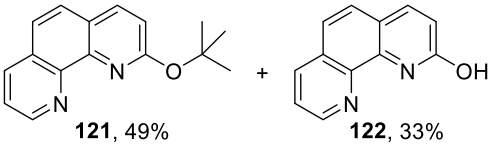 **121**, 49% + **122**, 33%
4	EDA (4.0 equiv.) $Cu(OAc)_2$ (40 mol%) $Ph\text{-}NHNH_2$ (20 mol%) DMSO 90 °C, o/n *or* EDA (2.0 equiv.) $Cu(OAc)_2$ (10 mol%) KOH (2.0 equiv.) DMSO (0.4 M) 90 °C, o/n	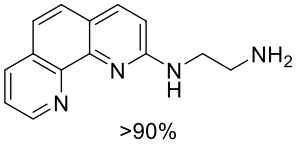 >90% phen-NCCN (**113**)

First, 2-bromo-1,10-phenanthroline (**119**) was reacted with ethylene diamine in presence of a Cu catalyst and a base in DMF as solvent. *N,N*-dimethyl-1,10-phenanthrolin-2-amine (**120**), which was the coupling product with DMF, was isolated in 65% yield (entry 1). This undesired reaction was observed regardless of using $Cu(OAc)_2$ with KOH or CuI with NaOAc.[282] No reaction was observed using Cu powder in water, as described by Jiao *et al*. (entry 2).[283] Applying Buchwald-Hartwig conditions with $Pd(dppf)Cl_2$ and KO*t*Bu in THF, the coupling product with KO*t*Bu, 2-(*tert*-butoxy)-1,10-phenanthroline (**121**), was isolated in 49% yield together with the hydrolyzed coupling product, 1,10-phenanthrolin-2-ol (**122**), in 33% yield (entry 3). However, following the procedure of Ballestero, Abarca and co-workers or running the reactions with $Cu(OAc)_2$ in DMSO rather than in DMF, the desired product **113** was obtained as the sole product after removal of the Cu catalyst and the high-boiling solvent (entry 4).

The thermal nucleophilic aromatic substitution of 2-bromo-1,10-phenanthroline (**119**) with excess EDA as the solvent was successful, too, and was taken as the method of choice due to its operational simplicity. The reaction was complete after 24 h at 100 °C. The product was obtained in 92% isolated yield (Scheme 48).

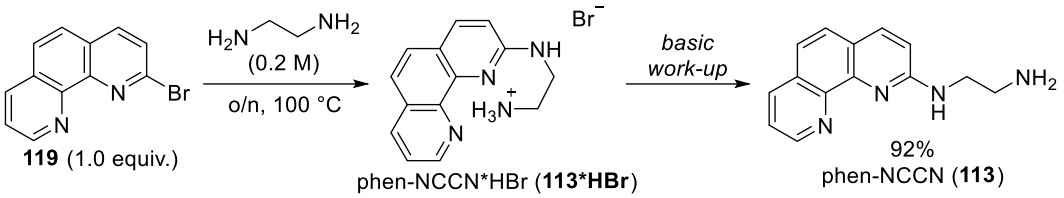

Scheme 48. Synthesis of phen-NCCN (**113**).

The coupling product was crystallized from the reaction mixture as hydrobromide salt (**113*HBr**, Figure 24). Interestingly, the crystal structure revealed a rather short bond length between N2 and the adjacent C3 atom (1.367(2) Å). According to Pyykkö and Atsumi, the interatomic distance can be assigned to a bonding situation between a single (1.46 Å) and a double bond (1.27 Å).[284]

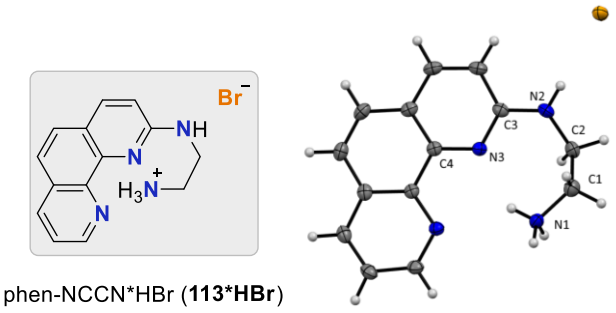

Figure 24. X-ray structure of phen-NCCN*HBr (**113*HBr**). Color code: grey (C), blue (N), orange (Br). Selected interatomic distances [Å]: N1-C1 1.484(2), N2-C2 1.457(2), N2-C3 1.367(2), N3-C3 1.325(2), N3-C4 1.360(2). Selected angles [°]: N1-C1-C2 111.1, C2-N2-C3 121.9.

The free amine was obtained upon treatment with aqueous NaOH solution as a yellow oil in 92% yield. Interestingly, the product readily crystallized in the NMR tube from deuterated chloroform. The crystals were identified as phen-NCCN hydrochloride salt (**113*HCl**), caused by traces of HCl in the deuterated chloroform. The substituted phenanthroline **113** was fully characterized including a ^{1}H-^{15}N HMBC NMR spectrum, which unambiguously illustrated the connectivity of the four different N nuclei (Figure 25).

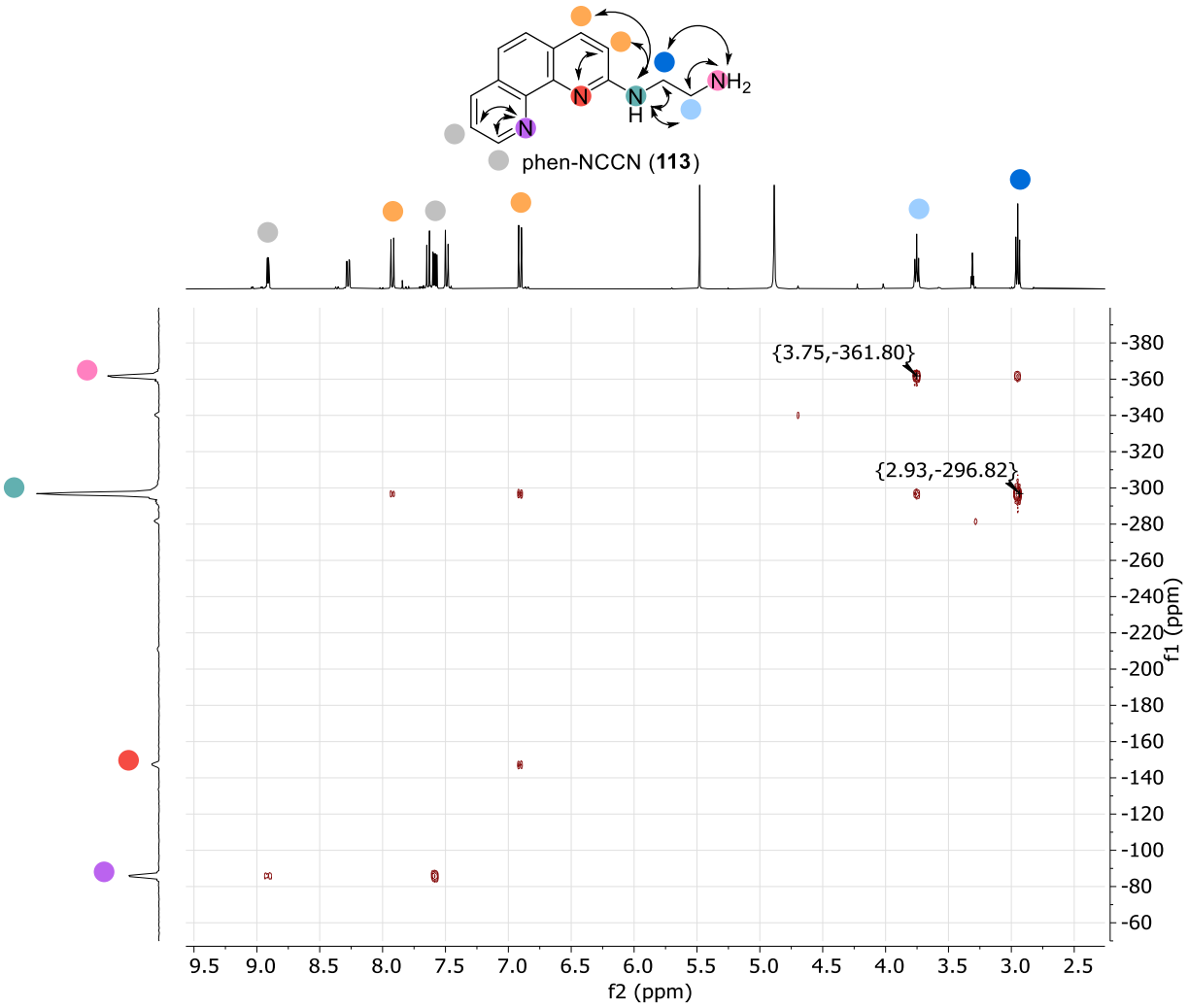

Figure 25. ^{1}H-^{15}N HMBC NMR spectrum of phen-NCCN (**113**).

The ^{15}N signal at –296.8 ppm showed an interaction with the aromatic protons, colored in orange, and the aliphatic protons, colored in blue. It was thus assigned to the secondary amine (green dot). Due to the high intensity of the signal, the aliphatic signal at 2.93 ppm was assigned to the adjacent methylene group (dark blue dot). The ^{15}N signal at –361.8 ppm showed an interaction with the aliphatic protons only, colored in blue. Hence, it was assigned to the primary amine (pink dot). Because of the higher intensity of the interaction signal from the interaction with the protons at 3.75 ppm, this signal was assigned to the second methylene group, colored in light blue. Likewise, the nitrogen atom included in the phenanthroline core were assigned to the signals shifted down-field (purple and red spot).

Promisingly, when the product was alkalized with aqueous K_2CO_3 instead of NaOH solution, the ^{13}C NMR spectrum of the product obtained an additional signal at 169.5 ppm, which hinted towards the formation of a carbamate species. Next, phen-NCCN (**113**) was reacted with $Pd(OAc)_2$ to examine the binding ability to a transition metal center for the further catalytic applications (Scheme 49).

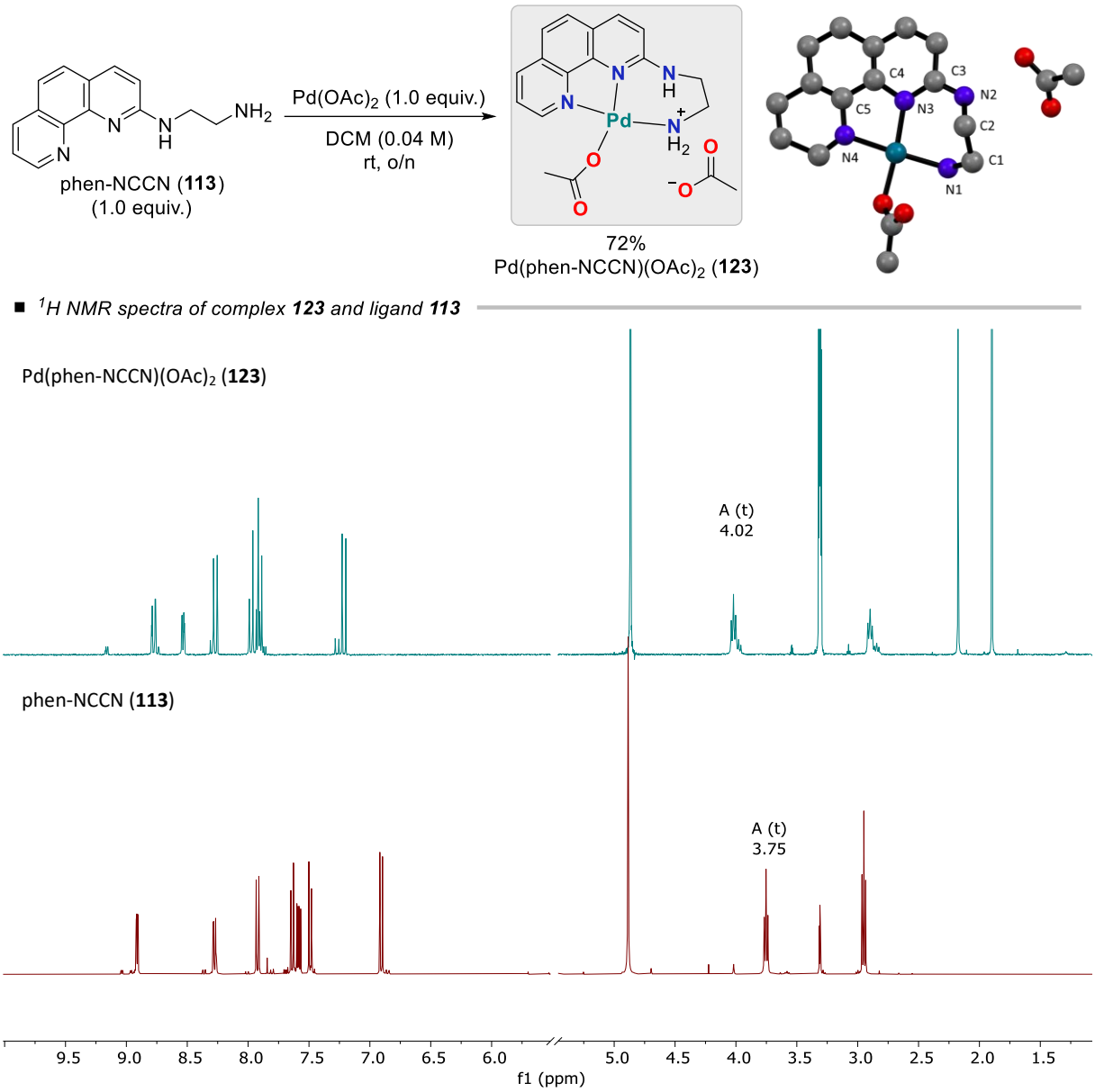

Scheme 49. Synthesis of Pd(phen-NCCN)$(OAc)_2$ (**123**), stacked ^{1}H NMR spectra of the Pd complex **123** (top) and the free ligand **113** (bottom), and X-ray structure of the complex **123**. Color code: grey (C), blue (N), red (O), teal (Pd). The position of the hydrogen atoms has not been determined due to the poor quality of the crystals. Selected interatomic distances [Å]: N1-C1 1.572, N2-C2 1.441, N2-C3 1.359, N3-C3 1.383, N3-C4 1.291, N4-C5 1.456, Pd-N1 2.053, Pd-N3 2.023, Pd-N4 2.025. Selected angles [°]: N1-C1-C2 111.2, C2-N2-C3 124.0.

The corresponding Pd complex Pd(phen-NCCN)$(OAc)_2$ (**123**) was synthesized in 72% yield. A down-field shift of most aromatic signals was observed in the ^{1}H NMR spectrum, confirming a coordination by the phenanthroline backbone. Interestingly, also the signal of one methylene group was shifted down-field (δ = 4.02 ppm i.o. 3.75 ppm). This can be explained by an additional coordination *via* the amine chain. According to the ^{1}H-^{15}N HMBC NMR spectrum of the free ligand (Figure 25), the respective proton signal can be assigned to the methylene group bearing the terminal amine. And indeed, the tridentate coordination was confirmed by X-ray crystallography (Scheme 49), even though the quality of the crystals was too low for a complete calculation of all parameters. The complexes were arranged

via π-stacking of the phenanthroline rings. The crystallographic data showed that the complex formed a cationic species. The square planar structure was in line with the 18-electron rule. Hence, one of the acetate ligands of the precursor formed the counterion. This was also observed in the ^{1}H NMR spectrum, as the methyl groups of the free and coordinated acetate groups were generating two independent singlets. Comparison of the bond lengths of the complex and the free ligand revealed two observations. First, the bond between N1 and C1 was elongated (1.572 Å), which was in line with the additional coordination of N1 by Pd. The interatomic distance between N1 and Pd (2.053 Å) was similar to those of N3 and N4 with Pd (2.023 Å and 2.025 Å, respectively) and matched literature-known Pd(phen)$(OAc)_2$ complexes.[266] Second, the bond lengths within the phenanthroline backbone differed much more from each other than in the free ligand. This suggested an incomplete delocalization of the electron density in the former aromatic system. In summary, the identified coordination modus of the phen-NCCN (**113**) ligand opened the possibility for CO_2 capture *via* the free NH group and subsequent transfer to the metal center to accomplish CCU.

The synthesis, characterization, and complexation of phen-NCCN (**113**) was followed by investigating its reactivity with CO_2 (Scheme 50).

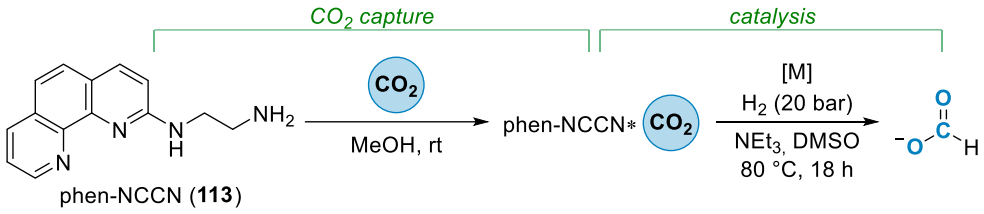

Scheme 50. Using phen-NCCN (**113**) for carbon capture and utilization.

In collaboration with Carolin Stein, M.Sc., it was tested if the molecule was able to capture CO_2. For this, a method of Wei *et al.* was applied that comprised stirring the reagent under CO_2 pressure for a certain time and analyzing the amount of captured CO_2 by quantitative ^{13}C NMR using THF as the internal standard.[272] A strong pressure and solvent dependency of CO_2 uptake was observed according to the researchers. Following the procedure from literature, the applied CO_2 pressure was varied between 20 bar, 2 bar and atmospheric concentrations. In contrast to Wei *et al*., MeOH was used as the solvent instead of water to avoid the formation of bicarbonate next to carbamate. Also, some of the substrates were not soluble in water. A theoretical CO_2 content of 100% per amine is possible for both ligand **113** and EDA, because no second molecule was required for proton uptake; this can be accomplished within one molecule by the second amine unit. In addition to the novel phen ligand **113**, also unsubstituted phenanthroline (**88**), EDA, a 1:1 mixture of both, and L-lysine were tested (Table 28).

Table 28. CO_2 capture by different substrates and at varied CO_2 pressures.

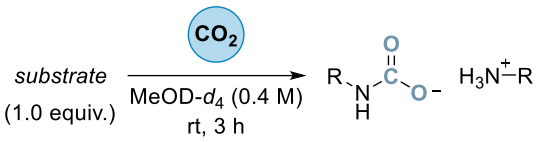

■ *CO_2 capture*

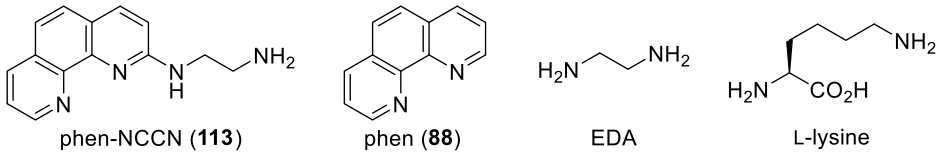

entry	substrate	CO_2 pressure [bar]	yield[a]
1	phen-NCCN (**113**)	20	30%
2	phen (**88**)	20	--
3	EDA	20	54%
4	EDA + phen 1:1	20	70%
5	L-lysine	20	25%
6	phen-NCCN (**113**)	2	39%
7	EDA	2	55%
8[b]	phen-NCCN (**113**)	0.0004	12%

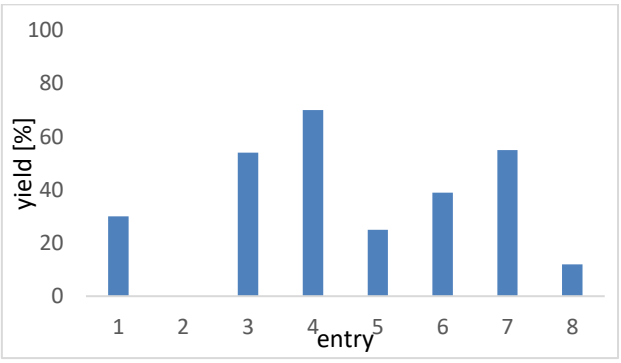

The reactions were performed on a 0.2 mmol scale. [a] NMR yield using THF as internal standard, calculated on the amount of substrate. [b] Diluted reaction (0.05 M), compressed air was bubbled through the reaction mixture for 3 days.

To our delight, additional signals were found in the carbamate region of the quantitative ^{13}C NMR spectra of phen-NCCN (**113**) after treatment with CO_2. Calculations using the internal standard THF revealed that the corresponding carbamates had been formed in 30% yield at 20 bar pressure (entry 1). Whereas unsubstituted phenanthroline (**88**) showed no reactivity with CO_2 (entry 2), EDA and L-lysine were both able to capture carbon dioxide in 54% and 25% yield, respectively (entries 3 and 5). The 1:1 mixture of phen and EDA even outcompeted the captured amount of pure EDA by reaching a yield of 70% (entry 4). Next, both ligand **113** and EDA were tested at a decreased CO_2 pressure of 2 bar (entries 6 and 7). No reduction in yield was observed. Instead, the amount of captured CO_2 was equal or higher as compared to the experiments at 20 bar, yielding the respective products in 39% for ligand **113** and 55% for EDA, respectively. As expected, applying atmospheric concentration of CO_2 from compressed air to phen-NCCN (**113**) resulted in a decreased amount of 0.12 mol of CO_2 uptake per mol of amine (entry 8).

However, discrepancies in the mass balance cast doubt on the quality of the applied methodology. When calculated from the internal standard THF, not the complete amount of substrate was recovered, although the NMR sample was directly taken from the homogenized reaction mixture. Deviations of 15% to 46% were found in the mass balance. Especially the experiments with pure EDA suffered from substrate loss.

In the reaction of phen-NCCN (**113**) with CO_2, two regiosiomeric carbamates, **124a** and **124b**, can be anticipated (Scheme 51).

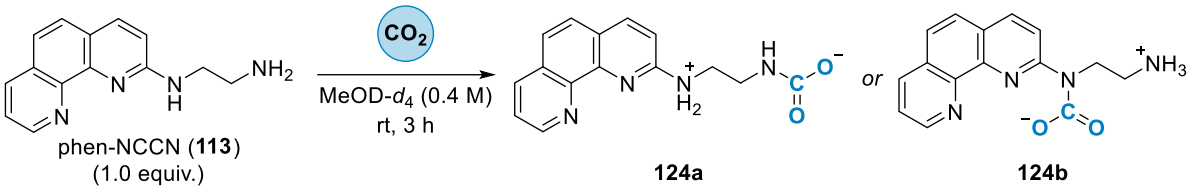

Scheme 51. Carbon dioxide capture with phen-NCCN (**113**): two different regioisomers (**124a**, **124b**) are possible.

To examine the binding situation after CO_2 capture, a full set of NMR spectra comprising 1D and 2D experiments was recorded after the reaction of phen-NCCN (**113**) with 20 bar CO_2. Four different species were identified in the ^{1}H NMR spectrum. According to the NOESY NMR spectrum, two of them were interchanging, resulting in multiple interaction signals. A ^{1}H-^{15}N HMBC NMR spectrum finally helped to assign the main product to one of the possible structures **124a** and **124b** (Figure 26).

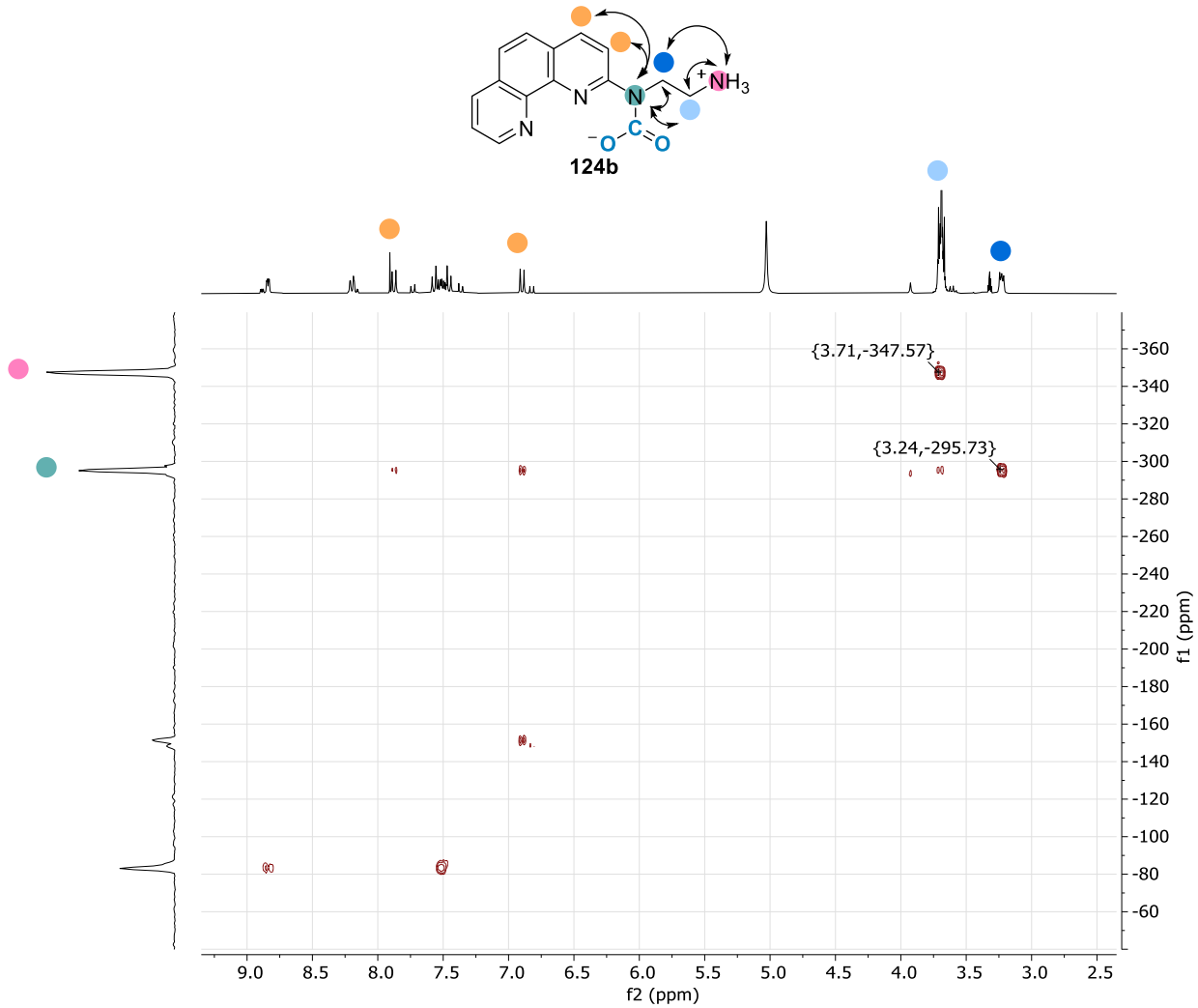

Figure 26. ^{1}H-^{15}N HMBC NMR spectrum of phen-NCCN after the reaction with CO_2.

The ^{1}H chemical shift of the methylene group next to the terminal amine, colored in light blue, remained almost unaltered (δ = 3.71 i.o. 3.75 ppm). In contrast, the signal of the methylene group next to the secondary amine group, colored in dark blue, showed a strong down-field shift (δ = 3.24 i.o. 2.93 ppm). This pointed towards the formation of carbamate **124b** as the main product, which

corresponded to the increased nucleophilicity of secondary as compared to primary amines.[285] The variations of the ^{15}N chemical shifts were not used to propose a structure for the carbamate, since it strongly depends on many external factors including concentration, solvent, and water content.[286]

An additional rational argument for the formation of the secondary carbamate **124b** is the possibility to stabilize the proton by formation of 6- or 7-membered cycles. This delocalization of the proton between the primary amine, the carbamate and both heterocyclic amines of the phenanthroline backbone would result in the formation of structures **124b'** and **124b''** (Scheme 52). Putatively, one of these tautomers caused the broad signals of the side product that had been observed to interchange with the main product. The other two side products might be assigned to the second possible carbamate species, **124a**, and its respective tautomer(s).

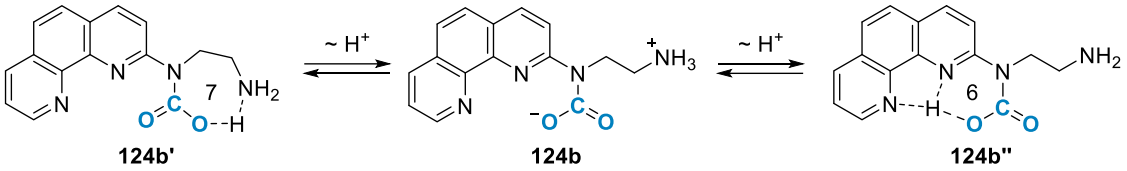

Scheme 52. Tautomeric equilibria of **124b** with **124b'** and **124b''**.

Next, the carbon capture experiment was repeated with palladium complex **123**. However, the compound decomposed in deuterated methanol during the reaction and gave palladium black, as it is known for $Pd(OAc)_2$ complexes in alcohols.[248] The analysis by NMR spectroscopy mainly showed the free ligand **113** and acetic acid but no carbamate species (Scheme 53).

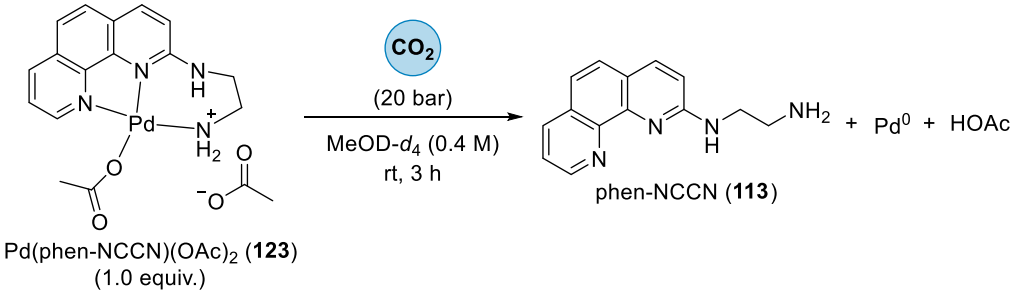

Scheme 53. Decomposition of complex **123** under the applied reaction conditions.

Therefore, subsequent CO_2 hydrogenation reactions to explore the utilization of phen-NCCN (**113**) for CCU were not only conducted with Pd precursors. Instead, also Ru, Rh, Ir, and Pt precursors were tested (Table 29). The CO_2 hydrogenation was undertaken by Carolin Stein, M.Sc., and analyzed by quantitative ^{13}C NMR spectroscopy using DMF as internal standard. The produced amounts of formate were calculated on the amount of TEA base to obtain a conversion and on the amount of metal to obtain a TON.

Table 29. Screening of metal precursors for the basic CO_2 hydrogenation to formate.

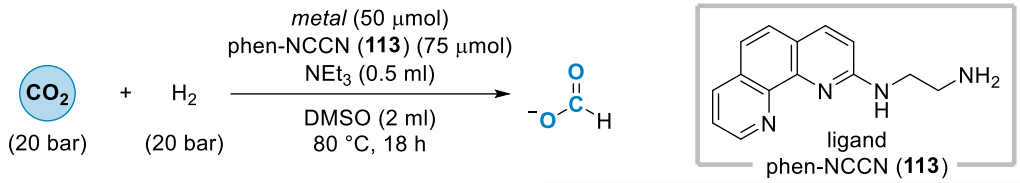

entry	metal precursor	conversion[a]	TON
1	$Pd(phen\text{-}NCCN)(OAc)_2$ (**123**)	40%	29
2	$Pd(OAc)_2$	26%	19
3	$PdCl_2(MeCN)_2$	33%	24
4	$Pd(acac)_2$	18%	13
5	Pd(COD)ClMe	8%	6
6	$[Ru(cymene)Cl_2]_2$	329%	238
7	$Ru(COD)Cl_2$	203%	147
8	$[Rh(acac)_2]_2$	39%	28
9	$[IrCl_2Cp^*]_2$	103%	74
10	$[Ir(COE)_2Cl]_2$	255%	184
11	Pt(acac)	--	--
12[b]	--	--	--

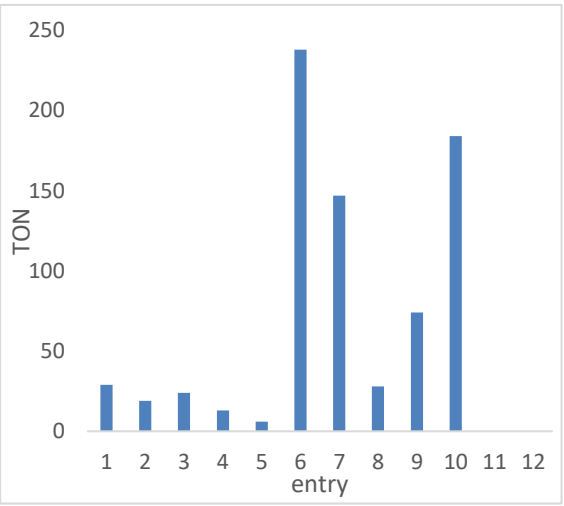

[a] The amount of formate was taken from ^{13}C quant. NMR using DMF as internal standard and used to calculate the conversion on the amount of base (3.6 mmol). [b] Control reaction without metal source.

All metal precursors except the Pt(I) complex were active in the hydrogenation of CO_2 to formate. The pre-synthesized Pd complex **123** afforded the product after 29 turnovers in 40% conversion with respect to the applied base (entry 1). When complex was formed *in situ* by addition of $Pd(OAc)_2$ and ligand **113**, the TON still amounted to 19 (entry 2). These entries as well as other Pd precursors all produced Pd black as the decomposition product (entries 3-5). Interestingly, much higher conversions were achieved using Ru precursors, yielding formate in TONs of 238 and 147, respectively (entries 6 and 7). Whereas the $[Rh(acac)_2]_2$ precursor only showed minor activity, giving formate in 39% conversion (entry 8), iridium(I) successfully afforded the product with a TON of 74 and 184, respectively (entries 9 and 10). Applying Pt(acac) as the metal precursor, no formate was detected (entry 11). A control reaction further confirmed the importance of the transition metal (entry 12). The amount of product exceeded the amount of base in the reactions catalyzed by Ru and Ir (entries 6, 7, 9, and 10). An equilibrium of formate with formic acid (FA) was postulated in the instances (Scheme 54).

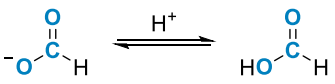

Scheme 54. Equilibrium of formate with formic acid.

It was assumed that CO_2 hydrogenation could also take place under neutral conditions without the addition of base to stabilize the product. This was appealing due to the simplified setup. Further experiments were conducted in an ongoing collaboration with Carolin Stein, M.Sc., to investigate this assumption (Table 30). Accordingly, $[Ru(cymene)Cl_2]_2$ was dissolved in dry DMSO and added phen-

NCCN (**113**), EDA, or phenanthroline (**88**) as the ligand. The formic acid yield was determined by quantitative ^{13}C NMR.

Table 30. Screening of ligands for the neutral CO_2 hydrogenation to formate.

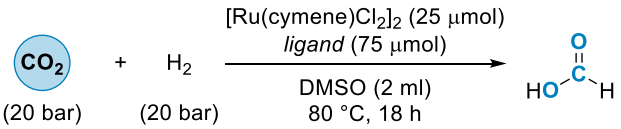

■ *CO_2 conversion*

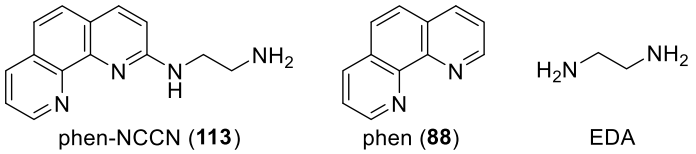

entry	ligand	n(FA)[a] [mmol]	TON
1	--	--	--
2	phen-NCCN (**113**)	0.59	12
3[b]	phen-NCCN (**113**)	0.75	15
4	EDA	--	--
5	phen (**88**)	0.59	12

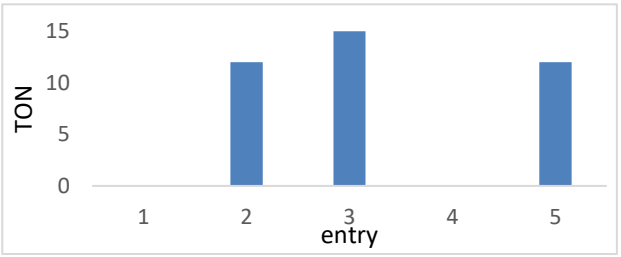

[a] The amount of formate was taken from ^{13}C quant. NMR using DMF as internal standard. [b] 250 µmol ligand (5.0 equiv.) were used.

The ligand screening in neutral conditions was commenced by testing if a ligand was required at all (entry 1). In this reaction, no formic acid was detected according to NMR spectroscopy, emphasizing the importance of the ligand. In the presence of novel phen ligand **113**, formic acid was produced with a TON of 12 (entry 2), equaling approx. 5% of the initial TON when base was added (Table 30, entry 6). However, it is known that basic hydrogenation is thermodynamically favored because the product is stabilized by deprotonation, which shifts the equilibrium to the side of the product.[287] Hence, it was not surprising to see that the amount of FA produced in the neutral CO_2 hydrogenation was lower. The amount of formate produced under neutral conditions was further increased if the amount of ligand **113** was raised from 1.5 to 5.0 equivalents (entry 3). This can be also caused by the basic properties of the tetraamine ligand **113** influencing the pH of the reaction mixture. To investigate the role of the ligand, the components phenanthroline (**88**) and EDA were tested individually (entries 4 and 5). While EDA as ligand did not support the formation of FA, unsubstituted phenanthroline (**88**) showed comparable activity as phen-NCCN (**113**).

These results were compared with the literature. $Ru(phen)(cymene)Cl_2$ is known to be active in the transfer hydrogenation of acetophenone with FA as the hydrogen source and in the heterogeneous hydrogenation of cyclohexanone with H_2 but so far not in CO_2 hydrogenation.[288-290] In contrast, basic CO_2 hydrogenation has been reported on utilizing $[Ru(cymene)Cl_2]_2$ complexes bearing bidentate nitrogen ligands like pyridyloxime (TON 50) and 8-aminoquinoline (TON 5562).[287, 291]

In summary, the novel phenanthroline derivative phen-NCCN (**113**) was successfully synthesized in one step from inexpensive starting materials. The synthesis was conducted on gram scale yielding the clean product **113** in >90% yield. The product was fully characterized by NMR spectroscopy and X-ray crystallography. Experiments with pressurized CO_2 confirmed the ability of the hydrocarbon chain bearing a primary and a secondary amine to capture carbon dioxide, while the respective product was assigned to internal carbamate **124b** based on ^{1}H-^{15}N HMBC NMR spectroscopy. Ligand phen-NCCN (**113**) was successfully applied in the hydrogenation of CO_2 under both basic and neutral conditions, producing formate with TONs of up to 238. However, it remained unclear if phen-NCCN (**113**) retained any bifunctional nature during the reaction or whether the side chain was potentially protonated by FA and, thus, inactivated. This would be in line with the similar behavior of phen-NCCN (**113**) and the parent compound phenanthroline (**88**) under neutral conditions. Also, the activities of EDA and phenanthroline (**88**) under basic conditions were still unknown and had to be compared to the performance of phen-NCCN (**113**) to rule out any mechanistic pathways. Lastly, an improved conversion of CO_2 might be possible if CO_2 capture and conversion were carried out consecutively and not simultaneously.

6 Summary and Outlook

During the work on this dissertation, the different components of a carbon dioxide-related circular economy were examined targeting the utility of CO_2 as C_1 building block in organic syntheses. This included investigations on the release, the capture, and the conversion of CO_2.

First, CO_2 release was explored starting from pharmaceutically relevant and natural carboxylic acids (Scheme 55). The method of choice was a photo-mediated decarboxylation reaction that was catalyzed by the inexpensive, organic tetra-*N*-propylpyrimidopteridine photoredox catalyst under basic conditions. The procedure was thoroughly optimized utilizing a statistical DoE approach. The scope comprised 26 examples including the decarboxylation of primary, secondary, and tertiary carboxylic acids. sp^2-Hybridized carboxylic acids and substrates bearing free amino groups could not be converted, *inter alia*. The aqueous reaction environment rendered this protocol potentially suitable for applications in wastewater treatment. When water was exchanged with deuterated water as an inexpensive deuterium source, the monodeuterated decarboxylated product was selectively formed with a high deuterium incorporation of up to 95%. Since more than 50% of the deuterated product are formed if the amount of D_2O is lowered to 5.0 equiv., this methodology can be suitable for tritium labeling studies. Furthermore, a sensitivity assessment revealed the high robustness of this reaction. The decarboxylation of naproxen was accomplished on gram scale, from commercially available tablets, and in non-degassed solvents by saturating the reaction mixture with inert gas for only 10 minutes. Various experiments were conducted to elucidate the reaction mechanism. Valuable insights were given by cyclic voltammetry and photoluminescence quenching experiments as well as EPR spectroscopy and radical quenching experiments. The proposed reaction mechanism underlined the dual role of PPTs as photoredox and hydrogen atom-transfer catalyst.

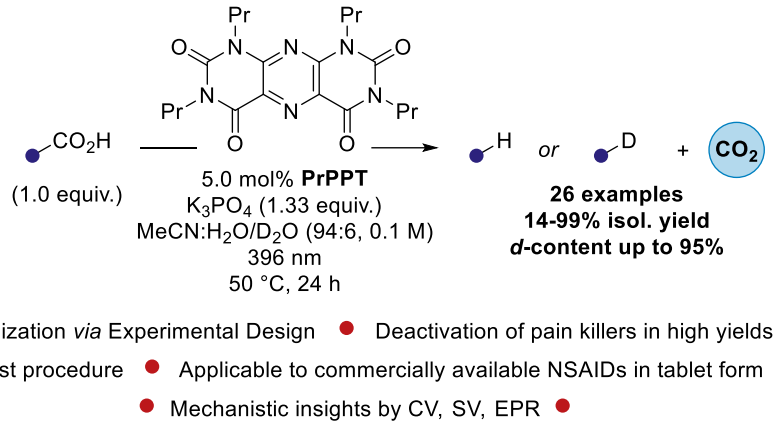

Scheme 55. CO_2 release by photomediated, PrPPT-catalyzed hydro- and deuterodecarboxylation of carboxylic acids.[37]

Next, the research was focused on CO_2 capture by waste materials like modified nylon (Scheme 56). A methodology for the selective hydrogenolysis of amides to the secondary amines, which are apt to bind carbon dioxide, was investigated. Based on the work of Klankermayer and Leitner, the reaction conditions were systematically optimized using *N*-hexylhexanamide as the model system.[151] For the ligand screening, novel triphos ligands with varying steric and electronic properties were synthesized. However, the conditions from literature remained unsurpassed, although it was shown that the reaction can also be run in other solvents than THF like butyl diglyme and HFIP. Next, the optimized reaction conditions were applied to convert nylon-6. Quantitative analysis proved challenging. Qualitative analysis was conducted by means of IR, NMR, and MALDI-TOF MS. Regardless of the choice of solvent, no hydrogenolysis of nylon-6 was observed under standard conditions. However, if the reaction temperature was increased above the melting point of nylon-6, the polymer was converted. The product of the reaction was isolated in 35 wt% yield and identified as a cross-linked oligoamine. Thermogravimetric analysis showed an increase of the sample mass that was caused by CO_2 uptake. Only minor amounts of 1.8 wt% CO_2 were captured and loosely bound to the oligomer, since it could be easily removed by blowing argon over the sample. This result further hinted towards undesired cross-linking in the obtained oligoamine.

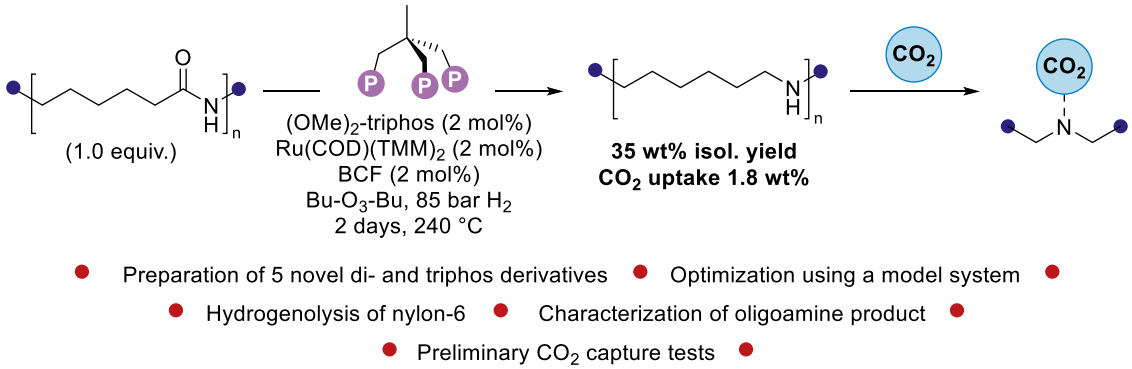

Scheme 56. CO_2 capture by modified nylon-6.

In a third project, the conversion of carbon dioxide by the application of bidentate and air-stable *N,N*-type ligands was examined (Scheme 57). Seminal investigations aimed at the dimerization of CO_2 *via* metalladicarboxylic acids, which were triggered to reductively eliminate oxalates by sterically demanding alkyl- and aryl-substituted phenanthroline and bipyridine ligands. The Pd-catalyzed oxidative carbonylation of MeOH to dimethyl oxalate was utilized as the model system. A library of ligands was synthesized and tested towards the stoichiometric formation of dimethyl oxalate. All substituted ligands resulted in increased yields of dimethyl oxalate as compared to unsubstituted phenanthroline and bipyridine. Various oxidants were then screened to transform the stoichiometric reaction into a catalytic process. Applying Wacker process-like conditions, consisting of $Cu(OMe)_2$ in the presence of oxygen, led to the formation of dimethyl oxalate with a maximum turnover number of 20. The control experiment without ligand afforded the product dimethyl oxalate in a similar amount

and the transfer of the reaction conditions onto the reductive coupling of CO_2 did not yield detectable amounts of product. Thus, the investigations on CO_2 conversion were continued from another angle.

The new approach combined CO_2 capture and CO_2 conversion. A bifunctional ligand was rationally designed, comprising a *N,N*-bidentate backbone and a flexible side chain with a terminal amino group. The terminal amine was meant to capture CO_2 *via* carbamate formation and forward it to a metal center that is ligated by the bidentate ligand, where the CO_2 can be transformed into value-added chemicals. The first ligand structure following this concept had a pyridyloxazoline scaffold and a C_4 side chain where the terminal amine was attached. It was synthesized starting from double protected L-lysine. However, the synthesis of pyrox-C_4N suffered from unexpected side product formation and decomposition, especially after deprotection of the side chain.

Therefore, effort was put into synthesizing a more stable ligand. The second ligand structure comprised a phenanthroline backbone and a diamine side chain. It was successfully synthesized in one step from inexpensive starting materials. Subsequent experiments showed its ability to capture CO_2 and to directly convert it into formate when reacted with molecular hydrogen. The molecular structure of the carbamate arising from CO_2 capture was determined with the aid of different 2D NMR spectra. Nevertheless, it remained unclear if any carbamate formation took place under CO_2 hydrogenation conditions due to the similar activity of unsubstituted phenanthroline.

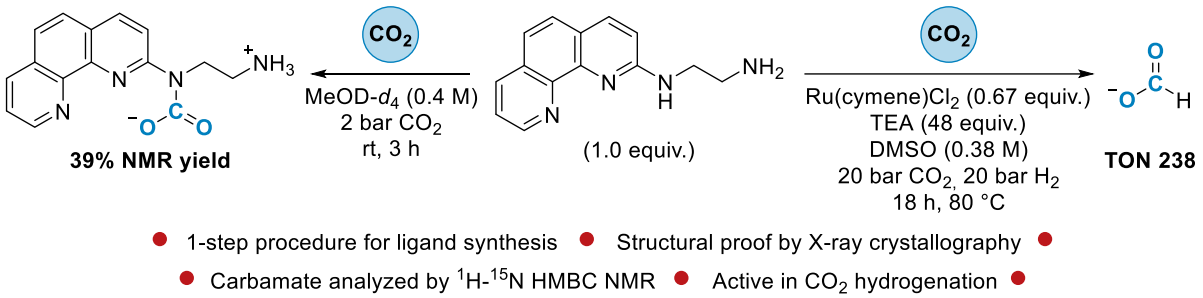

Scheme 57. CO_2 capture and conversion by a novel bifunctional phenanthroline ligand.

All in all, various concepts for all areas of a carbon dioxide-related circular economy were presented in order to promote the future use of CO_2 as a C_1 building block.

7 Experimental Section

7.1 General Remarks

All reactions involving moisture- or air-sensitive reagents or products were performed under an atmosphere of dry argon using standard Schlenk techniques and pre-dried (640 °C) glassware. Syringes for handling of dry solvents or liquid reagents were flushed with dry argon prior to use. All chemicals that have been purchased from commercial suppliers were used as received.

7.1.1 Solvents

Commercially available dry solvents were purchased from SIGMA-ALDRICH and ACROS ORGANICS. Dry acetonitrile, diethylether, pentane, and tetrahydrofuran were obtained by passing commercially available anhydrous, oxygen-free HPLC-grade solvents through activated alumina columns using an MBRAUN solvent purification system. Dry toluene was obtained by pre-drying over KH and distillation over sodium and benzophenone. All solvents used for column chromatography were distilled prior to application.

7.1.2 Analytical Data

Analytical data of substances that are known in literature (marked by corresponding references) were compared with those described in the literature.

7.1.3 Chromatography

Analytical thin layer chromatography (TLC) was performed with TLC-plates from MERCK (Geduran, Si 60, grain size 0.040-0.063 mm). Plates were visualized under ultraviolet light (254 nm or 366 nm) or developed by treatment with basic $KMnO_4$ solution (3.0 g $KMnO_4$, 20.0 g K_2CO_3 and 0.3 g KOH in 300 ml water).

Chromatographic purification of products was accomplished by flash column chromatography on MERCK silica gel, grade 60 (0.063-0.200 mm, 70–230 mesh ASTM).

7.1.4 Cyclic Voltammetry

All electrochemical investigations were performed at room temperature in dried acetonitrile p.A. (VWR) under an argon atmosphere with 0.1 M tetrabutylammonium hexafluorophosphate (Fluka) as conducting salt using an Autolab device (PGSTAT 204, Metrohm). A glassy carbon disk electrode (d = 2 mm) was used as working electrode and a glassy carbon electrode as the counter electrode. The reference electrode was an $Ag/AgCl/LiCl_{sat.}$ system in EtOH (all electrodes: Metrohm). All potentials were measured with respect to this reference system and were checked by using the ferrocenium/

ferrocene system as internal reference (potential of Fc^+/Fc: 0.54 V vs Ag/AgCl/$LiCl_{sat.}$ in EtOH). The potentials reported relative to the Fc^+/Fc redox couple were converted to SCE by adding 0.38 V.[292] The CV scans were done three times at a scan rate of 40 mV s^{-1}. Differential pulse voltammetry was measured using a step potential of 5 mV, modulation amplitude of 25 mV, modulation time 0.05 s, interval time 0.05 s.

7.1.5 Crystallographic Data

Crystallographic data were collected on a BRUKER KAPPA APEX II DUO diffractometer. The structure was solved by direct methods (SHELXS-97: Sheldrick, G. M. *Acta Crystallogr.* **2008**, *A64*, 112.) and refined by full-matrix least-squares procedures on F^2 (SHELXL-2018: G. M. Sheldrick, *Acta Crystallogr.* **2015**, *C71*, 3.). Mercury (C. F. Macrae, P. R. Edgington, P. McCabe, E. Pidcock, G. P. Shields, R. Taylor, M. Towler, J. van de Streek, *J. Appl. Crystallogr.* **2006**, *39*, 453.) was used for graphical representation. Displacement ellipsoids correspond to 30% probability.

For steroid **43**, the diffraction data were collected on an XtaLAB Synergy R diffractometer (DW system; HyPix-Arc 150; Cu K_α (λ = 1.54184 Å; rotating anode) at the Rigaku test center.

7.1.6 Electron Paramagnetic Resonance Spectroscopy (EPR)

EPR spectra were recorded on an X-band Bruker EMX CW-micro EPR spectrometer equipped with an ER4119HS high-sensitivity resonator using a microwave power of Ca 6.9 mW, modulation frequency of 100 kHz and modulation amplitude up to 5 G. The $h\nu = g\beta B_0$ equation was used to calculate g values with ν and B_0 being the frequency and resonance field, respectively. The g values calibration was performed using 2,2-Diphenyl-1-picrylhydrazyl as a standard (g = 2.0036 ± 0.0004). EPR spectrum simulation was done by Bruker SimFonia software.

7.1.7 High-Pressure Reactions

High-pressure reactions were carried out in WEATHON screw capped glass vials (5 mL) with silicone/PTFE septum, equipped with a magnetic stirring bar and a needle. The reaction mixtures were placed in a PARR 300 mL stainless steel autoclave and pressurized with carbon monoxide, carbon dioxide or hydrogen (LINDE).

7.1.8 Infrared Spectroscopy (IR)

Infrared spectra were recorded using an ALPHA FT-IR spectrometer (BRUKER). Liquid and solid probes were measured neat. Absorption is given in wave numbers (cm^{-1}). Spectra were recorded in the range of 4000–400 cm^{-1}. Following abbreviations were used for characterization: s (strong, 0-33% T), m (medium, 34-66% T), w (weak, 67-100% T).

7.1.9 Mass Spectrometry

Mass spectra were measured by the LIKAT analytic department on Agilent 6890/5973 (GC-MS), Agilent 7890/5977 (GC-MS), Agilent 1260/6130 Quadrupol (LC-MS), Agilent 1200/6210 Time-of-Flight (LC-MS). The ratio of mass to charge is indicated, intensities relative to the base peak (I = 100) are written in parentheses. High resolution mass spectra (HRMS) were recorded on Thermo Electron MAT 95-XP (EI) or Agilent 1200/6210 Time-of-Flight (ESI). Electron ionization (EI) spectra were performed at 70 eV using methane as the carrier gas, with time-of-flight (TOF) mass analyzer. Electrospray ionization (ESI) spectra were performed using a TOF mass analyzer.

7.1.10 Melting Points

Melting points were measured using a BÜCHI melting point apparatus. Reported values are uncorrected.

7.1.11 Nuclear Magnetic Resonance Spectroscopy (NMR)

NMR spectra were recorded at 300 or 400 MHz (^{1}H NMR), 75 or 125 MHz (^{13}C NMR), 282 or 376 MHz (^{19}F NMR), and 121 or 161 MHz (^{31}P NMR) on AV 400 (BRUKER), AV 300 (BRUKER) or Fourier 300 (BRUKER) instruments. The chemical shifts are reported as δ-values in ppm relative to the solvent residual peak.

	^{1}H NMR	^{13}C NMR
d_1-Chloroform	7.26 ppm	77.16 ppm
d_2-Water	4.79 ppm	
d_3-MeCN	1.94 ppm	1.32 ppm
d_4-MeOH	3.31 ppm	49.00 ppm
d_6-DMSO	2.50 ppm	39.52 ppm
d_6-Acetone	2.05 ppm	29.84 ppm
d_8-THF	1.72 ppm	25.31 ppm
d_8-Toluene	2.08 ppm	20.43 ppm

Coupling patterns in the NMR spectra are abbreviated as follows: s (singlet), d (doublet), t (triplet), q (quartet), p (pentets), hept (heptet), br (broad), dd (doublet of doublets), td (triplet of doublets), qd (quartet of doublets), dt (doublet of triplets), qt (quartet of triplets), dq (doublet of quartets), dp (doublet of pentets), tp (triplet of pentets), ddd (doublet of doublet of doublets), tdd (triplet of doublet of doublets), dtd (doublet of triplet of doublets), ddt (doublet of doublet of tripplets), ddh (doublet of doublet of heptet), dddd (doublet of doublet of doublet of doublets), m (multiplet), and reported as follow: (multiplicity; coupling constant *J* in Hz; integration).

7.1.12 Photoluminescence Quenching Experiments (Stern-Volmer)

Fluorescence spectra were measured using a Varian Cary Eclipse spectrophotometer using scan rates of 1200 to 30 nm/min. The solutions to be measured were filled under inert gas into quartz glass cuvettes, which were sealed with a septum. The obtained data were processed by using Origin.

7.1.13 UV/vis Spectroscopy

UV/vis spectra were recorded in MeCN using a METTLER TOLEDO UV5Bio spectrophotometer. The concentration of the analyte in solution was adjusted to an absorption between 0.8 and 1.2, resulting in a concentration range of 20 to 240 µmol/l depending on the substrate.

7.1.14 Vacuum

Following pressures were measured on the used vaccuum pump and are not corrected: 3.1 mbar (membrane pump vacuum), 0.001 mbar (oil pump vacuum).

7.2 General Procedures

7.2.1 General Procedure A: Photomediated Hydro- and Deuterodecarboxylation

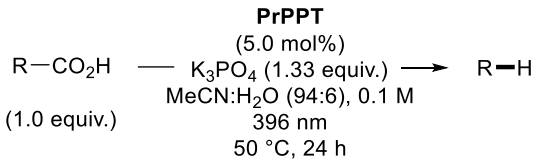

This protocol has been published by the author of this thesis.[37] The reactions were performed under Schlenk conditions using a 25 ml Schlenk tube. The appropriate carboxylic acid (0.50 mmol, 1.0 equiv.), photocatalyst PrPPT (5.0 mol%), and K_3PO_4 (1.33 equiv.) were added. Next, the flask was evacuated for 1 h and afterwards evacuated and purged with argon three times. Dry acetonitrile (4.7 ml) and degassed water or deuterated water (0.3 ml) were added, and the reaction mixture was irradiated for 24 h while stirred at 50 °C using an oil bath, before it was quenched upon exposure to air. Next, the crude mixture was added brine, and the product was extracted with dichloromethane three times, before it was concentrated under reduced pressure and purified by column chromatography.

7.2.2 General Procedure B: Synthesis of Differently Functionalized Triphos Ligands

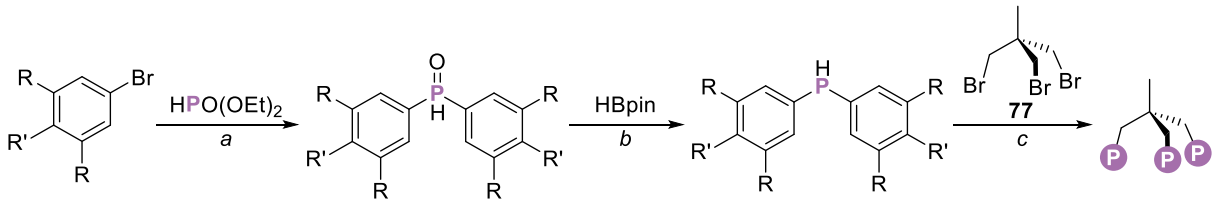

This protocol is a modified procedure from literature.[151] (*a*) A solution of aryl bromide (3.0 equiv.) in dry THF was added dropwise to a suspension of Mg (3.33 equiv.) in dry THF. The Grignard was started and then stirred o/n at room temperature before it was added to a solution of diethyl phosphite (1.0 equiv.) in dry THF at 0 °C. The green solution was stirred at room temperature for 1 h, and then quenched by adding 1 M HCl solution at 0 °C. The product was extracted with DCM (3x) and purified by column chromatography. (*b*) The diarylphosphine oxide (1.0 equiv.) was dissolved in dry MeCN (0.2 M). Pinacolborane (2.5 equiv.) was added by syringe and the reaction mixture was stirred art 60 °C o/n. Afterwards, the borane was quenched by adding *i*PrOH (1.5 equiv.) and the solvent was removed *in vacuo*. The residuals were dissolved in *n*-pentane and filtrated through basic aluminum oxide. The solvent was evaporated to yield the pure product. (*c*) The corresponding diarylphosphine (3.2 equiv.) and KO*t*Bu (3.2 equiv.) were dissolved in dry DMSO (0.1 M). To the very red solution, tribromide (1.0 equiv.) was added. The orange solution was stirred o/n at room temperature before the solvent was distilled off. The reaction mixture was added degassed water, and the resulting solution was

extracted with dry Et_2O (3x). The solvent was evaporated, and the product was crystallized from toluene/*n*-pentane (1:5).

7.2.3 General Procedure C: Hydrogenation of (Poly)Amides

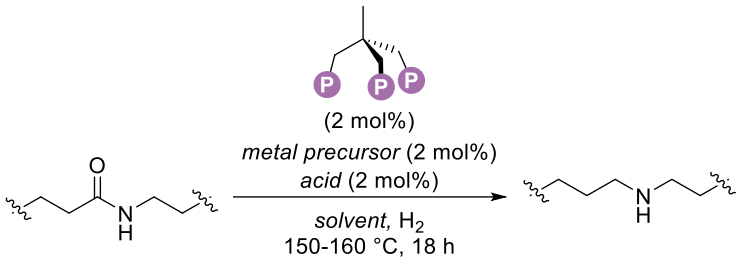

This protocol is a modified procedure from literature.[151] The reactions were prepared under inert conditions in the Glovebox. The (poly)amide (0.25 mmol, 1.0 equiv.), metal precursor (2 mol%), ligand (2 mol%), and acid (2 mol%) were added to a 5 ml vial equipped with a stirring bar. To the reagents was added dry solvent (1 ml). The vials were closed with a septum that is punctured by a needle and transferred to a 300 ml autoclave, which was pressurized with H_2 and heated for 18 h. After the reaction, the autoclaved was cooled and the remaining gas was released. To the vials was added 30 µl mesitylene as internal standard. The crude reaction mixture was filtrated through celite and analyzed by calibrated GC-FID.

7.2.4 General Procedure D: ortho-Functionalization of Heteroarenes

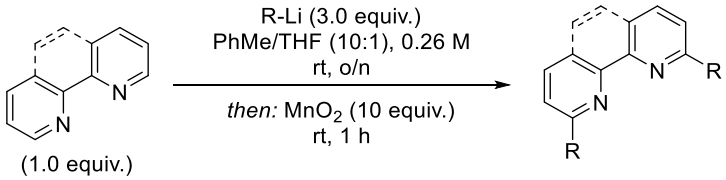

This protocol is a modified procedure from literature.[293] To a stirred solution of the heterocycle (2 mmol, 1.0 equiv.) in anhydrous toluene and THF (7 ml and 0.7 ml, respectively), the desired organolithium compound (6 mmol, 3.0 equiv.) was added dropwise under argon. The rate of addition was adjusted to maintain the reaction temperature around 30 °C. The dark red mixture was stirred at room temperature overnight and then quenched by slowly adding H_2O (10 ml) at 0 °C. The organic phase was separated, and the aqueous phase was extracted three times with DCM. The combined organic fractions were added excess MnO_2 (20 mmol, 10 equiv.). The mixture was stirred at room temperature for 1 h. Addition of anhydrous sodium sulfate was followed by filtration through celite and removing the filtrate *in vacuo*. The product was isolated by column chromatography.

7.2.5 General Procedure E: Alkoxycarbonylation to Dimethyloxalate

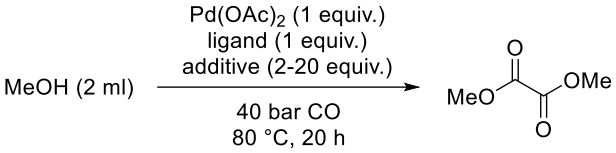

The reactions were prepared under inert conditions. The metal precursor (0.025-0.2 mmol, 1.0 equiv.), ligand (1.0 equiv.), and, if applicable, an additive (2-20 equiv.) were added to a 5 ml vial equipped with a stirring bar. To the reagents was added dry MeOH (2 ml). The vials were closed with a septum that is punctured by a needle and transferred to a 300 ml autoclave, which was pressurized with 40 bar CO (and, if applicable, 1 bar O_2) and heated for 20 h. After the reaction, the autoclaved was cooled and the remaining gas was released. To the vials was added EtOAc (2 ml) and tetradecane as internal standard. The crude reaction mixture was then filtrated through celite and analyzed by calibrated GC-FID.

7.2.6 General Procedure F: CO_2 Hydrogenation

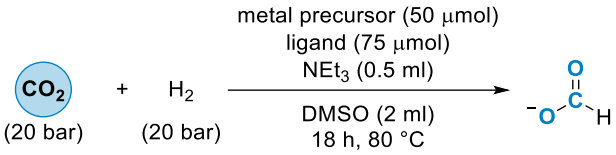

To a 10 ml vial equipped with a magnetic stirring bar were added a metal precursor (50 µmol, 1.0 equiv.) and ligand (75 µmol, 1.5 equiv.). The solids were dissolved in DMSO (2 ml) and added NEt_3 (0.5 ml), if required. The vials were closed with a septum, that was punctured by a needle, and transferred to a 300 ml autoclave, which was pressurized with CO_2 (20 bar) and H_2 (20 bar) and heated to 80 °C for 18 h.

7.3 Experimental Data

The experimental data is sorted according to the project it belongs to.

7.3.1 CO_2 Release by Photomediated Hydro- and Deuterodecarboxylation

Reaction set-up

Unless otherwise stated, all reactions were performed on a 0.5 mmol scale and a molarity of 0.1 M under inert atmosphere. The reactions were irradiated using 2 x 30 W lamps at 396 nm in 6.1 cm and 11.2 cm distance.

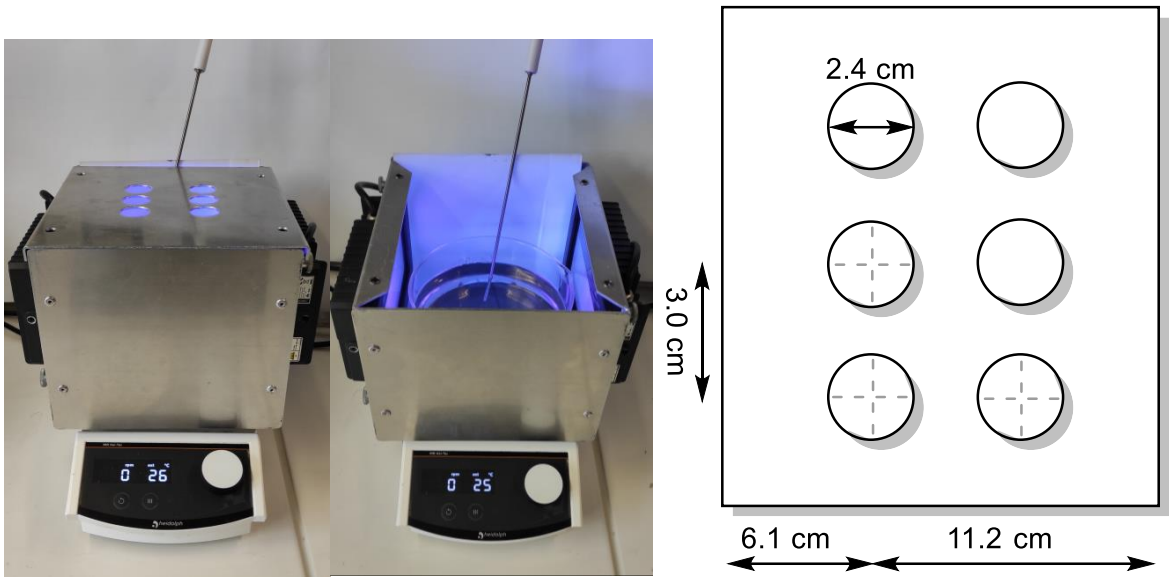

Figure 27. Reaction set-up.

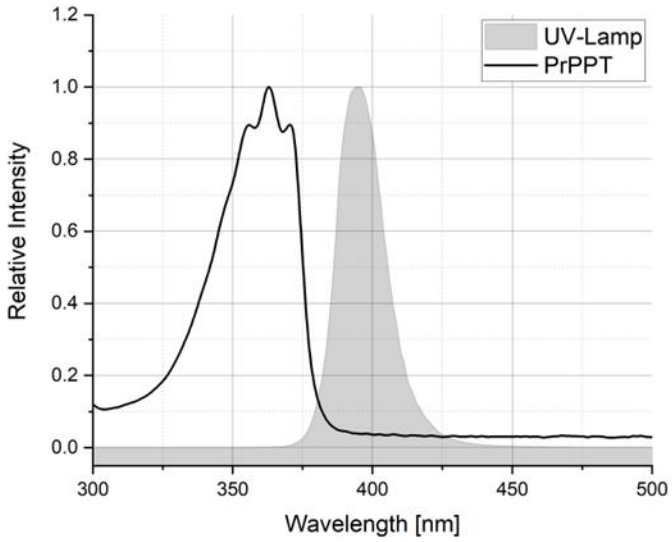

Figure 28. Emission spectrum of the utilized LED lamp ONFURO IP66 (30 W) and absorption spectrum of PrPPT.

Optimization of the reaction conditions

Table 31. Solvent screening.

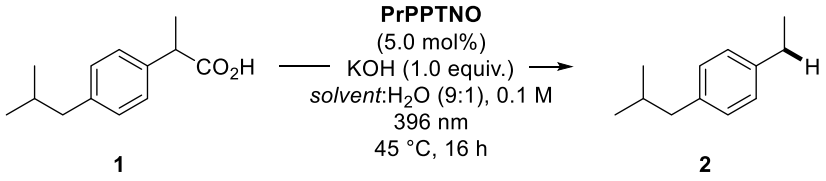

1 **2**

entry	solvent	yield [%][a]
1	MeCN	32
2	1,4-dioxane	16
3	acetone	13
4	toluene	13
5	methanol	12
6	DMSO	10
7	DMF	8

[a] Yields were determined by calibrated GC using biphenyl as internal standard.

Table 32. Base screening.

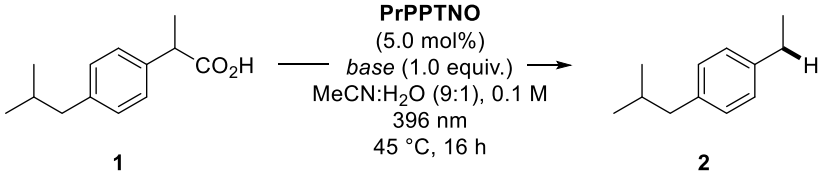

1 **2**

entry	base	yield [%][a]
1	K_3PO_4	39
2	K_2CO_3	37
3	Na_2CO_3	36
4	KOH	32
5	$NaHCO_3$	29
6	Cs_2CO_3	29
7	K_2HPO_4	20
8	NaOH	20
9	urotropin	13

[a] Yields were determined by calibrated GC using biphenyl as internal standard.

Table 33. Catalyst screening.

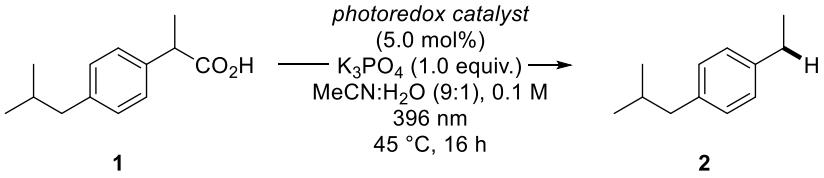

1 **2**

entry	photoredox catalyst	yield [%][a]
1	MePPTNO	24
2	PrPPTNO	39
3	PrPPT	42
4	BuPPTNO	34
5	BuPPT	38
6	PhPPTNO	10

[a] Yields were determined by calibrated GC using biphenyl as internal standard.

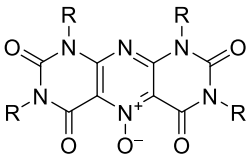

R = Me **MePPTNO**
Pr **PrPPTNO**
Bu **BuPPTNO**
Ph **PhPPTNO**

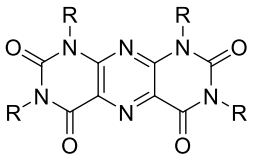

R = Pr **PrPPT**
Bu **BuPPT**

Design of Experiment (DoE)

A face-centered Box-Behnken Design with one center point was chosen. 13 experiments were carried out in a random order. To improve the mathematical model, six additional experiments (entries 14-19) were conducted. The program Design-Expert 13 was used for analyzing the responses.

Table 34. Experimental matrix.

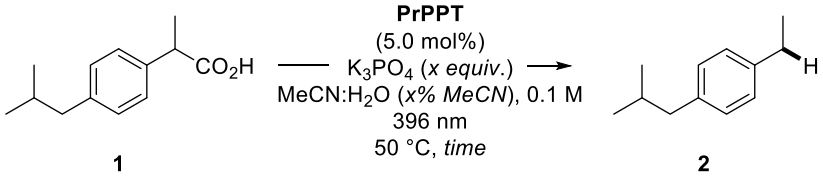

1 **2**

entry	*x equiv*. K_3PO_4	*x%* MeCN	*time* [h]	yield [%][a]
1	0.33	90	16	49
2	0.33	100	16	53
3	1.0	90	16	64
4	1.0	100	16	34
5	0.67	90	8	24
6	0.67	100	8	32
7	0.67	90	24	65
8	0.67	100	24	64
9	0.33	96	8	23
10	1.0	96	8	27
11	0.33	96	24	76
12	1.0	96	24	87
13	0.67	96	16	58
14	0.5	100	16	49
15	2.0	100	16	11
16	0.8	94	16	56
17	0.85	94	24	77
18	1.33	94	24	89
19	0.15	100	8	25

[a] Yields were determined by calibrated GC using biphenyl as internal standard.

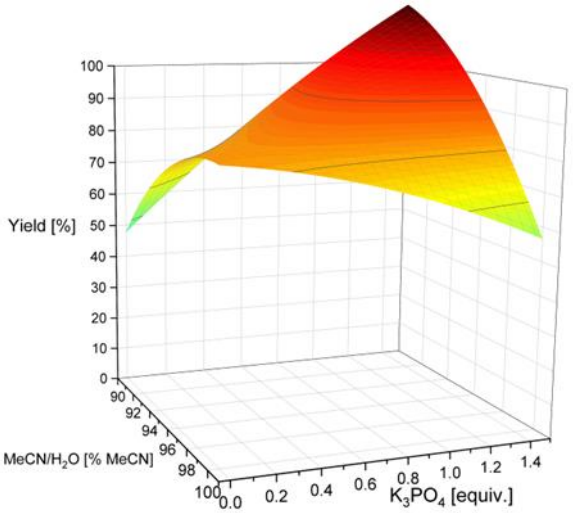

Figure 29. Response surface of the DoE after 24 h.

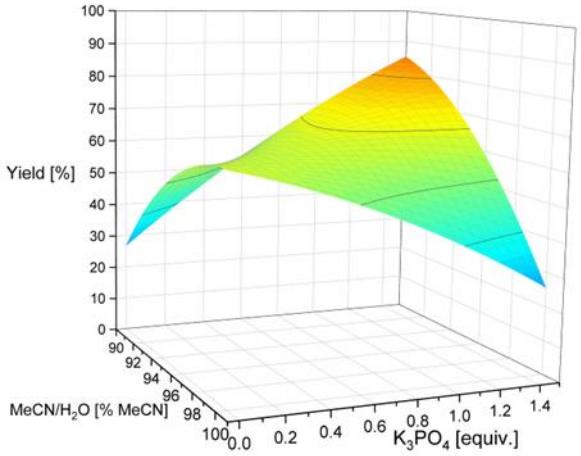

Figure 30. Response surface of the DoE after 16 h.

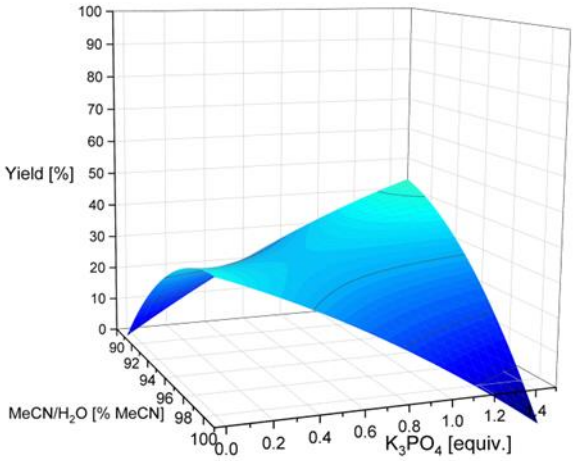

Figure 31. Response surface of the DoE after 8 h.

Table 35. Control experiments.

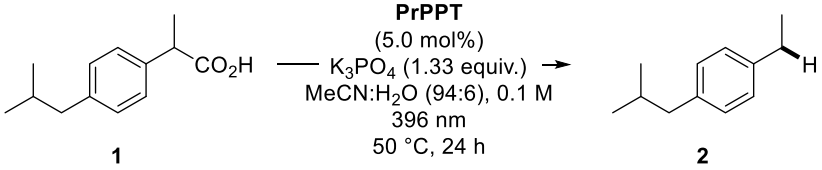

1 **2**

entry	deviation from optimized reaction conditions	yield [%][a]
1	no photocatalyst	0
2	in the dark	0
3	no base	35

[a] Yields were determined by calibrated GC using biphenyl as internal standard.

Synthesis of 1-ethyl-4-isobutylbenzene (2)

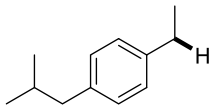

2

Compound **2** was prepared following general procedure A. Purification by column chromatography (*n*-pentane) yielded the title compound **2** in an average yield of 90% (#1: 67 mg, 0.41 mmol, 83%; #2: 78 mg, 0.48 mmol, 96%) as colorless liquid. The product was used to calibrate the GC by using biphenyl as internal standard.

R_f = 0.82 (*n*-pentane, UV)

^{1}H NMR (300 MHz, $CDCl_3$) δ 7.20 – 7.04 (m, 4H), 2.66 (q, *J* = 7.6 Hz, 2H), 2.48 (d, *J* = 7.1 Hz, 2H), 2.01 – 1.73 (m, 1H), 1.27 (t, *J* = 7.6 Hz, 3H), 0.95 (d, *J* = 6.6 Hz, 6H).

^{13}C NMR (75 MHz, $CDCl_3$) δ 141.6, 139.0, 129.2, 127.7, 45.2, 30.4, 28.6, 22.6, 15.8.

MS (EI): *m*/*z* (relative intensity) 162 (25), 120 (15), 119 (100), 91 (18), 77 (5).

HRMS (EI, *m*/*z*): calcd. for $C_{12}H_{18}$ $[M - H]^+$ 161.1325, observed 161.1328.

IR (ATR, neat, cm^{-1}): 3089 (w), 3049 (w), 3009 (w), 2955 (s), 2927 (s), 2868 (m), 2848 (w), 1896 (w), 1791 (w), 1682 (w), 1635 (w), 1558 (w), 1513 (m), 1463 (m), 1419 (w), 1383 (m), 1366 (m), 1339 (w), 1282 (w), 1242 (w), 1210 (w), 1167 (w), 1120 (w), 1085 (w), 1062 (w), 1045 (w), 1021 (w), 966 (w), 921 (w), 881 (w), 841 (s), 799 (s), 733 (w), 642 (w), 603 (w), 579 (m), 542 (m), 486 (m), 440 (w), 420 (w).

This data is in agreement with literature.[294]

GC calibration:

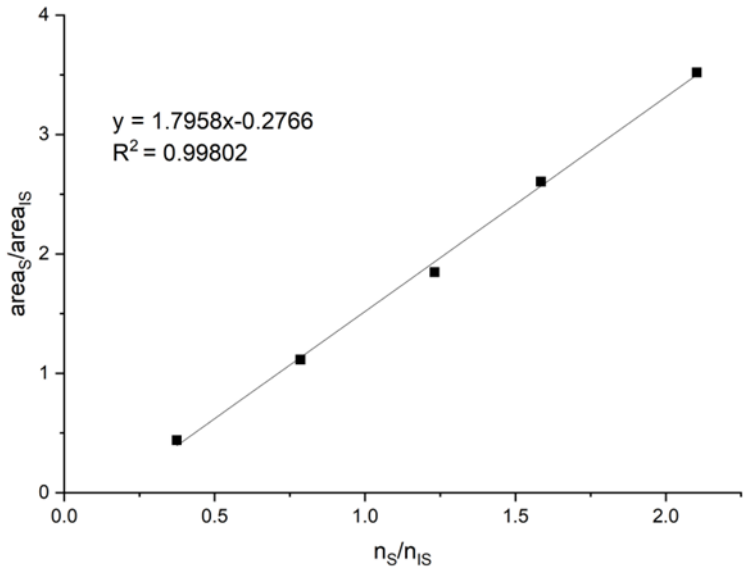

Figure 32. GC calibration graph for 1-ethyl-4-isobutylbenzene (**2**) as substrate (S) using biphenyl as internal standard (IS).

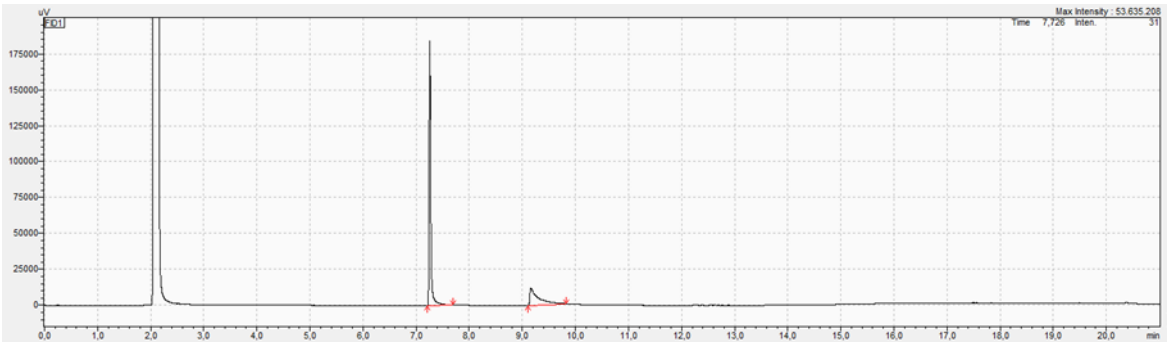

Figure 33. Exemplary gas chromatogram of 1-ethyl-4-isobutylbenzene (**2**, t_R = 7.26 min) and biphenyl (IS, t_R = 9.16 min) using a 20 min-method heating von 50 °C to 280 °C in 15 min.

Synthesis of 1-ethyl-3-phenoxybenzene (4)

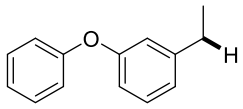

4

Compound **4** was prepared following general procedure A. Purification by column chromatography (*n*-pentane:EtOAc = 20:1) yielded the title compound **4** in an average yield of 93% (#1: 86 mg, 0.43 mmol, 86%; #2: 99 mg, 0.50 mmol, quant.) as a colorless oil.

R_f = 0.72 (*n*-pentane:EtOAc = 10:1, UV).

^{1}H NMR (300 MHz, $CDCl_3$) δ 7.38 – 7.31 (m, 2H), 7.31 – 7.20 (m, 1H), 7.17 – 7.05 (m, 1H), 7.08 – 6.97 (m, 2H), 6.96 (m, 1H), 6.90 (m, 1H), 6.89 – 6.79 (m, 1H), 2.65 (qd, *J* = 7.6, 0.6 Hz, 2H), 1.24 (t, *J* = 7.6 Hz, 3H).

^{13}C NMR (75 MHz, $CDCl_3$) δ 157.5, 157.3, 146.5, 129.8, 129.6, 123.2, 123.0, 118.9, 118.6, 116.2, 28.9, 15.6.

MS (EI): *m*/*z* (relative intensity) 199 (15), 198 (100), 183 (49), 169 (12), 155 (13), 77 (17).

HRMS (EI, *m*/*z*): calcd. for $C_{14}H_{14}O$ $[M]^+$ 198.1039, observed 198.1032.

IR (ATR, neat, cm^{-1}): 2965 (w), 2929 (w), 2872 (w), 1581 (s), 1484 (s), 1444 (m), 1330 (w), 1308 (w), 1249 (s), 1212 (s), 1161 (m), 1141 (m), 1091 (w), 1071 (w), 1051 (w), 1023 (w), 1002 (w), 984 (w), 918 (m), 874 (w), 812 (w), 754 (s), 723 (w), 689 (s), 614 (w), 485 (m), 449 (w), 419 (w).

This data is in agreement with literature.[294]

Synthesis of 2-ethyl-6-methoxynaphthalene (6)

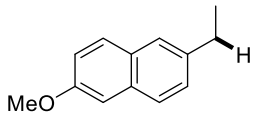

6

Compound **6** was prepared following general procedure A in 0.5 mmol-scale and in 5.5 mmol-scale, respectively. Purification by column chromatography (*n*-pentane:EtOAc = 20:1) yielded the title compound **6** in quantitative yield (#1: 93 mg, 0.50 mmol, quant.; #2: 1.02 g, 5.50 mmol, quant.) as colorless solid.

R_f = 0.22 (*n*-pentane, UV)

^{1}H NMR (300 MHz, $CDCl_3$) δ 7.72 – 7.68 (m, 1H), 7.68 – 7.65 (m, 1H), 7.57 (dt, *J* = 1.6, 0.8 Hz, 1H), 7.33 (dd, *J* = 8.4, 1.8 Hz, 1H), 7.18 – 7.09 (m, 2H), 3.92 (s, 3H), 2.79 (qt, *J* = 7.6, 0.6 Hz, 2H), 1.33 (t, *J* = 7.6 Hz, 3H).

^{13}C NMR (75 MHz, $CDCl_3$) δ 157.2, 139.6, 133.0, 129.3, 129.0, 127.7, 126.8, 125.6, 118.7, 105.8, 55.4, 29.0, 15.8.

MS (EI): *m*/*z* (relative intensity) 186 (52), 172 (13), 171 (100), 128 (30), 115 (11).

HRMS (EI, *m*/*z*): calcd. for $C_{13}H_{14}O$ $[M + H]^+$ 187.1123, observed 187.1121.

IR (ATR, neat, cm^{-1}): 3059 (w), 3008 (w), 2960 (m), 2926 (w), 2888 (w), 2867 (w), 2850 (w), 1632 (w), 1602 (m), 1504 (w), 1485 (m), 1458 (m), 1416 (w), 1390 (m), 1371 (w), 1341 (w), 1314 (w), 1263 (m), 1246 (m), 1222 (m), 1195 (m), 1161 (s), 1116 (w), 1067 (w), 1053 (w), 1028 (s), 963 (w), 917 (m), 886 (m), 852 (s), 831 (w), 815 (s), 785 (w), 749 (m), 675 (m), 660 (m), 636 (w), 625 (w), 594 (m), 568 (m), 508 (w), 483 (s), 474 (s), 438 (m).

This data is in agreement with literature.[294]

Synthesis of 4-ethyl-2-fluoro-1,1'-biphenyl (8)

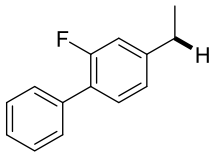

8

Compound **8** was prepared following general procedure A. Purification by column chromatography (*n*-pentane) yielded the title compound **8** in an average yield of 95% (#1: 93 mg, 0.46 mmol, 93%; #2: 96 mg, 0.48 mmol, 96%) as colorless oil.

R_f = 0.69 (*n*-pentane, UV)

^{1}H NMR (300 MHz, $CDCl_3$) δ 7.58 – 7.52 (m, 2H), 7.48 – 7.40 (m, 2H), 7.40 – 7.32 (m, 2H), 7.06 (ddt, *J* = 7.8, 1.8, 0.6 Hz, 1H), 7.04 – 6.98 (m, 1H), 2.70 (qt, *J* = 7.6, 0.7 Hz, 2H), 1.29 (t, *J* = 7.6 Hz, 3H).

^{13}C NMR (75 MHz, $CDCl_3$) δ 159.9 (d, *J* = 247.5 Hz), 146.1 (d, *J* = 7.6 Hz), 136.1, 130.6 (d, *J* = 4.0 Hz), 129.1 (d, *J* = 2.9 Hz), 128.5, 127.5, 126.4 (d, *J* = 13.5 Hz), 124.0 (d, *J* = 3.1 Hz), 115.5 (d, *J* = 22.6 Hz), 28.5 (d, *J* = 1.6 Hz), 15.4.

^{19}F NMR (282 MHz, $CDCl_3$) δ -118.8.

MS (EI): *m/z* (relative intensity) 200 (56), 186 (14), 185 (100), 183 (19), 170 (10), 165 (10), 133 (4).

HRMS (EI, *m/z*): calcd. for $C_{14}H_{13}F$ $[M]^+$ 200.0996, observed 200.0996.

IR (ATR, neat, cm^{-1}): 3058 (w), 3032 (w), 2966 (w), 2932 (w), 2874 (w), 1749 (w), 1717 (w), 1698 (w), 1625 (w), 1603 (w), 1581 (w), 1561 (w), 1516 (w), 1483 (m), 1451 (w), 1416 (m), 1375 (w), 1330 (w), 1288 (w), 1266 (m), 1229 (w), 1184 (w), 1150 (w), 1128 (m), 1075 (w), 1060 (w), 1038 (w), 1011 (w), 985 (w), 953 (w), 911 (m), 868 (m), 828 (m), 763 (s), 721 (m), 695 (s), 634 (w), 618 (w), 576 (m), 551 (w), 515 (w), 496 (w), 452 (w), 418 (w).

This data is in agreement with literature.[63]

Synthesis of 4-(ethyl-1-*d*)-2-fluoro-1,1'-biphenyl (*d*-8)

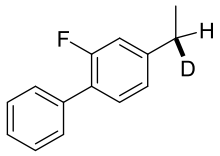

***d*-8**

Compound ***d*-8** was prepared following general procedure A using deuterated water. Purification by column chromatography (*n*-pentane) yielded the title compound ***d*-8** (98 mg, 0.49 mmol, 98%) as colorless oil. The deuterium content was determined by ^{1}H NMR spectroscopy (88%).

R_f = 0.69 (*n*-pentane, UV)

^{1}H NMR (400 MHz, $CDCl_3$) δ 7.59 – 7.53 (m, 2H), 7.48 – 7.42 (m, 2H), 7.40 – 7.34 (m, 2H), 7.08 – 6.99 (m, 2H), 2.75 – 2.64 (m, 1.12H, 88 % D), 1.29 (dt, *J* = 7.5, 1.2 Hz, 3H).

^{13}C NMR (101 MHz, $CDCl_3$) δ 159.9 (d, *J* = 247.5 Hz), 146.0 (d, *J* = 7.6 Hz), 136.1, 130.6 (d, *J* = 4.0 Hz), 129.1 (d, *J* = 3.1 Hz), 128.5, 127.5, 126.3 (d, *J* = 13.5 Hz), 124.0 (d, *J* = 3.2 Hz), 115.5 (d, *J* = 22.5 Hz), 28.5 (d, *J* = 1.6 Hz), 28.4 – 27.9 (td, J = 19.6, 1.6 Hz), 15.3.

^{19}F NMR (376 MHz, $CDCl_3$) δ -118.7 – -118.9 (m).

MS (EI): *m*/*z* (relative intensity) 201 (58), 187 (15), 186 (100), 184 (17), 166 (13), 152 (4), 133 (4).

HRMS (EI, *m*/*z*): calcd. for $C_{14}H_{12}{}^{2}HF$ $[M]^+$ 201.1059, observed 201.1060.

This data is in agreement with literature.[86]

Synthesis of 6-chloro-2-ethyl-9*H*-carbazole (10)

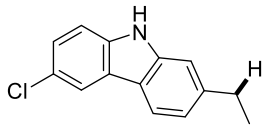

10

Compound **10** was prepared following general procedure A. Purification by column chromatography (*n*-pentane:EtOAc = 10:1) yielded the title compound **10** in an average yield of 58% (#1: 64 mg, 0.28 mmol, 56%; #2: 68 mg, 0.30 mmol, 59%) as a colorless solid.

R_f = 0.42 (*n*-pentane:EtOAc = 5:1, UV).

m.p. 171 – 181 °C

^{1}H NMR (300 MHz, DMSO-d_6) δ 11.27 (s, 1H), 8.14 (dt, *J* = 2.2, 0.6 Hz, 1H), 8.03 (dt, *J* = 8.0, 0.6 Hz, 1H), 7.46 (dd, *J* = 8.6, 0.6 Hz, 1H), 7.33 (dd, *J* = 8.6, 2.1 Hz, 1H), 7.30 (dd, *J* = 1.5, 0.7 Hz, 1H), 7.06 – 7.00 (m, 1H), 2.76 (q, *J* = 7.6 Hz, 2H), 1.26 (t, *J* = 7.6 Hz, 3H).

^{13}C NMR (75 MHz, DMSO-d_6) δ 142.4, 140.8, 138.1, 124.6, 123.8, 122.7, 120.4, 119.5, 119.3, 112.1, 109.8, 28.8, 16.0.

MS (EI): *m*/*z* (relative intensity) 231 (22), 230 (12), 229 (66), 216 (33), 215 (17), 214 (100), 179 (13), 178 (12).

HRMS (EI, *m*/*z*): calcd. for $C_{14}H_{12}NCl$ $[M]^+$ 229.0653, observed 229.0651; calcd. for $C_{14}H_{12}N^{37}Cl$ $[M]^+$ 231.0623, observed 231.0626.

IR (ATR, neat, cm^{-1}): 3393 (s), 3064 (w), 3029 (w), 2969 (w), 2957 (w), 2926 (w), 2864 (w), 1865 (w), 1719 (w), 1628 (w), 1605 (w), 1572 (w), 1468 (m), 1449 (m), 1426 (m), 1370 (w), 1335 (w), 1305 (w), 1293 (w), 1270 (m), 1237 (w), 1203 (w), 1125 (w), 1064 (m), 1051 (w), 1012 (w), 973 (w), 948 (w), 933 (w), 912 (w), 879 (m), 861 (m), 818 (s), 805 (s), 787 (m), 730 (m), 696 (m), 642 (w), 626 (w), 582 (s), 561 (w), 525 (w), 481 (s), 458 (s), 435 (s).

Synthesis of benzyl isobutylcarbamate (12)

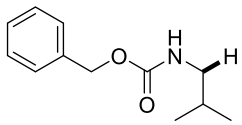

12

Compound **12** was prepared following general procedure A. Purification by column chromatography (CH_2Cl_2) yielded the title compound **12** in an average yield of 59% (#1: 67 mg, 0.32 mmol, 65%; #2: 55 mg, 0.27 mmol, 53%) as a colorless oil.

R_f = 0.54 (CH_2Cl_2, UV)

^{1}H NMR (300 MHz, $CDCl_3$) δ 7.39 – 7.27 (m, 5H), 5.10 (s, 2H), 4.80 (s, 1H), 3.02 (t, *J* = 6.3 Hz, 2H), 1.75 (dq, *J* = 13.3, 6.7 Hz, 1H), 0.91 (d, *J* = 6.7 Hz, 6H).

^{13}C NMR (75 MHz, $CDCl_3$) δ 156.7, 136.8, 128.7, 128.3, 128.2, 66.8, 48.7, 28.9, 20.1.

MS (EI): *m*/*z* (relative intensity) 207 (1), 108 (45), 107 (7), 91 (100), 79 (7), 65 (10), 41 (4).

HRMS (EI, *m*/*z*): calcd. for $C_{12}H_{17}NO_2$ $[M+Na]^+$ 230.1156, observed 230.1160.

IR (ATR, neat, cm^{-1}): 3321 (m), 3062 (w), 3032 (w), 2958 (m), 2925 (w), 2870 (w), 1688 (s), 1537 (s), 1499 (m), 1466 (m), 1454 (m), 1388 (w), 1367 (w), 1342 (w), 1304 (w), 1247 (s), 1145 (s), 1080 (w), 1006 (s), 971 (m), 909 (m), 892 (w), 847 (w), 818 (w), 780 (m), 746 (s), 712 (s), 694 (s), 673 (s), 621 (m), 591 (m), 572 (m), 489 (m), 423 (w).

This data is in agreement with literature.[295]

Synthesis of 4-ethylphenol (14)

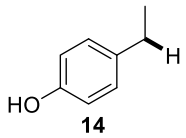

14

Compound **14** was prepared following general procedure A. Purification by column chromatography (*n*-pentane:EtOAc = 10:1) yielded the title compound **14** in an average yield of 79% (#1: 50 mg, 0.41 mmol, 82%; #2: 46 mg, 0.38 mmol, 76%) as a colorless solid.

R_f = 0.22 (*n*-pentane:EtOAc = 10:1, UV)

^{1}H NMR (300 MHz, $CDCl_3$) δ 7.12 – 7.04 (m, 2H), 6.82 – 6.74 (m, 2H), 4.91 (s, 1H), 2.68 – 2.53 (m, 2H), 1.22 (t, *J* = 7.6 Hz, 3H).

^{13}C NMR (75 MHz, $CDCl_3$) δ 153.5, 136.7, 129.0, 115.2, 28.1, 16.0.

MS (EI): *m*/*z* (relative intensity) 122 (29), 108 (8), 107 (100), 77 (18), 39 (4).

HRMS (ESI-TOF, *m*/*z*): calcd. for $C_8H_{10}O$ $[M]^+$ 122.0726, observed 122.0727.

IR (ATR, neat, cm^{-1}): 3222 (m), 3021 (w), 2960 (m), 2926 (w), 2892 (w), 2867 (w), 2702 (w), 2601 (w), 2487 (w), 1881 (w), 1792 (w), 1772 (w), 1749 (w), 1733 (w), 1717 (w), 1699 (w), 1684 (w), 1670 (w), 1647 (w), 1612 (m), 1599 (m), 1558 (w), 1541 (w), 1510 (s), 1449 (s), 1366 (m), 1218 (s), 1172 (m), 1109 (m), 1062 (m), 1015 (w), 969 (w), 928 (w), 818 (s), 729 (m), 709 (m), 642 (m), 539 (s), 479 (m), 419 (w).

This data is in agreement with literature.[296]

Synthesis of 4-(ethyl-1-*d*)phenol (*d*-14)

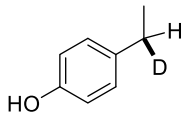

***d*-14**

Compound ***d*-14** prepared following general procedure A using deuterated water. Purification by column chromatography (*n*-pentane:EtOAc = 10:1) yielded the title compound ***d*-14** (49 mg, 0.39 mmol, 79%, 80% d-content) as a colorless solid. The deuterium content was determined by ^{1}H NMR spectroscopy (80%).

R_f = 0.22 (*n*-pentane:EtOAc = 10:1, UV)

^{1}H NMR (400 MHz, $CDCl_3$) δ 7.10 – 7.04 (m, 2H), 6.81 – 6.74 (m, 2H), 4.97 (s, 1H), 2.63 – 2.53 (m, 1.20H, 80 % D), 1.21 (dt, *J* = 7.6, 1.2 Hz, 3H).

^{13}C NMR (101 MHz, $CDCl_3$) δ 153.5, 136.7, 129.0, 115.3, 27.7 (t, *J* = 19.3 Hz), 15.9.

MS (EI): *m*/*z* (relative intensity) 123 (31), 108 (100), 107 (11), 78 (13).

HRMS (EI, *m*/*z*): calcd. for $C_8H_9{}^2HO$ $[M]^+$ 123.07889, observed 123.07914.

Synthesis of 1-chloro-4-ethylbenzene (16)

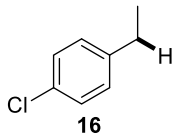

16

Compound **16** was prepared following general procedure A. Purification by column chromatography (*n*-pentane:EtOAc = 50:1) yielded the title compound **16** in an average yield of 77% (#1: 60 mg, 0.43 mmol, 85%; #2: 48 mg, 0.34 mmol, 68%) as colorless oil.

R_f = 0.76 (*n*-pentane:EtOAc = 50:1, UV)

^{1}H NMR (400 MHz, $CDCl_3$) δ 7.28 – 7.21 (m, 2H), 7.15 – 7.09 (m, 2H), 2.62 (q, *J* = 7.6 Hz, 2H), 1.22 (t, *J* = 7.6 Hz, 3H).

^{13}C NMR (101 MHz, $CDCl_3$) δ 142.8, 131.4, 129.3, 128.5, 28.4, 15.7.

MS (EI): *m*/*z* (relative intensity) 142 (12), 140 (37), 127 (32), 125 (100), 105 (43), 103 (11), 89 (15), 77 (13), 63 (8), 51 (8).

HRMS (EI, *m*/*z*): calcd. for $C_8H_9{}^{35}Cl$ $[M - H]^+$ 139.0309, observed 139.0321; calcd. for $C_8H_9{}^{37}Cl$ $[M - H]^+$ 141.0280, observed 141.0289.

IR (ATR, neat, cm^{-1}): 3027 (w), 2966 (w), 2931 (w), 2873 (w), 1892 (w), 1728 (w), 1649 (w), 1597 (w), 1491 (s), 1459 (w), 1408 (w), 1376 (w), 1331 (w), 1274 (w), 1231 (w), 1178 (w), 1109 (w), 1091 (s), 1050 (w), 1015 (m), 966 (w), 822 (s), 781 (m), 713 (w), 627 (m), 520 (m), 411 (w).

This data is in agreement with literature.[297]

Synthesis of undecane (18)

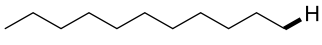

18

Compound **18** was prepared following general procedure A. The average yield of 20% was calculated as GC yield using the method below (#1: 19%; #2: 20%).

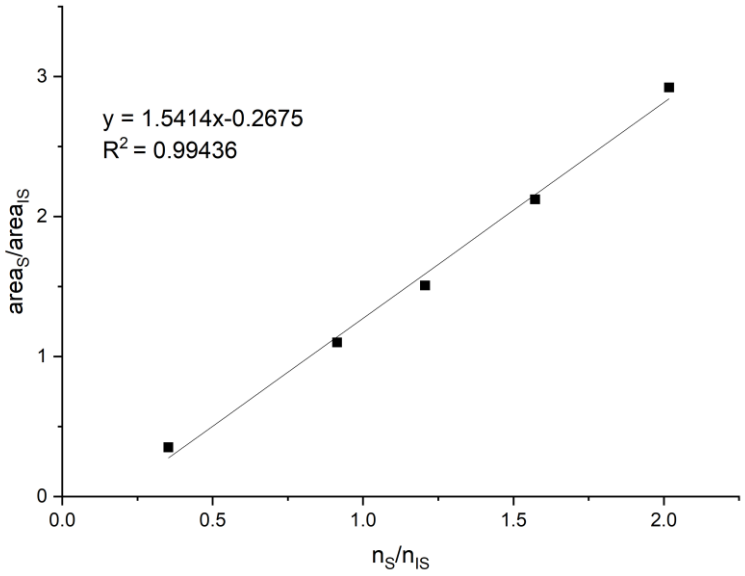

Figure 34. GC calibration graph for undecane (**18**) as substrate (S) using biphenyl as internal standard (IS).

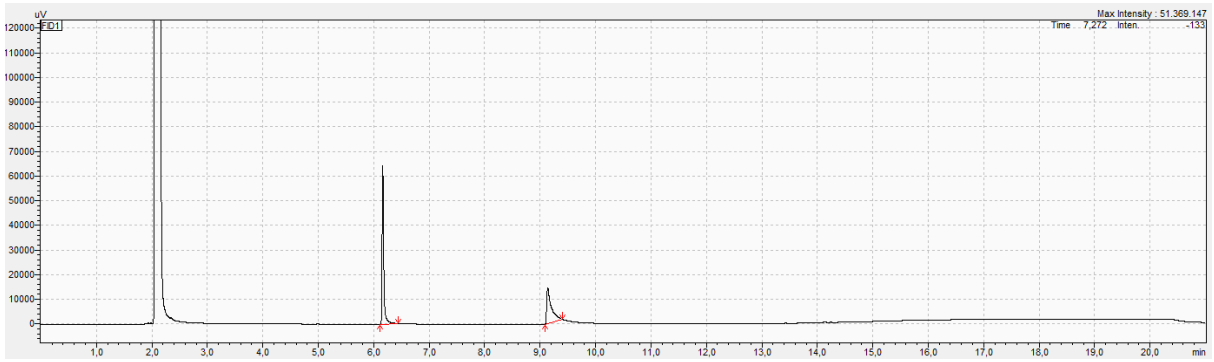

Figure 35. Exemplary gas chromatogram of undecane (**18**, t_R = 6.16 min) and biphenyl (IS, t_R = 9.14 min) using a 20 min-method heating von 50 °C to 280 °C in 15 min.

Synthesis of heptadecane (20)

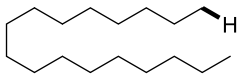

20

Compound **20** was prepared following general procedure A. Purification by column chromatography (*n*-pentane) yielded the title compound **20** in an average yield of 20% (#1: 28 mg, 0.12 mmol, 23%; #2: 19 mg, 0.08 mmol, 16%) as colorless oil.

R_f = 0.86 (*n*-pentane:EtOAc = 50:1, $KMnO_4$).

^{1}H NMR (300 MHz, $CDCl_3$) δ 1.40 – 1.16 (m, 30H), 0.94 – 0.82 (m, 6H).

^{13}C NMR (75 MHz, $CDCl_3$) δ 34.3, 32.1, 29.9, 29.8, 29.5, 22.9, 22.5, 14.3, 14.2.

MS (EI): *m*/*z* (relative intensity) 240 (5), 113 (8), 99 (15), 85 (51), 71 (72), 70 (12), 69 (12), 57 (100), 56 (15), 55 (23), 43 (67), 41 (35), 29 (12).

HRMS (EI, *m*/*z*): calcd. for $C_{17}H_{36}$ $[M]^+$ 240.2812, observed 240.2812.

IR (ATR, neat, cm^{-1}): 2956 (w), 2920 (s), 2852 (s), 1727 (w), 1465 (m), 1377 (w), 1308 (w), 1241 (w), 1149 (w), 1071 (w), 966 (w), 908 (w), 721 (w).

This data is in agreement with literature.[298]

Synthesis of (Z)-heptadec-8-ene (22)

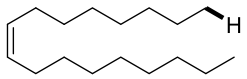

22

Compound **22** was prepared following general procedure A. Purification by column chromatography (*n*-pentane) yielded the title compound **22** in an average yield of 15% (#1: 17 mg, 0.07 mmol, 14%; #2: 18 mg, 0.08 mmol, 15%) as a colorless oil.

R_f = 0.83 (*n*-pentane:EtOAc = 50:1, $KMnO_4$)

^{1}H NMR (300 MHz, $CDCl_3$) δ 5.43 – 5.27 (m, 2H), 2.08 – 1.95 (m, 4H), 1.39 – 1.19 (m, 22H), 0.94 – 0.83 (m, 6H).

^{13}C NMR (75 MHz, $CDCl_3$) δ 130.1, 32.1, 32.0, 29.9, 29.7, 29.5, 29.4, 29.4, 27.4, 22.8, 14.3.

MS (EI): *m*/*z* (relative intensity) 239 (8), 238 (44), 126 (9), 125 (21), 112 (16), 111 (50), 98 (24), 97 (90), 96 (16), 85 (20), 84 (38), 83 (98), 82 (24), 81 (19), 71 (30), 70 (57), 69 (92), 68 (18), 67 (37), 57 (58), 56 (49), 55 (100), 54 (31), 53 (12), 43 (71), 42 (14), 41 (80), 39 (17).

HRMS (ESI-TOF, *m*/*z*): calcd. for $C_{17}H_{34}$ $[M]^+$ 238.2655, observed 238.2648.

IR (ATR, neat, cm^{-1}): 3005 (w), 2956 (m), 2921 (s), 2853 (s), 1654 (w), 1507 (w), 1464 (m), 1403 (w), 1378 (w), 1303 (w), 1114 (w), 1025 (w), 967 (w), 722 (m), 585 (w), 465 (w), 418 (w).

This data is in agreement with literature.[299]

Synthesis of toluene (24)

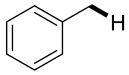

24

Compound **24** was prepared following general procedure A. The average yield of 17% was calculated as GC yield using the method below (#1: 16%, #2: 17%).

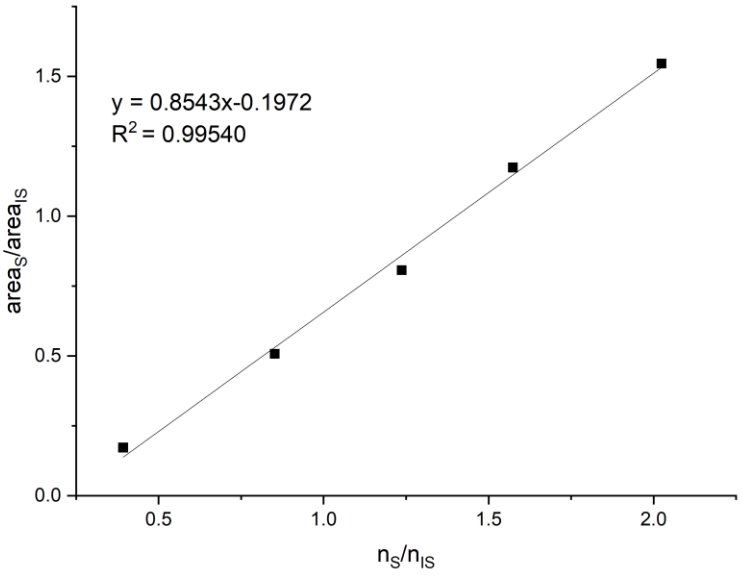

Figure 36. GC calibration graph for toluene (**24**) as substrate (S) using biphenyl as internal standard (IS).

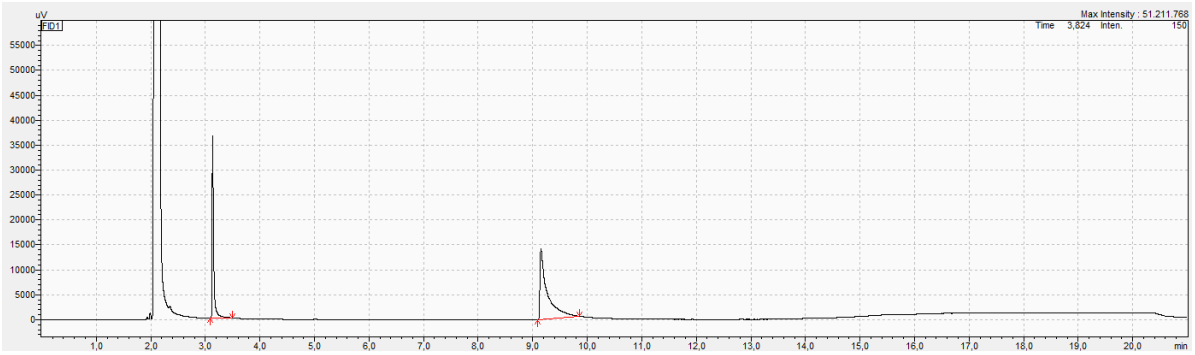

Figure 37. Exemplary gas chromatogram of toluene (**24**, t_R = 3.13 min) and biphenyl (IS, t_R = 9.15 min) using a 20 min-method heating von 50 °C to 280 °C in 15 min.

Synthesis of 1-methoxy-4-propylbenzene (26)

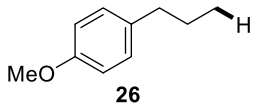

26

Compound **26** was prepared following general procedure A. Purification by column chromatography (*n*-pentane:CH_2Cl_2 = 5:1) yielded the title compound **26** in an average yield of 17% (#1: 12 mg, 0.08 mmol, 16%; #2: 14 mg, 0.09 mmol, 18%) as a colorless oil.

R_f = 0.37 (*n*-pentane, UV).

^{1}H NMR (300 MHz, $CDCl_3$) δ 7.13 – 7.06 (m, 2H), 6.86 – 6.80 (m, 2H), 3.79 (s, 3H), 2.57 – 2.48 (m, 2H), 1.69 – 1.53 (m, 2H), 0.93 (t, *J* = 7.3 Hz, 3H).

^{13}C NMR (75 MHz, $CDCl_3$) δ 157.6, 135.0, 129.4, 113.8, 55.4, 37.3, 24.9, 13.9.

MS (EI): *m*/*z* (relative intensity) 150 (21), 122 (9), 121 (100), 91 (6), 78 (7), 77 (7).

HRMS (EI, *m*/*z*): calcd. for $C_{10}H_{14}O$ $[M]^+$ 150.1039, observed 150.1043.

IR (ATR, neat, cm^{-1}): 2996 (w), 2955 (w), 2923 (m), 2852 (m), 2058 (w), 1991 (w), 1734 (w), 1612 (m), 1584 (w), 1511 (s), 1463 (m), 1442 (m), 1377 (w), 1340 (w), 1299 (m), 1244 (s), 1176 (m), 1114 (m), 1040 (s), 965 (w), 806 (m), 787 (m), 749 (m), 720 (m), 696 (m), 638 (w), 555 (m), 518 (m).

This data is in agreement with literature.[300]

Synthesis of butane-2,2-diylbis(4,1-phenylene) diacetate (28)

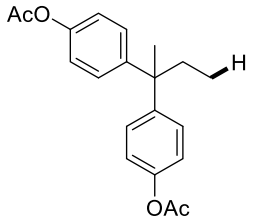

28

Compound **28** was prepared following general procedure A. Purification by column chromatography (CH_2Cl_2) yielded the title compound **28** in an average yield of 15% (#1: 23 mg, 0.07 mmol, 14%; #2: 25 mg, 0.08 mmol, 15%) as a colorless oil.

R_f = 0.48 (CH_2Cl_2, UV)

^{1}H NMR (300 MHz, $CDCl_3$) δ 7.22 – 7.15 (m, 4H), 7.03 – 6.94 (m, 4H), 2.28 (s, 6H), 2.11 (q, *J* = 7.4 Hz, 2H), 1.59 (s, 3H), 0.74 (t, *J* = 7.3 Hz, 3H).

^{13}C NMR (75 MHz, $CDCl_3$) δ 169.6, 148.6, 146.9, 128.5, 120.9, 46.2, 34.4, 27.3, 21.3, 9.3.

MS (EI): *m*/*z* (relative intensity) 326 (4), 297 (40), 255 (54), 214 (15), 213 (100), 197 (3), 169 (5), 119 (7), 43 (11).

HRMS (ESI-TOF, *m*/*z*): calcd. for $C_{20}H_{22}O_4$ $[M]^+$ 326.1513, observed 326.1515.

IR (ATR, neat, cm^{-1}): 3040 (w), 2969 (w), 2935 (w), 2879 (w), 1753 (s), 1604 (w), 1504 (m), 1458 (w), 1432 (w), 1409 (w), 1368 (m), 1307 (w), 1193 (s), 1167 (s), 1112 (w), 1101 (w), 1081 (w), 1043 (w), 1014 (m), 944 (w), 909 (s), 844 (m), 803 (w), 776 (w), 728 (s), 693 (w), 663 (w), 648 (w), 595 (m), 575 (w), 564 (w), 554 (m), 532 (m), 499 (w).

Synthesis of (4-chlorophenyl)(5-methoxy-2,3-dimethyl-1*H*-indol-1-yl)methanone (30)

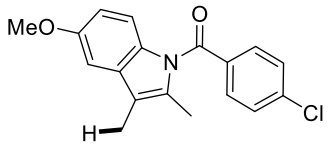

30

Compound **30** was prepared following general procedure A. Purification by column chromatography (*n*-pentane:CH_2Cl_2 = 1:1) yielded the title compound **30** in an average yield of 34% (#1: 50 mg, 0.16 mmol, 32%; #2: 55 mg, 0.18 mmol, 35%) as a yellow oil.

R_f = 0.32 (*n*-pentane:CH_2Cl_2 = 1:1, UV)

^{1}H NMR (300 MHz, $CDCl_3$) δ 7.68 – 7.61 (m, 2H), 7.49 – 7.43 (m, 2H), 6.94 – 6.88 (m, 2H), 6.67 (dd, *J* = 8.9, 2.6 Hz, 1H), 3.85 (s, 3H), 2.31 (q, *J* = 0.9 Hz, 3H), 2.19 (q, *J* = 0.8 Hz, 3H).

^{13}C NMR (75 MHz, $CDCl_3$) δ 168.3, 156.1, 139.0, 134.5, 133.9, 132.1, 131.2, 131.0, 129.1, 115.5, 115.0, 111.3, 101.4, 55.8, 13.4, 8.9.

MS (EI): *m*/*z* (relative intensity) 315 (17), 313 (47), 141 (33), 139 (100), 131 (11), 111 (25), 75 (8).

HRMS (ESI-TOF, *m*/*z*): calcd. for $C_{18}H_{16}O_2N^{35}Cl$ $[M]^+$ 313.0864, observed 313.0869.

IR (ATR, neat, cm^{-1}): 069 (w), 2924 (w), 2860 (w), 2832 (w), 1673 (s), 1608 (m), 1592 (m), 1474 (s), 1456 (s), 1436 (m), 1398 (m), 1391 (m), 1362 (s), 1353 (s), 1314 (s), 1285 (s), 1259 (m), 1216 (s), 1177 (m), 1154 (s), 1087 (s), 1047 (s), 1014 (s), 1004 (m), 925 (m), 876 (w), 830 (s), 800 (m), 753 (s), 738 (m), 716 (m), 689 (m), 643 (m), 629 (m), 608 (m), 589 (m), 560 (m), 549 (m), 480 (s), 433 (m).

This data is in agreement with literature.[43]

Synthesis of (4-chlorophenyl)(5-methoxy-2-methyl-3-(methyl-*d*)-1*H*-indol-1-yl)methanone (*d*-30)

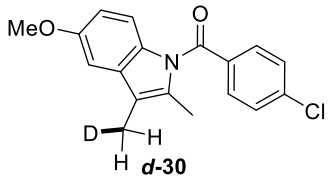

***d*-30**

Compound ***d*-30** prepared following general procedure A using deuterated water. Purification by column chromatography (*n*-pentane:CH_2Cl_2 = 1:1) yielded the title compound ***d*-30** (54 mg, 0.17 mmol, 34%) as a yellow oil. The deuterium content was determined by ^{1}H NMR spectroscopy (91%).

R_f = 0.32 (*n*-pentane:CH_2Cl_2 = 1:1, UV)

^{1}H NMR (400 MHz, $CDCl_3$) δ 7.67 – 7.62 (m, 2H), 7.49 – 7.44 (m, 2H), 6.94 – 6.88 (m, 2H), 6.67 (dd, *J* = 8.9, 2.6 Hz, 1H), 3.85 (s, 3H), 2.31 (s, 3H), 2.20 – 2.17 (m, 2.09H, 91 % D).

^{13}C NMR (101 MHz, $CDCl_3$) δ 168.3, 156.1, 139.0, 134.5, 133.9, 132.1, 131.1, 131.0, 129.1, 115.5, 115.0, 111.3, 101.4, 55.8, 13.4, 8.6 (t, *J* = 19.5 Hz).

MS (EI): *m*/*z* (relative intensity) 316 (20), 314 (53), 141 (51), 139 (100), 132 (13), 111 (37), 75 (10).

HRMS (EI-TOF, *m*/*z*): calcd. for $C_{18}H_{15}DO_2N^{35}Cl$ $[M]^+$ 314.0927, observed 314.0928; calcd. for $C_{18}H_{15}{}^2HO_2N^{37}Cl$ $[M]^+$ 316.0897, observed 316.0903.

This data is in agreement with literature.[86]

Synthesis of 1-(2,2-dichlorocyclopropyl)-4-isopropoxybenzene (33)

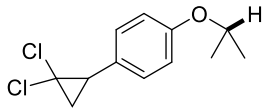

33

Compound **33** was prepared following general procedure A. Purification by column chromatography (*n*-pentane:CH_2Cl_2 = 1:1) yielded the title compound **33** in an average yield of 39% (#1: 46 mg, 0.19 mmol, 38%; #2: 48 mg, 0.20 mmol, 39%) as a colorless oil.

R_f = 0.18 (*n*-pentane, UV).

^{1}H NMR (300 MHz, $CDCl_3$) δ 7.18 – 7.12 (m, 2H), 6.90 – 6.84 (m, 2H), 4.55 (hept, *J* = 6.1 Hz, 1H), 2.89 – 2.79 (m, 1H), 1.94 (dd, *J* = 10.7, 7.4 Hz, 1H), 1.79 (dd, *J* = 8.4, 7.3 Hz, 1H), 1.34 (d, *J* = 6.1 Hz, 6H).

^{13}C NMR (75 MHz, $CDCl_3$) δ 157.5, 130.1, 126.6, 115.7, 70.0, 61.2, 35.0, 25.9, 22.2, 22.2.

MS (EI, 70 eV): *m/z* (relative intensity) 246 (2), 244 (4), 209 (17), 202 (10), 169 (33), 168 (11), 167 (100), 132 (28), 131 (82), 103 (19), 102 (10), 77 (13).

HRMS (ESI-TOF, *m/z*): calcd. for $C_{12}H_{14}O^{35}Cl_2$ $[M + H]^+$ 245.0500, observed 245.0500; calcd. for $C_{12}H_{14}O^{35}Cl^{37}Cl$ $[M + H]^+$ 247.0470, observed 247.0474.

IR (ATR, neat, cm^{-1}): 3036 (w), 2977 (w), 2933 (w), 1735 (w), 1612 (m), 1578 (w), 1510 (s), 1467 (w), 1453 (w), 1431 (w), 1384 (w), 1372 (w), 1334 (w), 1295 (w), 1243 (s), 1181 (m), 1111 (s), 1049 (m), 1012 (w), 955 (s), 861 (w), 829 (s), 798 (w), 758 (s), 727 (m), 704 (w), 637 (w), 585 (m), 550 (m), 512 (w), 457 (m), 415 (w).

This data is in agreement with literature.[80]

Synthesis of 1-(2,2-dichlorocyclopropyl)-4-((propan-2-yl-2-*d*)oxy)benzene (*d*-33)

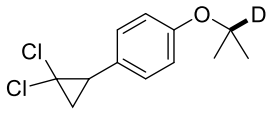

***d*-33**

Compound ***d*-33** was prepared following general procedure A using deuterated water. Purification by column chromatography (*n*-pentane:CH_2Cl_2 = 1:1) yielded the title compound ***d*-33** (43 mg, 0.18 mmol, 35%) as a colorless oil. The deuterium content was determined by ^{1}H NMR spectroscopy (83%).

R_f = 0.79 (*n*-pentane:CH_2Cl_2 = 1:1, UV)

^{1}H NMR (300 MHz, $CDCl_3$) δ 7.18 – 7.11 (m, 2H), 6.90 – 6.82 (m, 2H), 4.55 (hept, *J* = 6.1 Hz, 0.17H, 83 % D), 2.93 – 2.72 (m, 1H), 1.94 (dd, *J* = 10.7, 7.4 Hz, 1H), 1.79 (dd, *J* = 8.3, 7.3 Hz, 1H), 1.33 (s, 6H).

^{13}C NMR (101 MHz, $CDCl_3$) δ 157.5, 130.1, 126.6, 115.6, 69.6 (t, *J* = 21.7 Hz), 61.2, 35.0, 25.9, 22.1 (d, *J* = 1.6 Hz).

MS (EI): *m*/*z* (relative intensity) 247 (2), 245 (4), 210 (15), 202 (10), 169 (32), 168 (11), 167 (100), 132 (27), 131 (78), 103 (18), 102 (10), 77 (12).

HRMS (EI, *m*/*z*): calcd. for $C_{12}H_{13}{}^2HO^{35}Cl^{37}Cl$ $[M]^+$ 247.0450, observed 247.0445.

Synthesis of 4-chloro-*N*-(4-isopropoxyphenethyl)benzamide (35)

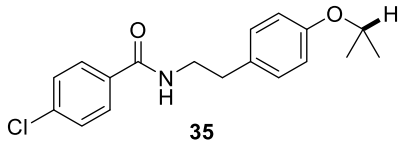

35

Compound **35** was prepared following general procedure A. Purification by column chromatography (*n*-pentane:EtOAc = 5:1) yielded the title compound **35** in an average yield of 33% (#1: 55 mg, 0.17 mmol, 35%; #2: 47 mg, 0.15 mmol, 30%) as a colorless solid.

R_f = 0.34 (*n*-pentane:EtOAc = 2:1, UV).

m.p. 176 – 178 °C

^{1}H NMR (300 MHz, $CDCl_3$) δ 7.65 – 7.59 (m, 2H), 7.40 – 7.34 (m, 2H), 7.16 – 7.08 (m, 2H), 6.88 – 6.81 (m, 2H), 6.11 (s, 1H), 4.52 (hept, *J* = 6.1 Hz, 1H), 3.67 (td, *J* = 6.9, 5.8 Hz, 2H), 2.85 (t, *J* = 6.8 Hz, 2H), 1.33 (d, *J* = 6.1 Hz, 6H).

^{13}C NMR (75 MHz, $CDCl_3$) δ 166.5, 156.8, 137.7, 133.2, 130.6, 129.9, 128.9, 128.4, 116.3, 70.1, 41.5, 34.8, 22.2.

MS (EI): *m*/*z* (relative intensity) 317 (2), 162 (61), 141 (14), 139 (42), 120 (100), 111 (19), 107 (41), 77 (8).

HRMS (ESI-TOF, *m*/*z*): calcd. for $C_{18}H_{20}ClNO_2$ $[M+H]^+$ 318.1261, observed 318.1260.

IR (ATR, neat, cm^{-1}): 3325 (w), 2983 (w), 2933 (w), 2862 (w), 1637 (s), 1611 (w), 1593 (w), 1579 (w), 1571 (w), 1541 (s), 1506 (m), 1480 (m), 1455 (m), 1383 (m), 1371 (w), 1355 (w), 1315 (m), 1294 (m), 1237 (s), 1193 (m), 1178 (m), 1155 (m), 1136 (m), 1118 (m), 1105 (m), 1090 (m), 1053 (m), 1036 (w), 1009 (m), 974 (w), 956 (m), 860 (m), 849 (s), 830 (s), 813 (s), 754 (m), 715 (m), 707 (m), 667 (m), 624 (m), 592 (w), 532 (s), 506 (m), 481 (w), 463 (m), 435 (w).

This data is in agreement with literature.[301]

Synthesis of isopropoxybenzene (37)

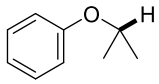

37

Compound **37** was prepared following general procedure A. The average yield of 35% was determined by ^{1}H NMR using 1,3,5-trimethoxybenzene (TMB, 0.22 mmol, 0.44 equiv.) as internal standard (#1: 32%; #2: 37%).

^{1}H NMR (300 MHz, $CDCl_3$) δ 7.33 – 7.24 (m, 2H), 6.98 – 6.85 (m, 3H), 4.56 (hept, *J* = 6.1 Hz, 1H), 1.35 (dd, *J* = 6.1, 0.4 Hz, 6H).

^{13}C NMR (75 MHz, $CDCl_3$) δ 158.0, 129.6, 120.6, 116.0, 69.9, 22.2.

This data is in agreement with literature.[302]

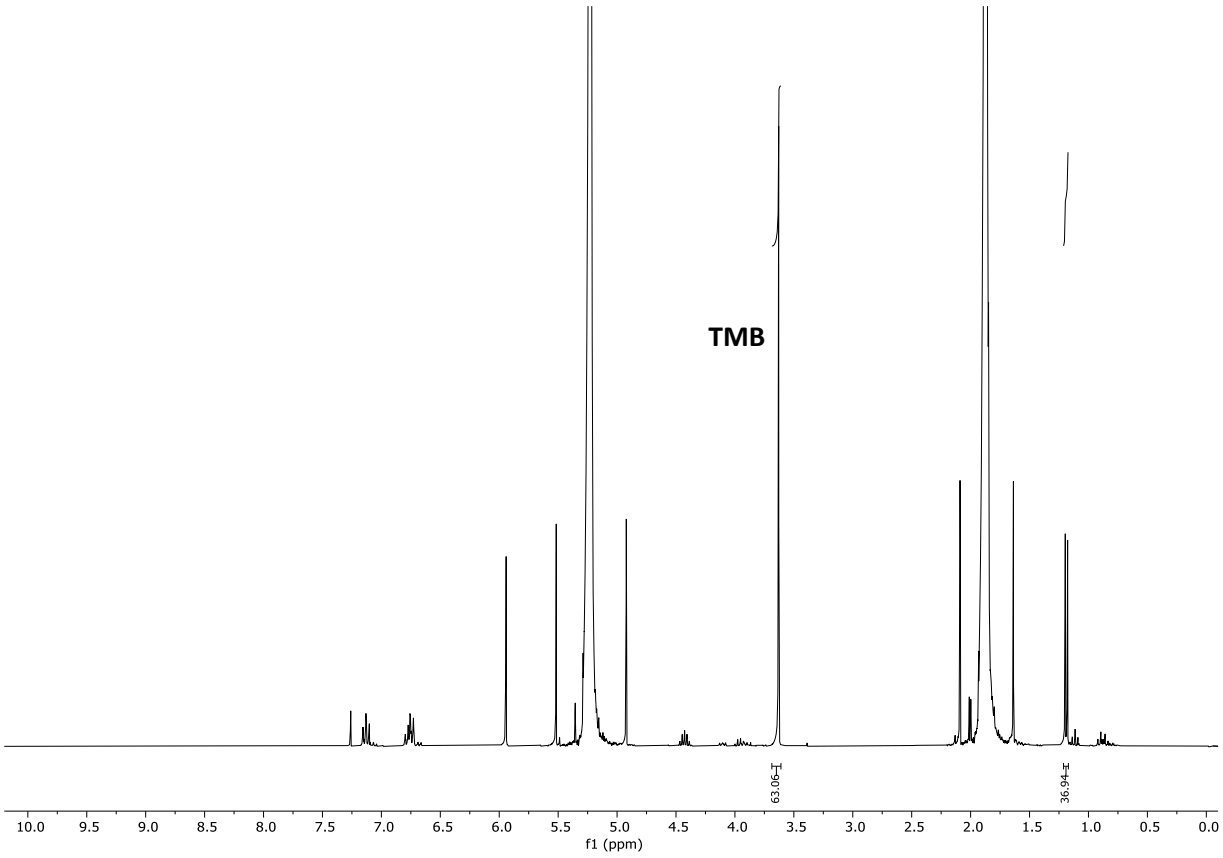

Figure 38. Crude NMR spectrum of ether **37** and 1,3,5-trimethoxybenzene (TMB).

Synthesis of (3s,5s,7s)-adamantan-1-ol (39)

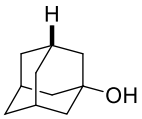

39

Compound **39** was prepared following general procedure A. Purification by column chromatography (CH_2Cl_2:MeOH = 100:1) yielded the title compound **39** in an average yield of 67% (#1: 48 mg, 0.31 mmol, 63%; #2: 54 mg, 0.36 mmol, 71%) as colorless solid.

R_f = 0.30 (n-pentane:EtOAc = 2:1, $KMnO_4$)

^{1}H NMR (300 MHz, $CDCl_3$) δ 2.14 (s, 3H), 1.71 (d, *J* = 2.9 Hz, 6H), 1.68 – 1.54 (m, 6H), 1.44 (s, 1H).

^{13}C NMR (75 MHz, $CDCl_3$) δ 68.4, 45.5, 36.2, 30.9.

MS (EI): *m*/*z* (relative intensity) 152 (29), 95 (100), 94 (13), 79 (6), 77 (8).

HRMS (EI, *m*/*z*): calcd. for $C_{10}H_{16}O$ $[M]^+$ 152.1196, observed 152.1201.

IR (ATR, neat, cm^{-1}): 3267 (m), 2914 (s), 2898 (s), 2847 (m), 2654 (w), 2324 (w), 1701 (w), 1474 (w), 1451 (m), 1420 (w), 1368 (w), 1352 (m), 1335 (w), 1316 (w), 1301 (m), 1281 (w), 1263 (w), 1227 (m), 1173 (w), 1114 (s), 1101 (m), 1086 (s), 1038 (w), 981 (m), 926 (s), 880 (w), 812 (m), 776 (w), 722 (m), 655 (w), 643 (w), 551 (m), 464 (w), 429 (m), 411 (w).

This data is in agreement with literature.[303]

Synthesis of adamantane (41)

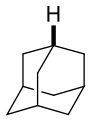

41

Compound **41** was prepared following general procedure A. The average yield of 23% was calculated as GC yield using the method below (#1: 22%; #2: 24%).

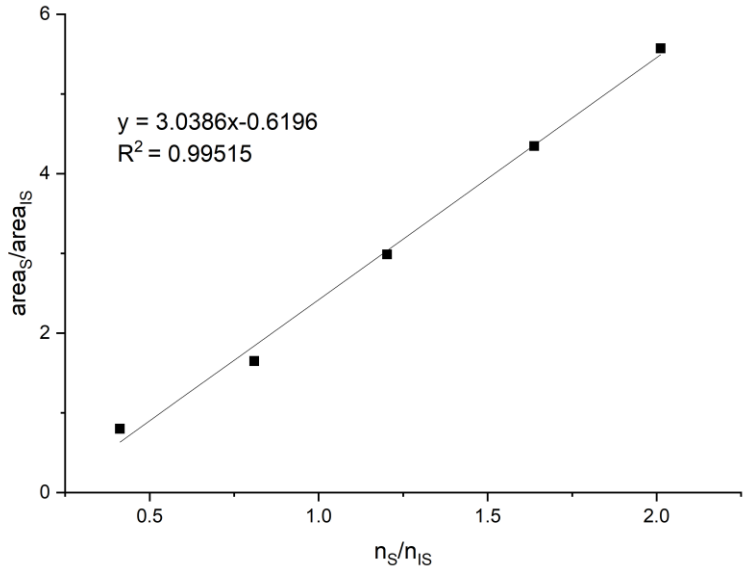

Figure 39. GC calibration graph for adamantane (**41**) as substrate (S) using biphenyl as internal standard (IS).

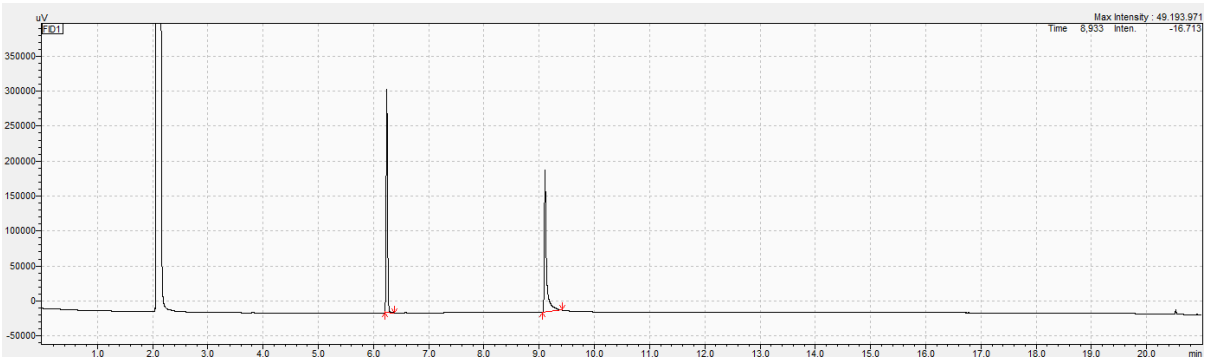

Figure 40. Exemplary gas chromatogram of adamantane (**41**, t_R = 6.24 min) and biphenyl (IS, t_R = 9.11 min) using a 20 min-method heating von 50 °C to 280 °C in 15 min.

Synthesis of (4a*R*,6a*S*,6b*R*,8a*R*,10*S*,12a*S*,12b*R*,14b*R*)-10-hydroxy-2,4a,6a,6b,9,9,12a-heptamethyl-1,3,4,4a,5,6,6a,6b,7,8,8a,9,10,11,12,12a,12b,14b-octadecahydropicen-13(2*H*)-one (43)

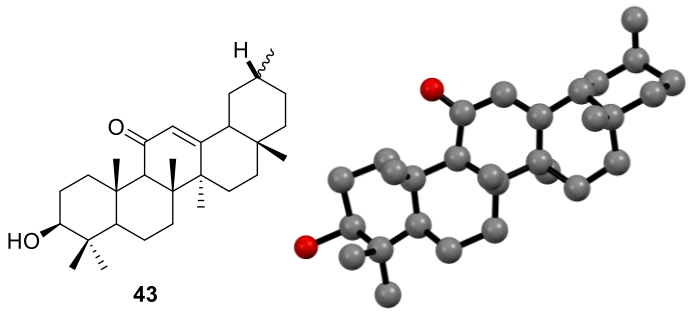

43

Compound **43** was prepared following general procedure A. Purification by column chromatography (*n*-pentane:EtOAc = 5:1) yielded the title compound **43** as a mixture of diastereomers in an average yield of 66% (#1: 146 mg, 0.34 mmol, 68%; #2: 137 mg, 0.32 mmol, 64%) as colorless solid. Crystals suitable for X-ray crystallography were obtained by crystallization from hot DMSO. Due to the low quality of the crystals, no complete data set was recorded.

R_f = 0.15 (*n*-pentane:EtOAc = 5:1, UV)

m.p. 105 – 120 °C

^{1}H NMR (300 MHz, $CDCl_3$) δ 5.58 (d, *J* = 5.2 Hz, 1H), 3.21 (ddd, *J* = 10.4, 6.3, 1.6 Hz, 1H), 2.78 (dtd, *J* = 13.4, 3.6, 1.8 Hz, 1H), 2.33 (s, 1H), 2.20 – 1.92 (m, 3H), 1.89 – 1.75 (m, 1H), 1.73 – 1.36 (m, 11H), 1.35 (s, 3H), 1.33 – 1.16 (m, 3H), 1.12 (s, 6H), 0.99 (s, 3H), 0.98 – 0.90 (m, 3H), 0.87 (d, *J* = 6.2 Hz, 2H), 0.83 (s, 1H), 0.82 (s, 2H), 0.79 (s, 3H), 0.69 (dd, *J* = 11.6, 2.0 Hz, 1H).

^{13}C NMR (75 MHz, $CDCl_3$) δ 200.5 (quart.), 171.0 (quart.), 170.5 (quart.), 128.1 (*C*H), 78.9 (*C*H), 61.9, 55.1, 51.8, 45.6 (quart.), 45.5 (quart.), 45.5, 43.5 (quart.), 43.5 (quart.), 41.5 (CH_2), 41.0 (CH_2), 39.3 (CH_2), 37.9 (CH_2), 37.2 (quart.), 34.4 (CH_2), 33.5, 32.9 (CH_2), 32.5 (quart.), 30.7 (CH_2), 29.1, 28.9, 28.2, 27.8, 27.4 (CH_2), 26.9 (CH_2), 26.8 (CH_2), 26.6 (CH_2), 26.6 (CH_2), 23.5, 22.5, 18.8, 18.8, 17.6 (CH_2), 17.0, 16.5, 15.7.

MS (EI): *m*/*z* (relative intensity) 426 (26), 393 (7), 260 (13), 259 (86), 219 (15), 218 (100), 203 (8), 193 (9), 192 (8), 175 (34), 149 (10), 135 (50), 121 (10), 107 (8), 105 (9), 95 (11), 81 (11).

HRMS (EI, *m*/*z*): calcd. for $C_{29}H_{46}O_2$ $[M]^+$ 426.3492, observed 426.3500.

IR (ATR, neat, cm^{-1}): 3420 (w), 2946 (m), 2923 (m), 2861 (m), 1654 (s), 1620 (w), 1454 (m), 1385 (m), 1362 (w), 1332 (w), 1289 (w), 1258 (w), 1207 (m), 1133 (w), 1088 (w), 1041 (s), 1013 (w), 994 (m), 980 (m), 948 (w), 918 (m), 879 (w), 867 (w), 856 (w), 840 (w), 829 (w), 808 (w), 779 (w), 730 (s), 700 (w), 673 (w), 646 (w), 624 (w), 577 (w), 542 (m), 495 (w), 475 (w), 461 (w), 435 (w), 418 (w).

This data is in agreement with literature.[48]

Synthesis of (4a*R*,6a*S*,6b*R*,8a*R*,10*S*,12a*S*,12b*R*,14b*R*)-10-hydroxy-2,4a,6a,6b,9,9,12a-heptamethyl-1,3,4,4a,5,6,6a,6b,7,8,8a,9,10,11,12,12a,12b,14b-octadecahydropicen-13(2*H*)-one-2-*d* (*d*-43)

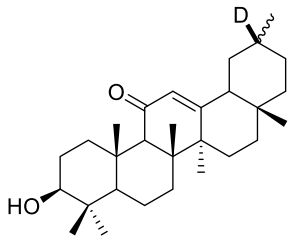

***d*-43**

Compound ***d*-43** was prepared following general procedure A using deuterated water. Purification by column chromatography (*n*-pentane:EtOAc = 5:1) yielded the title compound ***d*-43** as mixture of diastereomers (136 mg, 0.32 mmol, 64%) as colorless oil. The deuterium content was determined by GCMS analysis (95%).

R_f = 0.15 (*n*-pentane:EtOAc = 5:1, UV)

^{1}H NMR (400 MHz, $CDCl_3$) δ 5.59 (d, *J* = 6.9 Hz, 1H), 3.22 (ddd, *J* = 10.8, 5.4, 2.0 Hz, 1H), 2.78 (dt, *J* = 13.5, 3.3 Hz, 1H), 2.33 (s, 1H), 2.20 – 1.94 (m, 3H), 1.82 (td, *J* = 13.6, 6.9 Hz, 1H), 1.74 – 1.53 (m, 6H), 1.53 – 1.36 (m, 5H), 1.35 (d, *J* = 2.0 Hz, 3H), 1.34 – 1.19 (m, 3H), 1.13 (s, 6H), 1.03 – 0.91 (m, 6H), 0.91 – 0.83 (m, 1H), 0.84 (s, 1H), 0.82 (s, 2H), 0.80 (s, 3H), 0.69 (dd, *J* = 11.6, 1.9 Hz, 1H).

^{13}C NMR (101 MHz, $CDCl_3$) δ 200.6, 171.1, 170.6, 128.1, 128.1, 78.9, 61.9, 55.1, 51.8, 45.6, 45.5, 45.5, 43.5, 43.5, 41.4, 40.9, 39.3, 37.8, 37.2, 34.4, 34.3, 33.5, 32.9, 32.9, 32.5, 30.6, 29.8, 29.1, 28.9, 28.2, 27.8, 27.4, 26.8, 26.8, 26.6, 26.6, 23.5, 22.5, 22.4, 18.8, 18.8, 17.6, 16.9, 16.5, 15.7.

MS (EI): *m*/*z* (relative intensity) 427 (17), 394 (6), 261 (11), 260 (53), 220 (19), 219 (100), 204 (10), 193 (11), 192 (13), 175 (41), 150 (15), 135 (50), 121 (16), 107 (13), 105 (15), 95 (18), 81 (14).

HRMS (EI, *m*/*z*): calcd. for $C_{29}H_{45}{}^2HO_2$ $[M]^+$ 427.3555, observed 427.3549.

This data is in agreement with literature.[86]

TEMPO quenching experiment

The TEMPO quenching experiment was performed under Schlenk conditions using a 25 ml Schlenk tube. 1-adamantanecarboxylic acid (**40**, 92.5 mg, 0.50 mmol, 1.0 equiv.), photocatalyst PrPPT (10.4 mg, 25 µmol, 5.0 mol%), K_3PO_4 (145 mg, 0.67 mmol, 1.33 equiv.) and 2,2,6,6-tetramethylpiperidin-1-yl)oxyl (100.3 mg, 0.625 mmol, 1.25 equiv.) were added. Next, the flask was evacuated and purged with argon three times. Acetonitrile (4.7 mL) and degassed water (0.3 mL) were added and the reaction mixture was then irradiated for 24 h while stirred at 50 °C, before it was quenched upon exposure to air. Subsequently, a 0.5 ml sample was taken and analyzed by LC-MS (see LC-MS spectrum, below).

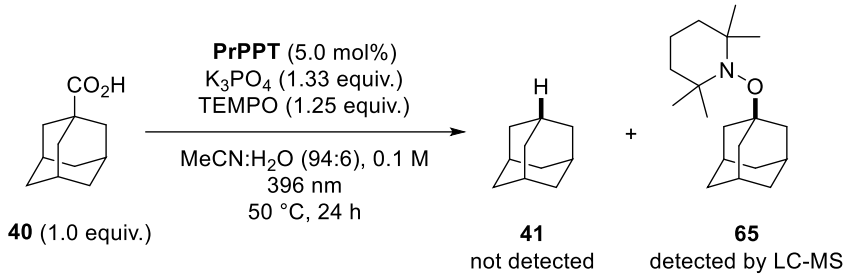

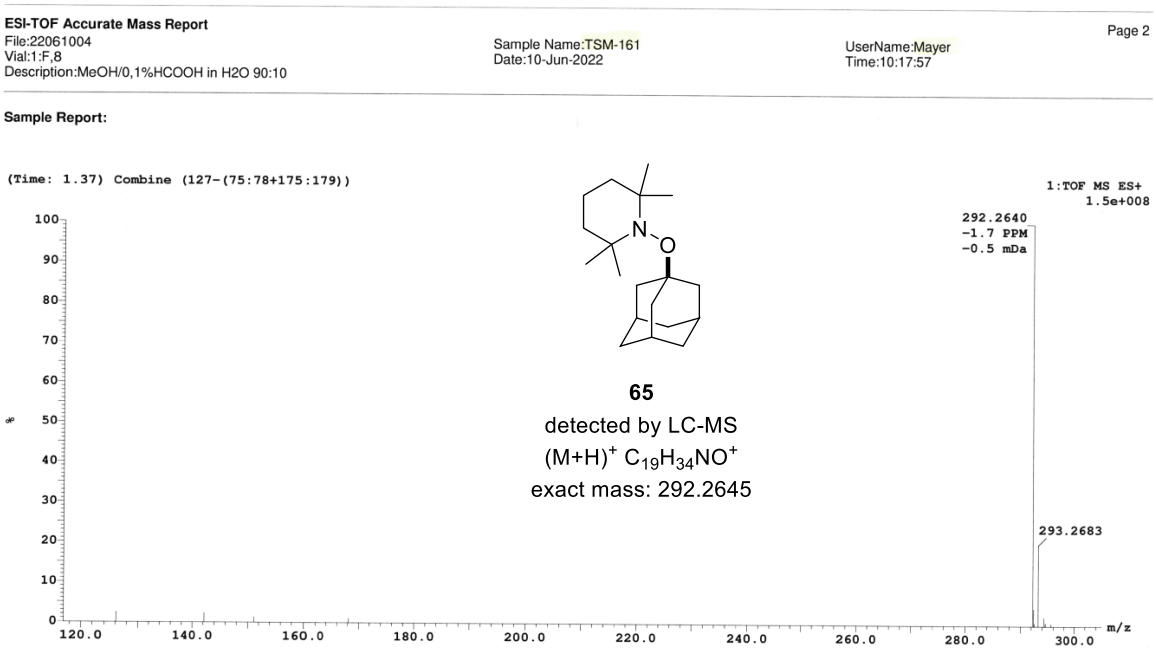

Figure 41. LC-MS spectrum of the decarboxylation reaction of 1-adamantanecarboxylic acid (**40**) in presence of 1.25 equiv. TEMPO.

Electrochemistry

The measurements were performed with 10 μM compound dissolved in the electrolyte. Afterwards, 1 equiv. TBAOH (40 wt% aqueous solution) was added to the electrochemical cell to form the corresponding carboxylate and the potentials were measured again.

Table 36. Redox potentials according to DPV peak maxima.

entry	compound	$E_{1/2}^{ox}$ (carboxylic acid, V vs SCE)	$E_{1/2}^{ox}$ (carboxylate, V vs SCE)
1	ibuprofen (**1**)	+2.15	+1.04
2	naproxen (**5**)	+1.64 +1.33	+1.55 +1.47 +1.33 +1.18
3	Cbz-Val-OH (**11**)	+2.53	+1.86 +1.62
4	hydroxyadamantane carboxylic acid (**38**)	+2.48	+1.31 +1.02
5	2-methyl-2-phenoxy-propanoic acid (**36**)	+1.83	+1.77 +1.01

Stern-Volmer experiments

The Stern-Volmer quenching experiments were run with freshly prepared solutions of PrPPT (0.2 mM in dry MeCN) at room temperature under argon. The solutions were irradiated at 355 nm and luminescence was measured at 384 nm for ibuprofen or at 385 nm for tetrabutylammonium ibuprofen carboxylate. The data shows that tetrabutylammonium ibuprofen carboxylate (**62**, K_{SV} = 34.1 M^{-1}) is a better quencher than ibuprofen itself (**1**, K_{SV} = 14.3 M^{-1}).

Table 37. Fluorescence quenching data of a solution of PrPPT by a solution of ibuprofen (**1**).

I_x [a.u.]	$I_0/I_x - 1$ [a.u.]	Q [mM]
$I_0 = 580.7570$	0	0
$I_1 = 565.4917$	0.0270	2.8015
$I_2 = 545.2892$	0.0650	5.3483
$I_3 = 526.9082$	0.1022	7.6737
$I_4 = 513.7072$	0.1305	9.8052
$I_5 = 499.6016$	0.1624	11.7663
$I_6 = 486.3278$	0.1942	13.5765
$I_7 = 475.2461$	0.2220	15.2526
$I_8 = 463.3983$	0.2533	16.8090

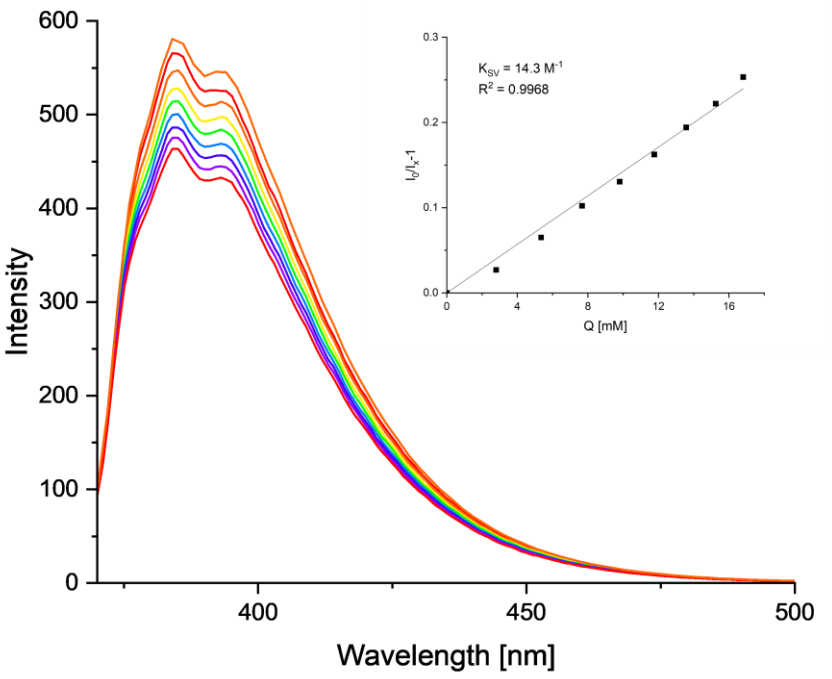

Figure 42. Quenching of luminescence and Stern-Volmer plot (inset) of PrPPT with varying concentrations of ibuprofen (**1**).

Table 38. Fluorescence quenching of a solution of PrPPT by a solution of tetrabutylammonium ibuprofen carboxylate (**62**).

I_x [a.u.]	$I_0/I_x - 1$ [a.u.]	Q [mM]
I_0 = 581.9404	0	0
I_1 = 535.9709	0.0858	2.8609
I_2 = 501.4997	0.1604	5.4617
I_3 = 471.5145	0.2342	7.8363
I_4 = 442.0692	0.3164	10.0130
I_5 = 416.0481	0.3987	12.0156
I_6 = 396.1945	0.4688	13.8642
I_7 = 375.3892	0.5502	15.5758
I_8 = 359.9533	0.6167	17.1652

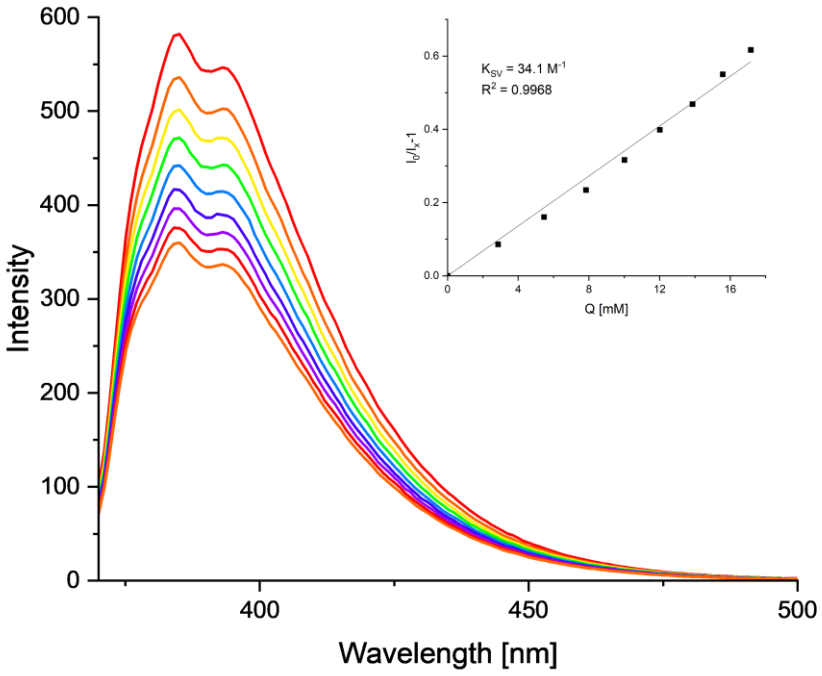

Figure 43. Quenching of luminescence and Stern-Volmer plot (inset) of PrPPT with varying concentrations of tetrabutylammonium ibuprofen carboxylate (**62**).

Light on/off experiment

In a Schlenk-tube, ibuprofen (**1**, 105.6 mg, 0.5 mmol, 1.0 equiv.), K_3PO_4 (145.7 mg, 0.66 mmol, 1.33 equiv.), PrPPT (11.0 mg, 25 µmol, 0.05 equiv.) and biphenyl (38.0 mg, 0.25 mmol, 0.5 equiv.) were added under argon. The Schlenk tube was evacuated and purged with argon 3 times. Next, dry acetonitrile (4.7 mL) and degassed water (0.3 mL) were added under argon. The reaction mixture was heated to 50 °C and irradiated for 4 h, then the light source was switched off for 2 consecutive hours. This process was repeated alternately before the reaction was quenched with air after 24 h of irradiation (reaction time 30 h). A 100 µl Sample was taken every 2 hours from the acetonitrile phase, quenched with air, and analyzed by calibrated GC.

The light on/off experiment indicated that no product **2** was formed during the off phases. Therefore, a constant photoirradiation of the reaction mixture is essential for the transformation to proceed. A radical propagation mechanism can therefore be excluded.

The decreased overall yield, however, is due to the biphasic nature of the reaction mixture. Thus, samples were only taken from the overlaying MeCN-phase, increasing the water content in the reaction mixture. As observed in the DoE, this may lead to lower yields.

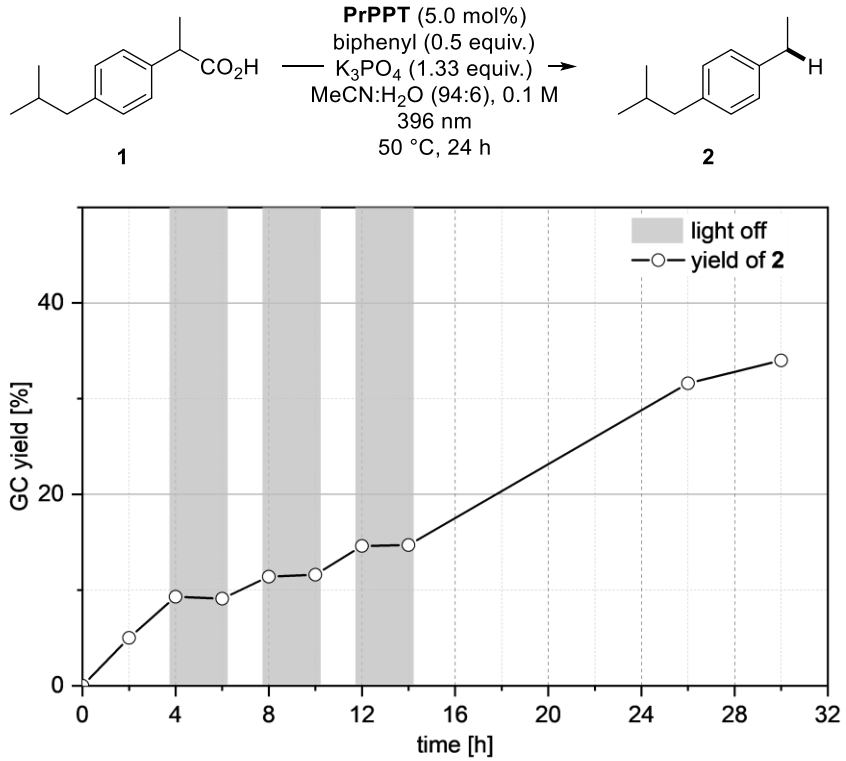

Figure 44. Conversion over time. Product formation calculated according to calibrated GC, using biphenyl as internal standard.

EPR spectroscopy

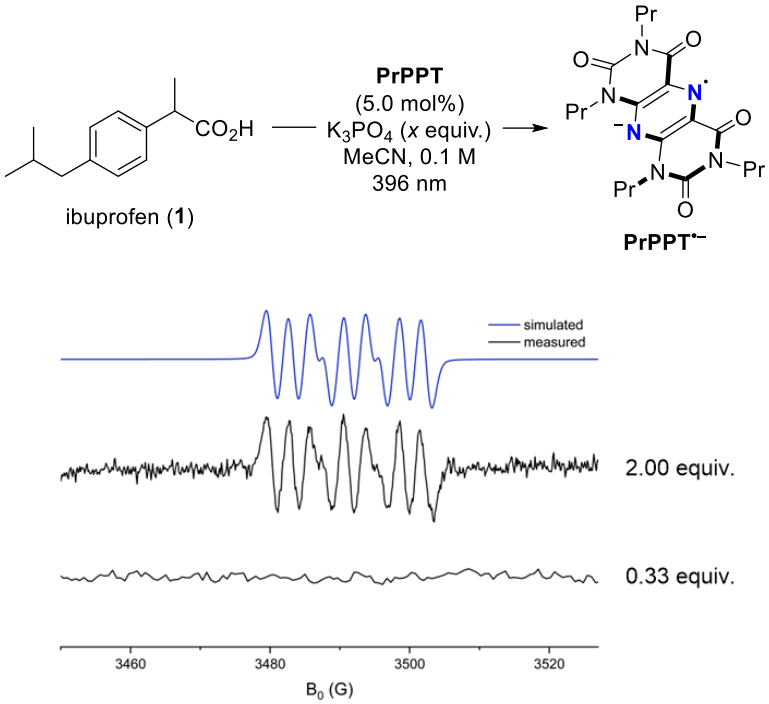

Figure 45. EPR spectrum of Ibuprofen (0.5 mmol), K_3PO_4 (2.00 equiv. or 0.33 equiv., respectively) and PrPPT (5.0 mol%, black line) in MeCN (5 ml); blue line is the simulated spectrum considering a hyperfine splitting from two non-equivalent nitrogen nuclei (g = 2.005; A_{N1} = 7.87 G, A_{N2} = 3.14 G).

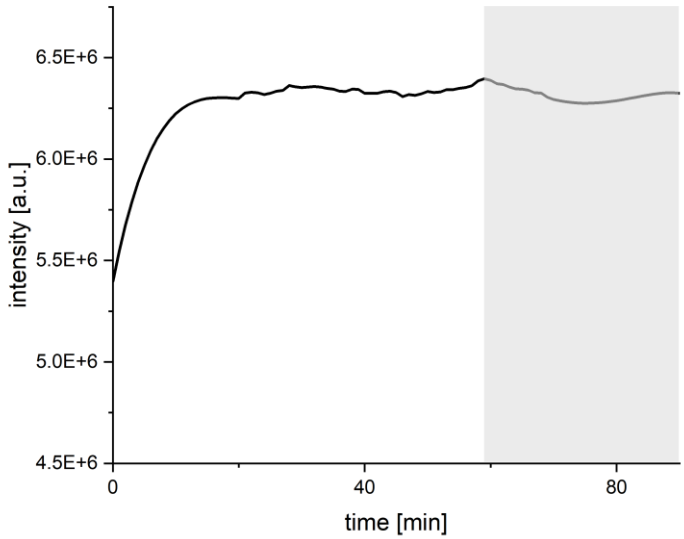

Figure 46. Intensity of the EPR signal of $PrPPT^{\bullet-}$ if the sample is irradiated or the irradiation is stopped (grey area).

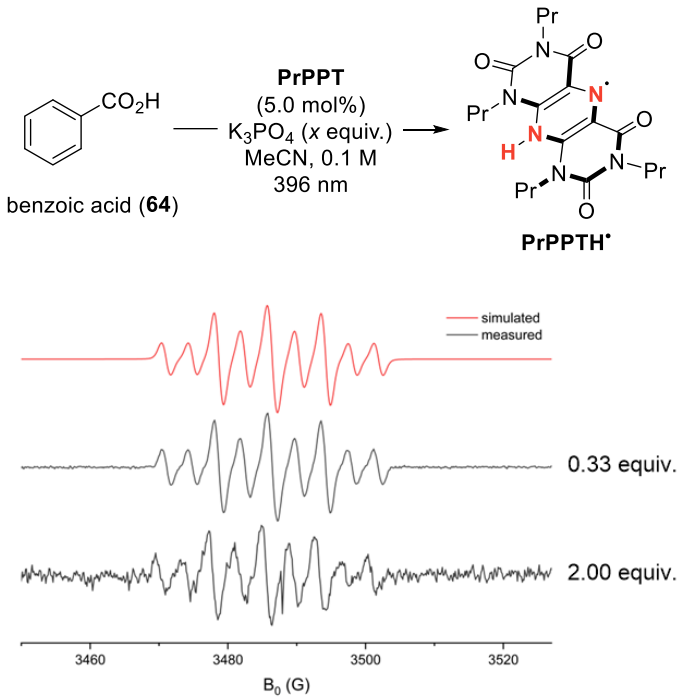

Figure 47. EPR spectrum of benzoic acid (**64**, 0.5 mmol), K_3PO_4 (0.33 equiv. or 2.00 equiv., respectively) and PrPPT (5.0 mol%, black line) in MeCN (5 ml); red line is the simulated spectrum considering a hyperfine splitting from two non-equivalent nitrogen nuclei and one hydrogen nucleus (g = 2.005; A_{N1} = 7.84 G, A_{N2} = 3.72 G and A_H= 7.45 G).

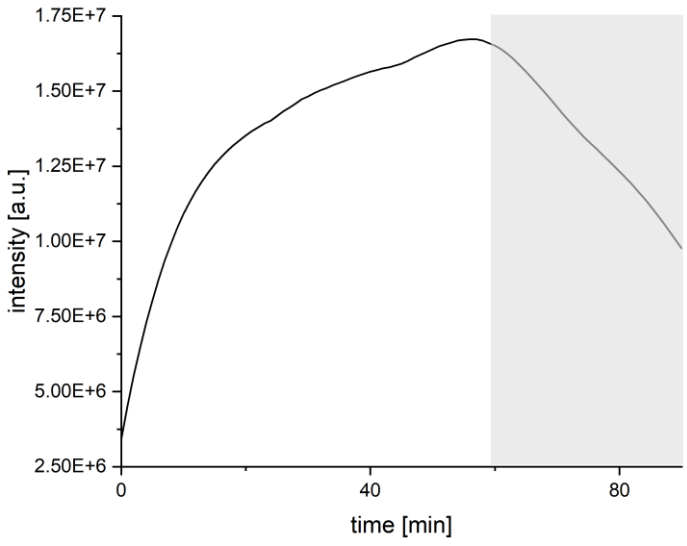

Figure 48. Intensity of the EPR signal of PrPPTH• if the sample is irradiated or the irradiation is stopped (grey area).

7.3.2 CO_2 Capture by (Poly)Amines Synthesized from Waste Nylon

Synthesis of *N*-hexylhexanamide (69)

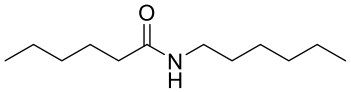

69

Hexylamine (2.6 ml, 20 mmol, 1.0 equiv.) and NEt_3 (3.4 ml, 24 mmol, 1.2 equiv.) were dissolved in dry THF (100 ml). The solution was added hexanoyl chloride (2.8 ml, 20 mmol, 1.0 equiv.) dropwise at 0 °C. The white suspension is stirred o/n at room temperature before it is quenched with water, extracted with DCM (3x) and dried over Na_2SO_4. After evaporation of the solvent, the product **69** is purified by column chromatography (*n*-pentane/EtOAc 2:1) to yield a colorless oil that slowly crystallized (4 g, 20 mmol, quant.).

R_f = 0.20 (*n*-pentane/EtOAc 1:3, $KMnO_4$).

^{1}H NMR (400 MHz, $CDCl_3$) δ 5.43 (s, 1H), 3.29 – 3.15 (m, 2H), 2.20 – 2.10 (m, 2H), 1.62 (dt, *J* = 15.0, 7.6 Hz, 2H), 1.48 (p, *J* = 8.0 Hz, 2H), 1.38 – 1.22 (m, 10H), 0.97 – 0.79 (m, 6H).

^{13}C NMR (75 MHz, $CDCl_3$) δ 173.3, 39.6, 37.0, 31.6, 29.7, 26.7, 25.7, 22.7, 22.5, 14.1, 14.1.

MS (EI): *m*/*z* (relative intensity) 199 (13), 170 (37), 157 (12), 156 (100), 143 (89), 129 (23), 128 (63), 116 (18), 114 (44), 99 (71), 86 (59), 73 (53), 55 (24).

HRMS (ESI-TOF, *m*/*z*): calcd. for $C_{12}H_{25}NO$ $[M + H]^+$ 200.2009, observed 200.2011; $[M + Na]^+$ 222.1828, observed 222.1832.

IR (ATR, neat, cm^{-1}): 3291 (m), 3087 (w), 2957 (s), 2924 (s), 2873 (m), 2857 (m), 1639 (s), 1552 (s), 1466 (w), 1435 (w), 1376 (w), 1327 (w), 1256 (w), 1223 (w), 1197 (w), 1158 (w), 962 (w), 724 (w).

This data is in agreement with literature.[304]

Synthesis of 1,1,1-tris(bromomethyl)ethane (77)

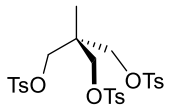

Tris(hydroxymethyl)ethane (1.2 g, 10 mmol, 1.0 equiv.) is dissolved in pyridine (20 ml) and slowly added tosyl chloride (8.75 g, 46 mmol, 4.6 equiv.) at 0 °C. The yellow suspension was stirred o/n at room temperature and quenched by slowly pouring it into a strongly stirred mixture of water (50 ml), conc. HCl (40 ml), and MeOH (100 ml). The white precipitate was filtered off, washed with MeOH (3x 5 ml) and water (2x 5 ml), and recrystallized from hot *n*-PrOH. The resulting needles were washed with cold MeOH (3x 5 ml) and dried to give tris(tosylmethyl)ethane (5.5 g, 9.5 mmol, 95%).

^{1}H NMR (400 MHz, $CDCl_3$) δ 7.71 (d, *J* = 8.3 Hz, 6H), 7.36 (d, *J* = 8.0 Hz, 6H), 3.76 (s, 6H), 2.47 (s, 9H), 0.89 (s, 3H).

This data is in agreement with literature.[305]

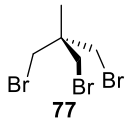

77

Next, tris(tosylmethyl)ethane (5.5 g, 9.5 mmol, 1.0 equiv.) was dissolved in diethylene glycol (30 ml) and added NaBr (9.8 g, 95 mmol, 10 equiv.). The solution was heated at 145 °C o/n. Then, the orange suspension was added water (30 ml) and extracted with DCM (6x 10 ml). The yellow solution was dried over Na_2SO_4, filtered off and concentrated before it was purified by column chromatography (*n*-pentane) to yield the product **77** as a colorless liquid (2.0 g, 6.4 mmol, 67%).

^{1}H NMR (400 MHz, $CDCl_3$) δ 3.50 (s, 6H), 1.29 (s, 3H).

This data is in agreement with literature.[306]

Synthesis of $(OMe)_2$-triphos (71)

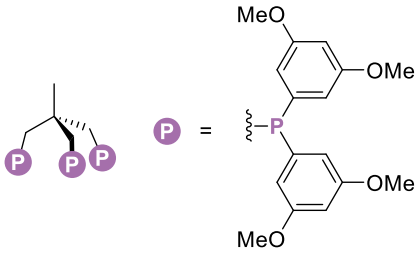

71

Compound **71** was prepared following general procedure B.

Diarylphosphine oxide (71-*a*):

The compound **71-*a*** was synthesized in 57% yield using *t*BuLi (6.0 equiv.) instead of Mg. The product was isolated by column chromatography (EtOAc to EtOAc/1% MeOH).

R_f = 0.24 (EtOAc, UV).

^{1}H NMR (300 MHz, $CDCl_3$) δ 7.93 (d, *J* = 485.1 Hz, 1H), 6.82 (dd, *J* = 15.1, 2.3 Hz, 4H), 6.60 (td, *J* = 2.3, 0.7 Hz, 2H), 3.79 (s, 12H).

^{13}C NMR (75 MHz, $CDCl_3$) δ 161.3 (d, *J* = 18.8 Hz), 133.2 (d, *J* = 101.1 Hz), 108.1 (d, *J* = 12.9 Hz), 105.0 (d, *J* = 2.3 Hz), 55.7.

^{31}P NMR (122 MHz, $CDCl_3$) δ 22.6.

This data is in agreement with literature.[307]

Diarylphosphine (71-*b*):

The compound **71-*b*** was synthesized in quantitative yield.

^{1}H NMR (300 MHz, CD_3CN) δ 6.66 (dd, *J* = 8.0, 2.3 Hz, 4H), 6.44 (t, *J* = 2.3 Hz, 2H), 5.14 (d, *J* = 220.6 Hz, 1H), 3.74 (s, 12H).

^{13}C NMR (75 MHz, CD_3CN) δ 162.0 (d, *J* = 8.7 Hz), 138.1, 112.3 (d, *J* = 18.1 Hz), 101.4, 56.1.

^{31}P(^{1}H) NMR (122 MHz, CD_3CN) δ -35.6.

$(OMe)_2$-triphos (71):

The compound **71** was isolated in 89% yield (51% over 3 steps).

^{1}H NMR (400 MHz, DMSO-d_6) δ 6.48 (dd, *J* = 7.9, 2.2 Hz, 12H), 6.42 (t, *J* = 2.2 Hz, 6H), 3.68 (s, 36H), 2.48 – 2.43 (m, 6H), 0.92 (s, 3H).

^{13}C NMR (101 MHz, DMSO-d_6) δ 160.2 (d, *J* = 9.7 Hz), 141.1, 110.2 (d, *J* = 21.7 Hz), 100.2, 55.1, 33.5, 21.8, 13.9.

^{31}P NMR (162 MHz, DMSO-d_6) δ -22.3.

Synthesis of (O*i*Pr)$_2$-triphos (72):

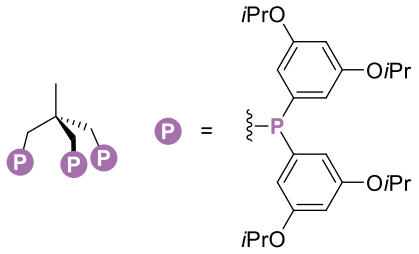

72

1-Bromo-3,5-di-*iso*-propoxybenzene was synthesized according to a literature procedure.[308] To a solution of 1-Bromo-3,5-dihydroxybenzene (756 mg, 4.0 mmol, 1.0 equiv.) in acetone (40 ml) were added K2CO3 (2.2 g, 16 mmol, 4.0 equiv.) and 2-bromopropane (1.5 ml, 16 mmol, 4.0 equiv.). The white suspension was refluxed o/n. After evaporation of the solvent, addition of water, and extraction with DCM (3x), the product was purified by column chromatography (*n*-pentane/EtOAc 10:1). The reaction yielded the mono-substituted product (339 mg, 37%) and di-substituted product (251 mg, 23%). Thus, the mono-substituted product was further converted using identical reagents in DMF (300 mg, 75%).

R$_f$ = 0.50 (*n*-pentane/EtOAc 10:1, UV).

^{1}H NMR (400 MHz, $CDCl_3$) δ 6.61 (d, *J* = 2.2 Hz, 2H), 6.34 (t, *J* = 2.2 Hz, 1H), 4.47 (hept, *J* = 6.1 Hz, 2H), 1.31 (d, *J* = 6.1 Hz, 12H).

^{13}C NMR (101 MHz, $CDCl_3$) δ 159.6, 122.9, 111.3, 102.9, 70.3, 22.0.

This data is in agreement with literature.[308]

Starting from the di-*iso*-propoxy-substituted aryl bromide, compound **72** was prepared following general procedure B.

Diarylphosphine oxide (72-*a*):

The compound **72-*a*** was synthesized in 62% yield after isolation by column chromatography (*n*-pentane/EtOAc 1:1 to 0:1).

R$_f$ = 0.40 (EtOAc, UV).

^{1}H NMR (400 MHz, $CDCl_3$) δ 7.88 (d, *J* = 483.0 Hz, 1H), 6.76 (dd, *J* = 15.2, 2.2 Hz, 4H), 6.56 (t, *J* = 2.1 Hz, 2H), 4.54 (hept, *J* = 6.1 Hz, 4H), 1.33 – 1.28 (m, 24H).

^{13}C NMR (101 MHz, $CDCl_3$) δ 159.6 (d, *J* = 18.9 Hz), 133.3 (d, *J* = 100.9 Hz), 109.7 (d, *J* = 12.8 Hz), 108.1 (d, *J* = 2.3 Hz), 70.4, 22.1 (d, *J* = 1.3 Hz).

^{31}P NMR (162 MHz, $CDCl_3$) δ 23.1 (dp, *J* = 483.2, 15.7 Hz).

Diarylphosphine (72-*b*):

The compound **72-*b*** was synthesized in 90% yield.

^{1}H NMR (400 MHz, Acetone-d_6) δ 6.61 (dd, *J* = 8.0, 2.2 Hz, 4H), 6.40 (t, *J* = 2.2 Hz, 2H), 5.11 (d, *J* = 217.3 Hz, 1H), 4.58 (hept, *J* = 6.0 Hz, 4H), 1.26 (d, *J* = 6.0 Hz, 24H).

^{13}C NMR (101 MHz, Acetone-d_6) δ 160.1 (d, *J* = 8.8 Hz), 138.6 – 136.0 (m), 113.8 (d, *J* = 18.0 Hz), 104.5, 70.3, 22.2.

^{31}P NMR (162 MHz, Acetone-d_6) δ -36.0 (dp, *J* = 217.4, 8.2 Hz, *P*–H), -37.4 (tp, *J* = 33.9, 7.9 Hz, *P*–D).

(O*i*Pr)$_2$-triphos (72):

The compound **72** was isolated in 83% yield (46% over 3 steps).

^{1}H NMR (400 MHz, Acetone-d_6) δ 6.58 (dd, *J* = 8.2, 2.2 Hz, 12H), 6.36 (t, *J* = 2.2 Hz, 6H), 4.53 (td, *J* = 11.7, 5.7 Hz, 12H), 1.24 (d, *J* = 5.9 Hz, 72H), 1.07 (s, 3H).

^{13}C NMR (101 MHz, Acetone-d_6) δ 159.9 (d, *J* = 9.6 Hz), 142.6 (d, *J* = 13.1 Hz), 129.4 (d, *J* = 72.4 Hz), 126.1, 112.7 (d, *J* = 21.2 Hz), 104.8, 70.3, 22.3, 22.2.

^{31}P NMR (162 MHz, Acetone-d_6) δ -20.9 (t, *J* = 8.7 Hz).

Synthesis of $(OMe)_2$F-triphos (73):

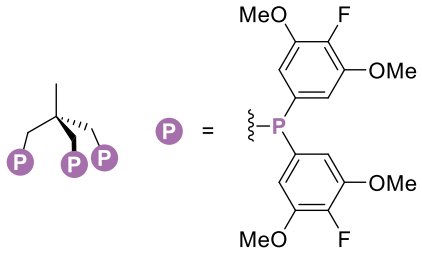

73

Compound **73** was prepared following general procedure B.

Diarylphosphine oxide (73-*a*):

The compound **73-*a*** was synthesized in 64% yield after isolation by column chromatography (EtOAc/MeOH 5%).

R_f = 0.15 (EtOAc, UV).

^{1}H NMR (400 MHz, $CDCl_3$) δ 7.98 (dd, *J* = 487.7, 1.7 Hz, 1H), 6.92 (ddd, *J* = 14.9, 6.9, 1.1 Hz, 4H), 3.90 (d, *J* = 1.2 Hz, 12H).

^{13}C NMR (101 MHz, $CDCl_3$) δ 149.3 (dd, *J* = 18.9, 8.6 Hz), 145.3 (dd, *J* = 253.0, 3.1 Hz), 125.8 (dd, *J* = 103.9, 5.1 Hz), 108.3 (dd, *J* = 13.6, 1.7 Hz), 56.9.

^{19}F NMR (376 MHz, $CDCl_3$) δ -149.6 (t, *J* = 7.1 Hz).

^{31}P NMR (162 MHz, $CDCl_3$) δ 21.5 (dp, *J* = 487.9, 15.1 Hz).

Diarylphosphine (73-*b*):

The compound **73-*b*** was synthesized in 84% yield. The eluent used was MeCN.

^{1}H NMR (400 MHz, Acetone-d_6) δ 6.98 – 6.86 (m, 4H), 5.25 (d, *J* = 219.1 Hz, 0.38H), 3.85 (s, 12H).

^{13}C NMR (101 MHz, Acetone-d_6) δ 149.4 (t, *J* = 8.6 Hz), 143.5 (d, *J* = 245.9 Hz), 130.6 (dd, *J* = 11.1, 5.7 Hz), 112.1 (d, *J* = 19.5 Hz), 56.8.

^{19}F NMR (376 MHz, Acetone-d_6) δ -158.5 (m).

^{31}P NMR (162 MHz, Acetone-d_6) δ -34.7 (dp, *J* = 219.2, 7.7 Hz, *P*–H), -36.1 (tp, *J* = 33.8, 7.5 Hz, *P*–D).

$(OMe)_2$F-triphos (73):

The compound **73** was isolated in 49% yield (26% over 3 steps).

^{1}H NMR (300 MHz, Toluene-d_8) δ 6.88 – 6.76 (m, 12H), 3.39 (s, 36H), 2.83 (d, *J* = 3.2 Hz, 6H), 1.40 (s, 3H).

^{13}C NMR (75 MHz, Toluene-d_8) δ 149.4, 145.7, 111.2 (d, *J* = 23.0 Hz), 56.2, 34.5, 22.8, 14.3.

^{19}F NMR (376 MHz, DMSO-d_6) δ -156.8 (t, *J* = 7.3 Hz).

$^{31}P(^{1}H)$ NMR (122 MHz, Toluene-d_8) δ -20.3.

Synthesis of $(OMe)_3$-triphos (74):

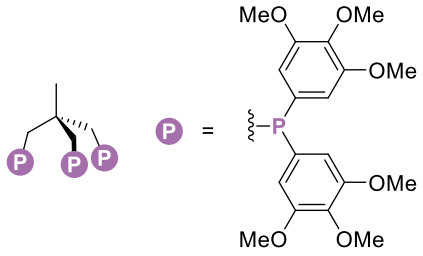

74

Compound **74** was prepared following general procedure B.

Diarylphosphine oxide (74-*a*):

The compound **74-*a*** was synthesized in 25% yield after isolation by column chromatography (*n*-pentane/EtOAc 1:4).

^{1}H NMR (400 MHz, $CDCl_3$) δ 7.92 (d, *J* = 484.6 Hz, 1H), 6.85 (d, *J* = 15.0 Hz, 4H), 3.82 (s, 6H), 3.80 (s, 12H).

^{13}C NMR (101 MHz, $CDCl_3$) δ 153.7 (d, *J* = 18.6 Hz), 141.6 (d, *J* = 2.7 Hz), 125.6 (d, *J* = 104.3 Hz), 107.5 (d, *J* = 13.5 Hz), 60.9, 56.3.

^{31}P NMR (162 MHz, $CDCl_3$) δ 22.5 (dp, *J* = 484.5, 15.0 Hz).

Diarylphosphine (74-*b*):

The compound **74-*b*** was synthesized in quantitative yield.

^{1}H NMR (400 MHz, MeOD-d_4) δ 6.79 (d, *J* = 7.8 Hz, 4H), 5.22 (d, *J* = 216.9 Hz, 1H), 3.80 (s, 12H), 3.76 (s, 6H).

^{13}C NMR (101 MHz, MeOD-d_4) δ 154.6 (d, *J* = 8.8 Hz), 139.8, 131.4, 112.1 (d, *J* = 19.2 Hz), 61.1, 56.7.

^{31}P NMR (162 MHz, MeOD-d_4) δ -35.2 (dp, *J* = 217.0, 7.8 Hz).

$(OMe)_3$-triphos (74):

The compound **74** was isolated in 23% yield (6% over 3 steps). Potassium *tert*-butoxide was exchanged for *n*-BuLi (3.6 equiv.).

^{1}H NMR (400 MHz, Toluene-d_8) δ 6.78 (d, *J* = 7.7 Hz, 12H), 3.79 (s, 18H), 3.37 (s, 36H), 1.55 (d, *J* = 4.2 Hz, 9H).

^{13}C NMR (101 MHz, Toluene-d_8) δ 154.3 (d, *J* = 9.0 Hz), 140.2, 135.4 (d, *J* = 13.6 Hz), 110.1 (d, *J* = 21.3 Hz), 60.3, 55.8, 14.3, 13.7, 13.6.

^{31}P NMR (162 MHz, Toluene-d_8) δ -21.8 (ddh, *J* = 11.9, 8.0, 4.1 Hz).

Synthesis of (*t*Bu)$_2$-triphos (75):

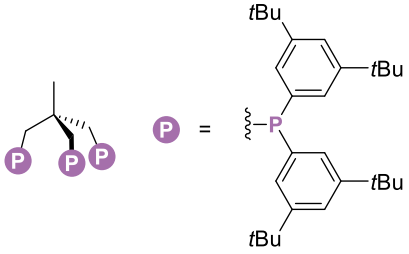

75

Compound **75** was prepared following general procedure B.

Diarylphosphine oxide (75-*a*):

The compound **75-*a*** was synthesized in 75% yield after isolation by column chromatography (*n*-heptane/EtOAc 4:1). Mg was exchanged for *t*BuLi (6.0 equiv.).

R$_f$ = 0.50 (EtOAc, UV).

^{1}H NMR (400 MHz, $CDCl_3$) δ 8.08 (d, *J* = 475.2 Hz, 1H), 7.54 (dd, *J* = 14.5, 1.9 Hz, 4H), 1.31 (s, 36H).

^{13}C NMR (101 MHz, $CDCl_3$) δ 151.6 (d, *J* = 12.5 Hz), 130.8 (d, *J* = 101.0 Hz), 126.7 (d, *J* = 2.9 Hz), 125.0 (d, *J* = 12.0 Hz), 35.2, 31.4.

^{31}P NMR (162 MHz, $CDCl_3$) δ 23.8 (dp, *J* = 475.3, 14.4 Hz).

This data is in agreement with literature.[309]

Diarylphosphine (75-*b*):

The compound **75-*b*** was synthesized in 97% yield. Et_2O was used as eluent.

^{1}H NMR (400 MHz, Acetone-d_6) δ 7.46 (t, *J* = 1.9 Hz, 2H), 7.37 (ddd, *J* = 8.1, 1.9, 1.0 Hz, 4H), 5.23 (d, *J* = 215.0 Hz, 0.55H), 1.29 (s, 36H).

^{13}C NMR (101 MHz, Acetone-d_6) δ 151.7 (d, *J* = 6.1 Hz), 134.8 (d, *J* = 9.3 Hz), 128.7 (d, *J* = 17.3 Hz), 123.3, 35.4, 31.7.

^{31}P NMR (162 MHz, Acetone-d_6) δ -39.6 (dp, *J* = 215.2, 8.0 Hz, *P*–H), -40.9 (tp, *J* = 33.4, 8.0 Hz, *P*–D).

(*t*Bu)$_2$-triphos (75):

The reaction yielded an undefined mixture of compounds that could not be purified further.

Synthesis of $(Me)_2$OMe-diphosphine (78):

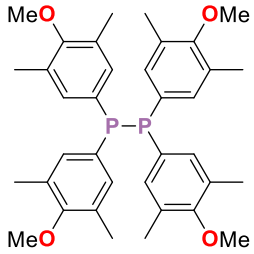

78

Compound **78** was prepared following general procedure B.

Diarylphosphine (78-*b*):

The compound **78-*b*** was synthesized in 40% yield.

^{1}H NMR (400 MHz, Acetone-d_6) δ 7.17 (dq, *J* = 7.5, 0.8 Hz, 4H), 5.03 (d, *J* = 216.5 Hz, 0.6H), 3.68 (s, 6H), 2.21 (s, 12H).

^{31}P NMR (162 MHz, Acetone-d_6) δ -42.1 (dp, *J* = 216.2, 7.3 Hz, *P*–H), -43.5 (tp, *J* = 33.7, 7.8 Hz, *P*–D).

This data is in agreement with literature.[310]

$(Me)_2$OMe-diphosphine (78):

Compound **78** was isolated by crystallization in 24% yield.

^{1}H NMR (400 MHz, THF-d_8) δ 6.97 (t, *J* = 2.9 Hz, 12H), 3.64 (s, 18H), 2.12 (s, 36H).

^{13}C NMR (101 MHz, THF-d_8) δ 158.7, 135.7 (t, *J* = 13.5 Hz), 131.8 – 131.5 (m), 131.1 (t, *J* = 3.7 Hz), 59.7, 16.1.

^{31}P NMR (162 MHz, THF-d_8) δ -17.4 (hept, *J* = 3.0 Hz).

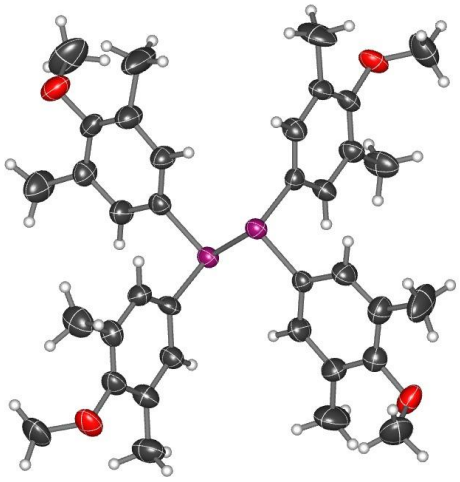

Table 39. Crystal data, data collection, and structure refinement for tetrakis(3,5-dimethyl-4-methoxyphenyl)diphosphine (**78**). A solvent mask was used to account for highly disordered co-crystallized toluene.

chemical formula	$C_{36}H_{44}O_4P_2$ ·3/4 PhMe
formula weight (g/mol)	602.69
crystal system, space group	triclinic, *P*1
T (K)	297
unit cell dimensions: *a, b, c* (Å)	*a* = 7.9890(4), *b* = 10.8924(5), *c* = 12.0959(4)
unit cell dimensions: *α, β, γ* (°)	*α* = 72.078(4), *β* = 87.979(3), *γ* = 82.764(4)
V (Å^3)	993.52(8)
Z	1
diffractometer, wavelength [Å]	Supernova, 0.71073
absorption coefficient *μ* (mm^{-1})	0.140
F (000)	322.0
crystal size (mm^3), crystal habit	0.50 · 0.50 · 0.30, colorless, clear block
transmission T_{min}, T_{max}	0.85737, 1.00000
reflections collected	21965
independent reflections	8653 [R_{int}=0.0317]
goodness-of-fit on F^2	1.077
final *R* indices [6711 data; *I* > 2σ(*I*)]	R_1 = 0.0676, ωR_2 = 0.1785
final *R* indices [all data]	R_1 = 0.0857, ωR_2 = 0.2067
no. of parameters	391
$\Delta\rho_{max}$, $\Delta\rho_{min}$ (e Å^{-3})	0.58, -0.34
R.M.S. deviation from mean (e Å^{-3})	0.079

Synthesis of complex [Ru(TMM)((OMe)$_2$-triphos)] (79):

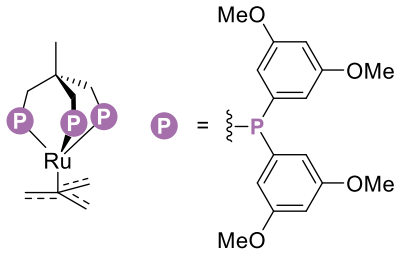

79

Compound **79** was synthesized according to a modified literature procedure.[151] In the glovebox, [Ru(COD)(TMM)$_2$] (16 mg, 0.05 mmol, 1.0 equiv.) and (OMe)$_2$-triphos (49 mg, 0.05 mmol, 1.0 equiv.) were weighed in a vial charged with a stir bar, and dry mesitylene (1 ml) was added. The vial was tightly closed, and the reaction mixture was stirred o/n at 110 °C. The dark brown solution turned into a greyish suspension that was transferred back to the glovebox and filtered through celite. The precipitate was further washed with dry mesitylene (1 ml) and dry pentane (3x 1 ml) before it was dried to give a yellow solid (33.5 mg, 0.029 mmol, 59%).

^{1}H NMR (400 MHz, THF-d_8) δ 6.36 – 6.28 (m, 12H), 6.18 (t, *J* = 2.1 Hz, 6H), 3.43 (s, 36H), 2.33 (s, 6H), 1.71 (s, 6H), 1.45 (s, 3H).

^{13}C NMR (101 MHz, THF-d_8) δ 160.8 (dd, *J* = 8.5, 4.0 Hz), 144.7, 110.3 (dd, *J* = 8.5, 4.7 Hz), 100.7, 64.3, 55.0, 34.9, 23.0, 14.2.

^{31}P NMR (162 MHz, THF-d_8) δ 37.7.

This data is in agreement with literature.[153]

Optimization of the reaction conditions

The screenings presented below (Table 40 to Table 47) were conducted following general procedure C.

Table 40. Screening of Ru precursors in THF. acac = acetylacetonate.

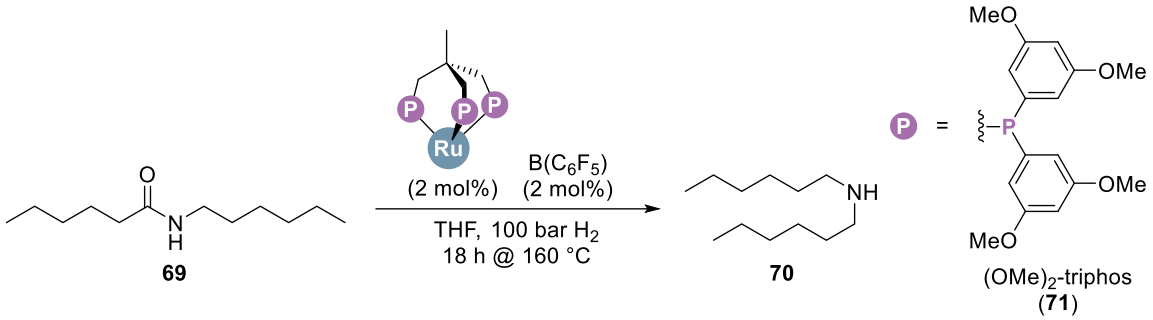

entry	metal precursor	comments	conversion[a]	yield Hex_2N[a]	yield of identified side products[a]	selectivity[b]
	$Ru(TMM)_2cod$	--	94%	61%	--	65%
	$Ru(TMM)_2cod$	--	19%	12%	--	63%
1	Ru(TMM)((OMe)$_2$-triphos) (**79**)	--	79%	54%	1%[c], 16%[d]	68%
2	$Ru(acac)_3$	--	15%	15%	--	100%
3	$Ru(acac)_3$	--	23%	15%	--	65%
4	$Ru(acac)_3$	without acid	--	--	--	--
5	$Ru(H)_2(PPh_3)_4$	--	29%	29%	--	100%
6	$Ru(H)_2(PPh_3)_4$	--	6%	6%	--	100%
7	$Ru(H)_2(PPh_3)_4$	without acid	--	--	--	--
8	$Ru(H)_2(PPh_3)_3(CO)$	--	--	--	--	--
9	$RuCl_2(PPh_3)_4$	--	--	--	--	--
10	$[RuCl_2(cod)]_n$	--	--	--	--	--
11	$[RuCl_2(p\text{-cymene})]_2$	--	--	--	--	--
12	Ru-MACHO	--	--	--	--	--
13	Ru-MACHO-BH	--	--	--	--	--

[a] GC yield using mesitylene as internal standard. [b] Calculated as the quotient of the yield (Hex_2N) and the conversion. [c] 1-HexOH was detected. [d] Hex_3N was detected.

Table 41. Solvent screening and variation of the water content. MS = molecular sieves.

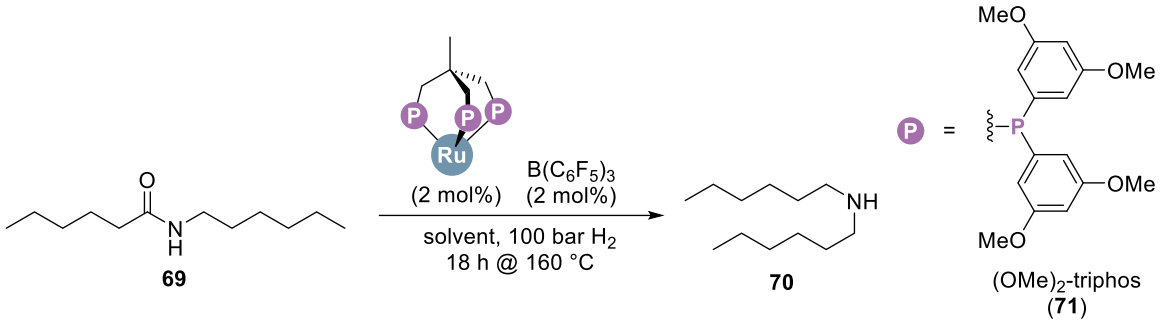

entry	metal precursor	solvent	conversion[a]	yield Hex_2N[a]	yield of identified side products[a]	selectivity[b]
	$Ru(TMM)_2cod$	THF	94%	61%	--	65%
	$Ru(TMM)_2cod$	THF	19%	12%	--	63%
1	$Ru(TMM)_2cod$	THF[c]	22%	19%	3%[d]	86%
2	$Ru(TMM)_2cod$	THF + MS	46%	42%	1%[d], 3%[e]	91%
3	$Ru(TMM)_2cod$	THF + MS	24%	24%	--	100%
4	$Ru(TMM)_2cod$	*n*-Bu_2O	5%	--	--	--
5	$Ru(TMM)_2cod$	DMSO	--	--	--	--
6	$Ru(TMM)_2cod$	*m*-cresol	--	--	--	--
7	$Ru(TMM)_2cod$	Bu-O_3-Bu	53%	40%	--	75%
8	$Ru(TMM)_2cod$	ethylene gylcol	8%	--	2%[f]	--

[a] GC yield using mesitylene as internal standard. [b] Calculated as the quotient of the yield (Hex_2N) and the conversion. [c] H2O (5.0 equiv.) was added. [d] 1-HexOH was detected. [e] Hex_3N was detected. [f] Hexanenitrile was detected.

Table 42. Ligand screening in THF. Experiments colored in red represent the standard reaction conditions.

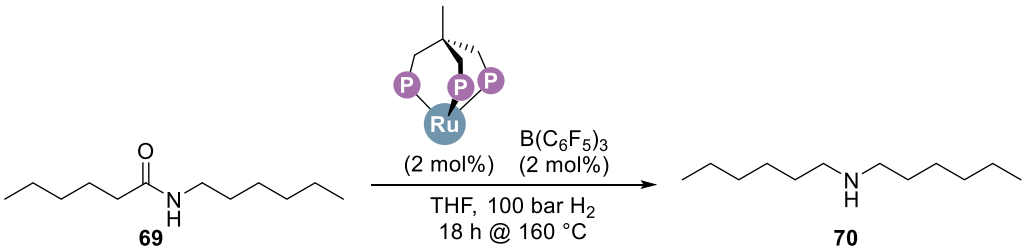

entry	metal precursor	ligand	conversion[a]	yield Hex_2N[a]	yield of identified side products[a]	selectivity[b]
	$Ru(TMM)_2cod$	$(OMe)_2$-triphos (**71**)	94%	61%	--	65%
	$Ru(TMM)_2cod$	$(OMe)_2$-triphos (**71**)	19%	12%	--	63%
1	$Ru(TMM)_2cod$	$(OiPr)_2$-triphos (**72**)	11%	8%	--	73%
2	$Ru(TMM)_2cod$	$(OMe)_3$-triphos (**74**)	--	--	--	--
3	$Ru(TMM)_2cod$	$(OMe)_2$F-triphos (**73**)	10%	10%	--	100%
4	$Ru(TMM)_2cod$	$(Me)_2$OMe-diphos (**78**)	--	--	--	--
5	$Ru(TMM)_2cod$	$(Me)_2$-triphos	68%	39%	--	57%
6	$Ru(TMM)_2cod$	Me-triphos	--	--	--	--
7	$Ru(TMM)_2cod$	CF_3-triphos	--	--	--	--
8	$Ru(TMM)_2cod$	triphos	--	--	--	--
9	$Ru(TMM)_2cod$	P(*n*-octyl)$_3$	--	--	--	--
10	$Ru(TMM)_2cod$	no ligand	--	--	--	--

[a] GC yield using mesitylene as internal standard. [b] Calculated as the quotient of the yield (Hex_2N) and the conversion.

Table 43. Acid screening in THF. Experiments colored in red represent the standard reaction conditions. pTSA = *para*-toluenesulfonic acid. MSA = methanesulfonic acid.

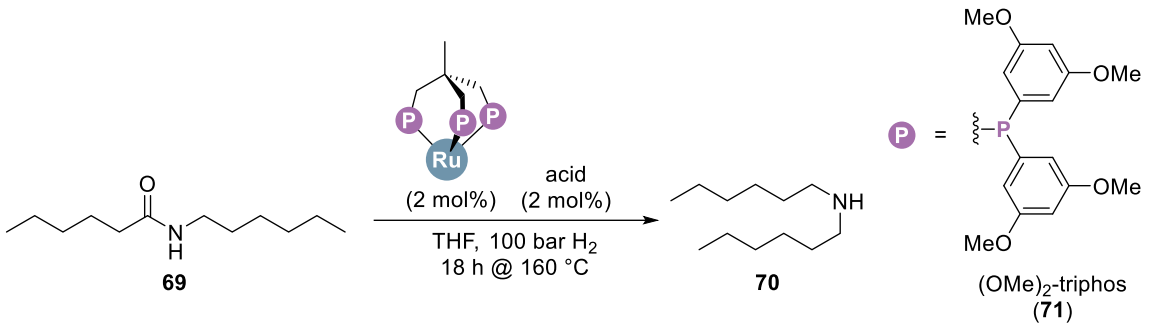

entry	metal precursor	acid	conversion[a]	yield Hex_2N[a]	yield of identified side products[a]	selectivity[b]
	$Ru(TMM)_2cod$	$B(C_6F_5)_3$	94%	61%	--	65%
	$Ru(TMM)_2cod$	$B(C_6F_5)_3$	19%	12%	--	63%
1	$Ru(TMM)_2cod$	$pTSA*H_2O$	83%	50%	--	59%
2	$Ru(TMM)_2cod$	MSA	--	--	--	--
3	$Ru(TMM)_2cod$	formic acid	22%	--	22%[c]	--
4	$Ru(TMM)_2cod$	$HNTf_2$	87%	54%	--	61%
5	$Ru(TMM)_2cod$	$Al(OTf)_3$	28%	21%	3%[c], 1%[d]	75%
6	$Ru(TMM)_2cod$	$Yb(OTf)_3$	64%	55%	--	88%
7	$Ru(TMM)_2cod$	$Hf(OTf)_4$	62%	45%	--	75%
8	$Ru(TMM)_2cod$	AgOTf	13%	12%	1%[c]	92%
9	$Ru(TMM)_2cod$	$ZnCl_2$	--	--	--	--
10	$Ru(TMM)_2cod$	TMSOTf	--	--	--	--

[a] GC yield using mesitylene as internal standard. [b] Calculated as the quotient of the yield (Hex_2N) and the conversion. [c] 1-HexOH was detected. [d] Hex_3N was detected.

Table 44. Metal screening after changing to HFIP as solvent.

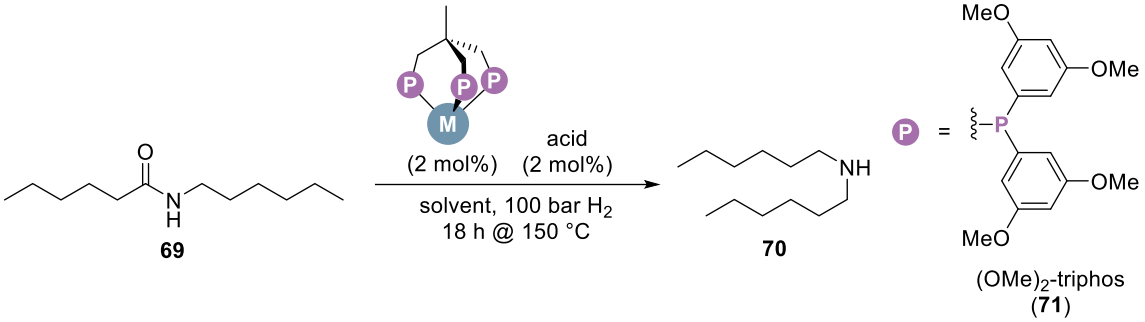

entry	metal precursor	acid	solvent	conversion[a]	yield Hex_2N[a]	yield Hex_3N[a]	selectivity[b]
1	$Ru(TMM)_2cod$	$B(C_6F_5)_3$	THF	66%	50%	10%	76%
2	$Ru(TMM)_2cod$	$B(C_6F_5)_3$	HFIP	86%	61%	17%	71%
3	$Ru(TMM)_2cod$	$B(C_6F_5)_3$	HFIP	100%	53%	15%	53%
4[c]	$Ru(TMM)_2cod$	$B(C_6F_5)_3$	HFIP	100%	61%	14%	61%
5[c,d]	$Ru(TMM)_2cod$	$B(C_6F_5)_3$	HFIP	26%	21%	6%	81%
6	$Co(NTf_2)_2$	$B(C_6F_5)_3$	HFIP	12%	--	--	--
7[c]	$Co(NTf_2)_2$	--	HFIP	24%	--	--	--
8	$Co(BF_4)_2(H_2O)_6$	$B(C_6F_5)_3$	HFIP	20%	--	--	--
9[c]	$Co(BF_4)_2(H_2O)_6$	--	HFIP	14%	--	--	--
10	$Co(acac)_3$	$B(C_6F_5)_3$	HFIP	15%	--	--	--

[a] GC yield using mesitylene as internal standard. [b] Calculated as the quotient of the yield (Hex_2N) and the conversion. [c] 60 bar. [d] 120 °C.

Table 45. Ligand screening in HFIP. Experiment colored in red represents the standard reaction conditions.

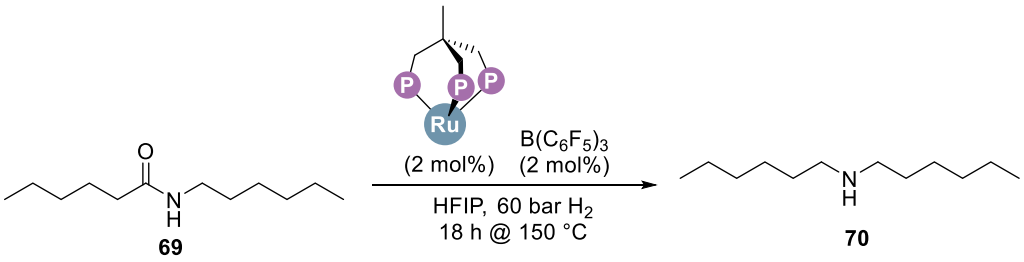

entry	metal precursor	ligand	conversion[a]	yield Hex_2N[a]	yield Hex_3N[a]	selectivity[b]
	$Ru(TMM)_2cod$	$(OMe)_2$-triphos (**71**)	100%	61%	14%	61%
1	$Ru(TMM)_2cod$	$(OiPr)_2$-triphos (**72**)	37%	18%	--	49%
2	$Ru(TMM)_2cod$	$(OMe)_3$-triphos (**74**)	20%	--	--	--
3	$Ru(TMM)_2cod$	$(OMe)_2$F-triphos (**73**)	39%	--	--	--
4	$Ru(TMM)_2cod$	$(Me)_2$-triphos	100%	40%	17 %	40%
5	$Ru(TMM)_2cod$	OMe-triphos	64%	21%	14 %	33%
6	$Ru(TMM)_2cod$	Me-triphos	51%	--	8 %	--
7	$Ru(TMM)_2cod$	triphos	32%	--	--	--

[a] GC yield using mesitylene as internal standard. [b] Calculated as the quotient of the yield (Hex_2N) and the conversion.

Table 46. Acid screening in HFIP. Experiment colored in red represents the standard reaction conditions. pTSA = *para*-toluenesulfonic acid. BA = phenylboronic acid.

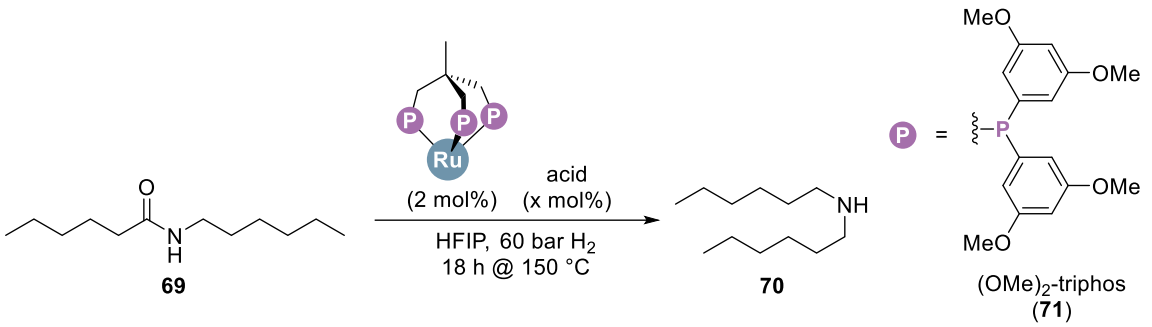

entry	metal precursor	acid	conversion[a]	yield Hex_2N[a]	yield Hex_3N[a]	selectivity[b]
	$Ru(TMM)_2cod$	$B(C_6F_5)_3$ (2 mol%)	100%	61%	14%	61%
1	$Ru(TMM)_2cod$	pTSA*H_2O (4 mol%)	40%	--	--	--
2	$Ru(TMM)_2cod$	F-BA (4 mol%)	71%	43%	14%	61%
3	$Ru(TMM)_2cod$	$B(OH)_3$ (5 mol%)	75%	55%	15%	73%
4	$Ru(TMM)_2cod$	BA (4 mol%)	89%	60%	17%	67%
4.2	$Ru(TMM)_2cod$	BA (2 mol%)	75%	55%	16%	73%
5	$Ru(TMM)_2cod$	CF_3-BA (3 mol%)	18%	--	6%	--
6	$Ru(TMM)_2cod$	F_5-BA (4 mol%)	94%	61%	15%	65%
7	$Ru(TMM)_2cod$	OMe-BA (4 mol%)	38%	24%	11%	63%

[a] GC yield using mesitylene as internal standard. [b] Calculated as the quotient of the yield (Hex_2N) and the conversion.

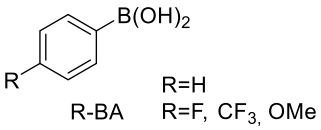

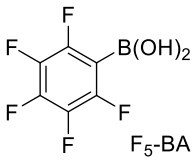

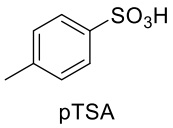

GC calibration

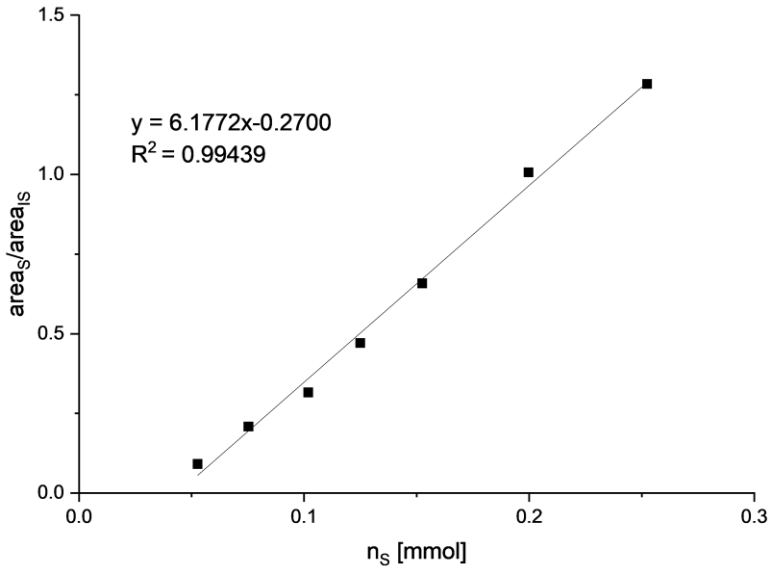

Figure 49. GC calibration graph for *N*-hexylhexanamide (**69**) as substrate (S) using 30 µl mesitylene as internal standard (IS).

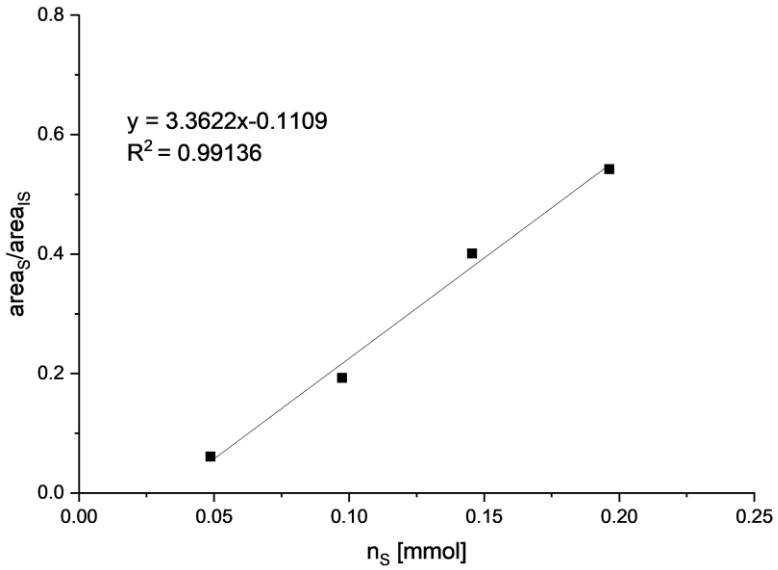

Figure 50. GC calibration graph for dihexylamine (**70**) as substrate (S) using 30 µl mesitylene as internal standard (IS).

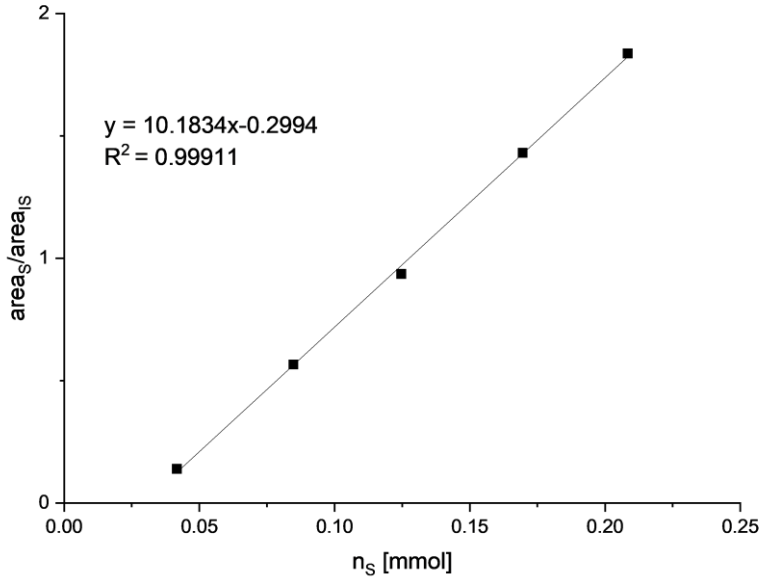

Figure 51. GC calibration graph for trihexylamine as substrate (S) using 30 µl mesitylene as internal standard (IS).

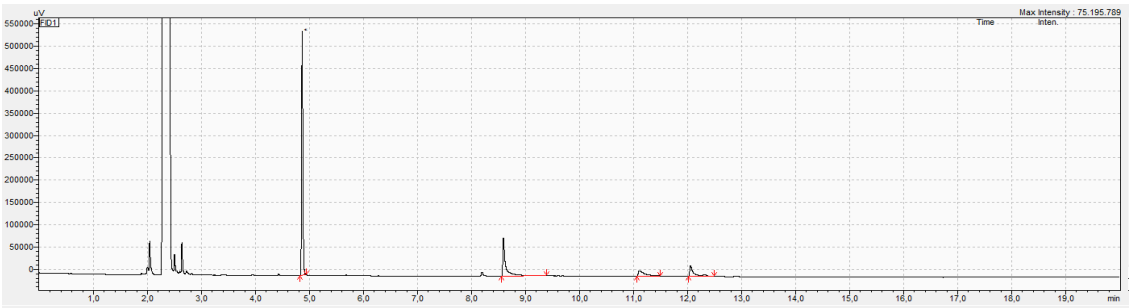

Figure 52. Exemplary gas chromatogram of mesitylene (IS, t_R = 4.86 min), dihexylamine (**70**, t_R = 8.58 min), *N*-hexylhexanamide (**69**, t_R = 11.12 min), and trihexylamine (t_R = 12.04 min) using a 20 min-method heating von 50 °C to 280 °C in 15 min.

Screening with nylon-6

Table 47. Screening of chaotropic additives.

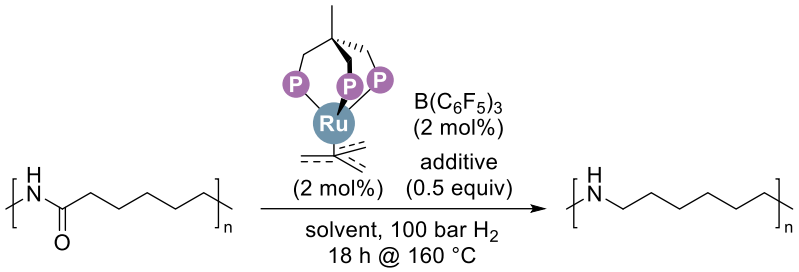

entry	chaotropic additive	solvent	IR
1	--	THF	C=O band
2	--	bu-O_3-bu	C=O band
3	LiCl	bu-O_3-bu	C=O band
4	$MgCl_2$	bu-O_3-bu	C=O band
5	SDS	bu-O_3-bu	C=O band
6	GHC	bu-O_3-bu	C=O band
7	urea	bu-O_3-bu	C=O band

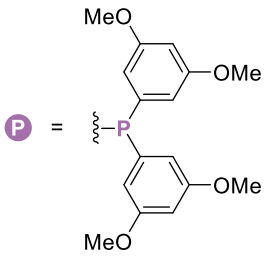

$(OMe)_2$-triphos (**71**)

IR spectra of nylon-6 and derivatives

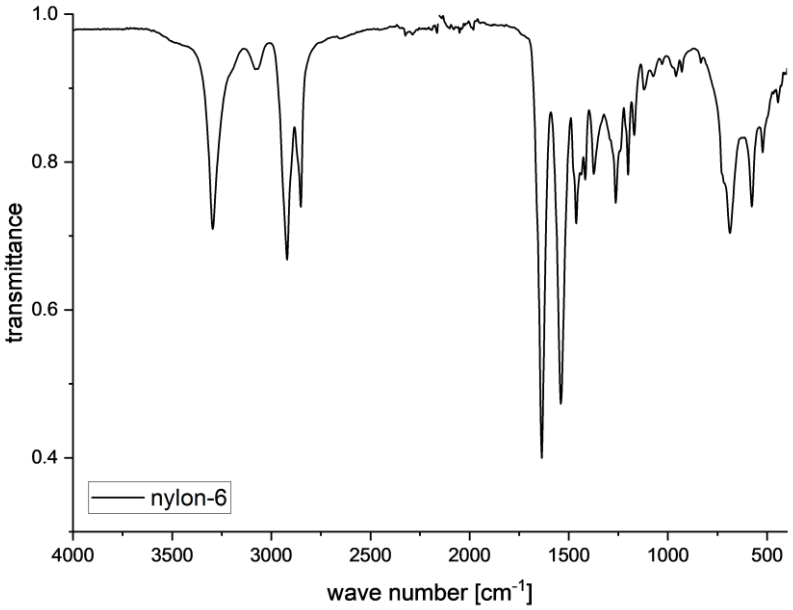

Figure 53. IR spectrum of PA6.

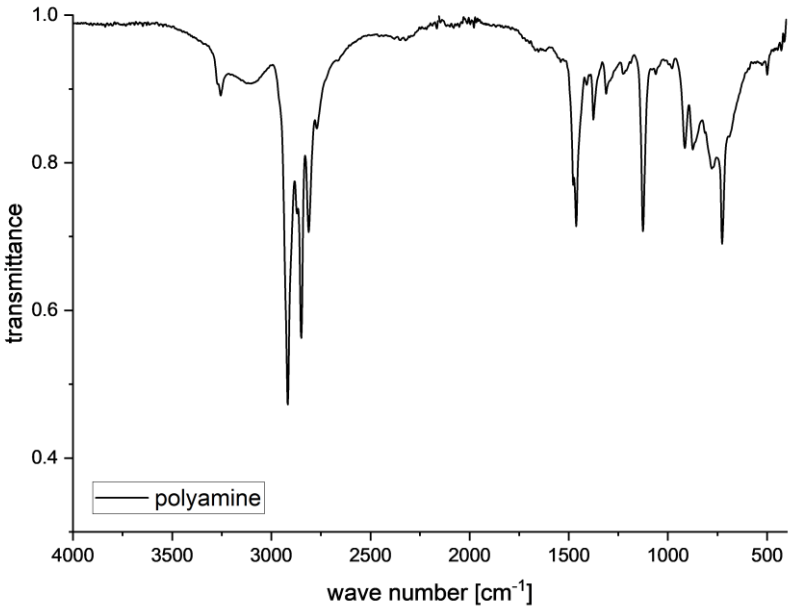

Figure 54. IR spectrum of the corresponding polyamine.

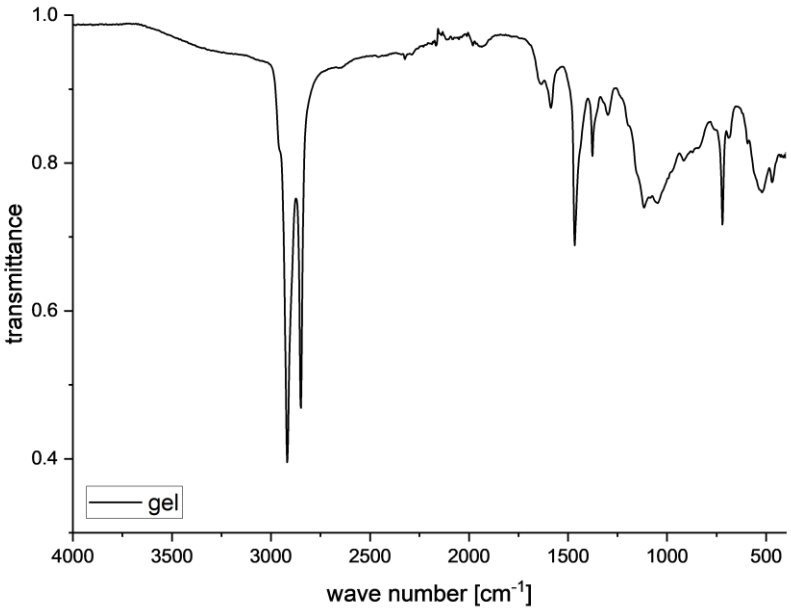

Figure 55. IR spectrum of the obtained gel after the hydrogenation reaction at 240 °C.

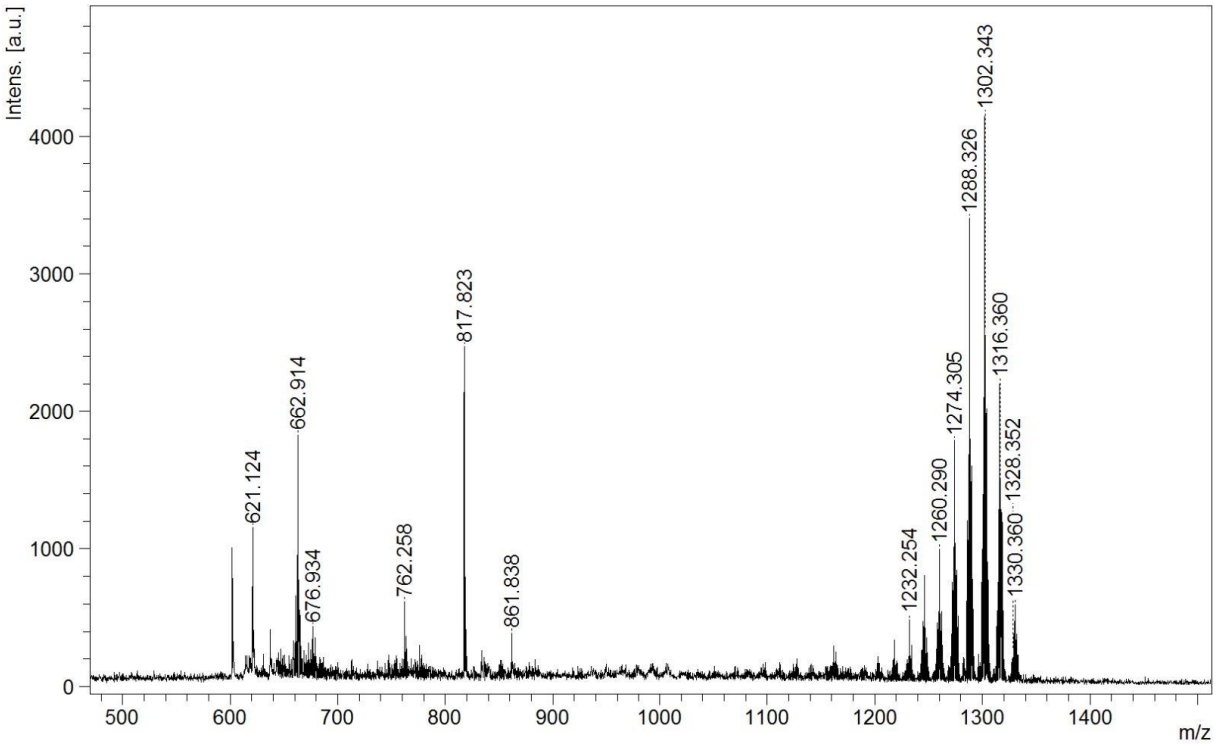

Figure 56. MALDI-TOF spectrum of the jelly-like solid using a HABA matrix.

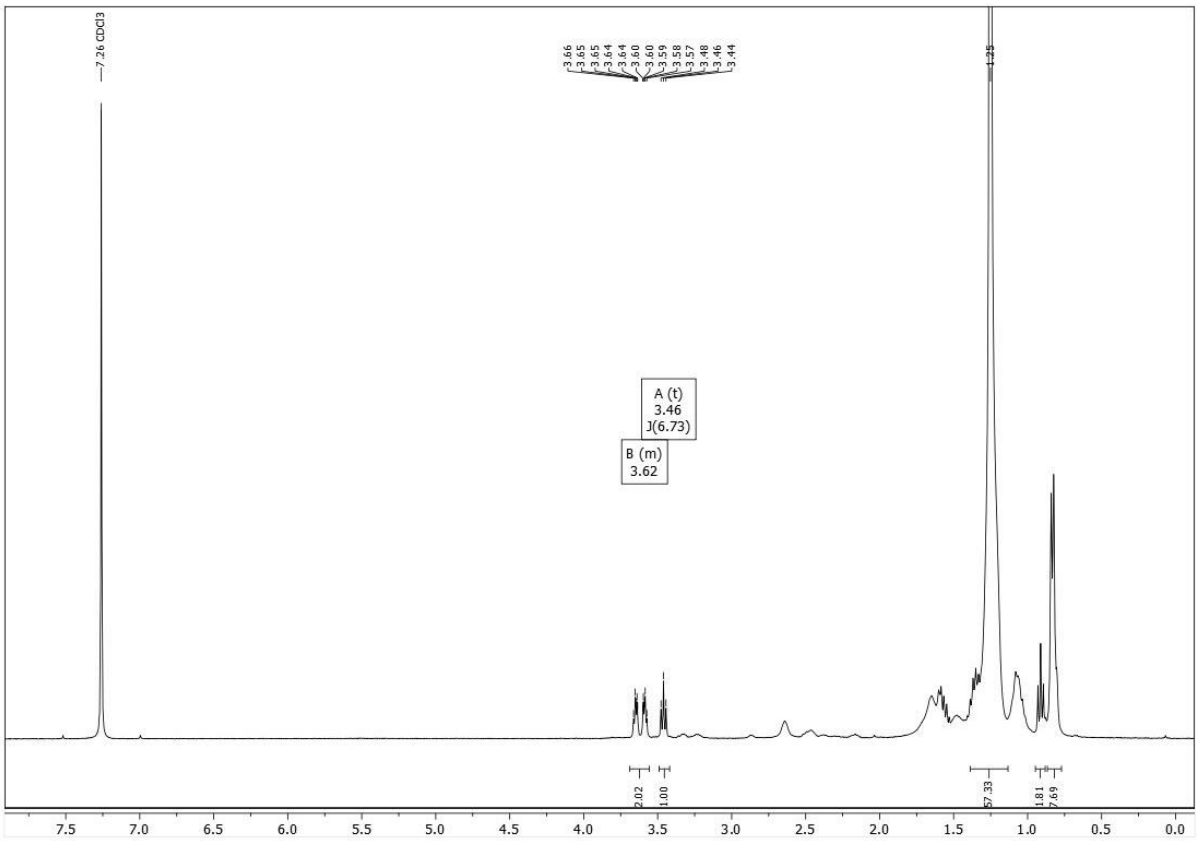

Figure 57. ^{1}H NMR spectrum of the gel obtained from the hydrogenation reaction at 240 °C.

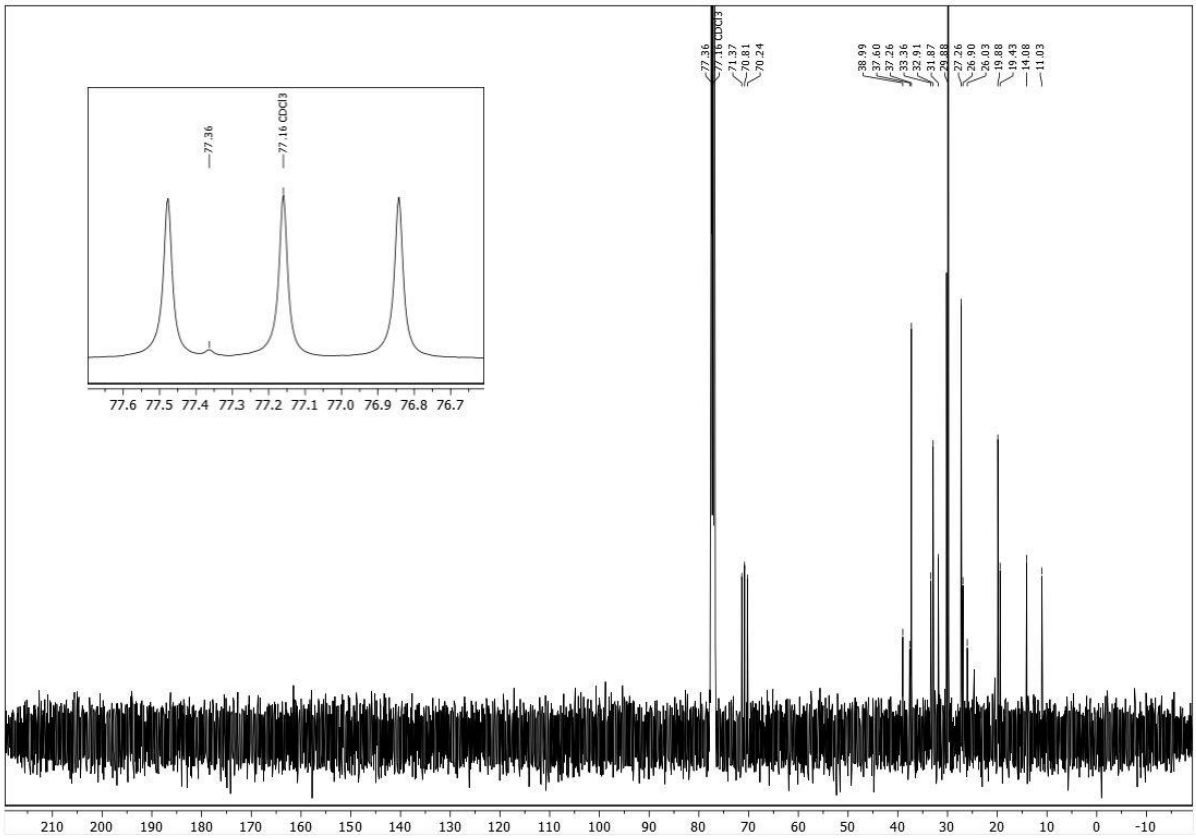

Figure 58. ^{13}C NMR spectrum of the gel obtained from the hydrogenation reaction at 240 °C.

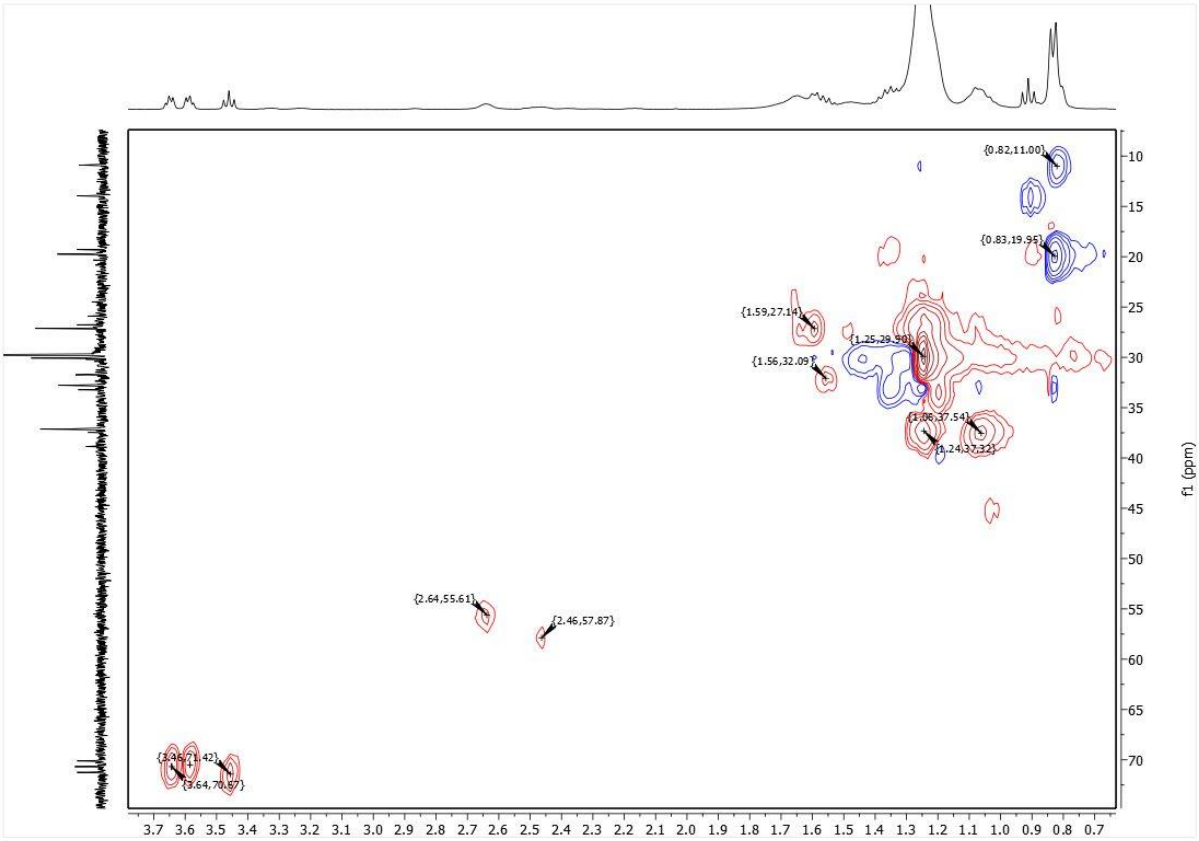

Figure 59. ^{1}H-^{13}C HSQC NMR spectrum of the gel obtained from the hydrogenation reaction at 240 °C.

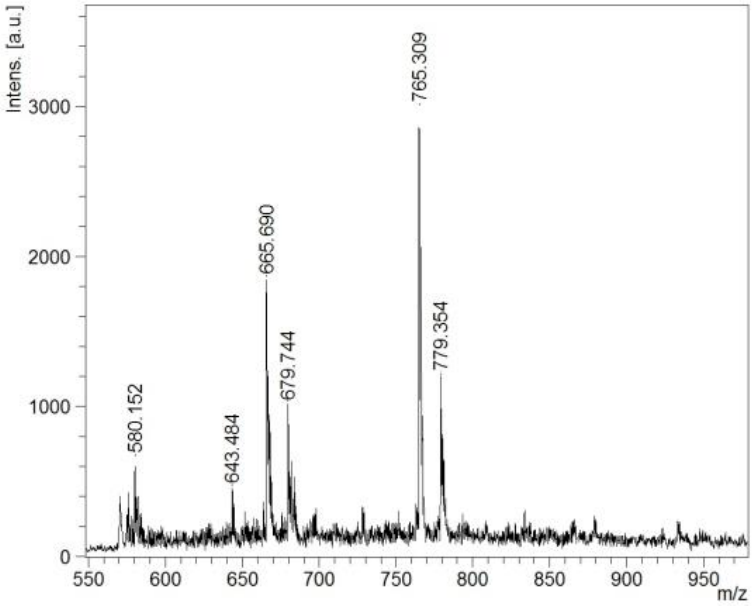

Figure 60. MALDI-TOF spectrum of the Bu-O_3-Bu solution after the hydrogenation reaction at 240 °C using a 2-(4-hydroxyphenylazo)benzoic acid (HABA) matrix. The MS was measured by Dr. Simon S. Pedersen.

7.3.3 CO_2 Conversion by Transition Metal Catalysis

7.3.3.1 Alkoxycarbonylation as a Model for the Dimerization of CO_2 *via* Metallacarboxylic Acids

Synthesis of dimethyl oxalate (87):

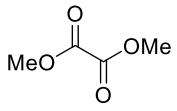

87

A solution of oxalic acid (450 mg, 5.0 mmol, 1.0 equiv.) in MeOH (10 ml) was treaded with concentrated sulfuric acid (0.16 ml, 3.0 mmol, 0.6 equiv.) and refluxed for one hour. The solution was cooled to room temperature and concentrated *in vacuo*. DCM was added and washed with saturated aqueous sodium bicarbonate solution followed by brine, then dried over Na_2SO_4. The solvent was evaporated to yield the title compound **87** in 63% yield (374 mg, 3.2 mmol) as colorless solid. The product was used to calibrate the GC by using tetradecane as internal standard.

m.p. 52-53 °C

^{1}H NMR (300 MHz, $CDCl_3$) δ 3.90 (s, 6H).

^{13}C NMR (75 MHz, $CDCl_3$) δ 158.1, 53.8.

MS (EI): *m*/*z* (relative intensity) 118 (4), 59 (100), 45 (24), 29 (13).

HRMS (ESI-TOF) was not possible due to the small size of the compound that already evaporated in the pre-vacuum.

IR (ATR, neat, cm^{-1}): 3025 (w), 2966 (w), 2859 (w), 1732 (s), 1438 (m), 1208 (s), 1156 (s), 924 (m), 779 (m), 523 (m).

This data is in agreement with literature.[311]

GC calibration:

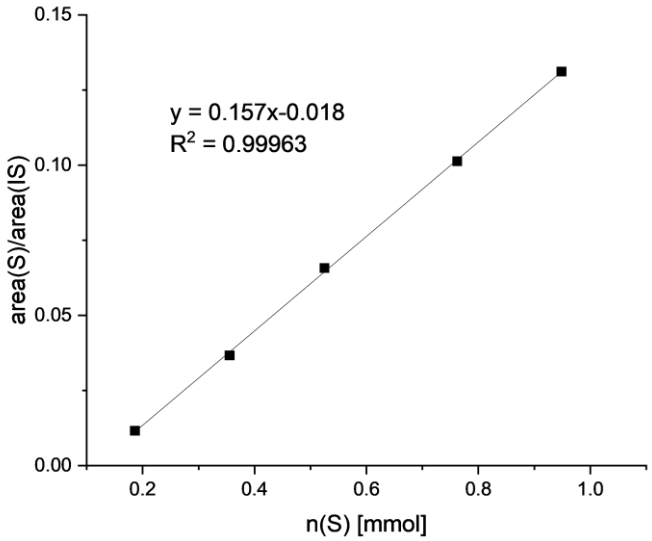

Figure 61. GC calibration graph for DMO (**87**) as substrate (S) using tetradecane as internal standard (IS).

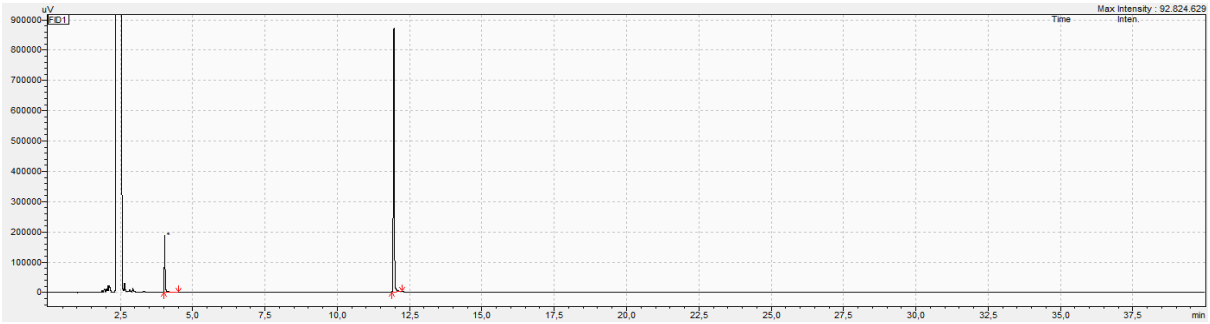

Figure 62. Exemplary gas chromatogram of dimethyl oxalate (**87**, t_R = 4.03 min) and tetradecane (IS, t_R = 11.96 min) using a 40 min-method heating von 50 °C to 280 °C with a heating rate of 10 °C/min.

Synthesis of Ph-phen (90):

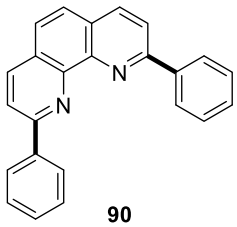

90

Compound **90** was prepared following general procedure D. Purification by column chromatography (DCM) yielded the title compound **90** in quantitative yield (662 mg, 1.99 mmol) as yellow solid.

R_f = 0.39 (DCM, UV).

^{1}H NMR (300 MHz, $CDCl_3$) δ 8.48 – 8.38 (m, 4H), 8.33 (d, *J* = 8.4 Hz, 2H), 8.14 (d, *J* = 8.4 Hz, 2H), 7.79 (s, 2H), 7.66 – 7.54 (m, 4H), 7.54 – 7.44 (m, 2H).

^{13}C NMR (75 MHz, $CDCl_3$) δ 156.9, 145.8, 139.4, 137.3, 129.7, 129.0, 128.1, 127.8, 126.2, 120.3.

MS (EI): *m*/*z* (relative intensity) 333 (24), 332 (100), 331 (58), 253 (8), 227 (4), 165 (5), 77 (9).

HRMS (EI, *m*/*z*): calcd. for $C_{24}H_{16}N_2$ $[M]^+$ 332.1308, observed 332.1300.

IR (ATR, neat, cm^{-1}): 3032 (w), 1605 (w), 1588 (w), 1574 (w), 1542 (w), 1504 (w), 1483 (m), 1417 (w), 1365 (w), 1313 (w), 1294 (w), 1275 (w), 1231 (w), 1184 (w), 1146 (w), 1106 (w), 1073 (w), 1023 (w), 919 (w), 906 (w), 883 (w), 841 (m), 807 (w), 758 (m), 732 (s), 685 (s), 635 (m), 614 (w), 571 (w), 547 (w), 494 (w), 467 (m), 433 (w).

This data is in agreement with literature.[312]

Synthesis of *n*Bu-phen (91):

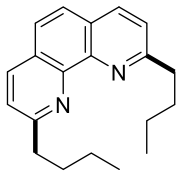

91

Compound **91** was prepared following general procedure D. Purification by column chromatography (DCM) yielded the title compound **91** in 69% yield (404 mg, 1.38 mmol) as yellow oil.

R_f = 0.09 (DCM, UV).

^{1}H NMR (300 MHz, $CDCl_3$) δ 8.13 (d, *J* = 8.3 Hz, 2H), 7.69 (s, 2H), 7.51 (d, *J* = 8.3 Hz, 2H), 3.30 – 3.14 (m, 4H), 1.97 – 1.81 (m, 4H), 1.61 – 1.42 (m, 4H), 0.99 (t, *J* = 7.3 Hz, 6H).

^{13}C NMR (75 MHz, $CDCl_3$) δ 163.3, 145.4, 136.3, 127.1, 125.5, 122.4, 39.3, 32.0, 23.0, 14.1.

MS (EI): *m*/*z* (relative intensity) 292 (4), 291 (7), 277 (25), 264 (17), 263 (60), 251 (60), 250 (100), 234 (17), 233 (21), 232 (10), 221 (37), 220 (36), 219 (23), 208 (57), 207 (59), 206 (31), 192 (24), 180 (11), 43 (19), 42 (14), 41 (39).

HRMS (ESI-TOF, *m*/*z*): calcd. for $C_{20}H_{23}N_2$ $[M + H]^+$ 293.2018, observed 293.2024.

IR (ATR, neat, cm^{-1}): 3040 (w), 2953 (m), 2925 (m), 2868 (m), 2856 (m), 1617 (w), 1609 (w), 1589 (m), 1545 (w), 1493 (s), 1464 (m), 1422 (w), 1400 (w), 1364 (m), 1297 (w), 1271 (w), 1194 (w), 1143 (w), 1113 (w), 1104 (w), 1080 (w), 969 (w), 932 (w), 881 (w), 851 (s), 742 (w), 700 (w), 633 (m), 599 (w), 497 (w), 421 (w), 409 (w).

This data is in agreement with literature.[312]

Synthesis of *s*Bu-phen (92):

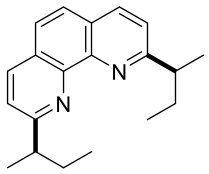

92

Compound **92** was prepared following general procedure D. Purification by column chromatography (DCM) yielded the title compound **92** in an average yield of 24% (#1: 150 mg, 0.51 mmol, 26%; #2: 129 mg, 0.44 mmol, 22%) as yellow oil.

R_f = 0.06 (DCM, UV).

^{1}H NMR (300 MHz, $CDCl_3$) δ 8.15 (d, *J* = 8.3 Hz, 2H), 7.69 (s, 2H), 7.50 (d, *J* = 8.4 Hz, 2H), 3.44 – 3.26 (m, 2H), 2.05 – 1.85 (m, 2H), 1.83 – 1.65 (m, 2H), 1.45 (d, *J* = 7.0 Hz, 6H), 0.98 (td, *J* = 7.4, 1.5 Hz, 6H).

^{13}C NMR (75 MHz, $CDCl_3$) δ 167.4, 167.4, 145.4, 136.5, 127.4, 125.6, 120.7, 44.3, 30.4, 30.2, 20.4, 20.3, 12.3.

MS (EI): *m*/*z* (relative intensity) 292 (6), 278 (10), 277 (50), 265 (20), 264 (100), 263 (49), 247 (23), 234 (12), 233 (36), 207 (9), 179 (6), 41 (4), 29 (20).

HRMS (EI, *m*/*z*): calcd. for $C_{20}H_{24}N_2$ $[M]^+$ 292.1934, observed 292.1925.

IR (ATR, neat, cm^{-1}): 3036 (w), 2960 (s), 2927 (m), 2872 (m), 1609 (w), 1591 (m), 1545 (w), 1494 (s), 1457 (m), 1421 (w), 1376 (m), 1349 (w), 1145 (w), 1116 (w), 1056 (w), 856 (m), 748 (w), 631 (w), 614 (w), 417 (w).

This data is in agreement with literature.[312]

Synthesis of *t*Bu-phen (93)

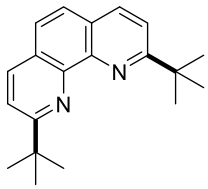

93

Compound **93** was prepared following general procedure D. Purification by column chromatography (DCM) yielded the title compound **93** in an average yield of 31% (#1: 191 mg, 0.65 mmol, 33%; #2: 483 mg, 1.65 mmol, 28%) as bright yellow solid.

m.p. 151 – 152 °C

R_f = 0.14 (DCM, UV).

^{1}H NMR (300 MHz, $CDCl_3$) δ 8.13 (d, *J* = 8.5 Hz, 2H), 7.72 (s, 1H), 7.70 (s, 3H), 1.61 (s, 18H).

^{13}C NMR (75 MHz, $CDCl_3$) δ 169.3, 144.9, 136.0, 127.0, 125.5, 119.7, 38.8, 30.4.

MS (EI): *m*/*z* (relative intensity) 292 (36), 291 (35), 277 (100), 261 (25), 247 (11), 236 (12), 221 (17), 219 (11), 57 (4), 41(7).

HRMS (EI, *m*/*z*): calcd. for $C_{20}H_{23}N_2$ $[M\text{-}H]^+$ 291.1856, observed 291.1856; calcd. for $C_{20}H_{24}N_2$ $[M]^+$ 292.1934, observed 292.1927.

IR (ATR, neat, cm^{-1}): 2957 (m), 2925 (w), 2864 (w), 1609 (w), 1589 (m), 1542 (w), 1504 (w), 1491 (s), 1477 (w), 1455 (w), 1420 (w), 1392 (w), 1365 (m), 1280 (w), 1157 (w), 1146 (w), 1131 (s), 1103 (w), 1022 (w), 917 (w), 885 (w), 856 (s), 845 (m), 749 (m), 736 (w), 703 (w), 632 (m), 616 (m), 512 (w), 427 (w).

This data is in agreement with literature.[313]

Synthesis of Ph-bipy (94):

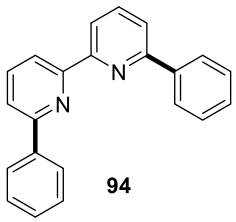

94

Compound **94** was prepared following general procedure D. Purification by column chromatography (*n*-pentane/DCM 1:1) yielded the title compound **94** in 19% yield (120 mg, 0.39 mmol) as bright yellow solid.

R_f = 0.56 (*n*-pentane/DCM 1:1, UV).

^{1}H NMR (300 MHz, $CDCl_3$) δ 8.68 – 8.59 (m, 2H), 8.22 – 8.12 (m, 4H), 7.95 (td, *J* = 7.8, 1.1 Hz, 2H), 7.81 (ddd, *J* = 7.8, 1.1, 0.4 Hz, 2H), 7.59 – 7.39 (m, 6H).

^{13}C NMR (75 MHz, $CDCl_3$) δ 156.5, 138.4, 129.5, 128.9, 127.3, 121.1, 120.5.

MS (EI): *m*/*z* (relative intensity) 309 (23), 308 (100), 307 (35), 204 (8), 154 (11), 127 (5).

HRMS (ESI-TOF, *m*/*z*): calcd. for $C_{22}H_{16}N_2$ $[M + H]^+$ 309.1392, observed 309.1383.

IR (ATR, neat, cm^{-1}): 3057 (w), 3034 (w), 2922 (w), 2852 (w), 1723 (w), 1561 (m), 1494 (w), 1451 (w), 1431 (s), 1374 (w), 1311 (w), 1284 (w), 1257 (w), 1181 (w), 1150 (w), 1107 (w), 1084 (m), 1069 (w), 1044 (w), 1020 (w), 1001 (w), 987 (w), 919 (w), 904 (w), 806 (m), 755 (s), 736 (s), 687 (s), 636 (m), 625 (m), 614 (m), 584 (m), 547 (w), 453 (w), 434 (w).

This data is in agreement with literature.[314]

Synthesis of *n*Bu-bipy (95):

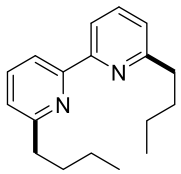

95

Compound **95** was prepared following general procedure D. Purification by column chromatography (DCM) yielded the title compound **95** in 39% yield (210 mg, 0.78 mmol) as yellow oil.

R_f = 0.16 (*n*-pentane/DCM 1:1, UV).

^{1}H NMR (300 MHz, $CDCl_3$) δ 8.24 (dd, *J* = 7.8, 1.0 Hz, 2H), 7.69 (t, *J* = 7.7 Hz, 2H), 7.13 (dd, *J* = 7.6, 1.1 Hz, 2H), 2.90 – 2.82 (m, 4H), 1.85 – 1.72 (m, 4H), 1.51 – 1.36 (m, 4H), 0.96 (t, *J* = 7.3 Hz, 6H).

^{13}C NMR (75 MHz, $CDCl_3$) δ 161.9, 156.1, 137.1, 129.2, 128.8, 122.6, 118.5, 38.3, 32.1, 22.6, 14.2.

MS (EI): *m*/*z* (relative intensity) 268 (3), 267 (4), 253 (16), 239 (26), 227 (16), 226 (100), 197 (35), 183 (8).

HRMS (ESI-TOF, *m*/*z*): calcd. for $C_{18}H_{24}N_2$ $[M + H]^+$ 269.2018, observed 269.2022.

IR (ATR, neat, cm^{-1}): 3060 (w), 2955 (m), 2928 (m), 2871 (w), 2858 (w), 1679 (w), 1572 (s), 1495 (w), 1437 (s), 1395 (w), 1378 (w), 1341 (w), 1286 (w), 1260 (w), 1228 (w), 1197 (w), 1150 (w), 1120 (w), 1103 (w), 1084 (m), 1030 (w), 991 (w), 933 (w), 900 (w), 779 (s), 748 (m), 700 (w), 635 (m), 615 (w), 591 (w), 559 (w), 460 (w), 420 (w).

This data is in agreement with literature.[315]

Synthesis of *s*Bu-bipy (96):

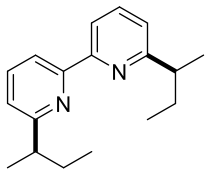

96

Compound **96** was prepared following general procedure D. Purification by column chromatography (*n*-pentane/DCM 1:1) yielded the title compound **96** in 15% yield (#1: 80 mg, 0.30 mmol) as yellow liquid.

R_f = 0.46 (DCM, UV).

^{1}H NMR (300 MHz, $CDCl_3$) δ 8.29 (dd, *J* = 7.8, 1.0 Hz, 2H), 7.70 (t, *J* = 7.7 Hz, 2H), 7.11 (dd, *J* = 7.7, 1.1 Hz, 2H), 2.85 (p, *J* = 7.0 Hz, 2H), 1.95 – 1.75 (m, 2H), 1.77 – 1.57 (m, 2H), 1.33 (d, *J* = 6.9 Hz, 6H), 0.88 (t, *J* = 7.4 Hz, 6H).

^{13}C NMR (75 MHz, $CDCl_3$) δ 165.7, 137.0, 129.2, 128.7, 121.5, 118.5, 43.8, 30.1, 20.6, 12.3.

MS (EI): *m*/*z* (relative intensity) 268 (8), 254 (11), 253 (62), 240 (100), 239 (48), 223 (18), 209 (22).

HRMS (ESI-TOF, *m*/*z*): calcd. for $C_{18}H_{24}N_2$ $[M + H]^+$ 269.2018, observed 269.2018.

IR (ATR, neat, cm^{-1}): 3059 (w), 2960 (m), 2929 (m), 2873 (w), 1682 (w), 1632 (w), 1571 (s), 1494 (w), 1458 (m), 1434 (s), 1399 (w), 1377 (w), 1265 (w), 1207 (w), 1151 (w), 1118 (w), 1082 (m), 1017 (w), 1003 (w), 991 (w), 960 (w), 908 (w), 880 (w), 801 (s), 750 (s), 700 (w), 634 (m), 559 (w), 517 (w), 460 (w), 424 (w).

Synthesis of (bipy)Pd(OAc)$_2$ (98):

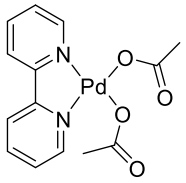

98

A solution of 2,2'-bipyridine (79 mg, 0.5 mmol, 1.0 equiv.) in DCM (2 ml) was added to a solution of Pd(OAc)$_2$ (115 mg, 0.5 mmol, 1.0 equiv.) in toluene (10 ml). The yellow suspension was stirred for 3 h at room temperature and then added *n*-pentane to fully precipitate the complex. The product was filtrated off, dried, and then recrystallized from DCM/*n*-pentane to yield the title compound **98** in 69% yield (132 mg, 0.35 mmol) as fine yellow needles.

m.p. 180 °C (decomposition).

^{1}H NMR (300 MHz, $CDCl_3$) δ 8.21 – 7.99 (m, 6H), 7.44 (ddd, *J* = 7.4, 5.6, 1.4 Hz, 2H), 2.05 (s, 6H).

^{13}C NMR (75 MHz, $CDCl_3$) δ 179.4, 155.6, 149.9, 140.7, 126.8, 122.9, 23.1.

MS (EI): *m*/*z* (relative intensity) was not possible for this compound.

HRMS (ESI-TOF, *m*/*z*): calcd. for $C_{12}H_{12}N_2O_3Pd$ $[M - OAc + OH]^+$ 337.9978, observed 337.9679.

IR (ATR, neat, cm^{-1}): 3389 (w), 3114 (w), 3081 (w), 2927 (w), 1626 (w), 1598 (w), 1498 (w), 1468 (w), 1448 (m), 1428 (m), 1400 (m), 1367 (s), 1314 (s), 1266 (m), 1252 (m), 1176 (w), 1163 (w), 1126 (w), 1111 (w), 1071 (w), 1061 (w), 1041 (w), 1024 (m), 925 (w), 900 (w), 823 (w), 806 (w), 767 (s), 742 (w), 722 (m), 691 (s), 652 (m), 618 (m), 567 (m), 549 (m), 483 (m), 448 (m), 416 (s).

Synthesis of (phen)Pd(OAc)$_2$ (99):

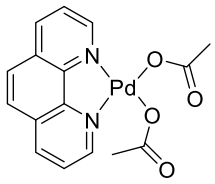

99

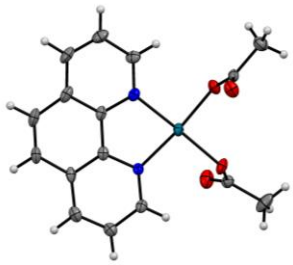

A solution of 1,10-phenanthroline (92 mg, 0.5 mmol, 1.0 equiv.) in DCM (2 ml) was added to a solution of Pd(OAc)$_2$ (115 mg, 0.5 mmol, 1.0 equiv.) in toluene (10 ml). The yellow suspension was stirred for 3 h at room temperature and then added *n*-pentane to fully precipitate the complex. The product was filtrated off, dried, and then recrystallized from DCM/*n*-pentane to yield the title compound **99** in 74% yield (150 mg, 0.37 mmol) as square yellow blocks suitable for X-ray crystallography.

^{1}H NMR (300 MHz, MeOD-d_4) δ 8.80 (d, *J* = 8.3 Hz, 2H), 8.42 (s, 2H), 8.08 (s, 2H), 8.02 – 7.86 (m, 2H), 2.15 (s, 6H).

^{13}C NMR (75 MHz, $CDCl_3$) δ 179.7, 150.1, 146.6, 139.2, 130.0, 127.3, 125.4, 23.0.

MS (EI): *m*/*z* (relative intensity) 181 (12), 180 (100), 179 (32), 154 (14), 90 (8), 76 (9), 60 (11), 45 (13), 43 (17). The complex decomposed upon ionization and the free ligand was detected.

HRMS (ESI-TOF, *m*/*z*): calcd. for $C_{14}H_{12}N_2O_3Pd$ $[M - OAc + OH]^+$ 361.9979, observed 361.9679.

IR (ATR, neat, cm^{-1}): 3086 (w), 3061 (w), 2920 (w), 1616 (w), 1597 (w), 1515 (w), 1493 (w), 1427 (m), 1406 (w), 1360 (s), 1308 (s), 1226 (m), 1207 (w), 1156 (w), 1110 (w), 1095 (w), 1044 (w), 1012 (w), 963 (w), 920 (w), 881 (w), 848 (s), 803 (w), 779 (w), 748 (w), 726 (w), 714 (s), 686 (s), 657 (w), 618 (m), 564 (w), 550 (w), 522 (w), 511 (w), 502 (w), 439 (m), 422 (w).

This data is in agreement with literature.[266]

Optimization of the reaction conditions

The screenings presented below (Table 48 to Table 51) were conducted following general procedure E.

Table 48. Stoichiometric ligand screening.

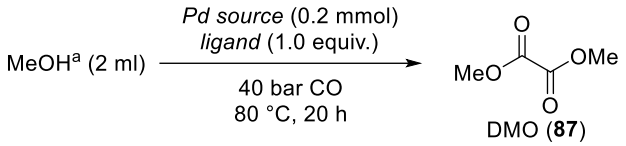

DMO (**87**)

entry	Pd source	ligand	yield[b]	2nd yield[b]
1	(bipy)Pd(OAc)$_2$ (**98**)	--	--[c]	
2	(phen)Pd(OAc)$_2$ (**99**)	--	--[c]	
3	Pd(OAc)$_2$	bipy (**89**)	--[c]	20%
4	Pd(OAc)$_2$	phen (**88**)	--[c]	28%
5	Pd(OAc)$_2$	*t*Bu-phen (**93**)	110%	61%
6	Pd(OAc)$_2$	*n*Bu-phen (**91**)	85%	45%
7	Pd(OAc)$_2$	*s*Bu-phen (**92**)	67%	61%
8	Pd(OAc)$_2$	Ph-phen (**90**)	66%	28%[d]

[a] Anhydrous MeOH from the SPS was used. [b] GC yield using tetradecane as internal standard. [c] MeOH from an AcroSeal bottle was used. [d] PVP was added as nanoparticle dispersant.

Table 49. Screening of oxidants to achieve a turn-over.

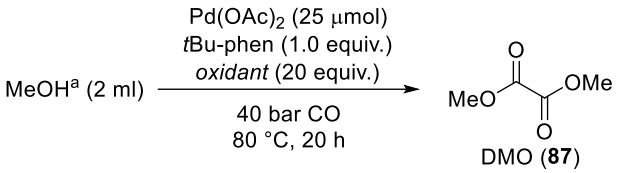

DMO (**87**)

entry	*oxidant*	yield[b]
1	$CuCl_2$	--
2	$Cu(OAc)_2$	--
3	$Cu(OMe)_2$	--
4	$Cu(OMe)_2$[c]	--
5	MnO_2	--
6	I_2	--
7	benzoquinone	--
8	duroquinone	--
9	DDQ	--
10	O_2 (1 bar)	--
11	O_2[d] (1 bar)	--

[a] Anhydrous MeOH from the SPS was used. [b] GC yield using tetradecane as internal standard. [c] PVP was added as nanoparticle dispersant. [d] 7.5 μmol Pd were used.

Table 50. Screening of Wacker process-like conditions.

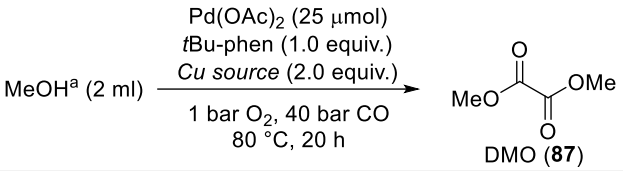

entry	*Cu source*	TON[b]	2nd TON[b]
1	$Cu(OMe)_2$	10	2.8
2[c]	$Cu(OMe)_2$	<1	
3[d]	$Cu(OMe)_2$	1.9	<1
4	$Cu(OMe)_2$[e]	1.6	1.5
5	$Cu(OMe)_2$[f]	4.7	5.9
6	Cu(0)	1.1	0.61
7	$Cu(OAc)_2$	--	--
8[g]	$Cu(OMe)_2$	--	

[a] Anhydrous MeOH from the SPS was used. [b] TON using tetradecane as internal standard. [c] 50 μmol Pd were used. [d] 12.5 μmol Pd were used. [e] 1.0 equiv. $Cu(OMe)_2$ were used. [f] 4.0 equiv. $Cu(OMe)_2$ were used. [g] control reaction without Pd.

Table 51. Screening of ligands in Wacker process-like DMO (**87**) synthesis.

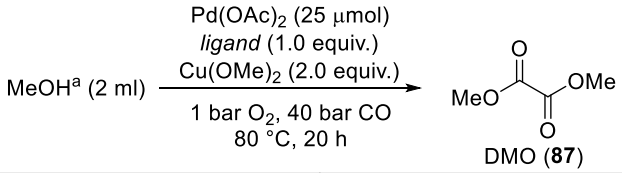

entry	*ligand*	TON[b]	2nd TON[b]
1	*t*Bu-phen (**93**)	10	2.8
2	phen (**88**)	2.1	1.2
3	bipy (**89**)	6.2	2.7
4	Ph-phen (**90**)	21	17
5[c]	Ph-phen (**90**)	2.9	
6	Ph-phen[d] (**90**)	17	
7	Ph-phen[e] (**90**)	14	
8	*n*Bu-phen (**91**)	22	17
9	*s*Bu-phen (**92**)	6.8	4.0
10	5,6-$(Me)_2$-phen	1.2	1.1
11	Ph-bipy (**94**)	15	
12	*n*Bu-bipy (**95**)	18	
13	*s*Bu-bipy (**96**)	14	
14	4,4'-$(Me)_2$-bipy	3.9	4.4
15	5,5'-$(Me)_2$-bipy	3.0	1.5
16	4,4'-$(OMe)_2$-bipy	1.8	<1
17	5,5'-$(CF_3)_2$-bipy	3.5	4.1
18	--	15	16

[a] Anhydrous MeOH from the SPS was used. [b] TON using tetradecane as internal standard. [c] 1.0 equiv. $Cu(OMe)_2$ were used. [d] 1.5 equiv. Ph-phen were used. [e] 2.0 equiv. Ph-phen were used.

Table 52. Screening of Pd nanoparticles (NP) for the oxidative carbonylation of methanol.

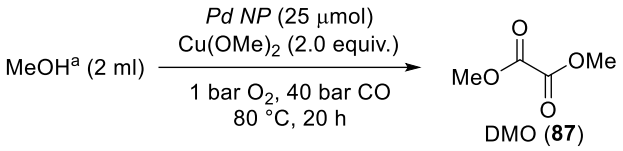

entry	*Pd nanoparticles*	TON[b]
1	Pd/CeO_2-SiO_2 (AW-UN-01)	--
2	Pd/CeO_2-SiO_2 (AW-UN-02)	--
3	$Pd/CeAl/SiO_2$, (2nd batch)	--
4	$Pd/Ce_{0.8}ZrO_x$ (direct irradiaton)	--
5	$Pd/Ce_{0.8}ZrO_x$ (irradiaton through glass)	--
6[c]	Cbz-010-400	--

[a] Anhydrous MeOH from the SPS was used. [b] TON using tetradecane as internal standard. [c] Control reaction without Pd, only support material.

Table 53. Unsuccessful transfer of reaction conditions from the oxidative carbonylation to the reductive CO_2 dimerization.

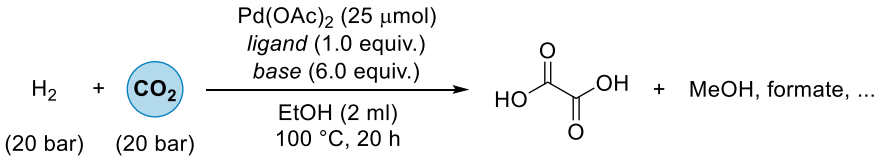

entry	*ligand*	*base*	product?
1	Ph-bipy	--	n.d.
2	Ph-phen	--	n.d.
3	*t*Bu-phen	--	n.d.
4	Ph-phen	NaOEt	n.d.
5	Ph-phen	K_3PO_4	n.d.
6	Ph-phen	PPTS	n.d.

PPTS = pyridinium *p*-toluenesulfonate.

7.3.3.2 Rational Ligand Design for Carbon Capture and Utilization

Ligand idea: Pyrox-C_4N

Synthesis of Cbz-Lys(Boc)-CH_2OH (104):

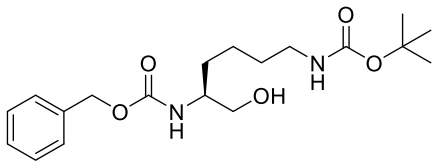

104

Compound **104** was synthesized according to a modified literature procedure.[316] Cbz-Lys(Boc)-OH (**103**, 1.0 equiv.) was loaded into a round-bottomed flask equipped with a stirring bar. Dry THF (1 M) was added, and the resulting solution was cooled to -10 °C. DIPEA (1.0 equiv.) was added, followed by isobutyl chloroformate (1.0 equiv.). The yellow suspension was stirred for 15 min and vacuum filtered into a second round-bottomed flask. The filtrate was again cooled to -10 °C. $NaBH_4$ (0.75 equiv.) was dissolved in H_2O (3 M) and very slowly added by syringe, followed by a second portion of $NaBH_4$ (0.75 equiv.) in H_2O (3 M). After the addition is complete and the gas evolution has stopped, the reaction is diluted with water and extracted with DCM (3x). The combined organic fractions were dried over Na_2SO_4, filtered, and purified by column chromatography using *n*-pentane/EtOAc (1:1 to 1:3) as eluent. The product **104** was isolated in an average yield of 65% (#1: 132 mg, 0.36 mmol, 72%; #2: 705 mg, 1.9 mmol, 64%; #3: 3.2 g, 8.7 mmol, 60%) as a colorless wax.

R_f = 0.47 (pentane/EtOAc 1:3, UV).

^{1}H NMR (300 MHz, $CDCl_3$) δ 7.40 – 7.27 (m, 5H), 5.13 (br s, 1H), 5.09 (s, 2H), 4.58 (br s, 1H), 3.76 – 3.49 (m, 3H), 3.23 – 2.96 (m, 2H), 2.48 (br s, 1H), 1.68 – 1.16 (m, 6H), 1.42 (s, 9H).

^{13}C NMR (75 MHz, $CDCl_3$) δ 156.9, 156.5, 136.6, 128.6, 128.2, 128.2, 79.4, 66.9, 65.0, 53.1, 39.8, 30.7, 30.0, 28.5, 22.8.

MS (EI): *m/z* (relative intensity) 128 (26), 108 (13), 91 (100), 84 (56), 57 (26).

HRMS (ESI-TOF, *m/z*): calcd. for $C_{19}H_{30}N_2O_5$ $[M + Na]^+$ 389.2052, observed 389.2058.

IR (ATR, neat, cm^{-1}): 3327 (w), 2933 (w), 2864 (w), 1684 (s), 1519 (s), 1454 (m), 1392 (w), 1365 (m), 1342 (w), 1246 (s), 1166 (s), 1049 (m), 1026 (m), 912 (w), 864 (w), 823 (w), 776 (w), 732 (s), 696 (s), 646 (m), 576 (m), 489 (m), 460 (m).

This data is in agreement with literature.[317]

Synthesis of H-Lys(Boc)-CH_2OH (105):

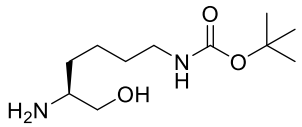

105

Compound **105** was synthesized according to a modified literature procedure.[317] A solution of Z-Lys(Boc)-CH_2OH (**104**, 1.0 equiv.) in MeOH (0.05 M) was added Pd/C (5 mol%) and stirred under an atmosphere of H_2 o/n. Then, the solution was filtered through a filter paper on a layer of celite, washed with methanol and concentrated *in vacuo* to afford the title compound **105** in quantitative yield (#1: 467 mg, 2.0 mmol, quant.; #2: 2.2 g, 9.5 mmol, quant.) as a colorless solid.

^{1}H NMR (300 MHz, $CDCl_3$) δ 4.65 (br s, 1H), 3.58 (dd, *J* = 10.8, 3.8 Hz, 1H), 3.30 (dd, *J* = 10.8, 7.5 Hz, 1H), 3.10 (q, *J* = 6.5 Hz, 2H), 2.84 (br s, 1H), 2.51 (s, 3H), 1.43 (s, 9H), 1.60 – 1.21 (m, 6H).

^{13}C NMR (75 MHz, $CDCl_3$) δ 156.3, 79.3, 66.3, 52.9, 40.3, 33.7, 30.2, 28.6, 23.2.

MS (EI): *m*/*z* (relative intensity) 201 (9), 159 (11), 145 (11), 128 (40), 84 (100), 60 (19), 59 (13), 57 (46), 56 (20), 43 (12), 41 (21).

HRMS (ESI-TOF, *m*/*z*): calcd. for $C_{11}H_{24}N_2O_3$ $[M + H]^+$ 233.1865, observed 233.1862.

IR (ATR, neat, cm^{-1}): 3367 (w), 3290 (w), 3117 (w), 2970 (w), 2935 (m), 2890 (w), 2856 (w), 1680 (s), 1597 (m), 1519 (s), 1476 (w), 1460 (w), 1446 (w), 1392 (w), 1363 (m), 1289 (m), 1271 (m), 1248 (s), 1227 (m), 1165 (s), 1131 (m), 1082 (w), 1053 (m), 1040 (m), 1018 (m), 993 (m), 969 (m), 909 (w), 859 (m), 824 (w), 780 (m), 767 (w), 733 (w), 604 (m), 569 (m), 550 (w), 496 (w), 471 (w), 424 (w).

This data is in agreement with literature.[318]

Synthesis of pyrox-C_4N(Boc) (106):

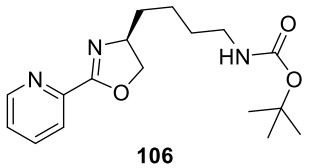

106

Compound **106** was synthesized according to a modified literature procedure.[275] To a 25 ml Schlenk finger were added the imidate (**109**, 1.0 equiv.), the amino alcohol (**105**, 1.2 equiv.), and dry toluene (0.4 M). The mixture was heated to 100 °C for 22 h under inert atmosphere. The crude mixture was cooled to room temperature, concentrated, and analyzed by NMR to calculate the ratio of pyrox **106** and compound **110**. The title compound **106** was obtained in quantitative yield with an average purity of 92% (#1: 1.28 g, 4.0 mmol, 96%; #2: 1.34 g, 4.2 mmol, 94%; #3: 1.16 g, 3.6 mmol, 86%) as a colorless oil. If necessary, the product was purified by column chromatography (*n*-pentane/EtOAc 1:5).

R_f = 0.13 (EtOAc, UV).

^{1}H NMR (300 MHz, $CDCl_3$) δ 8.66 (ddd, *J* = 4.8, 1.8, 0.9 Hz, 1H), 7.98 (dt, *J* = 7.9, 1.1 Hz, 1H), 7.73 (td, *J* = 7.7, 1.8 Hz, 1H), 7.34 (ddd, *J* = 7.6, 4.8, 1.2 Hz, 1H), 4.61 (s, 1H), 4.54 (dd, *J* = 9.5, 8.2 Hz, 1H), 4.30 (ddt, *J* = 9.5, 8.1, 6.4 Hz, 1H), 4.06 (dd, *J* = 8.2 Hz, 1H), 3.09 (q, *J* = 6.4 Hz, 2H), 1.79 – 1.44 (m, 6H), 1.39 (s, 9H).

^{13}C NMR (75 MHz, $CDCl_3$) δ 162.7, 156.0, 149.8, 146.8, 136.7, 125.6, 123.9, 79.1, 73.1, 66.9, 40.4, 35.5, 30.1, 28.5, 23.2.

MS (EI): *m/z* (relative intensity) 319 (1), 263 (6), 246 (50), 218 (11), 203 (21), 202 (71), 201 (27), 189 (21), 175 (21), 174 (13), 162 (16), 161 (63), 157 (37), 148 (43), 147 (100), 134 (16), 133 (15), 131 (10), 123 (21), 119 (21), 107 (11), 106 (41), 105 (62), 97 (33), 96 (59), 93 (26), 92 (52), 84 (11), 79 (31), 78 (64), 70 (17), 59 (14), 57 (67), 56 (19).

HRMS (ESI-TOF, *m/z*): calcd. for $C_{17}H_{25}N_3O_3$ $[M + H]^+$ 320.1969, observed 320.1975; $[M + Na]^+$ 342.1788, observed 342.1793.

IR (ATR, neat, cm^{-1}): 3324 (w), 3058 (w), 2973 (w), 2930 (w), 2862 (w), 1695 (s), 1643 (m), 1583 (w), 1569 (w), 1520 (s), 1469 (m), 1440 (m), 1390 (w), 1363 (s), 1270 (m), 1247 (s), 1167 (s), 1100 (m), 1043 (m), 995 (m), 963 (m), 909 (w), 867 (w), 800 (m), 782 (w), 745 (m), 705 (m), 682 (m), 620 (m), 463 (w), 403 (w).

Synthesis of pyrox-C_4N*HCl (107*HCl):

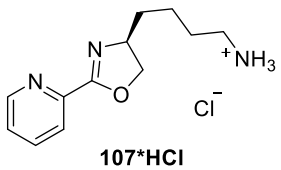

107*HCl

Pyrox-C_4N(Boc) (**106**, 318 mg, 1.0 mmol, 1.0 equiv.) was dissolved in dry Et_2O (3 ml). A solution of 2 M HCl in Et_2O (3 ml, 6.0 equiv.) was added dropwise and the mixture was stirred for 1 h at room temperature. The precipitate was isolated by filtration and washed with Et_2O to afford the title compound **107*HCl** in 97% yield (313 mg, 0.97 mmol) as a bright yellow solid.

m.p. 106 – 108 °C

^{1}H NMR (300 MHz, D_2O) δ 8.81 (ddd, *J* = 5.4, 1.6, 0.8 Hz, 1H), 8.46 (td, *J* = 7.9, 1.7 Hz, 1H), 8.33 (dt, *J* = 8.0, 1.1 Hz, 1H), 8.00 (ddd, *J* = 7.8, 5.4, 1.3 Hz, 1H), 4.47 – 4.33 (m, 1H), 3.86 (dd, *J* = 11.5, 4.2 Hz, 1H), 3.74 (dd, *J* = 11.5, 6.9 Hz, 1H), 2.99 (t, *J* = 7.6 Hz, 2H), 1.92 – 1.61 (m, 5H), 1.59 – 1.37 (m, 3H).

^{13}C NMR (101 MHz, D_2O) δ 162.7, 146.2, 144.9, 144.5, 129.9, 125.2, 52.5, 47.4, 39.9, 31.2, 27.0, 22.9.

MS (ESI): *m*/*z* (relative intensity) 256 (100, $[M + Cl]^+$), 220 (48, $[M]^+$).

HRMS (ESI-TOF, *m*/*z*): calcd. for $C_{12}H_{18}N_3O^+$ $[M]^+$ 220.1455, observed 220.1451.

IR (ATR, neat, cm^{-1}): 3391 (w), 3207 (w), 2930 (m), 2865 (m), 2049 (w), 1748 (w), 1680 (s), 1602 (s), 1556 (m), 1518 (s), 1456 (m), 1353 (m), 1296 (m), 1226 (m), 1156 (m), 1121 (m), 1095 (m), 1039 (m), 999 (m), 962 (m), 871 (w), 807 (m), 752 (s), 660 (s), 621 (s), 567 (m), 497 (m), 442 (m).

Synthesis of ethyl 2-pyridinecarboximidate (109):

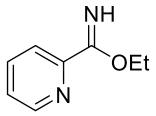

109

Compound **109** was synthesized according to a modified literature procedure.[275] To a solution of substituted 2-cyanopyridine (1.0 equiv.) in dry ethanol (0.67 M) was added a substoichiometric amount of sodium metal (0.37-0.52 equiv.) under argon. The colorless solution was stirred at room temperature overnight and became yellow. The solvent was removed under reduced pressure. Purification by column chromatography (*n*-pentane/EtOAc/NEt_3 10:1:0.01) yielded the title compound **109** in an average yield of 77% (#1: 301 mg, 2.0 mmol, 67%; #2: 1.3 g, 8.6 mmol, 87%) as a slightly yellow liquid.

R_f = 0.42 (pentane/EtOAc/NEt_3 10:1:0.01, UV).

^{1}H NMR (300 MHz, $CDCl_3$) δ 8.64 (ddd, *J* = 4.8, 1.7, 0.9 Hz, 1H), 7.87 (ddt, *J* = 7.9, 1.3, 0.9 Hz, 1H), 7.78 (dddd, *J* = 7.8, 7.4, 1.7, 0.7 Hz, 1H), 7.36 (dddd, *J* = 7.4, 4.7, 1.3, 0.8 Hz, 1H), 4.44 (qd, *J* = 7.1, 1.0 Hz, 2H), 1.44 (td, *J* = 7.1, 0.7 Hz, 3H).

^{13}C NMR (75 MHz, $CDCl_3$) δ 166.3, 149.3, 147.8, 137.3, 125.4, 121.1, 62.5, 14.4.

MS (EI): *m*/*z* (relative intensity) 149 (1), 134 (8), 122 (11), 106 (25), 105 (23), 79 (100), 78 (37), 52 (15), 51 (19).

HRMS (ESI-TOF, *m*/*z*): calcd. for $C_8H_{10}N_2O$ $[M + H]^+$ 151.0871, observed 151.0872.

IR (ATR, neat, cm^{-1}): 3423 (w), 3288 (w), 3059 (w), 2981 (w), 2903 (w), 1733 (w), 1716 (w), 1698 (w), 1648 (s), 1617 (w), 1583 (m), 1571 (m), 1541 (w), 1521 (w), 1507 (w), 1473 (w), 1457 (w), 1433 (w), 1406 (m), 1377 (s), 1338 (s), 1291 (w), 1256 (w), 1189 (m), 1175 (w), 1099 (s), 1085 (s), 1047 (w), 1022 (w), 995 (m), 878 (m), 802 (m), 747 (m), 670 (m), 621 (w), 502 (w), 459 (w), 443 (w), 404 (w).

This data is in agreement with literature.[319]

Synthesis of (*S*)-2-amino-6-((*tert*-butoxycarbonyl)amino)hexyl picolinate (110):

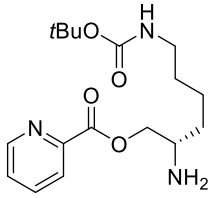

110
postulated structure

Compound **110** was synthesized according to a modified literature procedure.[320] To a 5 ml vial equipped with a stirring bar were added picolinic acid (31.0 mg, 0.25 mmol, 1.25 equiv.) and DCM (0.5 ml). After addition of $SOCl_2$ (36 µl, 0.50 mmol, 2.5 equiv.) and one drop DMF, the beige suspension was stirred over night at room temperature to form the acyl chloride. Next, a pre-mixed solution of the amino alcohol **105** (46.6 mg, 0.20 mmol, 1.0 equiv.) and Hünig base (102 µl, 0.60 mmol, 3.0 equiv.) was added. The light orange solution was stirred over the weekend at room temperature. At the next day, the reaction mixture was added 1 M KOH in methanol (1.5 equiv.) and stirred for another 30 min., before it was adjusted to neutral pH with 1 M aqueous HCl solution. The aqueous phase is extracted with DCM. The combined organic phases were washed with brine, dried over Na_2SO_4, and concentrated. Purification by column chromatography (*n*-pentane/EtOAc 2:1) afforded the title compound **110** in 34% yield as a colorless oil (23 mg, 0.07 mmol).

Compound **110** was also obtained as side-product from the synthesis of pyrox-C_4N(Boc) (**106**).

R_f = 0.33 (EtOAc, UV).

^{1}H NMR (300 MHz, $CDCl_3$) δ 8.53 (ddd, *J* = 4.8, 1.7, 0.9 Hz, 1H), 8.20 (d, *J* = 8.0 Hz, 1H), 8.17 (dt, *J* = 7.8, 1.1 Hz, 1H), 7.84 (td, *J* = 7.7, 1.7 Hz, 1H), 7.42 (ddd, *J* = 7.6, 4.8, 1.3 Hz, 1H), 4.64 (s, 1H), 4.11 (tdd, *J* = 9.2, 7.3, 3.7 Hz, 1H), 3.76 (dd, *J* = 11.3, 3.8 Hz, 1H), 3.70 (dd, *J* = 11.3, 5.3 Hz, 1H), 3.09 (dh, *J* = 13.1, 6.5 Hz, 2H), 2.86 (s, 1H), 1.84 – 1.59 (m, 2H), 1.59 – 1.47 (m, 2H), 1.47 – 1.41 (m, 2H), 1.40 (s, 9H).

^{13}C NMR (75 MHz, $CDCl_3$) δ 164.8, 156.2, 149.6, 148.0, 137.5, 126.3, 122.4, 79.1, 65.2, 51.9, 40.0, 30.6, 29.9, 28.4, 23.0.

MS (EI): *m*/*z* (relative intensity) 337 (1), 281 (2), 264 (11), 184 (17), 147 (10), 124 (11), 123 (63), 114 (20), 106 (46), 84 (100), 79 (20), 78 (56), 57 (26).

HRMS (ESI-TOF, *m*/*z*): calcd. for $C_{17}H_{27}N_3O_4$ $[M + Na]^+$ 360.1894, observed 360.1895.

IR (ATR, neat, cm^{-1}): 3350 (m), 3056 (w), 2975 (w), 2932 (m), 2863 (w), 1660 (s), 1590 (w), 1570 (w), 1519 (s), 1462 (m), 1433 (m), 1391 (w), 1364 (m), 1272 (w), 1248 (m), 1164 (m), 1089 (w), 1042 (w), 997 (w), 865 (w), 820 (w), 748 (w), 693 (w), 620 (w).

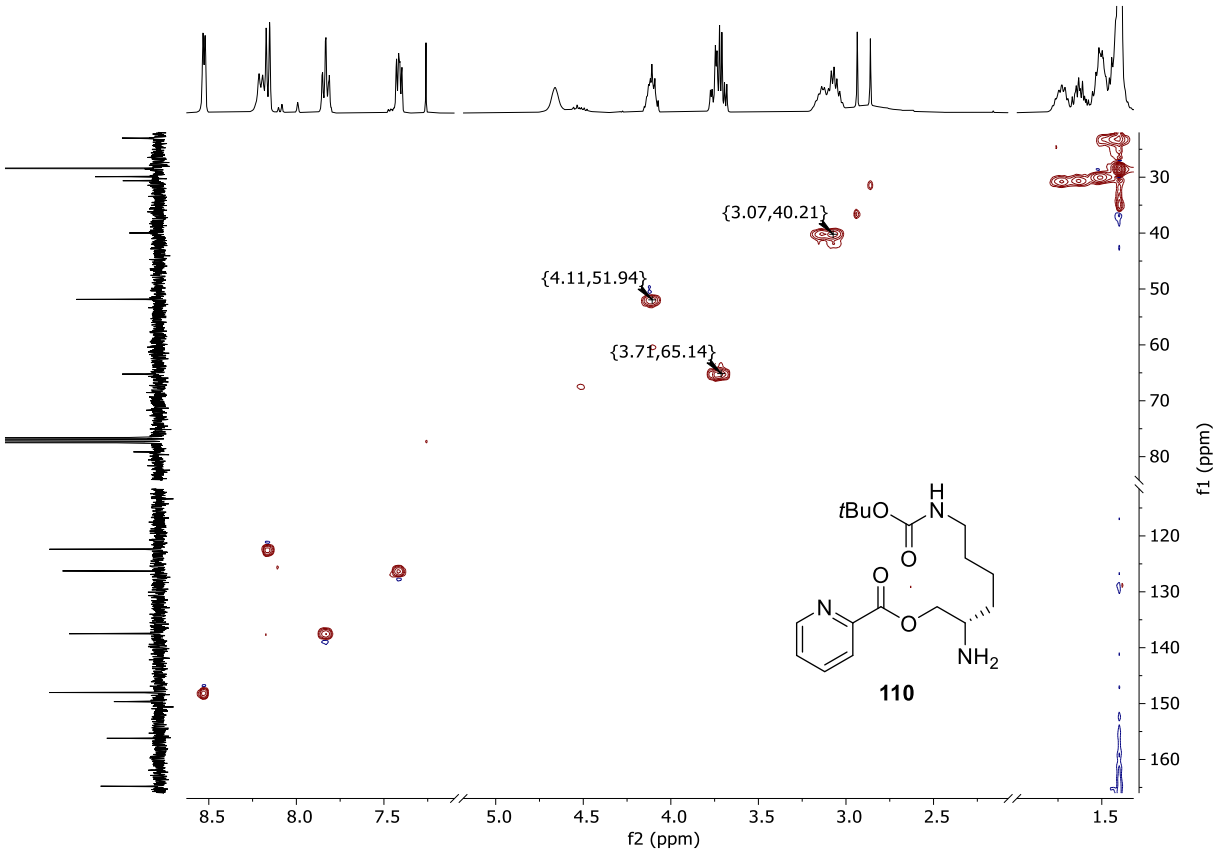

Figure 63. ^{1}H-^{13}C HSQC NMR spectrum of compound **110**.

Synthesis of *tert*-butyl-(*S*)-(6-hydroxy-5-(picolinamido)hexyl)carbamate (112):

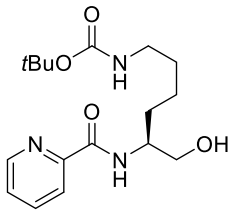

112
postulated structure

Compound **112** was synthesized according to a modified literature procedure.[320] To a 5 ml vial equipped with a stirring bar were added picolinic acid (28.3 mg, 0.23 mmol, 1.15 equiv.) and DCM (1 ml). After addition of $SOCl_2$ (34 µl, 0.46 mmol, 2.3 equiv.), the white suspension was stirred for 30 min. at room temperature to form the acyl chloride. Next, the amino alcohol **105** (46.6 mg, 0.20 mmol, 1.0 equiv.) was added, followed by the addition of Hünig base (102 µl, 0.60 mmol, 3.0 equiv.). The white suspension turned into a yellow solution that was stirred over night at room temperature. At the next day, the light green suspension was poured into an Erlenmeyer flask and stirred with 1 M KOH in methanol for another 30 min., before it was adjusted to neutral pH with 1 M aqueous HCl solution. The aqueous phase is extracted with DCM. The combined organic phases were washed with brine, dried over Na_2SO_4, and concentrated. Purification by column chromatography (n-pentane/EtOAc 2:1) afforded the title compound **112** in 15% yield as a colorless oil (10 mg, 0.03 mmol).

Compound **112** was also obtained from stirring pyrox-C_4N(Boc) (**106**, 1.28 g, 4.0 mmol) with HCl (2 M in Et_2O, 3.0 equiv.) at room temperature for 1 h, followed by basic work-up using aqueous NaOH solution (2.5 M) and extraction with DCM (3x). Purification by column chromatography using EtOAc as eluent afforded the title compound **112** in 48% yield (645 mg, 1.9 mmol).

R_f = 0.76 (EtOAc, UV).

^{1}H NMR (300 MHz, $CDCl_3$) δ 8.57 (ddd, *J* = 4.8, 1.7, 0.9 Hz, 1H), 8.21 (d, *J* = 8.0 Hz, 1H), 8.20 (dt, *J* = 7.8, 1.1 Hz, 1H), 7.87 (td, *J* = 7.7, 1.7 Hz, 1H), 7.45 (ddd, *J* = 7.6, 4.8, 1.3 Hz, 1H), 4.56 (s, 1H), 4.48 – 4.34 (m, 1H), 3.77 (dd, *J* = 11.2, 4.3 Hz, 1H), 3.70 (dd, *J* = 11.2, 3.9 Hz, 1H), 3.20 – 3.01 (m, 2H), 2.32 (s, 1H), 1.82 – 1.70 (m, 2H), 1.62 – 1.47 (m, 2H), 1.41 (s, 9H).

^{13}C NMR (75 MHz, $CDCl_3$) δ 164.1, 156.1, 149.5, 148.1, 137.7, 126.5, 122.6, 79.2, 49.7, 48.1, 40.4, 31.8, 29.9, 28.5, 23.2.

HRMS (ESI-TOF, *m*/*z*): calcd. for $C_{17}H_{27}N_3O_4$ $[M]^+$ 338.2080, observed 338.2083; calcd. for $C_{17}H_{25}N_3O_3$ $[M - H_2O]^+$ 320.1974, observed 320.1979.

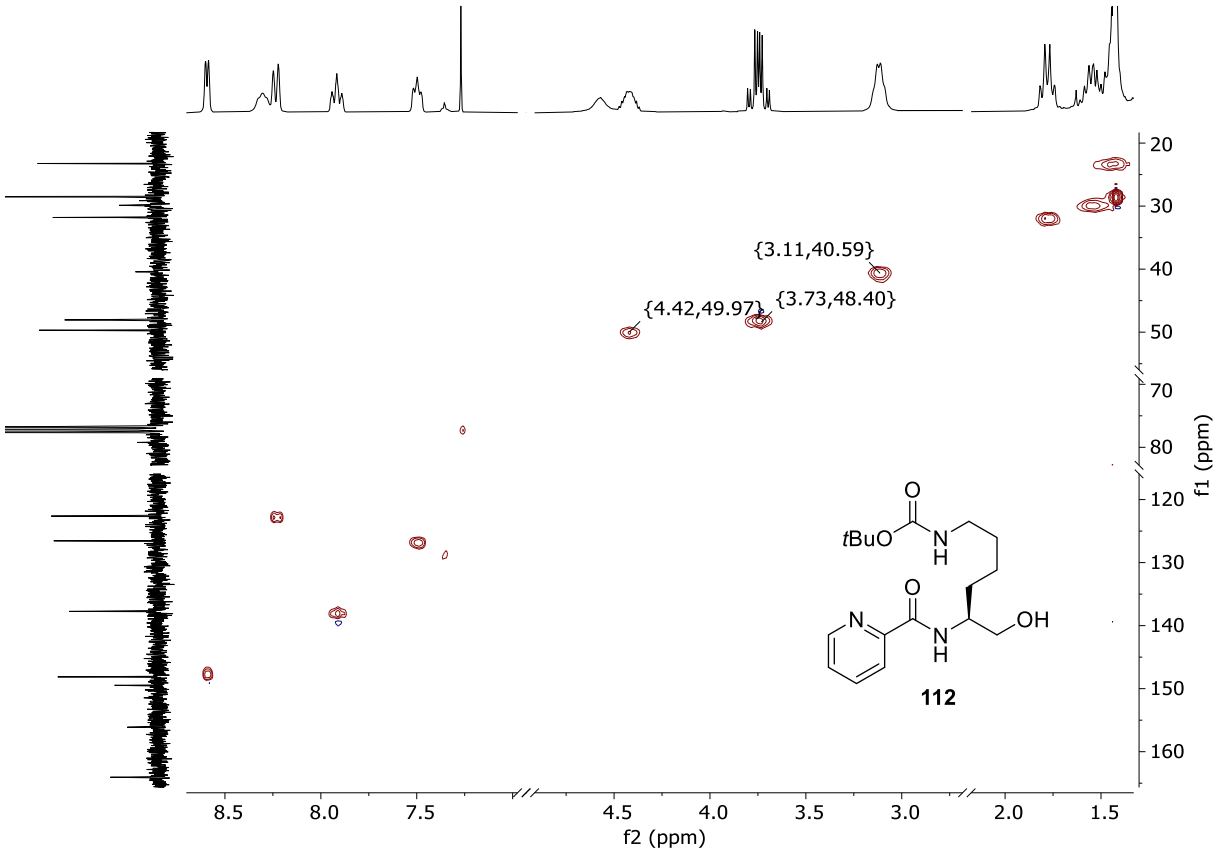

Figure 64. ^{1}H-^{13}C HSQC NMR spectrum of compound **112**.

Calculations on pyrox-C_4N (107):

The geometry optimization and frequency analysis of the pyrox ligand was calculated by using the semiempirical tight-binding model from Grimme *et al*. (gfn2-xtb version 6.5.1) with tight convergence criteria and subsequent calculation of the Hessian (notation: "xtb --ohess --opt tight").[321-322] The conformational space was scanned with Grimme's Conformer-Rotamer Ensemble Sampling Tool (CREST version 2.12, notation: crest --gfn-xtb).[323-324] Next, the lowest lying conformer (Figure 65) was chosen for a potential energy surface scan of the distance between the primary nitrogen atom ($-NH_2$) and the quaternary carbon atom of the oxazole ring using xtb. This resulted in formation of the eight membered azocine heterocycle.

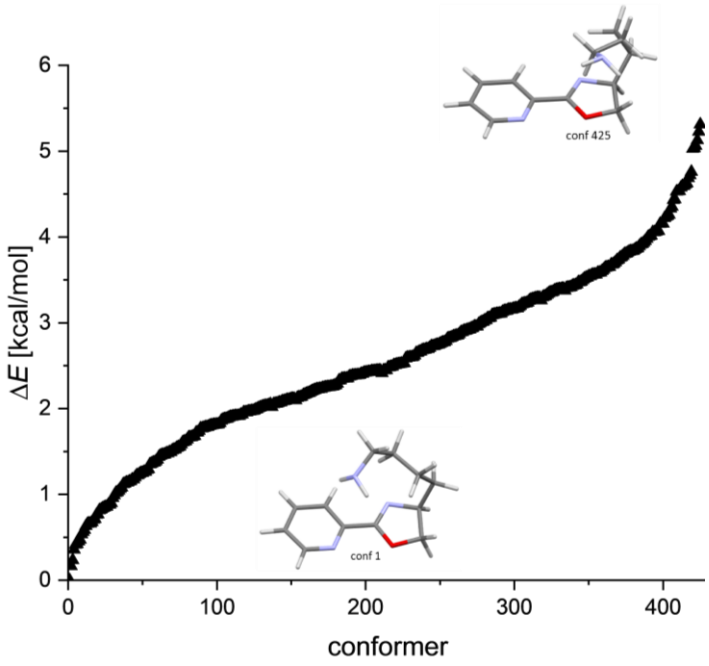

Figure 65. Relative energies of the conformers of the pyrox ligand **107** from CREST calculation.

Optimized structures

pyrox-C_4N *@ xtb pyrox.xyz --ohess --opt tight*

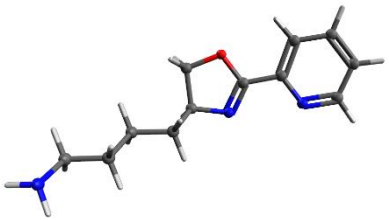

C	-1.08491	0.11886	-0.02022
C	0.28889	-0.12409	-0.06134
C	1.14817	0.95941	-0.11832
C	0.61146	2.23698	-0.13298
C	-0.77150	2.36690	-0.09014
N	-1.59871	1.34410	-0.03531
H	2.21793	0.80938	-0.15054
H	0.65538	-1.13801	-0.04771
H	1.24587	3.10866	-0.17678
H	-1.24060	3.34214	-0.10088
C	-2.02463	-0.99974	0.04255
N	-3.28196	-0.90381	0.13647
O	-1.49620	-2.25627	0.00530
C	-3.84330	-2.23349	0.15684
H	-4.38324	-2.36338	1.10190
C	-4.82608	-2.41557	-1.00148
C	-5.60965	-3.72068	-0.89704
H	-4.27546	-2.38317	-1.94428
H	-5.51174	-1.56737	-0.98875
C	-6.56462	-3.89721	-2.07414
H	-6.17880	-3.72540	0.03578
H	-4.91806	-4.56589	-0.86432
C	-7.36868	-5.19149	-1.97214
H	-6.00481	-3.91377	-3.01018
H	-7.25297	-3.04983	-2.11400
H	-6.68398	-6.04255	-1.90774
H	-7.96819	-5.17296	-1.04479
N	-8.17122	-5.37061	-3.17186
H	-8.70413	-6.23170	-3.11759
H	-8.83030	-4.60475	-3.26806
C	-2.59520	-3.15626	0.07633
H	-2.59422	-3.77848	-0.82321
H	-2.47278	-3.79075	0.95782

Azocin-pyrox *obtained after PES-Scan*

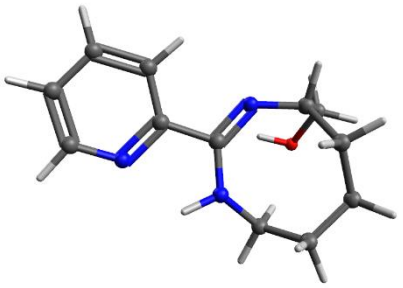

C	1.68360	-0.29819	-0.38450
C	2.28717	0.81772	-0.95968
C	3.65327	0.79858	-1.17070
C	4.37316	-0.33122	-0.80812
C	3.68142	-1.39217	-0.24638
N	2.37779	-1.37900	-0.03647
H	4.15305	1.64854	-1.61296
H	1.67039	1.66053	-1.22280
H	5.44017	-0.38789	-0.95698
H	4.19072	-2.29914	0.05471
C	0.21222	-0.33270	-0.13054
N	-0.39925	0.73572	-0.45571
O	-1.78223	1.12460	1.99014
C	-1.79696	1.04782	-0.49708
H	-1.84097	1.84433	-1.25952
C	-2.76483	-0.04093	-1.02058
C	-3.42352	-1.00673	-0.03572
H	-2.22847	-0.61249	-1.78271
H	-3.56662	0.50118	-1.52898
C	-2.57926	-2.22525	0.31825
H	-4.35105	-1.36099	-0.49372
H	-3.69199	-0.48387	0.88289
C	-1.35068	-1.85752	1.15524
H	-2.25916	-2.73831	-0.59135
H	-3.19641	-2.91739	0.89502
H	-1.61346	-1.01852	1.80707
H	-1.07740	-2.70611	1.78705
N	-0.18491	-1.53351	0.36698
H	0.59689	-2.17294	0.43889
H	-0.81762	1.10981	1.94114
C	-2.24369	1.74323	0.81546
H	-3.33326	1.75517	0.87754
H	-1.88610	2.78159	0.78879

Ligand idea: Phen-NCCN

Synthesis of phen-NCCN (113):

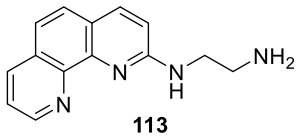

113

Compound **113** was synthesized according to a modified literature procedure.[280] In a 5 ml vial equipped with a magnetic stirrer, a suspension of 2-bromophenanthroline (**119**, 0.5 g, 1.96 mmol, 1.0 equiv.) in excess amine (1 ml) was heated to 100 °C for 24 h. On the next day, the thick yellow solution was cooled to room temperature and the excess amine was removed *in vacuo* to provide the phen-NCCN hydrobromide salt as yellow needles. The HBr salt was then dissolved in water and acidified using 1 M aqueous HCl. The water phase was washed with DCM (3x) followed by addition of 2.5 M NaOH until a basic pH was gained. Afterwards, the product was extracted with DCM (3x). The combined organic fractions were dried over Na_2SO_4 and concentrated. The title compound **113** was obtained in an average yield of 92% (#1: 444.9 mg, 1.9 mmol, 95%; #2: 415.7 mg, 1.7 mmol, 89%) as a yellow oil that slowly solidified upon storage.

m.p. 150 °C (decomposition)

^{1}H NMR (300 MHz, MeOD-d_4) δ 8.75 (dd, *J* = 4.4, 1.8 Hz, 1H), 8.03 (dd, *J* = 8.2, 1.4 Hz, 1H), 7.70 (d, *J* = 8.9 Hz, 1H), 7.37 (td, *J* = 7.1, 2.5 Hz, 2H), 7.24 (dd, *J* = 8.7, 2.2 Hz, 1H), 6.77 (dd, *J* = 8.8, 0.7 Hz, 1H), 3.66 (t, *J* = 6.0 Hz, 2H), 2.89 (t, *J* = 6.0 Hz, 2H).

^{1}H NMR (300 MHz, $CDCl_3$) δ 9.06 (dd, *J* = 4.3, 1.7 Hz, 1H), 8.15 (dd, *J* = 8.1, 1.8 Hz, 1H), 7.96 (d, *J* = 8.7 Hz, 1H), 7.61 (d, *J* = 8.7 Hz, 1H), 7.50 (dd, *J* = 8.2, 4.4 Hz, 1H), 7.46 (d, *J* = 8.7 Hz, 1H), 6.89 (d, *J* = 8.8 Hz, 1H), 5.73 (s, 1H), 3.57 (q, *J* = 5.7 Hz, 2H), 3.03 (dd, *J* = 6.3, 5.4 Hz, 2H), 1.85 (s, 2H).

^{13}C NMR (75 MHz, MeOD-d_4) δ 159.4, 149.2, 145.9, 145.3, 138.3, 137.6, 130.5, 127.7, 123.3, 121.7, 113.5, 44.2, 42.6.

^{13}C NMR (75 MHz, $CDCl_3$) δ 158.4, 149.5, 146.1, 145.2, 138.1, 136.0, 129.5, 126.7, 122.4, 121.3, 109.5, 45.4, 41.9.

MS (EI): *m*/*z* (relative intensity) 238 (1), 210 (19), 209 (100), 208 (60), 195 (23), 181 (28), 180 (68), 179 (51), 154 (12), 125 (6).

HRMS (ESI-TOF, *m*/*z*): calcd. for $C_{14}H_{14}N_4$ $[M + H]^+$ 239.1291, observed 239.1292; $[M + Na]^+$ 261.1111, observed 261.1112.

IR (ATR, neat, cm^{-1}): 3303 (w), 3042 (w), 2928 (w), 2867 (w), 2418 (m), 2231 (w), 2200 (w), 2133 (w), 2061 (m), 1945 (w), 1619 (s), 1607 (m), 1590 (m), 1552 (w), 1519 (s), 1486 (m), 1474 (m), 1423 (m),

1387 (m), 1358 (m), 1297 (w), 1193 (w), 1146 (w), 1119 (w), 1077 (w), 1034 (w), 975 (m), 836 (m), 775 (w), 736 (w), 714 (w), 683 (w), 659 (w), 628 (w), 422 (w).

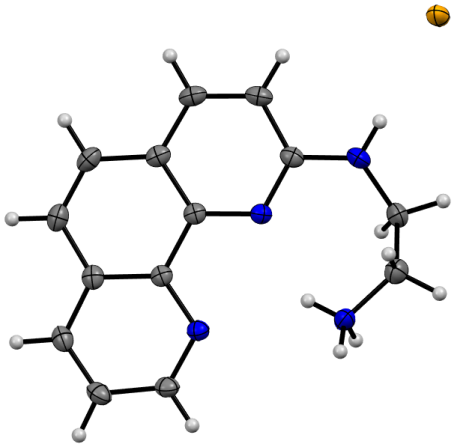

Table 54. Crystal data, data collection, and structure refinement for phen-NCCN*HBr (**113*HBr**).

chemical formula	$C_{14}H_{15}N_4Br$
formula weight (g/mol)	319.21
crystal system, space group	monoclinic, *P* 2_1/n
T (K)	150
unit cell dimensions: *a, b, c* (Å)	*a* = 9.6824(5), *b* = 7.0993(4), *c* = 19.9532(11)
unit cell dimensions: *α, β, γ* (°)	*α* = 90, *β* = 90.374(2), *γ* = 90
V (Å^3)	1371.59(13)
Z	4
absorption coefficient *μ* (mm^{-1})	4.013
F (000)	648.0
crystal size (mm^3), crystal habit	0.323 · 0.163 · 0.093, colorless block
transmission T_{min}, T_{max}	0.360, 0.710
reflections collected	2435
independent reflections	2435
reflections with *I* > 2σ(*I*)	2419
goodness-of-fit on F^2	1.079
final *R* indices [*I* > 2σ(*I*)]	R_1 = 0.0187, ωR_2 = 0.0494
final *R* indices [all data]	R_1 = 0.0188, ωR_2 = 0.0495
no. of parameters	188
$\Delta\rho_{max}$, $\Delta\rho_{min}$ (e Å^{-3})	0.229, -0.297
R.M.S. deviation from mean (e Å^{-3})	0.048

Synthesis of 1-methyl-1,10-phenanthrolin-1-ium iodide (117):

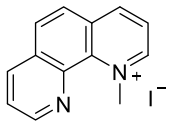

117

Compound **117** was synthesized according to a modified literature procedure.[281] 1,10-phenanthroline (**88**, 180 mg, 1.0 mmol, 1.0 equiv.) was dissolved in MeCN (2 ml). Methyliodide (186 µl, 3.0 mmol, 3.0 equiv.) was added and the solution was heated to 45 °C and stirred overnight. To the yellow suspension was added Et_2O. The yellow solid was filtered off, washed with Et_2O, and dried. This procedure was repeated after concentration of the mother liquor. The title compound **117** was obtained in 78% yield (250.7 mg, 0.78 mmol) as a yellow solid.

^{1}H NMR (300 MHz, DMSO-d_6) δ 9.58 (ddd, *J* = 6.0, 1.6, 0.7 Hz, 1H), 9.40 (dd, *J* = 8.2, 1.5 Hz, 1H), 9.32 (dd, *J* = 4.3, 1.8 Hz, 1H), 8.81 (dd, *J* = 8.2, 1.8 Hz, 1H), 8.47 – 8.37 (m, 3H), 8.07 (dd, *J* = 8.2, 4.3 Hz, 1H), 5.28 (d, *J* = 0.6 Hz, 3H).

^{13}C NMR (75 MHz, DMSO-d_6) δ 151.4, 149.7, 146.7, 140.5, 137.6, 137.4, 132.1, 131.6, 130.5, 126.8, 125.2, 124.3, 54.1.

This data is in agreement with literature.[281]

Synthesis of 1-methyl-1,10-phenanthrolin-2(1*H*)-one (118):

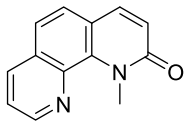

118

Compound **118** was synthesized according to a modified literature procedure.[281] Potassium hexacyanoferrate(III) (593 mg, 1.8 mmol, 2.4 equiv.) was dissolved in water (2.5 ml) and heated to 45 °C. A solution of NaOH (300 mg, 7.5 mmol, 10 equiv.) in water (2.5 ml) was added with a syringe and (phen-Me)I (**117**, 242 mg, 0.75 mmol, 1.0 equiv.) was added simultaneously in small portions. Water (5.0 ml) was also added in portions to the yellow suspension. The reaction mixture was stirred for 18 h at 60 °C. After completion, the reaction mixture was extracted with dichloromethane three times. The combined organic extracts were dried over Na_2SO_4 and filtered, and the solvent was removed. The residue was dissolved in EtOAc/MeOH (8:2) and filtered through AlOx in a column. The title compound **118** was obtained in 95% yield (150 mg, 0.71 mmol) as yellow crystals.

^{1}H NMR (300 MHz, $CDCl_3$) δ 8.94 (dd, *J* = 4.2, 1.9 Hz, 1H), 8.17 (dd, *J* = 8.2, 1.9 Hz, 1H), 7.77 (d, *J* = 9.3 Hz, 1H), 7.55 (d, *J* = 2.0 Hz, 2H), 7.49 (dd, *J* = 8.2, 4.1 Hz, 1H), 6.90 (d, *J* = 9.3 Hz, 1H), 4.48 (s, 3H).

^{13}C NMR (75 MHz, $CDCl_3$) δ 164.4, 147.3, 140.4, 139.2, 138.1, 136.3, 130.3, 126.9, 122.5, 122.4, 122.0, 120.6, 38.0.

This data is in agreement with literature.[281]

Synthesis of Pd(phen-NCCN)$(OAc)_2$ (123):

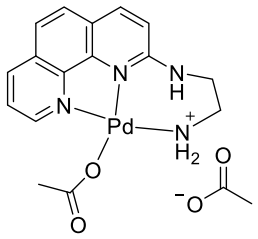

123

A solution of phen-NCCN (**113**, 94.3 mg, 0.42 mmol, 1.0 equiv.) in DCM (5 ml) was added to a solution of $Pd(OAc)_2$ (100 mg, 0.42 mmol, 1.0 equiv.) in DCM (5 ml). The orange suspension was stirred for at room temperature overnight. The precipitate was filtrated off, dried, and then recrystallized from EtOH/*n*-heptane to yield the title compound **123** in 72% yield (140 mg, 0.30 mmol) as orange crystals suitable for X-ray crystallography.

m.p. 200-205 °C (decomposition)

^{1}H NMR (300 MHz, MeOD-d_4) δ 8.73 (dd, *J* = 8.4, 1.4 Hz, 1H), 8.50 (dd, *J* = 5.2, 1.4 Hz, 1H), 8.23 (d, *J* = 9.1 Hz, 1H), 7.97 – 7.79 (m, 4H), 7.22 (d, *J* = 9.1 Hz, 1H), 4.01 (dd, *J* = 8.2, 2.7 Hz, 2H), 2.95 – 2.87 (m, 2H), 2.18 (s, 3H), 1.90 (s, 4H).

^{13}C NMR (75 MHz, MeOD-d_4) δ 181.9, 180.0, 164.1, 149.8, 147.2, 145.9, 141.3, 138.8, 131.3, 128.7, 125.4, 125.1, 124.2, 47.6, 46.8, 24.1, 23.4.

MS (EI): the compound decomposed upon measurement.

HRMS (ESI-TOF, *m*/*z*): calcd. for $C_{15}H_{15}N_4O_2{}^{106}Pd$ $[M - OAc + HCOO]^+$ 389.0225, observed 389.0230; calcd. for $C_{15}H_{15}N_4O_2{}^{108}Pd$ $[M - OAc + HCOO]^+$ 391.0229, observed 391.0234.

IR (ATR, neat, cm^{-1}): 3430 (w), 3324 (w), 3187 (w), 2955 (w), 2918 (m), 2853 (w), 1629 (m), 1590 (s), 1562 (s), 1486 (m), 1472 (m), 1419 (m), 1360 (s), 1319 (s), 1307 (s), 1232 (m), 1217 (m), 1154 (m), 1103 (w), 1038 (w), 1007 (w), 913 (w), 842 (m), 779 (w), 722 (w), 689 (w), 644 (w), 616 (w), 471 (w), 432 (w).

CO_2 capture tests

The ability to capture CO_2 was examined using a modified procedure from literature.[272]

2-20 bar:

A 4 ml vial equipped with a stirring bar was filled with 0.2 mmol of the respective substrate and 0.5 ml dry MeOD-d_4. The vials were placed in a 300 ml autoclave that was purged with CO_2 3 times before it was pressurized with 2 or 20 bar CO_2. After a reaction time of 3 h at room temperature, the gas was slowly released. The reaction mixtures were added 0.2 mmol THF and transferred to NMR tubes. If required, D_2O was added until all precipitates were dissolved. The solutions were analyzed by ^{13}C quant. NMR spectroscopy.

Ambient air:

A glass reactor equipped with a stirring bar was filled with 0.2 mmol of phen-NCCN and 4 ml dry MeOD-d_4. Compressed air was bubbled through the reaction mixture for 3 days. The reaction mixture was added 0.2 mmol THF and transferred to an NMR tube. The solution was analyzed by ^{13}C quant. NMR spectroscopy.

Table 55. CO_2 capture with varying substrates and CO_2 pressures.

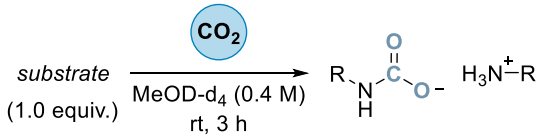

entry	substrate	CO_2 pressure [bar]	carbamates[a] [µmol]	bicarbonate[a,b] [µmol]	yield[a]
1	L-lysine	20	--	49	25%
2	phen-NCCN (**113**)	20	12	47	30%
3	EDA	20	49	59	54%
4	phen (**88**)	20	--	--	--
5	EDA + phen 1:1	20	113	28	70%
6	phen-NCCN (**113**	2	18	61	39%
7	EDA	*2*	89	22	55%
8[c]	phen-NCCN (**113**)	0.0004	24	--	12%

[a] Calculated by NMR using THF as the internal standard. [b] Formed after addition of D_2O to dissolve any precipitates before NMR spectroscopy. [c] Diluted reaction (0.05 M), CO_2 was taken from compressed air bubbling through the reaction mixture for 3 days.

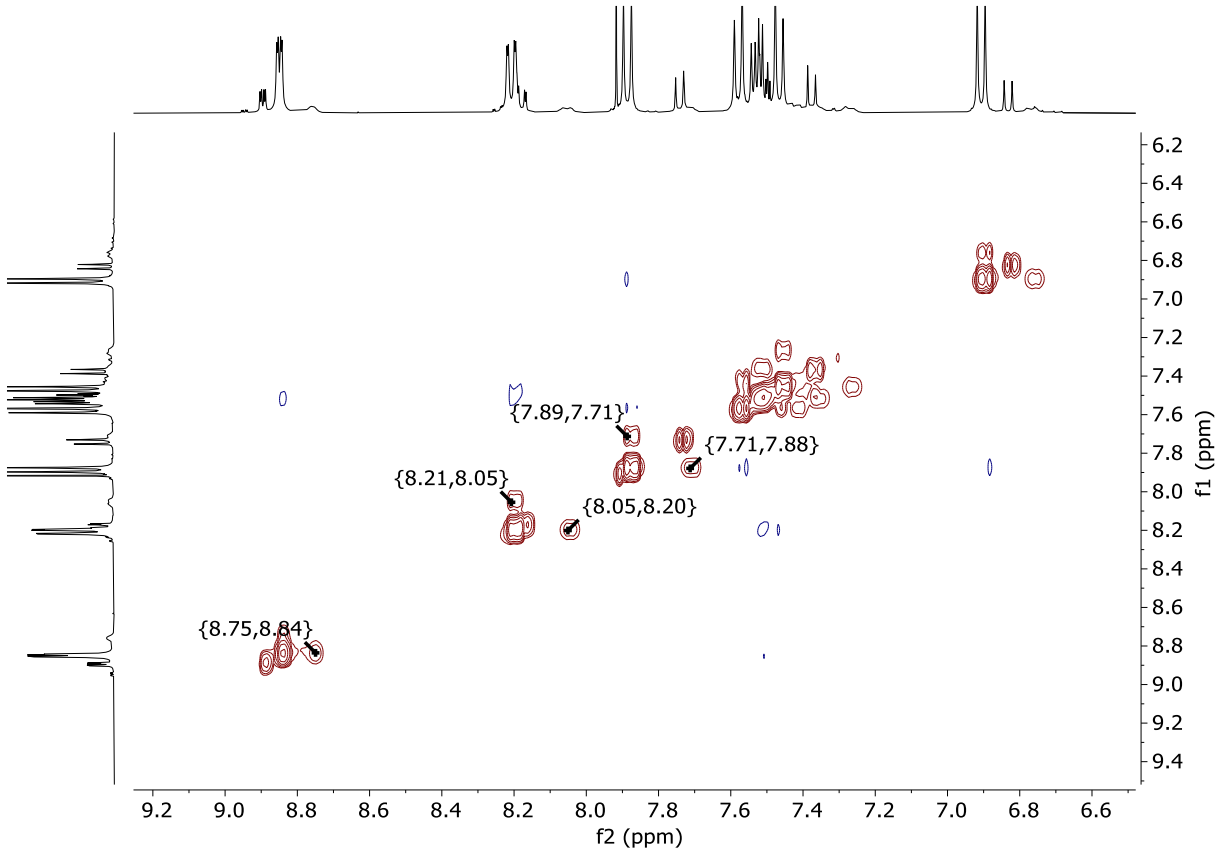

Figure 66. NOESY NMR spectrum of phen-NCCN (**113**) after the reaction with CO_2.

CO_2 hydrogenation

The CO_2 hydrogenation to formate/formic acid was accomplished following General Procedure F.

Table 56. Screening of metal precursors for CO_2 hydrogenation under basic conditions.

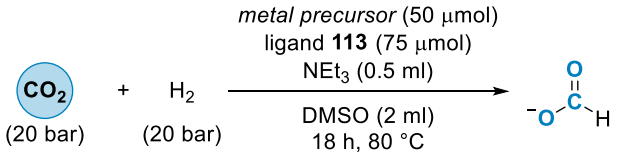

entry	metal precursor	n(formate)[a] [mmol]	conversion[b]	TON
1	$Pd(phen\text{-}NCCN)(OAc)_2$ (**123**)	1.45	40%	29
2	$Pd(OAc)_2$	0.93	26%	19
3	$PdCl_2(MeCN)_2$	1.20	33%	24
4	$Pd(acac)_2$	0.63	18%	13
5	Pd(COD)ClMe	0.28	8%	6
6	$Ru(cymene)Cl_2$	11.88	329%	238
7	$Ru(COD)Cl_2$	7.34	203%	147
8	$[Rh(acac)_2]_2$	1.41	39%	28
9	$[IrCl_2Cp^*]_2$	3.72	103%	74
10	$[Ir(COE)_2Cl]_2$	9.20	255%	184
11	Pt(acac)	--	--	--
12[c]	--	--	--	--

[a] Amount of formate taken from ^{13}C quant. NMR using DMF as internal standard. [b] Calculated on the amount of base. [c] Control reaction without metal.

Table 57. Screening of ligands for CO_2 hydrogenation under neutral/acidic conditions.

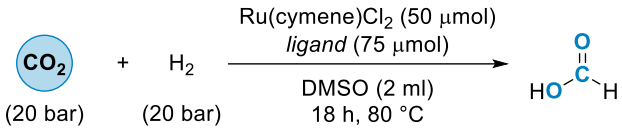

entry	ligand	n(FA)[a] [mmol]	TON
1	--	--	--
2	phen-NCCN (**113**)	0.59	12
3[b]	phen-NCCN (**113**)	0.75	15
4	EDA	--	--
5	phen (**88**)	0.59	12

[a] Amount of formate taken from ^{13}C quant. NMR using DMF as internal standard. [b] 250 µmol ligand (5.0 equiv.) were used.

8 References

[1] T. Wiedmann, M. Lenzen, L. T. Keyßer, J. K. Steinberger, *Nat. Commun.* **2020**, *11*, 3107.

[2] H. Bae, Y. Kim, *Mater. Adv.* **2021**, *2*, 3234-3250.

[3] J. Wang, W. Azam, *Geosci. Front.* **2024**, *15*, 101757.

[4] C. Alewell, B. Ringeval, C. Ballabio, D. A. Robinson, P. Panagos, P. Borrelli, *Nat. Commun.* **2020**, *11*, 4546.

[5] T. Dinh, Z. Dobo, H. Kovacs, *Chemosphere* **2022**, *286*, 131805.

[6] T. Watari, K. Nansai, K. Nakajima, *Resour., Conserv. Recycl.* **2021**, *164*, 105107.

[7] Bundesministerium for Umwelt, Naturschutz, nukleare Sicherheit und Verbraucherschutz, "Waste incineration", can be found under https://www.bmuv.de/en/topics/water-management/circular-economy-overview/waste-treatment-and-technology/waste-incineration, **2021** (accessed 02.04.2024).

[8] NASA, "Carbon Dioxide | Vital Signs - Climate Change: Vital Signs of the Planet", can be found under https://climate.nasa.gov/vital-signs/carbon-dioxide/, **2024** (accessed 18.03.2024).

[9] W. Steffen, J. Grinevald, P. Crutzen, J. McNeill, *Philos. Trans. R. Soc., A* **2011**, *369*, 842-867.

[10] United States Environmental Protection Agency (EPA), "Climate Change Indicators: Atmospheric Concentrations of Greenhouse Gases", can be found under https://www.epa.gov/climate-indicators/climate-change-indicators-atmospheric-concentrations-greenhouse-gases, **2022** (accessed 02.04.2024).

[11] S. Chen, N. Wang, H. Zhang, M. Qiu, L. Shi, Y. Xia, J. Zhang, Y. Huang, F. Cheng, P. Gu, X. Zhang, Q. Yi, *Ind. Eng. Chem. Res.* **2024**, *63*, 3443-3464.

[12] Scripps Institution of Oceanography, "The Keeling Curve", can be found under https://keelingcurve.ucsd.edu/, **2024** (accessed 02.04.2024).

[13] S. Jin, Z. Hao, K. Zhang, Z. Yan, J. Chen, *Angew. Chem. Int. Ed.* **2021**, *60*, 20627-20648.

[14] M. Bergmann, F. Collard, J. Fabres, G. W. Gabrielsen, J. F. Provencher, C. M. Rochman, E. van Sebille, M. B. Tekman, *Nat. Rev. Earth Environ.* **2022**, *3*, 323-337.

[15] P. G. C. Nayanathara Thathsarani Pilapitiya, A. S. Ratnayake, *Cleaner Mater.* **2024**, *11*, 100220.

[16] Eurostat, "Packaging waste statistics", can be found under https://ec.europa.eu/eurostat/statistics-explained/index.php?title=Packaging_waste_statistics, (accessed 01.03.2024).

[17] European Environment Agency, "Reducing loss of resources from waste management is key to strengthening the circular economy in Europe", can be found under https://www.eea.europa.eu/publications/reducing-loss-of-resources-from, **2023** (accessed 03.04.2024).

[18] European Parliament, "Circular economy: definition, importance and benefits", can be found under https://www.europarl.europa.eu/news/en/headlines/economy/20151201STO05603/circular-economy-definition-importance-and-benefits, **2023** (accessed 03.01.2024).

[19] B. Ramasubramanian, J. Tan, V. Chellappan, S. Ramakrishna, *Mater. Circ. Econ.* **2023**, *5*, 6.

[20] S. Schmidt, D. Laner, *J. Ind. Ecol.* **2023**, *27*, 1447-1460.

[21] R. Demets, K. Van Kets, S. Huysveld, J. Dewulf, S. De Meester, K. Ragaert, *Resour., Conserv. Recycl.* **2021**, *174*, 105826.

[22] N. A. Rosli, I. Ahmad, in *Recent Developments in Plastic Recycling* (Eds.: J. Parameswaranpillai, S. Mavinkere Rangappa, A. Gulihonnehalli Rajkumar, S. Siengchin), Springer Singapore, **2021**, pp. 239-258.

[23] J. Harder, *Recovery* **2018**, *05*, can be found under https://www.recovery-worldwide.com/en/artikel/glass-recycling-current-market-trends-3248774.html (accessed 12.04.2024).

[24] G. P. Agnusdei, M. G. Gnoni, F. Sgarbossa, *Sci. Total Environ.* **2022**, *851*, 158256.

[25] Der Grüne Punkt, "Glass Recycling is Simple and Effective", can be found under https://www.gruener-punkt.de/en/politics-and-society/consumer-information/glass-recycling, **2024** (accessed 12.04.2024).
[26] T. Bristogianni, F. Oikonomopoulou, *Glass Struct. Eng.* **2023**, *8*, 255-302.
[27] A. Zupanc, J. Install, M. Jereb, T. Repo, *Angew. Chem. Int. Ed.* **2023**, *62*, e202214453.
[28] D. Raabe, D. Ponge, P. J. Uggowitzer, M. Roscher, M. Paolantonio, C. Liu, H. Antrekowitsch, E. Kozeschnik, D. Seidmann, B. Gault, F. De Geuser, A. Deschamps, C. Hutchinson, C. Liu, Z. Li, P. Prangnell, J. Robson, P. Shanthraj, S. Vakili, C. Sinclair, L. Bourgeois, S. Pogatscher, *Prog. Mater. Sci.* **2022**, *128*, 100947.
[29] X. Tian, J. Sarkis, *Nature* **2024**, *625*, 241.
[30] D. Raabe, *Chem. Rev.* **2023**, *123*, 2436-2608.
[31] G. A. Olah, G. K. S. Prakash, A. Goeppert, *J. Am. Chem. Soc.* **2011**, *133*, 12881-12898.
[32] Petrochemicals Europe, "Discover the interactive flowchart", can be found under www.petrochemistry.eu, **2023** (accessed 15.12.2023).
[33] C. Netzer, T. Li, T. Løvås, *Energy Fuels* **2021**, *35*, 7030-7049.
[34] M. Aresta, A. Dibenedetto, A. Angelini, *Chem. Rev.* **2014**, *114*, 1709-1742.
[35] M. M. F. Hasan, L. M. Rossi, D. P. Debecker, K. C. Leonard, Z. Li, B. C. E. Makhubela, C. Zhao, A. Kleij, *ACS Sustainable Chem. Eng.* **2021**, *9*, 12427-12430.
[36] T. aus der Beek, F.-A. Weber, A. Bergmann, S. Hickmann, I. Ebert, A. Hein, A. Küster, *Environ. Toxicol. Chem.* **2016**, *35*, 823-835.
[37] T. S. Mayer, T. Taeufer, S. Brandt, J. Rabeah, J. Pospech, *J. Org. Chem.* **2023**, *88*, 6347-6353.
[38] A. Yagmur Goren, D. Erdemir, I. Dincer, *Environ. Res.* **2024**, *240*, 117503.
[39] U. Asghar, S. Rafiq, A. Anwar, T. Iqbal, A. Ahmed, F. Jamil, M. S. Khurram, M. M. Akbar, A. Farooq, N. S. Shah, Y.-K. Park, *J. Environ. Chem. Eng.* **2021**, *9*, 106064.
[40] H. A. Alalwan, A. H. Alminshid, *Sci. Total Environ.* **2021**, *788*, 147850.
[41] K. Kaneto, S. Uto, *Chem. Lett.* **2022**, *51*, 924-926.
[42] Y. K. Kharaka, W. W. Carothers, R. J. Rosenbauer, *Geochim. Cosmochim. Acta* **1983**, *47*, 397-402.
[43] T. Qin, L. R. Malins, J. T. Edwards, R. R. Merchant, A. J. E. Novak, J. Z. Zhong, R. B. Mills, M. Yan, C. Yuan, M. D. Eastgate, P. S. Baran, *Angew. Chem. Int. Ed.* **2017**, *56*, 260-265.
[44] E. B. McLean, D. T. Mooney, D. J. Burns, A.-L. Lee, *Org. Lett.* **2022**, *24*, 686-691.
[45] Y.-L. Sun, F.-F. Tan, R.-G. Hu, C.-H. Hu, Y. Li, *Chin. J. Chem.* **2022**, *40*, 1903-1908.
[46] S. Karmakar, A. Silamkoti, N. A. Meanwell, A. Mathur, A. K. Gupta, *Adv. Synth. Catal.* **2021**, *363*, 3693-3736.
[47] A. V. Iosub, Š. Moravčík, C.-J. Wallentin, J. Bergman, *Org. Lett.* **2019**, *21*, 7804-7808.
[48] J. D. Griffin, M. A. Zeller, D. A. Nicewicz, *J. Am. Chem. Soc.* **2015**, *137*, 11340-11348.
[49] A. Adili, A. B. Korpusik, D. Seidel, B. S. Sumerlin, *Angew. Chem. Int. Ed.* **2022**, *61*, e202209085.
[50] O. De Garmo (Monsanto Chemical Company), US 2561324 A, **1951**.
[51] M. Sako, K. Shimada, K. Hirota, Y. Maki, *Tetrahedron Lett.* **1985**, *26*, 6493-6496.
[52] T. S. Mayer, J. Fessler, J. Pospech, *Manuscript in preparation* **2024**.
[53] M. Sako, K. Shimada, K. Hirota, Y. Maki, *J. Am. Chem. Soc.* **1986**, *108*, 6039-6041.
[54] K. Shimada, M. Sako, K. Hirota, Y. Maki, *Tetrahedron Lett.* **1987**, *28*, 207-210.
[55] M. Sako, S. Ohara, K. Hirota, Y. Maki, *J. Chem. Soc., Perkin Trans. 1* **1990**, 3339-3344.
[56] Y. Maki, I. Oyabu, S. Ohara, M. Sako, Y. Kitade, K. Hirota, *Chem. Pharm. Bull.* **1989**, *37*, 3239-3242.
[57] Y. Maki, M. Sako, I. Oyabu, T. Murase, Y. Kitade, K. Hirota, *J. Chem. Soc., Chem. Commun.* **1989**, 1780-1782.
[58] R. Hauptmann, A. Petrosyan, F. Fennel, M. A. Argüello Cordero, A.-E. Surkus, J. Pospech, *Chem. - Eur. J.* **2019**, *25*, 4325-4329.
[59] T. Taeufer, M. A. Argüello Cordero, A. Petrosyan, A.-E. Surkus, S. Lochbrunner, J. Pospech, *ChemPhotoChem* **2021**, *5*, 999-1003.

[60] A. Joshi-Pangu, F. Lévesque, H. G. Roth, S. F. Oliver, L.-C. Campeau, D. Nicewicz, D. A. DiRocco, *J. Org. Chem.* **2016**, *81*, 7244-7249.

[61] T. Taeufer, R. Hauptmann, F. El-Hage, T. S. Mayer, H. Jiao, J. Rabeah, J. Pospech, *ACS Catal.* **2021**, *11*, 4862-4869.

[62] A. Petrosyan, L. Zach, T. Taeufer, T. S. Mayer, J. Rabeah, J. Pospech, *Chem. - Eur. J.* **2022**, *28*, e202201761.

[63] F. El-Hage, C. Schöll, J. Pospech, *J. Org. Chem.* **2020**, *85*, 13853-13867.

[64] D. D. M. Wayner, D. J. McPhee, D. Griller, *J. Am. Chem. Soc.* **1988**, *110*, 132-137.

[65] S. Chopra, D. Kumar, *Heliyon* **2020**, *6*, e04087.

[66] L. Ferrando-Climent, N. Collado, G. Buttiglieri, M. Gros, I. Rodriguez-Roda, S. Rodriguez-Mozaz, D. Barceló, *Sci. Total Environ.* **2012**, *438*, 404-413.

[67] T. Ding, M. Yang, J. Zhang, B. Yang, K. Lin, J. Li, J. Gan, *J. Hazard. Mater.* **2017**, *330*, 127-134.

[68] J. L. Tambosi, L. Y. Yamanaka, J. J. Moreira, H. F. Schroder, *Quim. Nova* **2010**, *33*, 411-420.

[69] L. L. Mazaleuskaya, K. N. Theken, L. Gong, C. F. Thorn, G. A. FitzGerald, R. B. Altman, T. E. Klein, *Pharmacogenet. Genomics* **2015**, *25*, 96-106.

[70] R. Leardi, *Anal. Chim. Acta* **2009**, *652*, 161-172.

[71] A. P. Schellinger, P. W. Carr, *LCGC North Am.* **2004**, *22*, 544-548.

[72] S. Jana, C. Empel, T. V. Nguyen, R. M. Koenigs, *Chem. - Eur. J.* **2021**, *27*, 2628-2632.

[73] Y. Nacheva, A. Garkinin, I. Trenchev, Z. Velkov, *Bulg. Chem. Commun.* **2022**, *54*, 61-65.

[74] V. Thavasi, R. P. A. Bettens, L. P. Leong, *J. Phys. Chem. A* **2009**, *113*, 3068-3077.

[75] L. Buglioni, F. Raymenants, A. Slattery, S. D. A. Zondag, T. Noël, *Chem. Rev.* **2022**, *122*, 2752-2906.

[76] F. A. Carey, R. J. Sundberg, in *Organische Chemie* (Eds.: H. J. Schäfer, D. Hoppe, G. Erker), VCH Weinheim, **1995**, pp. 660-661.

[77] M. Arroyo, L. Briones, H. Hernando, J. M. Escola, D. P. Serrano, *Energy Fuels* **2021**, *35*, 17167-17181.

[78] A. Kiméné, R. Wojcieszak, S. Paul, F. Dumeignil, *J. Chem. Technol. Biotechnol.* **2019**, *94*, 658-669.

[79] M. Valentovic, in *xPharm: The Comprehensive Pharmacology Reference* (Eds.: S. J. Enna, D. B. Bylund), Elsevier, New York, **2007**, pp. 1-3.

[80] H. Oelschläger, D. Rothley, K.-H. Hellwich, W. Schmidt, *Arch. Pharm. (Weinheim, Ger.)* **1989**, *322*, 629-632.

[81] M. R. Shah, M. Imran, S. Ullah, in *Nanocarriers for Cancer Diagnosis and Targeted Chemotherapy*, Elsevier, **2019**, pp. 79-106.

[82] J. Atzrodt, V. Derdau, W. J. Kerr, M. Reid, *Angew. Chem. Int. Ed.* **2018**, *57*, 1758-1784.

[83] E. M. Isin, C. S. Elmore, G. N. Nilsson, R. A. Thompson, L. Weidolf, *Chem. Res. Toxicol.* **2012**, *25*, 532-542.

[84] Y. Y. Loh, K. Nagao, A. J. Hoover, D. Hesk, N. R. Rivera, S. L. Colletti, I. W. Davies, D. W. C. MacMillan, *Science* **2017**, *358*, 1182-1187.

[85] F. Legros, P. Fernandez-Rodriguez, A. Mishra, R. Weck, A. Bauer, M. Sandvoss, S. Ruf, M. Méndez, H. Mora-Radó, N. Rackelmann, C. Pöverlein, V. Derdau, *Chem. - Eur. J.* **2020**, *26*, 12738-12742.

[86] N. Li, Y. Ning, X. Wu, J. Xie, W. Li, C. Zhu, *Chem. Sci.* **2021**, *12*, 5505-5510.

[87] S. Kubosaki, H. Takeuchi, Y. Iwata, Y. Tanaka, K. Osaka, M. Yamawaki, T. Morita, Y. Yoshimi, *J. Org. Chem.* **2020**, *85*, 5362-5369.

[88] T. H. James, A. Weissberger, *J. Am. Chem. Soc.* **1938**, *60*, 98-104.

[89] L. Pitzer, F. Schäfers, F. Glorius, *Angew. Chem. Int. Ed.* **2019**, *58*, 8572-8576.

[90] W. M. Haynes, *CRC Handbook of Chemistry and Physics*, 95 ed., CRC Press, **2014-2015**.

[91] C. D. Herzfeldt, R. Kümmel, *Drug Dev. Ind. Pharm.* **1983**, *9*, 767-793.

[92] L. Li, Y. Yao, N. Fu, *Eur. J. Org. Chem.* **2023**, *26*, e202300166.

[93] D. M. Kitcatt, S. Nicolle, A.-L. Lee, *Chem. Soc. Rev.* **2022**, *51*, 1415-1453.

[94] Y. Patehebieke, *Beilstein J. Org. Chem.* **2020**, *16*, 1418-1435.

[95] X. Bao, W. Yu, G. Wang, *Adv. Synth. Catal.* **2023**, *365*, 2299-2309.
[96] A. M. Varghese, G. N. Karanikolos, *Int. J. Greenhouse Gas Control* **2020**, *96*, 103005.
[97] National Energy Technology Laboratory (USA), "Point Source Carbon Capture from Power Generation Sources", can be found under https://netl.doe.gov/carbon-capture/power-generation, (accessed 05.03.2024).
[98] T. Wilberforce, A. G. Olabi, E. T. Sayed, K. Elsaid, M. A. Abdelkareem, *Sci. Total Environ.* **2021**, *761*, 143203.
[99] S. A. Theofanidis, A. N. Antzaras, A. A. Lemonidou, *Curr. Opin. Chem. Eng.* **2023**, *39*, 100902.
[100] Carbon Engineering, "Our technology", can be found under https://carbonengineering.com/our-technology/, (accessed 05.03.2024).
[101] Intergovernmental Panel on Climate Change, "AR6 Synthesis Report: Climate Change", can be found under https://www.ipcc.ch/report/ar6/syr/, **2023** (accessed 03.03.2024).
[102] Aker Carbon Capture, "Capturing carbon for a brighter future", can be found under https://akercarboncapture.com/, (accessed 05.03.2024).
[103] Shell, "Quest Carbon Capture and Storage", can be found under https://www.shell.ca/en_ca/about-us/projects-and-sites/quest-carbon-capture-and-storage-project.html, (accessed 05.03.2024).
[104] Carbfix, "We turn CO2 into stone", can be found under https://www.carbfix.com/, **2024** (accessed 05.03.2024).
[105] Global CCS Institute, "CO2RE Facilities Report", can be found under https://co2re.co/FacilityData, **2024** (accessed 10.03.2024).
[106] CORDIS (European Commission), "New process produces methanol renewably", can be found under https://cordis.europa.eu/article/id/435360-new-process-produces-methanol-renewably, **2021** (accessed 03.03.2024).
[107] Carbon Recycling International, "Circlenergy", can be found under https://www.carbonrecycling.is/circlenergy, **2022** (accessed 04.03.2024).
[108] Columbus, "Pioneer of the energy transition", can be found under https://columbus-project.com/, (accessed 05.03.2024).
[109] F. E. Liew, R. Nogle, T. Abdalla, B. J. Rasor, C. Canter, R. O. Jensen, L. Wang, J. Strutz, P. Chirania, S. De Tissera, A. P. Mueller, Z. Ruan, A. Gao, L. Tran, N. L. Engle, J. C. Bromley, J. Daniell, R. Conrado, T. J. Tschaplinski, R. J. Giannone, R. L. Hettich, A. S. Karim, S. D. Simpson, S. D. Brown, C. Leang, M. C. Jewett, M. Köpke, *Nat. Biotechnol.* **2022**, *40*, 335-344.
[110] A. Sattari, A. Ramazani, H. Aghahosseini, M. K. Aroua, *J. CO2 Util.* **2021**, *48*, 101526.
[111] L. Shi, T. Hu, R. Xie, H. Wang, J. Li, S. Li, Y. Liu, Y. Zhi, K. Yao, S. Shan, *Chem. Eng. J.* **2024**, *481*, 148566.
[112] C. Yu, Q. Ding, J. Hu, Q. Wang, X. Cui, H. Xing, *Chem. Eng. J.* **2021**, *405*, 126937-126944.
[113] A. Pal, S. Chand, S. M. Elahi, M. C. Das, *Dalton Trans.* **2017**, *46*, 15280-15286.
[114] P. G. Boyd, A. Chidambaram, E. García-Díez, C. P. Ireland, T. D. Daff, R. Bounds, A. Gładysiak, P. Schouwink, S. M. Moosavi, M. M. Maroto-Valer, J. A. Reimer, J. A. R. Navarro, T. K. Woo, S. Garcia, K. C. Stylianou, B. Smit, *Nature* **2019**, *576*, 253-256.
[115] P. Hu, H. Liu, H. Wang, J. Zhou, Y. Wang, H. Ji, *J. Mater. Chem. A* **2022**, *10*, 881-890.
[116] G. T. Rochelle, *Science* **2009**, *325*, 1652-1654.
[117] D. J. Heldebrant, P. K. Koech, V.-A. Glezakou, R. Rousseau, D. Malhotra, D. C. Cantu, *Chem. Rev.* **2017**, *117*, 9594-9624.
[118] S. Kikkawa, K. Amamoto, Y. Fujiki, J. Hirayama, G. Kato, H. Miura, T. Shishido, S. Yamazoe, *ACS Environ. Au* **2022**, *2*, 354-362.
[119] H. F. Svendsen, A. A. Trollebø (Advanced Carbon Capture AS), WO 2013/000953 A2, **2013**.
[120] Z. Qi, F. Liu, H. Ding, M. Fang, *Fuel* **2023**, *350*, 128726.
[121] S. K. Shukla, S. G. Khokarale, T. Q. Bui, J.-P. T. Mikkola, *Front. Mater.* **2019**, *6*, 1-8.
[122] L. A. Blanchard, Z. Gu, J. F. Brennecke, *J. Phys. Chem. B* **2001**, *105*, 2437-2444.
[123] M. Ramdin, T. W. de Loos, T. J. H. Vlugt, *Ind. Eng. Chem. Res.* **2012**, *51*, 8149-8177.
[124] R. Biswas, *J. Mol. Model.* **2022**, *28*, 231.

[125] S. F. R. Taylor, C. McCrellis, C. McStay, J. Jacquemin, C. Hardacre, M. Mercy, R. G. Bell, N. H. de Leeuw, *J. Solution Chem.* **2015**, *44*, 511-527.

[126] X. An, P. Wang, X. Ma, X. Du, X. Hao, Z. Yang, G. Guan, *Carbon Resour. Convers.* **2023**, *6*, 85-97.

[127] F. Liu, Y. Shen, L. Shen, C. Sun, L. Chen, Q. Wang, S. Li, W. Li, *Environ. Sci. Technol.* **2020**, *54*, 3520-3529.

[128] Y. Zhang, Y. Huang, S. Chen, L. Shi, J. Wang, Q. Yi, F. Pei, *Chem. Eng. J.* **2023**, *471*, 144580.

[129] N. Noorani, A. Mehrdad, *ACS Omega* **2024**, *9*, 9516-9525.

[130] C.-J. Yoo, P. Narayanan, C. W. Jones, *J. Mater. Chem. A* **2019**, *7*, 19513-19521.

[131] X. Chen, J. Lin, H. Wang, Y. Yang, C. Wang, Q. Sun, X. Shen, Y. Li, *Carbohydr. Polym.* **2023**, *302*, 120389.

[132] J. Hack, N. Maeda, D. M. Meier, *ACS Omega* **2022**, *7*, 39520-39530.

[133] L. B. Hamdy, C. Goel, J. A. Rudd, A. R. Barron, E. Andreoli, *Mater. Adv.* **2021**, *2*, 5843-5880.

[134] H. T. Kwon, M. A. Sakwa-Novak, S. H. Pang, A. R. Sujan, E. W. Ping, C. W. Jones, *Chem. Mater.* **2019**, *31*, 5229-5237.

[135] M. Y. Zorainy, M. Gar Alalm, S. Kaliaguine, D. C. Boffito, *J. Mater. Chem. A* **2021**, *9*, 22159-22217.

[136] G. Férey, C. Mellot-Draznieks, C. Serre, F. Millange, J. Dutour, S. Surblé, I. Margiolaki, *Science* **2005**, *309*, 2040-2042.

[137] O. Guselnikova, O. Semyonov, E. Sviridova, R. Gulyaev, A. Gorbunova, D. Kogolev, A. Trelin, Y. Yamauchi, R. Boukherroub, P. Postnikov, *Chem. Soc. Rev.* **2023**, *52*, 4755-4832.

[138] Z. Fu, I. M. A. Mohamed, J. Li, C. Liu, *J. Taiwan Inst. Chem. Eng.* **2019**, *97*, 381-388.

[139] X. Dong, A. Akram, B. Comesaña-Gándara, X. Dong, Q. Ge, K. Wang, S.-P. Sun, B. Jin, C. H. Lau, *ACS Appl. Polym. Mater.* **2020**, *2*, 2586-2593.

[140] W. A. Algozeeb, P. E. Savas, Z. Yuan, Z. Wang, C. Kittrell, J. N. Hall, W. Chen, P. Bollini, J. M. Tour, *ACS Nano* **2022**, *16*, 7284-7290.

[141] L. D. Ellis, N. A. Rorrer, K. P. Sullivan, M. Otto, J. E. McGeehan, Y. Román-Leshkov, N. Wierckx, G. T. Beckham, *Nat. Catal.* **2021**, *4*, 539-556.

[142] M. Shakiba, E. Rezvani Ghomi, F. Khosravi, S. Jouybar, A. Bigham, M. Zare, M. Abdouss, R. Moaref, S. Ramakrishna, *Polym. Adv. Technol.* **2021**, *32*, 3368-3383.

[143] A. Kumar, N. von Wolff, M. Rauch, Y.-Q. Zou, G. Shmul, Y. Ben-David, G. Leitus, L. Avram, D. Milstein, *J. Am. Chem. Soc.* **2020**, *142*, 14267-14275.

[144] J. R. Cabrero-Antonino, R. Adam, V. Papa, M. Beller, *Nat. Commun.* **2020**, *11*, 3893.

[145] W. Stuyck, K. Janssens, M. Denayer, F. De Schouwer, R. Coeck, K. V. Bernaerts, J. Vekeman, F. De Proft, D. E. De Vos, *Green Chem.* **2022**, *24*, 6923-6930.

[146] L. Ye, X. Liu, K. B. Beckett, J. O. Rothbaum, C. Lincoln, L. J. Broadbelt, Y. Kratish, T. J. Marks, *Chem* **2024**, *10*, 172-189.

[147] J. B. Jakobsen, M. H. Rønne, K. Daasbjerg, T. Skrydstrup, *Angew. Chem. Int. Ed.* **2021**, *60*, 9174-9179.

[148] Federal Ministry for Economic Cooperation and Development, "Green hydrogen and Power-to-X products", can be found under https://www.bmz.de/en/issues/green-hydrogen, **2023** (accessed 11.01.2023).

[149] J. R. Cabrero-Antonino, R. Adam, M. Beller, *Angew. Chem. Int. Ed.* **2019**, *58*, 12820-12838.

[150] J. Coetzee, D. L. Dodds, J. Klankermayer, S. Brosinski, W. Leitner, A. M. Z. Slawin, D. J. Cole-Hamilton, *Chem. - Eur. J.* **2013**, *19*, 11039-11050.

[151] J. Klankermayer, S. Westhues, W. Leitner, R. T. Hembre, WO 2019/222063 A1, **2019**.

[152] M. Meuresch, S. Westhues, W. Leitner, J. Klankermayer, *Angew. Chem. Int. Ed.* **2016**, *55*, 1392-1395.

[153] T. vom Stein, M. Meuresch, D. Limper, M. Schmitz, M. Hölscher, J. Coetzee, D. J. Cole-Hamilton, J. Klankermayer, W. Leitner, *J. Am. Chem. Soc.* **2014**, *136*, 13217-13225.

[154] P. Pyykkö, M. Atsumi, *Chem. - Eur. J.* **2009**, *15*, 186-197.

[155] M. J. Burk, R. L. Harlow, *Angew. Chem. Int. Ed.* **1990**, *29*, 1462-1464.

[156] M. Meuresch, PhD thesis, RWTH Aachen University (DE), **2016**.

[157] J. Chen, J. Wang, T. Tu, *Chem. - Asian J.* **2018**, *13*, 2559-2565.
[158] W. Zhou, P. Neumann, M. Al Batal, F. Rominger, A. S. K. Hashmi, T. Schaub, *ChemSusChem* **2021**, *14*, 4176-4180.
[159] B. Herzog, M. I. Kohan, S. A. Mestemacher, R. U. Pagilagan, K. Redmond, R. Sarbandi, in *Ullmann's Encyclopedia of Industrial Chemistry*, **2020**, pp. 1-47.
[160] V. Papa, J. R. Cabrero-Antonino, A. Spannenberg, K. Junge, M. Beller, *Catal. Sci. Technol.* **2020**, *10*, 6116-6128.
[161] Y. Zhou, J. Rodríguez-López, J. S. Moore, *Nat. Commun.* **2023**, *14*, 4847.
[162] Carbolution, "1,1,1,3,3,3-hexafluoropropan-2-ol, 99%", can be found under https://www.carbolution.de/product_info.php?products_id=134, **2024** (accessed 09.04.2024).
[163] B. Gleede, M. Selt, R. Franke, S. R. Waldvogel, *Chem. - Eur. J.* **2021**, *27*, 8252-8263.
[164] E. Kaiser, R. L. Colescott, C. D. Bossinger, P. I. Cook, *Anal. Biochem.* **1970**, *34*, 595-598.
[165] W. F. Rowe, in *Kirk-Othmer Encyclopedia of Chemical Technology*, 5 ed., John Wiley & Sons, Inc, **2015**, pp. 89-107.
[166] D. J. McCaldin, *Chem. Rev.* **1960**, *60*, 39-51.
[167] M. Friedman, L. David Williams, *Bioorg. Chem.* **1974**, *3*, 267-280.
[168] K. I. Assaf, W. M. Nau, *Angew. Chem. Int. Ed.* **2018**, *57*, 13968-13981.
[169] Z. Fan, Z. Zhang, C. Xi, *ChemSusChem* **2020**, *13*, 6201-6218.
[170] N. Sutin, C. Creutz, E. Fujita, *Comments Inorg. Chem.* **1997**, *19*, 67-92.
[171] M. Aresta, A. Dibenedetto, *Dalton Trans.* **2007**, 2975-2992.
[172] S. Das, *CO2 as a Building Block in Organic Synthesis*, Wiley-VCH, **2020**.
[173] J. Wu, Y. Huang, W. Ye, Y. Li, *Adv. Sci.* **2017**, *4*, 1700194.
[174] L. Rotundo, D. C. Grills, R. Gobetto, E. Priola, C. Nervi, D. E. Polyansky, E. Fujita, *ChemPhotoChem* **2021**, *5*, 526-537.
[175] J. Li, H. Zeng, X. Dong, Y. Ding, S. Hu, R. Zhang, Y. Dai, P. Cui, Z. Xiao, D. Zhao, L. Zhou, T. Zheng, J. Xiao, J. Zeng, C. Xia, *Nat. Commun.* **2023**, *14*, 340.
[176] S. D. Friis, A. T. Lindhardt, T. Skrydstrup, *Acc. Chem. Res.* **2016**, *49*, 594-605.
[177] G. H. Han, J. Bang, G. Park, S. Choe, Y. J. Jang, H. W. Jang, S. Y. Kim, S. H. Ahn, *Small* **2023**, *19*, 2205765.
[178] F. Bertini, M. Glatz, N. Gorgas, B. Stöger, M. Peruzzini, L. F. Veiros, K. Kirchner, L. Gonsalvi, *Chem. Sci.* **2017**, *8*, 5024-5029.
[179] D. Wei, R. Sang, P. Sponholz, H. Junge, M. Beller, *Nat. Energy* **2022**, *7*, 438-447.
[180] A. Kumar, P. Daw, N. A. Espinosa-Jalapa, G. Leitus, L. J. W. Shimon, Y. Ben-David, D. Milstein, *Dalton Trans.* **2019**, *48*, 14580-14584.
[181] K. Schlenker, E. G. Christensen, A. A. Zhanserkeev, G. R. McDonald, E. L. Yang, K. T. Lutz, R. P. Steele, R. T. VanderLinden, C. T. Saouma, *ACS Catal.* **2021**, *11*, 8358-8369.
[182] A. M. Bahmanpour, A. Hoadley, S. H. Mushrif, A. Tanksale, *ACS Sustainable Chem. Eng.* **2016**, *4*, 3970-3977.
[183] S. Zhao, H.-Q. Liang, X.-M. Hu, S. Li, K. Daasbjerg, *Angew. Chem. Int. Ed.* **2022**, *61*, e202204008.
[184] B. Kim, D. Kwon, J.-O. Baeg, M. Austeria P, G. H. Gu, J.-H. Lee, J. Jeong, W. Kim, W. Choi, *Adv. Funct. Mater.* **2023**, *33*, 2212453.
[185] J. K. Soeherman, A. J. Jones, P. J. Dauenhauer, *ACS Eng. Au* **2023**, *3*, 114-127.
[186] T. Diehl, P. Lanzerath, G. Franciò, W. Leitner, *ChemSusChem* **2022**, *15*, e202201250.
[187] S.-T. Bai, G. De Smet, Y. Liao, R. Sun, C. Zhou, M. Beller, B. U. W. Maes, B. F. Sels, *Chem. Soc. Rev.* **2021**, *50*, 4259-4298.
[188] G. A. McCarver, T. Yildirim, W. Zhou, *ChemPhysChem* **2023**, *24*, e202300645.
[189] Y. Xiong, H. Chen, Y. Hu, S. Yang, X. Xue, L. He, X. Liu, J. Ma, Z. Jin, *Nano Lett.* **2021**, *21*, 8693-8700.
[190] Y. Ling, Q. Ma, Y. Yu, B. Zhang, *Trans. Tianjin Univ.* **2021**, *27*, 180-200.
[191] S. Zhang, Q. Fan, R. Xia, T. J. Meyer, *Acc. Chem. Res.* **2020**, *53*, 255-264.
[192] H.-Q. Liang, T. Beweries, R. Francke, M. Beller, *Angew. Chem. Int. Ed.* **2022**, *61*, e202200723.

[193] X. Yuan, S. Chen, D. Cheng, L. Li, W. Zhu, D. Zhong, Z.-J. Zhao, J. Li, T. Wang, J. Gong, *Angew. Chem. Int. Ed.* **2021**, *60*, 15344-15347.

[194] C. Xiao, J. Zhang, *ACS Nano* **2021**, *15*, 7975-8000.

[195] Y. Lum, J. W. Ager, *Nat. Catal.* **2019**, *2*, 86-93.

[196] J. Gao, H. Zhang, X. Guo, J. Luo, S. M. Zakeeruddin, D. Ren, M. Grätzel, *J. Am. Chem. Soc.* **2019**, *141*, 18704-18714.

[197] C. Peng, G. Luo, J. Zhang, M. Chen, Z. Wang, T.-K. Sham, L. Zhang, Y. Li, G. Zheng, *Nat. Commun.* **2021**, *12*, 1580.

[198] E. Schuler, M. Demetriou, N. R. Shiju, G.-J. M. Gruter, *ChemSusChem* **2021**, *14*, 3636-3664.

[199] J. H. H. Meurs (Shell Oil Company), WO 2016/124646 A1, **2016**.

[200] M. Rudolph, S. Dautz, E.-G. Jäger, *J. Am. Chem. Soc.* **2000**, *122*, 10821-10830.

[201] K. Kobayashi, K. Tanaka, *Inorg. Chem.* **2015**, *54*, 5085-5095.

[202] R. S. Costa, B. S. R. Aranha, A. Ghosh, A. O. Lobo, E. T. S. G. da Silva, D. C. B. Alves, B. C. Viana, *J. Phys. Chem. Solids* **2020**, *147*.

[203] W. J. Evans, C. A. Seibel, J. W. Ziller, *Inorg. Chem.* **1998**, *37*, 770-776.

[204] T. T. Adamson, S. P. Kelley, W. H. Bernskoetter, *Organometallics* **2020**, *39*, 3562-3571.

[205] B. J. Cook, G. N. Di Francesco, K. A. Abboud, L. J. Murray, *J. Am. Chem. Soc.* **2018**, *140*, 5696-5700.

[206] J. Pospech, T. S. Mayer, *Nachr. Chem.* **2023**, *71*, 64-67.

[207] F. Khamespanah, M. Marx, D. B. Crochet, U. R. Pokharel, F. R. Fronczek, A. W. Maverick, M. Beller, *Nat. Commun.* **2021**, *12*, 1997.

[208] M. Marx, H. Frauendorf, A. Spannenberg, H. Neumann, M. Beller, *JACS Au* **2022**, *2*, 731-744.

[209] A. Béthegnies, Y. Escudié, N. Nuñez-Dallos, L. Vendier, J. Hurtado, I. del Rosal, L. Maron, S. Bontemps, *ChemCatChem* **2019**, *11*, 760-765.

[210] D. Zhang, C. Jarava-Barrera, S. Bontemps, *ACS Catal.* **2021**, *11*, 4568-4575.

[211] G. Jin, C. G. Werncke, Y. Escudié, S. Sabo-Etienne, S. Bontemps, *J. Am. Chem. Soc.* **2015**, *137*, 9563-9566.

[212] H. Kolbe, *Justus Liebigs Ann. Chem.* **1860**, *113*, 125-127.

[213] R. Schmitt, *J. Prakt. Chem.* **1885**, *31*, 397-411.

[214] A. S. Lindsey, H. Jeskey, *Chem. Rev.* **1957**, *57*, 583-620.

[215] World Health Organization, "Model List of Essential Medicines - 23rd list", can be found under https://www.who.int/publications/i/item/WHO-MHP-HPS-EML-2023.02, **2023** (accessed 03.03.2024).

[216] J. Davies, D. Janssen-Müller, D. P. Zimin, C. S. Day, T. Yanagi, J. Elfert, R. Martin, *J. Am. Chem. Soc.* **2021**, *143*, 4949-4954.

[217] M. Börjesson, D. Janssen-Müller, B. Sahoo, Y. Duan, X. Wang, R. Martin, *J. Am. Chem. Soc.* **2020**, *142*, 16234-16239.

[218] X.-W. Chen, J.-P. Yue, K. Wang, Y.-Y. Gui, Y.-N. Niu, J. Liu, C.-K. Ran, W. Kong, W.-J. Zhou, D.-G. Yu, *Angew. Chem. Int. Ed.* **2021**, *60*, 14068-14075.

[219] G. Kemper, M. Hölscher, W. Leitner, *Sci. Adv.* **2023**, *9*, eadf2966.

[220] D.-Y. Zhu, L. Fang, H. Han, Y. Wang, J.-B. Xia, *Org. Lett.* **2017**, *19*, 4259-4262.

[221] C. Bosch, W. Meiser (BASF), US 1429483 A, **1922**.

[222] C. Chen, X. Zhu, X. Wen, Y. Zhou, L. Zhou, H. Li, L. Tao, Q. Li, S. Du, T. Liu, D. Yan, C. Xie, Y. Zou, Y. Wang, R. Chen, J. Huo, Y. Li, J. Cheng, H. Su, X. Zhao, W. Cheng, Q. Liu, H. Lin, J. Luo, J. Chen, M. Dong, K. Cheng, C. Li, S. Wang, *Nature Chem.* **2020**, *12*, 717-724.

[223] P. Mampuys, H. Neumann, S. Sergeyev, R. V. A. Orru, H. Jiao, A. Spannenberg, B. U. W. Maes, M. Beller, *ACS Catal.* **2017**, *7*, 5549-5556.

[224] A. Del Vecchio, F. Caillé, A. Chevalier, O. Loreau, K. Horkka, C. Halldin, M. Schou, N. Camus, P. Kessler, B. Kuhnast, F. Taran, D. Audisio, *Angew. Chem. Int. Ed.* **2018**, *57*, 9744-9748.

[225] A. Paparakis, R. C. Turnell-Ritson, J. S. Sapsford, A. E. Ashley, M. Hulla, *Catal. Sci. Technol.* **2023**, *13*, 637-644.

[226] H. Niu, L. Lu, R. Shi, C.-W. Chiang, A. Lei, *Chem. Commun.* **2017**, *53*, 1148-1151.

[227] S.-S. Ma, R. Sun, Z.-H. Zhang, P.-X. Guan, J.-Q. Lin, C.-S. Li, B.-H. Xu, *Green Chem.* **2023**, *25*, 8625-8632.
[228] X. Li, Z. Liu, H. Hong, L. Han, N. Zhu, *RSC Adv.* **2022**, *12*, 18107-18114.
[229] T.-X. Zhao, G.-W. Zhai, J. Liang, P. Li, X.-B. Hu, Y.-T. Wu, *Chem. Commun.* **2017**, *53*, 8046-8049.
[230] C. L. Rooney, Y. Wu, Z. Tao, H. Wang, *J. Am. Chem. Soc.* **2021**, *143*, 19983-19991.
[231] S. Liu, T. Wang, L. Elbaz, Q. Li, *Mater. Rep.: Energy* **2023**, *3*, 100178.
[232] Y. Wu, Z. Jiang, Z. Lin, Y. Liang, H. Wang, *Nat. Sustain.* **2021**, *4*, 725-730.
[233] CarbonCure, "CarbonCure's Sustainable Concrete Solution - Concrete Technology Reducing Carbon Impact", can be found under https://www.carboncure.com/, **2024** (accessed 18.03.2024).
[234] Solidia Technologies, "Sustainable Concrete, Cement Solutions", can be found under https://www.solidiatech.com/, **2024** (accessed 18.03.2024).
[235] International Energy Agency (IEA), "Putting CO2 to Use", can be found under https://www.iea.org/reports/putting-co2-to-use, **2019** (accessed 14.03.2024).
[236] P. P. Pescarmona, *Curr. Opin. Green Sustainable Chem.* **2021**, *29*, 100457.
[237] M. Usman, A. Rehman, F. Saleem, A. Abbas, V. C. Eze, A. Harvey, *RSC Adv.* **2023**, *13*, 22717-22743.
[238] J. Martínez, F. de la Cruz-Martínez, M. Martínez de Sarasa Buchaca, J. Fernández-Baeza, L. F. Sánchez-Barba, M. North, J. A. Castro-Osma, A. Lara-Sánchez, *ChemPlusChem* **2021**, *86*, 460-468.
[239] B. Limburg, C. Maquilón, A. W. Kleij, in *CO2 as a Building Block in Organic Synthesis* (Ed.: S. Das), **2020**, pp. 1-28.
[240] C. Maquilón, B. Limburg, V. Laserna, D. Garay-Ruiz, J. González-Fabra, C. Bo, M. Martínez Belmonte, E. C. Escudero-Adán, A. W. Kleij, *Organometallics* **2020**, *39*, 1642-1651.
[241] C. Qiao, W. Shi, A. Brandolese, J. Benet-Buchholz, E. C. Escudero-Adán, A. W. Kleij, *Angew. Chem. Int. Ed.* **2022**, *61*, e202205053.
[242] X. Li, A. Villar-Yanez, C. Ngassam Tounzoua, J. Benet-Buchholz, B. Grignard, C. Bo, C. Detrembleur, A. W. Kleij, *ACS Catal.* **2022**, *12*, 2854-2860.
[243] Z. Guo, B. Yang, J. Jia, X. Wei, *Asian J. Org. Chem.* **2023**, *12*, e202300097.
[244] N. Westhues, M. Belleflamme, J. Klankermayer, *ChemCatChem* **2019**, *11*, 5269-5274.
[245] G. Gastelu, D. Savary, M. Hulla, D. Ortiz, J. G. Uranga, P. J. Dyson, *ACS Catal.* **2023**, *13*, 2403-2409.
[246] M. Siebert, M. Seibicke, A. F. Siegle, S. Kräh, O. Trapp, *J. Am. Chem. Soc.* **2019**, *141*, 334-341.
[247] K. Beydoun, J. Klankermayer, *Chem. - Eur. J.* **2019**, *25*, 11412-11415.
[248] T. A. Stephenson, S. M. Morehouse, A. R. Powell, J. P. Heffer, G. Wilkinson, *J. Chem. Soc.* **1965**, 3632-3640.
[249] A. Sinha, T. Ghatak, J. K. Bera, *Dalton Trans.* **2010**, *39*, 11301-11313.
[250] S. Tahara, K. Fujii, K. Nishihira, M. Matsuda, K. Mizutare (Ube Industries), US 4,467,109, **1983**.
[251] F. Rivetti, U. Romano, *J. Organomet. Chem.* **1978**, *154*, 323-326.
[252] F. Rivetti, U. Romano, *J. Organomet. Chem.* **1979**, *174*, 221-226.
[253] H. Hoberg, F. Javier Fañanás, H. Josef Riegel, *J. Organomet. Chem.* **1983**, *254*, 267-271.
[254] P. L. Burk, D. Van Engen, K. S. Campo, *Organometallics* **1984**, *3*, 493-495.
[255] H. E. Bryndza, S. A. Kretchmar, T. H. Tulip, *J. Chem. Soc., Chem. Commun.* **1985**, 977-978.
[256] D. M. Fenton, P. J. Steinwand, *J. Org. Chem.* **1974**, *39*, 701-704.
[257] S. P. Current, *J. Org. Chem.* **1983**, *48*, 1779-1780.
[258] E. Amadio, PhD thesis, Ca'Foscari University Venice (IT), **2009**.
[259] E. Amadio, G. Cavinato, A. Dolmella, L. Toniolo, *Inorg. Chem.* **2010**, *49*, 3721-3729.
[260] E. Amadio, Z. Freixa, P. W. N. M. van Leeuwen, L. Toniolo, *Catal. Sci. Technol.* **2015**, *5*, 2856-2864.
[261] G. D. Smith, B. E. Hanson, J. S. Merola, F. J. Waller, *Organometallics* **1993**, *12*, 568-570.
[262] R. Santi, A. M. Romano, R. Garrone, R. Millini, *J. Organomet. Chem.* **1998**, *566*, 37-43.
[263] E. Gallo, F. Ragaini, S. Cenini, F. Demartin, *J. Organomet. Chem.* **1999**, *586*, 190-195.

[264] A. Ariafard, B. F. Yates, *J. Organomet. Chem.* **2009**, *694*, 2075-2084.
[265] C. S. Day, S. J. Ton, R. T. McGuire, C. Foroutan-Nejad, R. Martin, *Organometallics* **2022**, *41*, 2662-2667.
[266] B. Milani, E. Alessio, G. Mestroni, A. Sommazzi, F. Garbassi, E. Zangrando, N. Bresciani-Pahor, L. Randaccio, *J. Chem. Soc., Dalton Trans.* **1994**, 1903-1911.
[267] K. M. Koczkur, S. Mourdikoudis, L. Polavarapu, S. E. Skrabalak, *Dalton Trans.* **2015**, *44*, 17883-17905.
[268] G. Cavinato, L. Toniolo, *J. Organomet. Chem.* **1993**, *444*, C65-C66.
[269] J. Smidt, W. Hafner, R. Jira, R. Sieber, J. Sedlmeier, A. Sabel, *Angew. Chem. Int. Ed.* **1962**, *1*, 80-88.
[270] J. A. Keith, P. M. Henry, *Angew. Chem. Int. Ed.* **2009**, *48*, 9038-9049.
[271] Z.-N. Xu, J. Sun, C.-S. Lin, X.-M. Jiang, Q.-S. Chen, S.-Y. Peng, M.-S. Wang, G.-C. Guo, *ACS Catal.* **2013**, *3*, 118-122.
[272] D. Wei, H. Junge, M. Beller, *Chem. Sci.* **2021**, *12*, 6020-6024.
[273] C. E. Roth, A. Dibenedetto, M. Aresta, *Eur. J. Inorg. Chem.* **2015**, *2015*, 5066-5073.
[274] D. P. Hickey, C. Sandford, Z. Rhodes, T. Gensch, L. R. Fries, M. S. Sigman, S. D. Minteer, *J. Am. Chem. Soc.* **2019**, *141*, 1382-1392.
[275] Z.-Q. Li, Y. Fu, R. Deng, V. T. Tran, Y. Gao, P. Liu, K. M. Engle, *Angew. Chem. Int. Ed.* **2020**, *59*, 23306-23312.
[276] M. A. Schmidt, X. Qian, *Tetrahedron Lett.* **2013**, *54*, 5721-5726.
[277] J. A. Frump, *Chem. Rev.* **1971**, *71*, 483-505.
[278] H. Li, Y. Li, J. Jiao, C. Lin, *Results Chem.* **2023**, *5*, 100859.
[279] G. A. Dawson, Q. Lin, M. C. Neary, T. Diao, *J. Am. Chem. Soc.* **2023**, *145*, 20551-20561.
[280] L. Chiassai, R. Ballesteros-Garrido, M. P. Clares, E. García-España, R. Ballesteros, B. Abarca, *Synthesis* **2019**, *51*, 4034-4042.
[281] M. Böttger, B. Wiegmann, S. Schaumburg, P. G. Jones, W. Kowalsky, H.-H. Johannes, *Beilstein J. Org. Chem.* **2012**, *8*, 1037-1047.
[282] K. Okano, H. Tokuyama, T. Fukuyama, *Org. Lett.* **2003**, *5*, 4987-4990.
[283] J. Jiao, X.-R. Zhang, N.-H. Chang, J. Wang, J.-F. Wei, X.-Y. Shi, Z.-G. Chen, *J. Org. Chem.* **2011**, *76*, 1180-1183.
[284] P. Pyykkö, M. Atsumi, *Chem. - Eur. J.* **2009**, *15*, 12770-12779.
[285] F. Brotzel, Y. C. Chu, H. Mayr, *J. Org. Chem.* **2007**, *72*, 3679-3688.
[286] H. Meier, in *Spektroskopische Methoden in der organischen Chemie, Vol. 9* (Eds.: S. Bienz, L. Bigler, T. Fox, H. Meier), Georg Thieme Verlag, **2016**, pp. 248-253.
[287] S. Kushwaha, J. Parthiban, S. K. Singh, *Organometallics* **2023**, *42*, 3066-3076.
[288] P. Štěpnička, J. Ludvík, J. Canivet, G. Süss-Fink, *Inorg. Chim. Acta* **2006**, *359*, 2369-2374.
[289] M. Chen, J. Xia, H. Li, X. Zhao, Q. Peng, J. Wang, H. Gong, S. Dai, P. An, H. Wang, Z. Hou, *ChemCatChem* **2021**, *13*, 3801-3814.
[290] J. Canivet, L. Karmazin-Brelot, G. Süss-Fink, *J. Organomet. Chem.* **2005**, *690*, 3202-3211.
[291] J. Fidalgo, M. Ruiz-Castañeda, G. García-Herbosa, A. Carbayo, F. A. Jalón, A. M. Rodríguez, B. R. Manzano, G. Espino, *Inorg. Chem.* **2018**, *57*, 14186-14198.
[292] V. V. Pavlishchuk, A. W. Addison, *Inorg. Chim. Acta* **2000**, *298*, 97-102.
[293] J. Li, W. Yan, Y. Kishi, *J. Am. Chem. Soc.* **2015**, *137*, 6226-6231.
[294] Q.-Y. Meng, T. E. Schirmer, A. L. Berger, K. Donabauer, B. König, *J. Am. Chem. Soc.* **2019**, *141*, 11393-11397.
[295] Y. Ye, G. Ma, K. Yao, H. Gong, *Synlett* **2021**, *32*, 1625-1628.
[296] S. Iimura, K. Manabe, S. Kobayashi, *J. Org. Chem.* **2003**, *68*, 8723-8725.
[297] M. Yasuda, Y. Onishi, M. Ueba, T. Miyai, A. Baba, *J. Org. Chem.* **2001**, *66*, 7741-7744.
[298] M. Shimoi, K. Maeda, S. J. Geib, D. P. Curran, T. Taniguchi, *Angew. Chem. Int. Ed.* **2019**, *58*, 6357-6361.
[299] E. J. Ko, G. P. Savage, C. M. Williams, J. Tsanaktsidis, *Org. Lett.* **2011**, *13*, 1944-1947.
[300] P. V. Kattamuri, J. G. West, *J. Am. Chem. Soc.* **2020**, *142*, 19316-19326.

[301] E. de Pedro Beato, D. Spinnato, W. Zhou, P. Melchiorre, *J. Am. Chem. Soc.* **2021**, *143*, 12304-12314.
[302] J. Bai, T. Wang, B. Dai, Q. Liu, P. Yu, T. Jia, *Org. Lett.* **2021**, *23*, 5761-5765.
[303] H.-T. Song, W. Ding, Q.-Q. Zhou, J. Liu, L.-Q. Lu, W.-J. Xiao, *J. Org. Chem.* **2016**, *81*, 7250-7255.
[304] K. Dong, X. Fang, R. Jackstell, G. Laurenczy, Y. Li, M. Beller, *J. Am. Chem. Soc.* **2015**, *137*, 6053-6058.
[305] V. Chandrasekaran, T. K. Lindhorst, *Chem. Commun.* **2012**, *48*, 7519-7521.
[306] A. D. Ure, I. A. Lázaro, M. Cotter, A. R. McDonald, *Org. Biomol. Chem.* **2016**, *14*, 483-494.
[307] R. Gorre, D. Enagandhula, S. Balasubramanian, S. M. Akondi, *Org. Biomol. Chem.* **2020**, *18*, 1354-1358.
[308] A. Kabro, G. Ghattas, T. Roisnel, C. Fischmeister, C. Bruneau, *Dalton Trans.* **2012**, *41*, 3695-3700.
[309] Y.-D. Zhang, X.-Y. Li, Q.-K. Mo, W.-B. Shi, J.-B. Zhao, S.-F. Zhu, *Angew. Chem. Int. Ed.* **2022**, *61*, e202208473.
[310] T. Senda, M. Ogasawara, T. Hayashi, *J. Org. Chem.* **2001**, *66*, 6852-6856.
[311] Y. Ye, H. Chen, J. L. Sessler, H. Gong, *J. Am. Chem. Soc.* **2019**, *141*, 820-824.
[312] T. Wang, F. Chen, J. Qin, Y.-M. He, Q.-H. Fan, *Angew. Chem. Int. Ed.* **2013**, *52*, 7172-7176.
[313] Z. Wang, X. Ji, J. Zhao, H. Huang, *Green Chem.* **2019**, *21*, 5512-5516.
[314] D. E. Stephens, J. Lakey-Beitia, J. E. Burch, H. D. Arman, O. V. Larionov, *Chem. Commun.* **2016**, *52*, 9945-9948.
[315] Y. Zhang, J. Ma, J. Chen, L. Meng, Y. Liang, S. Zhu, *Chem* **2021**, *7*, 3171-3188.
[316] B. H. Rotstein, A. K. Yudin, *Synthesis* **2012**, *44*, 2851-2858.
[317] A. S. Ripka, K. A. Satyshur, R. S. Bohacek, D. H. Rich, *Org. Lett.* **2001**, *3*, 2309-2312.
[318] W. Li, A. Zhang, *Sci. China: Chem.* **2010**, *53*, 2509-2519.
[319] G. Orellana, C. Alvarez-Ibarra, M. L. Quiroga, *Bull. Soc. Chim. Belg.* **1988**, *97*, 731-742.
[320] M. R. Krout, J. T. Mohr, B. M. Stoltz, *Org. Synth.* **2009**, *86*, 181.
[321] C. Bannwarth, S. Ehlert, S. Grimme, *J. Chem. Theory Comput.* **2019**, *15*, 1652-1671.
[322] C. Bannwarth, E. Caldeweyher, S. Ehlert, A. Hansen, P. Pracht, J. Seibert, S. Spicher, S. Grimme, *Wiley Interdiscip. Rev.: Comput. Mol. Sci.* **2021**, *11*, e1493.
[323] S. Grimme, *J. Chem. Theory Comput.* **2019**, *15*, 2847-2862.
[324] P. Pracht, F. Bohle, S. Grimme, *Phys. Chem. Chem. Phys.* **2020**, *22*, 7169-7192.

9 Curriculum Vitae

THEA SIRI MAYER

Leibniz Institute for Catalysis e.V. (LIKAT)
Albert-Einstein-Straße 29A, 18059 Rostock, Germany
Phone: +493811281206
Email: thea.mayer@catalysis.de
Born 18th August 1997 in Lübeck, Germany
Languages: German (native), English (proficient), French (intermediate), Latinum

EDUCATION

2021 – 2024	**PhD in Chemistry** at the LIKAT, Rostock, Germany. Supervisors: Dr. Jola Pospech, Prof. Matthias Beller. Thesis: *"Exploring CO_2 as C_1 building block in synthetic processes: Steps towards a circular economy"* Date of submission: 14th May 2024; date of defense: 15th October 2024. Invited to participate in the 71st Lindau Nobel Laureate Meeting as one of 600 young scientists from all around the world.
2018 – 2020	**MSc in Chemistry** at the University of Rostock, Germany and Aarhus University, Denmark. Master thesis: *"Synthesis of chiral photosensitizers and their application in the asymmetric hydroamination of stilbenes"* (1.0); carried out under supervision of Dr. Jola Pospech. Final grade: 1.1 Supported by an Erasmus+ scholarship.
2015 – 2018	**BSc in Chemistry** at the University of Rostock, Germany. Bachelor thesis: "*Synthesis of new P-stereogenic ligands*" (1.0); carried out under supervision of Prof. Armin Börner. Final grade: 1.4 Valedictorian of the Bachelor class in Chemistry (2018).
2007 – 2015	**Abitur** at Gymnasium Hittfeld in Seevetal, Germany. Final grade: 1.2 GDCh (Gesellschaft Deutscher Chemiker)-Award for the school's best Abitur in chemistry (2015); awardee of the Glemser Foundation For Future Excellency (2015).

ADDITIONAL RESEARCH AND WORK EXPERIENCE

11/2023	Two-day seminar at the Graduate Academy Rostock, Germany. *Speed reading for academics*.
05/2023	Two-day online seminar at the National Institute for Science Communication (NaWik), Germany. *Comprehensible writing (Verständlich schreiben)*.
04/2023 – 06/2023	Research stay as part of the PhD studies at the Interdisciplinary Nanoscience Center (iNANO), Aarhus University, Denmark. Supervisor: Prof. Troels Skrydstrup.
04/2023	Two-day seminar at the Graduate Academy Rostock, Germany. *Presence training and self-marketing (Präsenztraining und Selbstmarketing).*
11/2022 – 03/2023	Deputy lab leader during the maternal leave of Dr. Jola Pospech.

10/2020 – 03/2021	Industry intern at Bayer AG, Wuppertal, Germany. *Process optimization and special technologies*. Supervisor: Dr. Kai Lovis.
09/2019 – 12/2019	Research intern in catalysis at iNANO, Aarhus, Denmark. *Carbonylative access to trifluoromethyl ketones and labeling of aliphatic ketones* via *the* in situ *formation of thioesters.* Supervisor: Prof. Troels Skrydstrup.
10/2018 – 01/2019	Research associate in organic chemistry and catalysis at LIKAT, Rostock, Germany. *Synthesis of an organic, Cu(I) specific sensor.* Supervisor: Dr. Jola Pospech.
06/2017 – 06/2018	Student associate in physical chemistry at the University of Rostock, Germany. *Dynamic light scattering on charged hydrogels.* Supervisor: Prof. Joachim Wagner.
06/2015	Internship in polymer chemistry at the Karlsruhe Institute for Technology (KIT), Germany. Supervisor: Prof. Leonie Barner.

PUBLICATIONS

6. Thea Siri Mayer, and Jola Pospech, "Künstliche Photosyntheseprozesse: Kupplungsreaktionen mit CO_2" *Nachr. Chem*. **2023**, *71*, 64–67.
5. Thea Siri Mayer, Tobias Taeufer, Sina Brandt, Jabor Rabeah, and Jola Pospech, "Photomediated Hydro- and Deuterodecarboxylation of Pharmaceutically Relevant and Natural Aliphatic Carboxylic Acids" *J. Org. Chem*. **2023**, *88*, 6347–6353.
4. Thea Siri Mayer, and Jola Pospech, "Der richtige Dreh mit Licht" *Nachr. Chem*. **2022**, 70, 81–85.
3. Andranik Petrosyan, Luisa Zach, Tobias Taeufer, Thea Siri Mayer, Jabor Rabeah, and Jola Pospech, "Pyrimidopteridine-catalyzed Photo-mediated Hydroacetoxylation" *Chem. – Eur. J*. **2022**, *28*, e2022017.
2. Tobias Taeufer, Richy Hauptmann, Firas El-Hage, Thea Siri Mayer, Haijun Jiao, Jabor Rabeah, and Jola Pospech, "Pyrimidopteridine-Catalyzed Hydroamination of Stilbenes with Primary Amines: A Dual Photoredox and Hydrogen Atom Transfer Catalyst" *ACS Catal.* **2021**, *11*, 4862–4869.
1. Martin Bundgaard Johansen, Oliver Rae Gedde, Thea Siri Mayer, and Troels Skrydstrup, "Access to Aryl and Heteroaryl Trifluoromethyl Ketones from Aryl Bromides and Fluorosulfates with Stoichiometric CO" *Org. Lett*. **2020**, *22*, 4068–4072.

PARTICIPATION IN INTERNATIONAL CONFERENCES

5. **Poster** "Approaches to Photo-mediated Deuterodecarboxylation, Direct Air Capture and Transition Metal-catalyzed CO_2 Valorization" at the International Symposium on Organometallic Chemistry Directed Towards Organic Synthesis (OMCOS) XXI in Vancouver, Canada (2023). Supported by a DAAD scholarship.
4. **Poster** "Photo-mediated Hydro- and Deuterodecarboxylation of Pharmaceutically Relevant and Natural Aliphatic Carboxylic Acids" at the Belgian Organic Synthesis Symposium (BOSS) XVII in Namur, Belgium (2022).
3. **Participation** in the 71st Lindau Nobel Laureate Meeting, dedicated to Chemistry, Lindau, Germany (2022).
2. **Poster** "Photo-mediated Hydro- and Deuterodecarboxylation of Pharmaceutically Relevant and Natural Aliphatic Carboxylic Acids" at the 3rd ComBioCat Symposium in Rostock, Germany (2022).
1. **Participation** in the 5th Torkil Holm Symposium in Copenhagen, Denmark (2020).

VOLUNTEERING

04/2024	Reviewer activity for *Green Chemistry* (RSC).
11/2022 – 11/2023	PhD representative at LIKAT, Rostock.
12/2018 – 09/2020	Head of the student council and representative of the Master students and international students at the Institute for Chemistry, University of Rostock.
10/2018 – 09/2019	Head of the mentoring program for freshmen at the Institute for Chemistry, University of Rostock.